Aus dem Max von Pettenkofer-Institut für Hygiene und
Medizinische Mikrobiologie/ Lehrstuhl Virologie der
Ludwig-Maximilians-Universität München

Vorstand: Prof. Dr. med. Oliver T. Keppler

Characterization of the E4 protein of human papillomaviruses as an enhancer of HIV infection

Dissertation
zum Erwerb des Doktorgrades der Naturwissenschaften
an der Medizinischen Fakultät der
Ludwig-Maximilians-Universität zu München

vorgelegt von
Dipl.-Biologe Marcel Stern

aus
Worms

2020

Mit Genehmigung der Medizinischen Fakultät
der Universität München

Betreuer:	Prof. Dr. rer. nat. Karl-Klaus Conzelmann
Zweitgutachter:	Prof. Dr. rer. nat. Thomas Brocker
Dekan:	Prof. Dr. med. dent. Reinhard Hickel
Tag der mündlichen Prüfung:	06.02.2020

Eidesstattliche Versicherung

Stern, Marcel

Ich erkläre hiermit an Eides statt, dass ich die vorliegende Dissertation mit dem Titel

"Characterization of the E4 protein
of human papillomaviruses as an enhancer
of HIV infection"

selbständig verfasst, mich außer der angegebenen keiner weiteren Hilfsmittel bedient und alle Erkenntnisse, die aus dem Schrifttum ganz oder annähernd übernommen sind, als solche kenntlich gemacht und nach ihrer Herkunft unter Bezeichnung der Fundstelle einzeln nachgewiesen habe.

Ich erkläre des Weiteren, dass die hier vorgelegte Dissertation nicht in gleicher oder in ähnlicher Form bei einer anderen Stelle zur Erlangung eines akademischen Grades eingereicht wurde.

München, 27.02.2020	Marcel Stern
Ort, Datum	Unterschrift des Doktoranden

„Es wird dich niemals jemand fragen, wie lange hast du gebraucht, sondern immer, wer hat das gemacht…“

- Für meine Familie -

This thesis has been prepared in the laboratories of Prof Dr. Oliver Keppler and Prof. Dr. Karl-Klaus Conzelmann at the Max von Pettenkofer-Institute of the Ludwig-Maximilians-University Munich

Danksagung

Diese Doktorarbeit wäre ohne die Vielzahl von Menschen, die mich in den letzten Jahren auf vielerlei Art und Weise unterstützt haben, nicht möglich gewesen.

Zunächst möchte ich mich bei meinen Betreuern **Prof. Dr. Oliver T. Keppler** und **Prof. Dr. Karl-Klaus Conzelmann** für ihr Vertrauen bedanken, dass ich meine Doktorarbeit in ihren Arbeitsgruppen anfertigen durfte. Beide haben mir mit ihrem Anspruch an gutes wissenschaftliches Arbeiten, der Freiheit eigenen Idee nachgehen zu können, der Anregung zur kritischen Auseinandersetzung mit dem Thema sowie den gewonnenen Daten, menschlich und fachlich perfekte Rahmenbedingungen geboten. Durch ihre Führung haben sie mir dabei geholfen mich stetig weiter zu entwickeln. Auch möchte ich mich für das interessante, aktuelle und translationale Thema bedanken.

Weiterhin möchte ich mich bei den Kollaborationspartnern bedanken ohne die diese Arbeit nicht möglich gewesen wäre: Prof. Klein (bNAbs), Prof. Dürst/ Prof. Brockmeyer (IHC), Prof. Baur (MELC), Dr. Neßling/ Dr. Richter (EM Bilder) und Prof. Cinatl (AdV).

Aus der Zeit in Frankfurt möchte ich **Margarethe, Lena, Ina, Sebe und Sarah** für ihre Freundschaft und Unterstützung danken, sowie **Sarah-Marie**, welche mir auch weit über die Zeit in Frankfurt hinaus eine treue Wegbegleiterin geblieben ist.

Beim Neustart in München waren mir **Christian** und **Ari** eine sehr große Unterstützung. Ich danke euch für eure Freundschaft und euren Rat. Christian, du als einer meiner wichtigsten Kritiker, hast mich mit Oliver und Klaus zusammen zu dem Wissenschaftler ausgebildet, der ich heute bin. Ich danke dir sehr für die Korrektur meiner Doktorarbeit.

Außerdem möchte ich meinen Kollegen aus der **AG Keppler, Madeleine, Manuel, Ernesto, Steffi, Robin, Hong-Ru und Qianhao** danken, ihr seid spitze! Die vielen konstruktiven und kritischen Gespräche sowie die tolle Zeit abseits des Arbeitsalltags waren stets eine Bereicherung für mich. Ich danke **Hanna-Mari**, **Fabian, Ramya, Rebecca, Lin, Johanna, Kathi, Augusto, Ina** sowie meinen Kollegen aus der **AG Conzelmann Belex, Verena, Chloé** und **Max** für ihre Unterstützung und Geduld. **Xaver** danke ich für seine großartige Unterstützung bei den Experimenten der Konfokal-Mikroskopie, seine Kritik und Anregung zum wissenschaftlichem Denken und Arbeiten. Für die tolle Zeit in Frankfurt und in München danke ich außerdem **Patricia**, du warst mir immer eine sehr gute Kollegin und Freundin.

Meinen Freunden **Robert, Rebecca, Dominik, Stefanie, Hannah, Sebastian, Marc und Tina** gilt ein weiterer besonderer Dank. Ihr ward mir immer eine Stütze. Ich danke euch sehr für die tolle Zeit, die wir gemeinsam verbracht haben. Ihr seid die besten! Ein besonderer Dank gilt auch meiner ehemaligen Stammkursleiterin/ Biologie-Lehrerin **Vera.**

Für den Schluss habe ich mir die wichtigsten Menschen aufgehoben. Ein ganz besonderer Dank gilt **meiner Familie**, die mich immer unterstützt hat. So lange ich denken kann ward ihr immer für mich da, habt mich aufgerichtet und mir Kraft gegeben. Ich danke euch dafür, dass ihr mich immer gefördert habt und es mir somit ermöglicht habt diesen langen Weg zu gehen. Deshalb widme ich euch diese Doktorarbeit.

Table of Contents

I Summary

Transmission of the human immunodeficiency virus (HIV) across anogenital epithelial tissue is the primary route of HIV dissemination worldwide. Genital human papillomavirus (HPV) infection is the most common sexually transmitted disease (STD) with global prevalence of above 10%. It is well established that sexually transmitted infections of the anogenital tract are important cofactors for HIV transmission in both men and women, and epidemiological studies indicate that preexisting infections by mucotropic HPV types enhance the risk of HIV acquisition by up to 5-fold. It has been speculated that HPV-induced inflammatory lesions in the mucosal barrier and the recruitment of HIV-susceptible immune cells might be involved, yet little is known about molecular mechanisms in the cross-talk of these pathogens that may be involved in the increased rate of HIV transmission. Specific peptides present in seminal fluid, including SEVI, are able to form amyloid fibrils and enhance HIV infection. Interestingly, the E4 protein of HPV, which accumulates to high levels in infected, disintegrating keratinocytes in the outermost layers of the anogenital mucosa, spontaneously aggegrates into amyloids.

Here we find that the E4 protein of oncogenic and non-oncogenic HPV types enhances HIV infection of CD4 T cells by up to 300-fold. Naturally occurring, *N-terminally* cleaved E4 self-assembled into cationic, intermediate amyloid fibrils that captured and concentrated HIV particles, protecting virion infectivity, impairing the efficiency of HIV broadly neutralizing antibodies and promoting fusion to and infection of multiple types of primary target cells. E4 drastically lowered the virus titer required for productive HIV infection in *ex vivo*-lymphoid organ cultures and infection enhancement occurred efficiently in vaginal fluid. Low amounts of E4 induced the amyloid formation and functionality of SEVI. Analysis of structural HPV16 E4 mutants identified the *C-terminal* 22 amino acids to be critical for HIV infection enhancement. Moreover, exposure of other clinically relevant viruses, i.e. herpes simplex virus type 1, rabies virus, measles virus and adenoviruses, to E4 amyloids also increased their ability to infect target cells. Comparison of the impact of E4 and a panel of naturally occurring amyloids (SEVI, β-amyloid, α-synuclein, islet amyloid polypeptide) on infection of this set of viruses revealed a broad, yet variable degree of enhancement.

These results demonstrate the potency of the papillomaviral E4 protein to boost virus infections, most notably HIV, and suggest a potential cross-talk of pathogen-associated and physiological infection-enhancing peptides for transmission and disease induction of viruses. Together with epidemiological evidence these findings provide a strong rationale for the development of polyvalent prophylactic HPV vaccines that protect from infection with all circulating mucosal HPV types as a strategy to lower the risk of HIV transmission and confine the pandemic.

II Zusammenfassung

Die Übertragung des Humanen Immundefizienz-Viruses (HIV) über die anogenitale Schleimhaut ist weltweit die häufigste Art der Verbreitung. Die verbreitetste sexuell übertragbare Infektion (STI) stellt mit einer globalen Prävalenz von mehr als 10% die Gruppe der genital vorkommenden humanen Papillomaviren (HPV) dar. Es ist allgemein anerkannt, dass sowohl bei Männer als auch bei Frauen Koinkfetionen mit anderen STIs im Anogenitaltrakt die HIV-Übertragung begünstigen können. Epidemiologische Studien zeigen zudem, dass eine vorbestehende Infektion mit mukotropen HPV-Typen das Risiko eine HIV-Infektion um bis zu 5-fach erhöht. Als mögliche Ursache hierfür werden u.a. die HPV-induzierten entzündlichen Läsionen der mukosalen Schutzschicht und die damit verbundene Rekrutierung von HIV-suszeptiblen Immunzellen genannt. Über die zugrundeliegenden molekularen Mechanismen, die bei der Wechselwirkung der beiden Pathogene im Hinblick auf die erhöhte HIV-Übertragung eine Rolle spielen, ist bisher noch wenig bekannt. Samenflüssigkeit enthält speziellen Peptide, wie z.B. SEVI, die in der Lage sind, amyloide Fibrillen auszubilden und hierdurch die HIV-Infektion von Zielzellen zu verstärken. Das E4-Protein von HPV, welches in großen Mengen in infizierten, abschilfernden Keratinozyten der äußersten Schichten der anogenitalen Mukosa zu finden ist, aggregiert spontan zu solchen Amyloiden.

In der vorliegenden Arbeit wird gezeigt, dass das E4-Protein von onkogenen und nicht-onkogenen HPV-Typen die Infektion von CD4 T-Zellen mit HIV um bis zu 300-fach erhöht. Natürlich vorkommendes, *N-terminal* prozessiertes E4 bildet kationische, intermediäre amyloide Fibrillen, welche HIV-Partikel binden und konzentrieren können, die Infektiosität der Virionen verlängern, die Effizienz von breitneutralisierenden Antikörpern gegen HIV beeinträchtigen, und sowohl die virale Fusion als auch die Infektion verschiedener primären Zielzelltypen erhöhen können. E4 ist zudem in der Lage, die Virustiter, welche benötigt werden, um ein produktive HIV-Infektion in lymphatischen Organkulturen *ex vivo* auszulösen, deutlich zu senken. Außerdem ist die E4-vermittele Infektionsverstärkung von HIV in Gegenwart von Vaginalsekret möglich. Kleine Mengen E4-Protein sind in der Lage, die Aggregation von monomerem SEVI auszulösen. Die Analyse verschiedener struktureller HPV16 E4-Mutanten konnte darüber hinaus die 22 *C-terminalen* Aminosäuren des Proteins als wichtig für die Verstärkung der HIV-Infektion identifizieren. Ferner konnte die HPV E4-Exposition anderer klinisch relevanter Viren, wie z.B. Herpes simples Virus 1, Tollwut-Virus, Masern-Virus und Adenovirus, die Infektion ihrer Zielzellen erhöhen. Vergleichende Experiment mit E4 und einer Gruppe anderer natürlich vorkommender Amyloide (SEVI, β-Amyloid, α-Synuclein, Insel-Amyloid-Polypeptid) zeigten einen breiten, jedoch variablen Einfluss auf die Verstärkung der Infektion mit den zuvor genannten Viren.

II - Zusammenfassung

Die dargestellten Ergebnisse belegen die Wirksamkeit von HPV-E4, die Infektion von Viren, insbesondere von HIV, zu verstärken. Auch deuten sie auf ein mögliches Wechselspiel zwischen Pathogen-assoziierten and physiologischen infektionsverstärkenden Peptiden im Hinblick auf Übertragung und Ausprägung des jeweiligen Virus-assoziierten Krankheitsbildes hin. Zusammen mit epidemiologischen Studien untermauern diese neuen Erkenntnisse die Forderung nach der Entwicklung eines polyvalenten, prophylaktischen HPV-Impfstoffes, welcher vor der Infektion mit allen zirkulierenden mukosalen HPV-Typen schützt. Diese Strategie könnte das Risiko der HIV-Übertragung minimieren und damit die weltweite HIV-Pandemie eindämmen.

1 Introduction

1.1 The human immunodeficiency virus - HIV

1.1.1 The HIV pandemic - a global burden

In the early 1980s, “homosexual men in urban centers began presenting with advanced and unexplained immunodeficiency” [1], which was later termed acquired immunodeficiency syndrome (AIDS) and has been attributed in 1983 to the etiologic agent human immunodeficiency virus type 1 (HIV-1). In 1986, a second HIV-related retrovirus was discovered, termed HIV type 2 (HIV-2). HIV-1 is the virus responsible for the majority of today’s pandemic of approximately 36.9 million people living with HIV and 1.8 million people becoming newly infected in 2017. More than half of the HIV-infected individuals are women. HIV infection has caused so far more than 35 million deaths and, although numbers are declining (-38% between 2000 and 2017), 940,000 people still died in 2017. The increasing availability of antiretroviral therapy (ART) has helped to ban HIV from the “global top 10 list” of disease-related death; however, HIV can still be found in this group in low-income countries. To date, 59% of adults and 52% of children infected with HIV are under ART treatment. The main region of the HIV pandemic is located in Africa, especially sub-Saharan Africa, which accounts for over two thirds of the global HIV burden [1, 2] (“WHO HIV update”/ “The top 10 causes of death”/ “HIV/AIDS key facts”, WHO 2018).

Similarities to the monkey-derived simian immunodeficiency virus (SIV) and epidemiological evidence strongly suggest that HIV was the consequence of zoonotic transmissions. Since both viruses can spread through blood, the species transfer could have occurred during hunting and butching of monkey “bush meat”. Interestingly, the collection of fecal samples from several monkeys and subsequent phylogenetic analysis revealed that HIV-1 is closely related to SIV strains in chimpanzee (SIVcpz) as well as gorilla (SIVgor), and HIV-2 to SIV strains in sooty mangabeys (SIVsmm). In addition, these studies indicated that for both, HIV-1 and HIV-2, independent transmission events likely occurred several times, which is represented by the four HIV-1 groups (M, N, O and P) and at least eight HIV-2 groups (A-H). HIV-1 group M, which accounts for the majority of the global HIV burden, can be divided into multiple subtypes (A-D, F-H, J and K). Since recombination of the viral genome is an intrinsic feature of HIV, genetical exchange between subtypes as well as groups can occur, resulting in so-called CRFs (circulating recombinant form) or URF (unique recombinant form), depending on their property to spread in the population. Looking at the worldwide contribution to the pandemic (**Fig. 1**), HIV-1 group M subtype C (Africa, India) dominates, followed by subtype A (Africa, Eastern Europe) and subtype B (America, Western Europe, Australia). In contrast, HIV-2 being less pathogenic

and less transmittable, is mostly restricted to West Africa, where it is in most cases represented by group A and B [2].

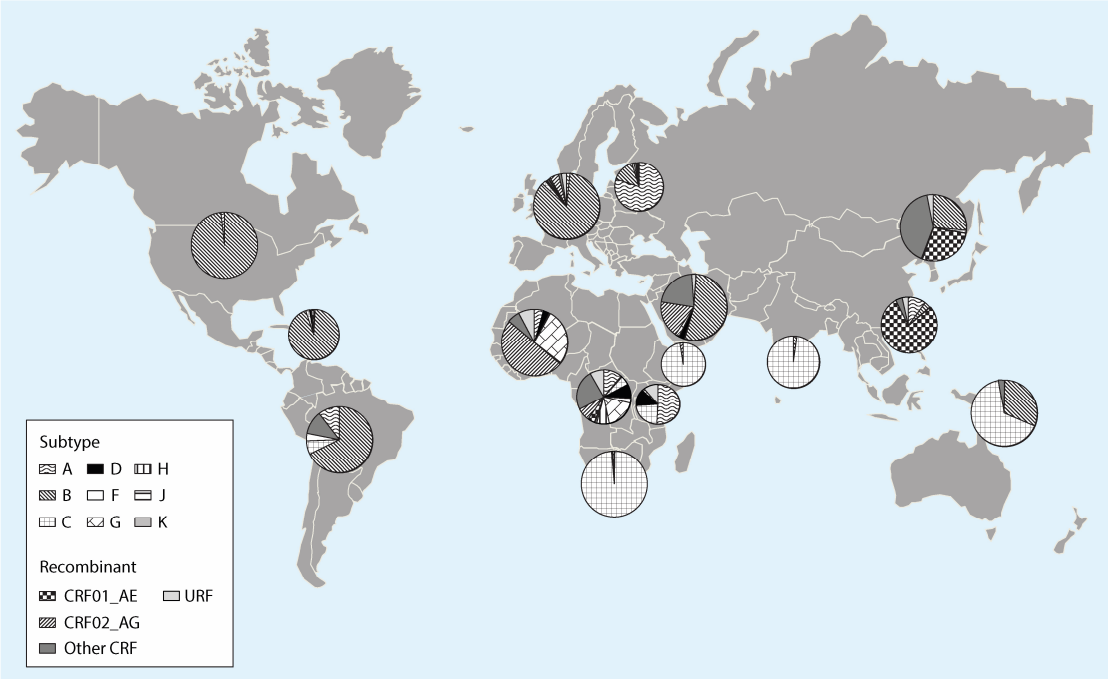

Figure 1: Geographic distribution of HIV-1 group M. Depicted is the regional prevalence of the different subtypes and CRFs of HIV-1group M in 2007. The main subtypes found are clade C, followed by A and B. CRFs are also largely present especially in eastern Asia. Graphic taken from Peeters et al. [2].

1.1.2 HIV transmission and interplay with the host

Transmission of HIV occurs mainly through heterosexual intercourse, which accounts for around 70% of HIV infections worldwide and a risk of transmission of 1:200-3,000. The remaining transmission events can be attributed to man having sex with men (MSM, transmission risk 1:20-300), mother-to-child transmission (*in utero*, perinatal and post-natal by breastfeeding) and needle sharing during injection drug use (IDU). Importantly, the transmission risk can be markedly increased, up to 10-fold, by confounding risk factors like other sexually transmitted diseases (STDs) or surgery impairing the mucosal integrity, the stage of HIV disease and the corresponding viral load (vL) of the donor as well as the exposure route. Moreover, certain groups have an increased risk including people with low-income or sex workers. Both, MSM and heterosexual individuals have an increased risk for HIV acquisition related to a frequent change of partners. In all cases, early diagnosis of HIV infection plays a crucial role, since it allows early onset of ART. Afterwards, continuous as well as for efficiency monitored (avoiding viral escape and drug resistance) ART is important, because only in that way efficient control of viral replication is possible, lowering the plasma viral load in infected individuals and

thereby also decreasing the risk of sexual transmission by >96%. Additional ways to limit transmission can be the use of condoms, monogamy, treatment of co-infections and circumcision [3, 4].

Other factors that can affect the efficiency of the transmission event are characteristics of the transmitted virus itself, the environment present within the transmission fluid, the composition and fitness of the mucosa at the transmission site as well as the presence of HIV target cells [4]. To study the characteristics of recently transmitted viruses in more detail, methods were established to create viral consensus sequences from patients recently infected with HIV, which were termed transmitted/ founder (T/F) viruses. HIV requires interaction of viral Env (envelope) surface receptor with two different cellular receptors to infect new cells: the initial binding of the primary receptor CD4 and subsequent interaction with one of the two major co-receptors, CCR5 or CXCR4 (both chemokine receptors). Analysis of the T/F and their chronic counterparts showed that the T/F viruses almost exclusively target cells expressing CCR5, hence are termed as R5-tropic. Only in few rare cases, the T/F viruses are dual-tropic (R5X4). The trimeric HIV Env consists of heterodimers formed by the viral proteins gp (glycoprotein) 41 and gp120, the latter containing several variable loops. Typically, chronic HIV variants present few Env molecules on their surface, which exhibit long variable loops and are extensively glycosylated, whereas T/F viruses frequently display the opposite phenotype. This indicates that features of the virus acquired within the chronically infected host, may protect important conserved regions and support evasion from immune recognition, but might be detrimental for transmission. A context where this could conceivably be of importance is the transmission fluid, which can possibly select for the transmitted viruses by factors present in semen or cervicovaginal fluid, such as lectins (able to bind glycosylated proteins) or neutralizing antibodies. Furthermore, T/F viruses did not exhibit an altered behavior compared to their chronic counterparts in studies examining tiered-neutralization using bNAbs (see chapter 1.1.7) [3-5].

The mucosa present at transmission sites imposes as a first line of defense a barrier to incoming pathogens. In the case of the female genital tract, the thin single-layered endocervix can be discriminated from the multi-layered ectocervix and vagina, the latter being under constant change in thickness due to hormonal changes as part of the menstrual cycle. Thinning of the mucosa can be important, since it brings incoming pathogens in proximity to target cells. It was reported that infection with HIV could occur within both regions as well as the transition zone [3, 6]. Besides antibodies and lectins, the mucus present at the transmission site may play an important role, due to its ability to immobilize pathogens including HIV [4, 6].

1.1.3 HIV-1 - establishment of infection and development of AIDS

After conquering the mucosa, the availability of target cells is crucial to establish infection in the new host. Comparing vaginal and anal sub-mucosa, the former contains lower numbers of CD4 T cells [3]. Studies in monkeys aiming to detect the first cells infected after transmission yielded controversial results, with some indicating that $CD4^+$ $CCR5^+$ T cells may be involved [7]. In contrast, dendritic cells (DCs) or Langerhans cells (LCs), which sample with their dendrites the lumen of the vaginal or anal tract, display low CD4 levels, which in most cases might allow attachment of HIV particles, but not infection [6]. The presence of CD4 T cells in the mucosa frequently occurs during inflammation, caused by microlesions due to sexual intercourse or other STDs. Productively infected CD4 T cells can lead to spread through either free virus particles or cell-to-cell transmission (virological synapse). Alternatively, DCs/ LCs with bound or internalized HIV particles can start migrating to the underlying lamina propria or draining lymph nodes, wherein infectious synapse formation can lead to infection of resident CD4 positive T helper cells or T follicular helper cells. This may also lead to B cell dysfunction and reduce the adaptive immune response to HIV. Nevertheless, all of these scenarios of initial spread have in common, that replication within these cells usually causes their death, creating a pro-inflammatory milieu leading to influx of additional target cells and local tissue destruction [3, 4, 6, 8]. Interestingly, all of the described factors important during transmission result in 60 to 80% of cases in the establishment of infection by only a single virus in the new host, although many different viruses might have been present at the transmission site or even transmitted initially [3, 4].

After establishing local infection, HIV spreads usually to other lymphatic organs, most importantly, the gut-associated lymphatic tissue (GALT), but eventually also to non-lymphatic tissues such as the brain [6]. This initial clinically in many cases silent phase of systemic spread in the new host is referred to as the “eclipse phase” and is also the time where the HIV reservoir is formed. As a retrovirus, HIV can integrate into the genome of an infected activated CD4 T cell, which can in some cases reconvert into a resting state, hence become a memory T cell. Here, HIV can reside as a latent provirus, from which it can rebound after direct or bystander activation. The next phase towards developing AIDS is the “acute phase”, where the initial systemic depletion of immune cells in various lymphatic organs occurs and flu-like symptoms are frequently reported. Destruction of CD4 T cells within the GALT is one of the most fatal actions during this period, causing an imbalance of the tightly regulated gut homeostasis, followed by the breakdown of the intestinal lining. Besides changing the mucosal microbiome, this event leads to microbial translocation and systemic immune activation, which is a hallmark of HIV infection. Afterwards, CD8 T cells as wells as NK cells in combination with antibodies against HIV manage to control the viremia and the “chronic phase” starts. Nevertheless, a constant low level of viral replication persists, which at its initial point is termed “virological set

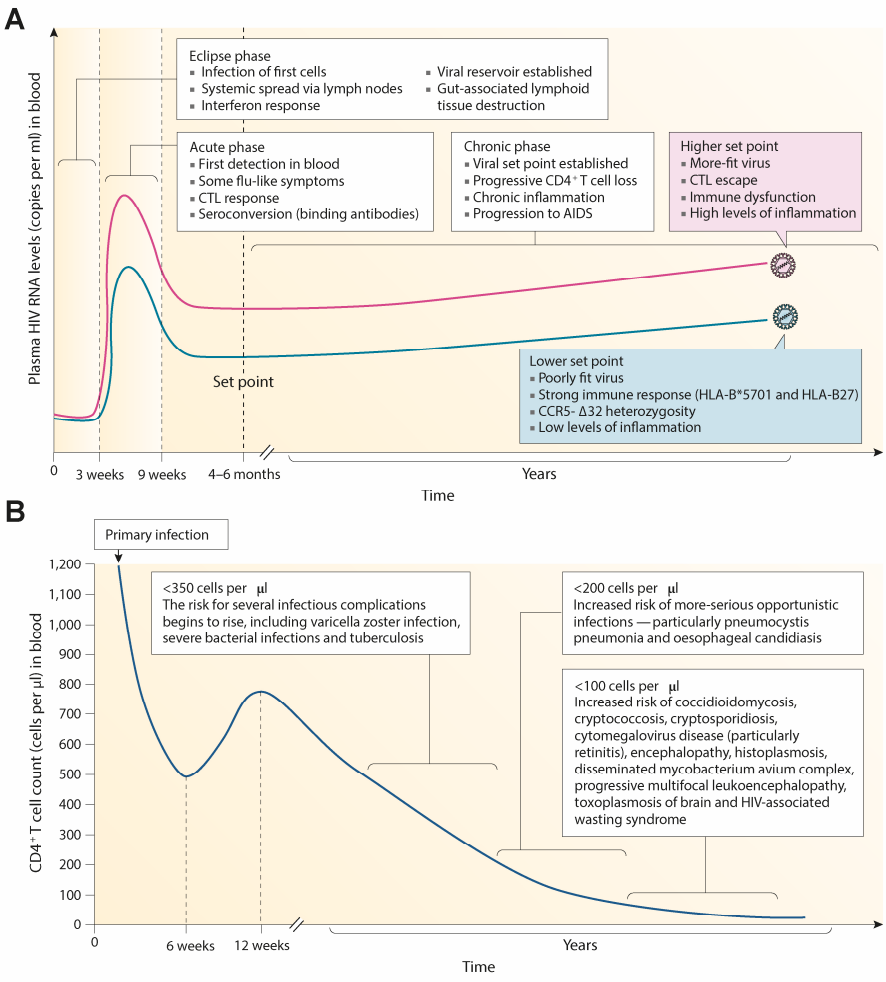

Figure 2: Stages of HIV infection leading to AIDS and related disease. (**A**) Different stages of HIV infection. Right after transmission, the “eclipse phase” takes place, where the viral reservoir is formed, and which is followed by the viremic/ symptomatic “acute phase”. The immune response controls the viremia to a certain degree, defining the “virological set point”, which is predictive for the further disease progression. The “chronic phase” is typically asymptomatic during the first years, but increasing CD4 T cell loss facilitates occurrence of opportunistic infections. (**B**) CD4 T cell decline and associated symptoms. HIV infection leads initially to a dramatic loss of CD4 T cells, which can recover to a certain degree due to the immune response controlling the “acute phase”. Over time, ongoing HIV replication and depletion of CD4 T cells leads to the development of AIDS. Figure modified from Deeks et al. [1].

point” and predictive for disease progression in infected patients. Control of HIV replication in this phase causes a partial recovery of CD4 T cell numbers, but gradual loss of CD4 T cells over several years leads to the development of AIDS (**Fig. 2A**) [1, 9].

Progressive immune dysfunction and exhaustion make the host permissive to opportunistic infections and certain types of cancer. Classical opportunistic co-infections are caused e.g. by *candida albicans*, *cryptococcus neoformans* or *mycobacterium tuberculosis*, different viruses including kaposi's sarcoma-associated herpesvirus (KSHV or human herpesvirus 8 (HHV-8)) and cytomegalovirus (CMV) and parasites like *toxoplasma gondii*. In addition, the incidence of several tumors, including Kaposi sarcoma and certain lymphomas, but also HPV-associated

cervical as well as anal cancers is increased in HIV-immunocompromised hosts (**Fig. 2B**). There are several non-AIDS defining but HIV-associated organ syndromes likely due to immune activation or endothelial dysfunction including ischemic heart disease, stroke, liver fibrosis and cognitive disorders [1, 9, 10]. Additionally, the immune reconstitution inflammatory response (IRIS), which occurs during the partial recovery of CD4 T cell counts, leads to local immune dysbalance and thereby aggravating previously suppressed disease manifestations [9].

1.1.4 HIV-patients not developing AIDS

Despite the fact that most HIV patients progress to AIDS if not treated with ART, there are several reports of individuals not developing a clinically relevant immunodeficiency. The most interesting ones are the group of elite controllers, which represent <1% of HIV-infected patients and which maintain low to undetectable levels of virus in the absence of treatment. Their protection seems to be associated with certain variants of the human leukocyte antigen (HLA) class I, indicating the importance of CD8 T cell and NK cell responses. In addition, the development of broadly neutralizing antibodies (bNAbs), which target a broad variety of HIV strains, as well as HIV-specific protective (cytolytic) CD4 T cell responses, were reported within this population. Other hypotheses include an initial transmission of viruses with low fitness or a low “virological set point” as reasons for this phenotype [1, 6]. Another interesting population in the context of HLA class I-association was found in a population in Africa, where in cases of vertically (mother-to-child) transmitted HIV infection a long-term survival of so far unknown reasons was observed [11]. Finally, an interesting group of patients was reported in the context of ART: Post-treatment controller are patients, in whom early HIV diagnosis and initiation of ART followed by long-term treatment resulted in an apparent control when therapy was discontinued. These patients do not show a CD8 T cell-mediated protection but are characterized by very low levels of proviral DNA, indicating a small reservoir, and low levels of immune activation [1].

1.1.5 HIV-1 structure and replication cycle

The human immunodeficiency virus 1 and 2 belong to the genus *Lentivirus*, which are part of the family of *Retroviridae*, bearing two copies of a positive single stranded RNA (+ssRNA) genome. The latter has a size of 9-10 kb (HIV-1: 9.2-9.6kb; HIV-2: 9.8kb) and consists of the *gag*, the *pol* as well as the *env* region, which are flanked by the 5’- and the 3’-LTR (long terminal repeat). Initiation and regulation of viral replication is mediated by the promoter region within the 5’-LTR. HIV-1 *gag* encodes for several structural proteins (capsid, matrix, nucleoprotein and p6), *pol* for enzymes involved in viral replication (protease, reverse transcriptase, RNase

H and integrase) and *env* for the particle's surface proteins involved in viral entry as well as fusion (gp120 and gp41). In addition, the genome of HIV encodes for two factors regulating replication – the HIV-derived transcription factor Tat (transactivator of transcription) and the splicing factor Rev (Regulator of expression of virion proteins). Finally, HIV encodes several accessory proteins: Vif (viral infectivity factor), Vpu (viral protein U) (HIV-1)/ Vpx (HIV-2) and Nef (negative regulatory factor). These proteins restrict the host defense and modulate the cellular metabolism to support HIV replication [12].

As an enveloped virus, HIV is covered by a lipid bilayer, which displays on its surface only few Env molecules (around 10 [13], between 4-35 Env molecules reported corresponding to an average of 7 Env trimers [14]), and at the inner side the matrix and p6 proteins. The two viral RNAs are bound by nucleoproteins as well as the reverse transcriptase, and are further protected by the cone-shaped capsid (consisting of hexamers/ pentamers of the capsid protein). In addition, this structure contains the viral integrase and accessory proteins (**Fig. 3**) [12, 15, 16].

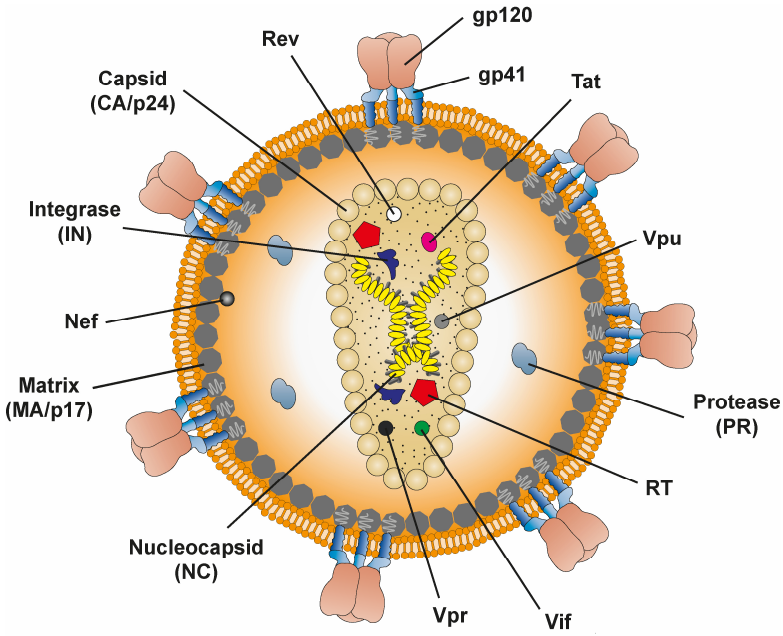

Figure 3: Schematic representation of the HIV-1 particle. Shown are the lipid bilayer carrying Env (gp41/gp120 trimer) spikes and matrix protein, forming the shell of the virion. Inside the HIV-1 particle, the capsid harboring the two viral RNA as well as the different indicated proteins can be found. Schematic modified from Chen et al. [17].

HIV attachment and fusion is mediated by interaction of the HIV Env trimer with cellular receptor, first CD4 (primary receptor) and then the chemokine receptors CCR5 or CXCR4 (co-receptors). After entering the cytoplasm, transport to the nucleus, reverse transcription (RT) and uncoating take place. It is so far under debate, if the latter occurs directly after release of the

capsid core into the cytoplasm (early uncoating) or if the RT reaction takes place within the capsid core and uncoating occurs briefly before nuclear import (late uncoating). In both cases, reverse transcription requires the formation of an RTC (reverse transcription complex), which involves the viral RNA, the RNaseH as well as the reverse transcriptase and leads to the production of a viral cDNA (complementary DNA). The cDNA forms together with the viral integrase the PIC (pre-integration complex), which is subsequently imported into the nucleus. After integration into the host genome, the provirus can serve as a template for transcription of viral RNAs by using the cellular RNA polymerase in combination with the Tat and Rev proteins as well as other cellular factors. After translation of viral proteins, Gag (group-specific antigen), Gag-Pol (Gag-polymerase polyprotein), regulatory and accessory proteins, they are subsequently shuttled, together with the viral RNAs, to the Env-decorated plasma membrane. Here, assembly and budding of immature particles take place, by hijacking of the cellular ESCRT (endosomal sorting complexes required for transport)-machinery. To infect new target cells a process called maturation has to take place, which requires cleavage of Gag and Gag-Pol proteins by the viral protease, resulting in viral particles of the described structure (**Fig. 4**) [1, 15, 16].

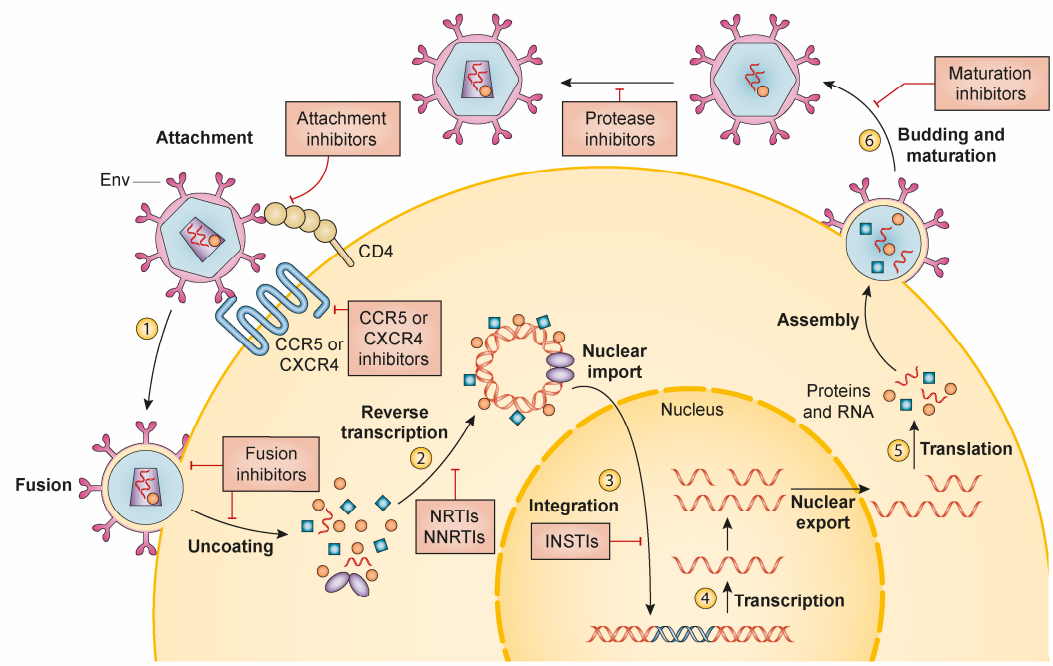

Figure 4: Replication cycle of HIV and potential therapeutic targets. Schematic showing the steps of the viral replication cycle and the different drugs used in ART (boxes): attachment and fusion (1), reverse transcription (2), integration of the viral cDNA after nuclear import (3), transcription of viral mRNA (4), translation of viral proteins in the cytoplasm (5) and finally budding as well as maturation of viral particles (6). Abbreviations, NRTIs: nucleoside reverse transcriptase inhibitor, NNRTIs: non-nucleoside reverse transcriptase inhibitor, INSTIs: integrase strand transfer inhibitor. Schematic modified from Deeks et al. [1].

During the replication cycle of HIV, several cellular restriction factors are induced for example by PRR (pattern recognition receptor)-mediated sensing. Here, receptors such as TLRs (Toll-like receptor), cGAS (cGAMP synthase), PQBP1 (polyglutamine-binding protein 1), IFI16 (gamma-interferon-inducible protein 16), and RIG-I (retinoic acid inducible gene I) cause an IFN (Interferon)-response [18]. The HIV accessory proteins counteract most of these so-called Interferon-stimulated genes (ISGs) [1]. For example, Vif inhibits APOBEC3 proteins (apolipoprotein B mRNA-editing catalytic polypeptide-like 3), which can cause G to A hyper-mutations in the viral genome during reverse transcription [19]. Vpu targets CD317 (BST-2 (bone marrow stromal antigen 2)/ tetherin), which represents a cellular factor that can retain budding particles at the cell surface [20]. Vpx encoded by HIV-2 and certain SIV strains, can induce proteasomal degradation of SAMHD1 (sterile alpha motif and histidine/aspartic domain containing protein 1), which is involved in the modulation of cellular dNTP pools and thereby indirectly also reverse transcription [21-24]. The Nef protein has several functions: it downregulates MHC (major histocompatibility complex) class I to avoid immune recognition, but also decreases cellular CD4 levels, likely contributing to the prevention of super-infection by other HI-viruses or infection of the same cell by budding virus particles. Recently, Nef-mediated inhibition of incorporation of SERINC (serine incorporator) proteins into virions was reported to counteract a loss of particle infectivity [25, 26]. SERINC 3 and 5 are supposed to change the flexibility of the viral membrane and the formation of the fusion pore, which interferes with virus entry [27].
Similar to cellular restriction factors, drugs used in antiretroviral therapy block different steps of the viral replication cycle. For example, inhibitors targeting attachment (maraviroc, CCR5), fusion (enfuvirtide/ T20), RT reaction (tenofovir, NRTI – nucleoside reverse transcriptase inhibitor; efavirenz, NNRTI – non-nucleoside reverse transcriptase inhibitor), integration (raltegravir) or the viral protease (atazanavir) (**Fig. 4**). In most cases, a combined ART (cART) is used, where Truvada® (NRTIs: tenofovir and emtricitabine) is used in combination with a drug of the other classes. More recently, for individuals that have a high risk to acquire HIV, a prophylactic treatment called PrEP (pre-exposure prophylaxis) has become available. In contrast to PEP (post-exposure prophylaxis) is given to individuals, who may have recently been exposed to HIV to either prevent infection of start ART extremely early to improve outcome [1, 9]. Nowadays, ART is in most cases well tolerated and highly efficient, as for example reported in PrEP studies examining transmission of HIV in gay couples [28-31].

1.1.6 Entry of HIV - a more detailed look

Both the composition of HIV Env and the processes occurring during viral entry will be important in the context of amyloid enhancers of infection and bNAbs. Therefore, a more detailed description will be given in the following paragraph. Entry of HIV into a target cell is mediated by the trimeric Env molecule on the virion surface, which is composed of heterodimers of gp41

and gp120. The gp120 subunit consists of five conserved regions (C1-5) and five variable loops (V1-V5) and is responsible for the receptor binding, whereas the gp41 subunit links the Env protein complex to the membrane by MPER (membrane-proximal external region) and contains the fusion peptide [32].

HIV entry includes the following steps: attachment to the target cell, fusion of viral and cellular membranes followed by the release of the capsid core into the cytoplasm. Initial binding to the target cell can occur in a rather unspecific manner through interaction of HIV Env with heparan sulfate proteoglycans (HSPG), α4β7 integrins (high expression on gut and mucosal CD4 T cells), or the pattern recognition receptor (PRR) DC-SIGN (dendritic cell-specific intercellular adhesion molecular 3-grabbing non-integrin). This brings Env in proximity to the cellular membrane and allows interaction of the CD4 binding site (CD4bs) within gp120 and the primary receptor for HIV, CD4. Next, conformational changes in the variable loops V1/V2 lead to a repositioning of V3, in parallel to the formation of a bridging sheet, which consists of two double-stranded β-sheets. Such rearrangements within gp120, allow the engagement and binding to one of the two co-receptors CCR5 or CXCR4, leading to the exposure of the hydrophobic fusion peptide within gp41. After insertion into the host cell membrane and formation of the six-helix bundle (6HB), the fusion pore forms because of close proximity of both membranes and the viral core is release into the cytoplasm of the target cell [32].

The requirement for specific receptors determines the cellular tropism, which is in most patients defined by the presence of CD4 and CCR5 on the surface of target cells. This complex is mainly found on activated CD4 T cells, monocytes, macrophages and DCs. The genome of HIV is highly variable, which has the biggest effect on the Env spike. Due to the high error rate of the reverse transcriptase, mutations occur constantly. Consequently, Env molecules of chronic HIV patients display long and heavily glycosylated variable loops allowing escape from immune recognition. In addition, the depletion of CCR5-positive target cells can drive the development of viruses, which use CXCR4 (X4-tropic) as a co-receptor. These occur in ~8% of patients [33]. Interestingly, a special mutation within the *ccr5* gene referred to as Δ32 (*ccr5Δ32*), which can be found with an allelic frequency of on average ~10% in the Caucasian population, is under homozygous conditions highly protective from HIV infection [1, 32]. Other studies report a north-south decline of the *ccr5Δ32 mutation*, with for example countries from northern Europe showing frequencies of up to 16% and countries from southern Europe of 4 to 6% allelic frequency [34].

1.1.7 HIV vaccination and bNAbs

Besides ART, generation of an efficient vaccine to cure and/or prevent HIV infections would be the ultimate goal in HIV research. The main epitopes used in the development of the different HIV vaccine trials are structures within the Env surface molecule, which is as described

above highly variable. Further variation comes from the fact, that the HIV Env is not static, with the gp120 subunits undergoing conformational changes also in the absence of CD4 or any co-receptor [1, 35, 36].

This makes the development of a potent vaccine difficult, which is reflected by so far only one at least partially successful field study - the “Thai trail” (RV144). This study was conducted in Thailand and used the so-called “prime-boost” strategy: participants were first primed with the Canarypox-vector ALVAC-HIV, followed by a boost using AIDSVAX (both vaccines contained antigens derived from HIV group M subtype A and E) [37, 38]. Analysis of the study revealed a partial protection (efficacy of 31.2%), the generation of neutralizing antibodies against the Env V1V2 region, as well as detection of polyfunctional memory CD4 T cells, targeting specific epitopes within the V2 region [37-40]. Although IgA antibodies are thought to lead to mucosal protection [41], and this at a first glance is important to protect from infection with a STD, the presence of monomeric Env-specific plasma IgA correlated with a risk of infection in RV144. This might have been due to the fact of pre-bound IgA, directly or indirectly inhibiting further IgG binding, which would otherwise be able to mediate ADCC (antibody-dependent cell-mediated cytotoxity) [37-40].

Although in the past adenovirus (AdV)-based HIV vaccine trials were not successful, the more recent study “APPROACH” used an AdV strain 26 (AdV26)-based strategy, which is believed to be more potent and safe than the previously used AdV5 vectors. In addition to applying a bivalent approach (antigens of HIV-1 subtype B and C), the usage of mosaic antigens was supposed to increase potency of the vaccine and elicit a broader immune response. As in the “RV144 trial” a “prime-boost” regimen was used, being the most successful in a scenario where priming and boosting was done using an AdV26-HIV-mosaic vector. On top, the boost was supplemented with adjuvanted gp140 (Ad26-Ad26 plus gp140). A special feature of this study was the parallel application to healthy individuals from the USA, east-/ south-Africa and Thailand as well as in the rhesus monkey model. The latter was used as a proof-of-concept study, in which repeated intrarectal SHIV challenge was performed following vaccination. Besides being well tolerated in both sub-studies, the vaccination strategy generated neutralizing antibodies against HIV, ADCP (antibody-dependent cellular phagocytosis) and HIV-specific T cell responses. However, although two thirds of the monkeys were protected from infection, neither in monkeys nor in humans, antibodies with broadly neutralizing activity could thus far be detected, longitudinal evaluations are ongoing [42-44].

Another strategy to prevent or treat HIV infection is the passive immunization using broadly neutralizing antibodies (bNAbs), which target a variety of HIV strains. Most HIV patients show autologous, strain-specific neutralizing antibody (NAbs) responses 3 to 12 month post infection, which can further develop to the broadly neutralizing phenotype, requiring somatic hypermutation causing affinity maturation. Here, extended HCDR3s (heavy-chain complementary-

determining regions 3) cause additional polyreactivity. Development of bNAbs occurs in ~20% of chronically infected individuals two to four years post infection, and is until now not inducible by vaccination [45-48].

Scientific progress has resulted in new isolation and screening methods, allowing establishment of plasma cell lines from HIV-infected patients, and these produce large amounts of highly potent anti-HIV antibodies, required for laboratory as well as clinical studies [49, 50]. Both NAbs and bNAbs usually can be separated into three groups according to their epitopes recognized: gp120 (V1/V2 loops, V3 loops and CD4bs), gp41/MPER as well as

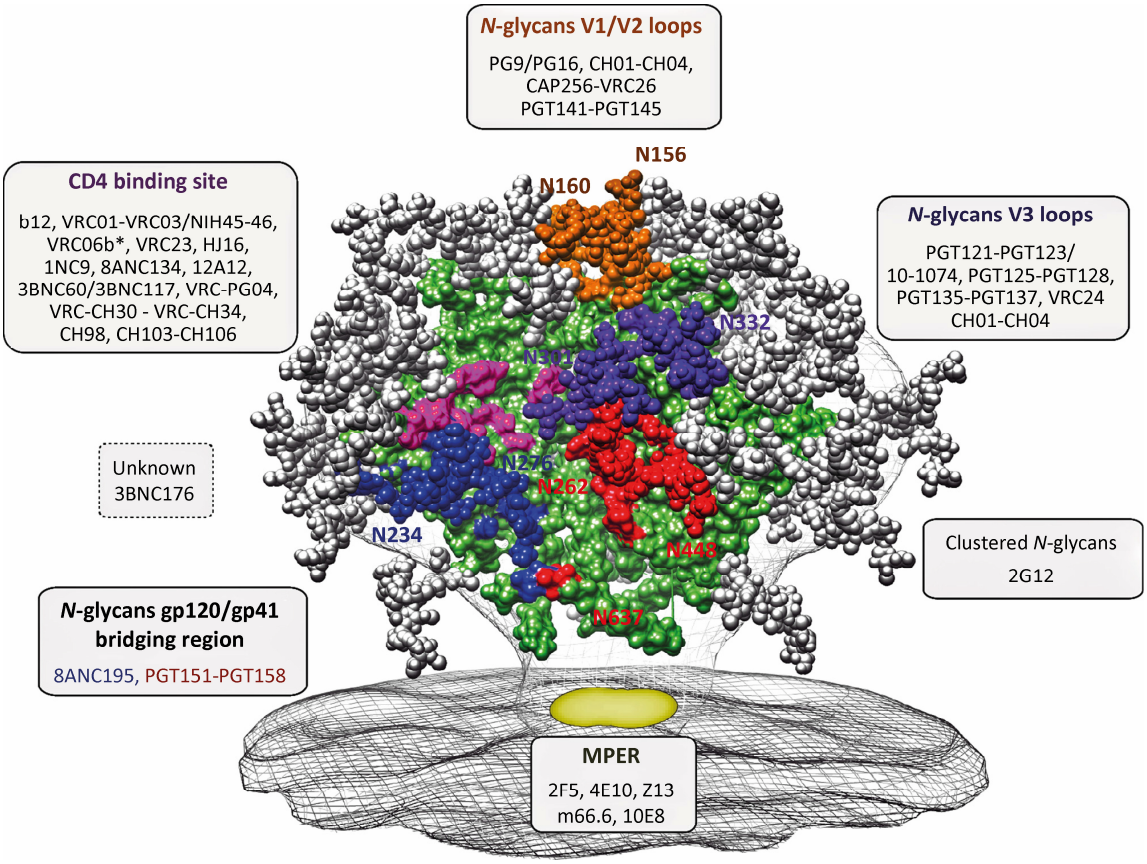

Figure 5: Schematic representation of an HIV Env spike and bNAb epitopes. Env structure and overview of the epitopes on Env as well as the corresponding bNAbs: gp120 (CD4 binding site, V1/V2 loops, V3 loops), gp41/ MPER and gp120/gp41 bridging. Image taken from Mouquet [51].

epitopes that span/bridge or are found at the interface of gp41/gp120, the latter so far being reported only for bNAbs (**Fig. 5**) [52, 53]. A described escape mechanism of HIV Env is the immune evasion through Env's glycan shield, which can surprisingly also be a target for bNAbs [45, 54]. In addition, antibodies against HIV are distinguished according to their neutralizing potency and while there are different ways of classification, in most cases the tiered-classification is used: starting from highly sensitive (tier-1 viruses) over more resistant, but genetically matched (tier-2 viruses) and ending with more resistant, genetically mismatched viruses (tier-

3 viruses) [55]. Moreover, there are also non-neutralizing antibodies, which show ADCC and ADCP [45]. Under lab conditions, the potency of bNAbs was assessed in cell culture, where infection with free viruses but also cell-to-cell spread could be inhibited [46, 55, 56]. *In vivo* studies in mice and primates indicated that infusions of bNAbs can mediate protection from virus transmission and thus represent a conceptional alternative to PrEP [47, 57-59]. In most cases, higher *in vivo* efficiency of antibodies was associated with a functional Fc-part, presumably also in association with ADCC/ ADCP, and modification of this antibody domain even increased the duration of protection [60]. Further, the use of antibodies targeting several epitopes on Env (e.g. “tri-mix”) enhanced the potency *in vitro* as well as *in vivo*, hindering viral escape [49, 61, 62]. Finally, studies in humans using single as well as combinations of different bNAbs were well tolerated and showed control of viral loads in patients where ART was discontinued [63-65].

1.2 Amyloids are potent enhancers of viral infection

1.2.1 Amyloids - an overview

Amyloid fibrils are elongated unbranched protein aggregates of 6 to 12 nm diameter, which are characterized by a β-sheet secondary structure, where β-strands are orientated upright to the fibril axis [66]. These amyloids are generated in a two-step nucleation polymerization process, requiring initially a partial un- or misfolding of a protein, forming an amyloid precursor. Interestingly, misfolded proteins can induce the unfolding of other proteins, thereby starting a chain reaction that creates several oligomers, which can range in size anywhere from dimers to large fibril-like aggregates (protofibril). Generation of a nucleus can either originate directly from amyloid precursors, or from protofibrils. This process represents the first step of amyloidogenesis, is rather slow and can under laboratory conditions be accelerated by agitation or seeding with already pre-formed aggregates. In a final step, conformational changes within the nucleus are required to form short amyloid fibrils, which can than elongate in a self-templated fashion (**Fig. 6**) [66-68].

The presence of biological membranes or hydrophobic surfaces can support the formation of amyloid fibrils. Extracellular accumulation of amyloid fibrils are a sign of amyloidosis, like Alzheimer’s disease, and intracellular aggregation of proteins is typical for Parkinson’s disease [68]. Prions, also termed infectious proteins, which can cause for example the bovine spongiform encephalopathy (BSE), are based on the principles of amyloidogenesis. To counteract the formation of amyloid fibrils, several attempts to control amyloid formation exist, for example stabilization of the native state or off-pathway oligomers, β-sheet breakers as wells as clearance by antibodies [66-68]. In addition, as found in many proteins of non-pathogenic origin and having an affinity to membranes as well as nucleic acids, the amyloid fold present

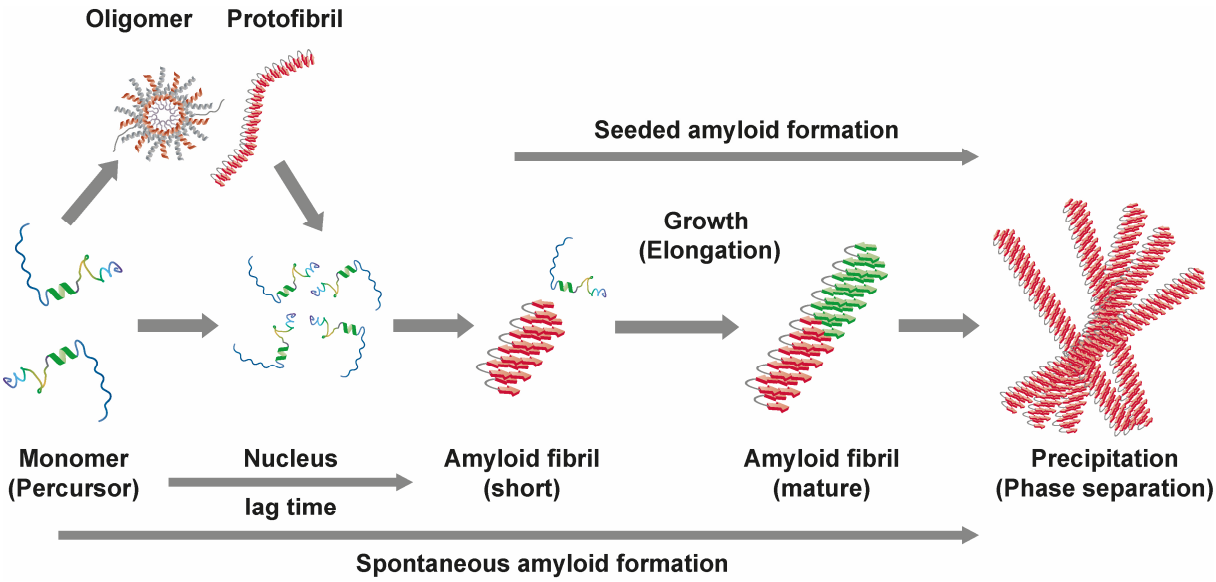

Figure 6: Schematic of amyloidogenesis. Refolding of peptides or proteins leads to formation of an amyloid precursor that can build oligomers/ protofibrils further creating a nucleus. The establishment of the latter creates a certain lag time and is required to generate short amyloid fibrils, which can afterwards elongate in a self-catalyzed fashion. Picture modified from Lee and Ramamoorthy et al. [67].

in many fibrils is “believed to represent a biological structure of early life” [69]. Interestingly, amyloids can also have a physiological function like the human defensin 6 (HD6), having anti-microbial function at mucosal surfaces and being able to form fibrillary nanonets, which can bind for example bacterial flagellae [70]. In contrast to being mostly pathogenic for eukaryotes, bacterial amyloids like the ones derived from Curli (found in enterobacteria, e.g. *E.coli* [71]), are part of the extracellular matrix and required for adhesion and biofilm formation. Since these aggregates are PAMPs (pathogen-associated molecular patterns), they can be recognized by the immune system in a TLR (toll-like receptor)-2-dependent fashion and as a consequence cause immune activation as well as clearance [72]. Taken together, this makes amyloids a very interesting field of research and the following chapters will give an overview on recently studied amyloids important in disease, but also as functional proteins within the body. Special attention will be given to amyloids already published to enhance viral infection and new potentially interesting candidates will be highlighted.

1.2.2 Semen-derived amyloids enhancing HIV and other viral infections

As described in chapter 1.1.2, HIV transmission by sexual intercourse is a process with relatively poor efficiency and neither the presence of lesions caused by STDs nor sexual practices can adequately explain the ongoing and fatal HIV pandemic. In the context of “semen being the main vector for HIV dissemination worldwide” [73], proteins present in the male ejaculate

as well as proteins present in the female genital tract or at anal mucosal surfaces might interfere with HIV infection in a supporting or inhibitory way. Hence, a group of scientists around Jan Münch and Frank Kirchhoff performed a huge screening approach to identify such proteins in pools of human seminal fluid derived from several donors. By using a fractionated testing approach, they found that certain cleavage products of the prostatic acidic phosphatase (PAP) were able to enhance HIV infection in a dose-dependent manner. The most potent and abundant enhancer was PAP 248-286, which was inactive when freshly prepared from synthesized peptides, but became active after overnight agitation. This finding, together with EM analysis, positive Thioflavin T staining (dye that intercalates into amyloid fibrils) as wells as several other methods, identified this peptide to form amyloid fibrils. The latter were able to enhance HIV infection as previously published for classical amyloids, like for example β-amyloid, and were termed Semen-derived enhancer of virus infection (SEVI) [74, 75]. More detailed analysis of the interplay between HIV particles, target cells and the peptide revealed that the fibrils of SEVI are cationic, and likely bind due to their positive charge efficiently to negatively charged cell as well as virion surfaces. Together with the local formation of helical structures, these amyloids increase attachment and fusion of HIV to its target cells, in a HIV Env-independent manner. Reflecting the most likely *in vivo* scenario of low viral loads being transmitted, infection enhancement potency was highest at low MOIs of HIV. In addition, infection enhancement was possible at different physiological pH, within *ex vivo* culture models and also in *in vivo* systems, where HIV together with SEVI was injected intravenously into hCD4/hCCR5 transgenic rats [67, 74, 76, 77]. The latter approach being interesting as a proof-of-concept, but not predictive for a mucosal route of HIV transmission, more physiologically relevant approaches were chosen. However, neither intra-vaginal challenge of rhesus macaques with SIV nor rectal challenge of humanized mice with HIV exhibited enhancing effects, possibly related to the importance of the protective mucosal barrier. The latter has to be disrupted in its integrity by mechanical, chemical or biological means to allow SEVI-dependent effects, being the main problem in finding an adequate *in vivo* model (**Fig. 7**) [78, 79].

In addition, these initial studies already suggested the presence of factors other than SEVI present in semen to play a role in enhancing HIV infection [80]. This was supported by studies monitoring presence of amyloids already in seminal vesicles, where PAP is absent [81]. Further analysis of semen by mass spectrometry revealed that cleavage products of semenogelin 1 (SEM1) and SEM2, which are responsible for the viscous gel-like structure of the male coagulum, could form amyloid fibrils [80]. This happens during a process called liquefaction, which transforms the ejaculate to a more fluid-like consistency, what is mainly due to prostate-specific antigen (PSA)-mediated proteolytic cleavage of SEM1/2. Also, PAP plays a role in degradation of semenogelins. Studies analyzing the temporal dynamics of this process showed that this process is fast and leads to the production of SEM(86-107) peptides at early

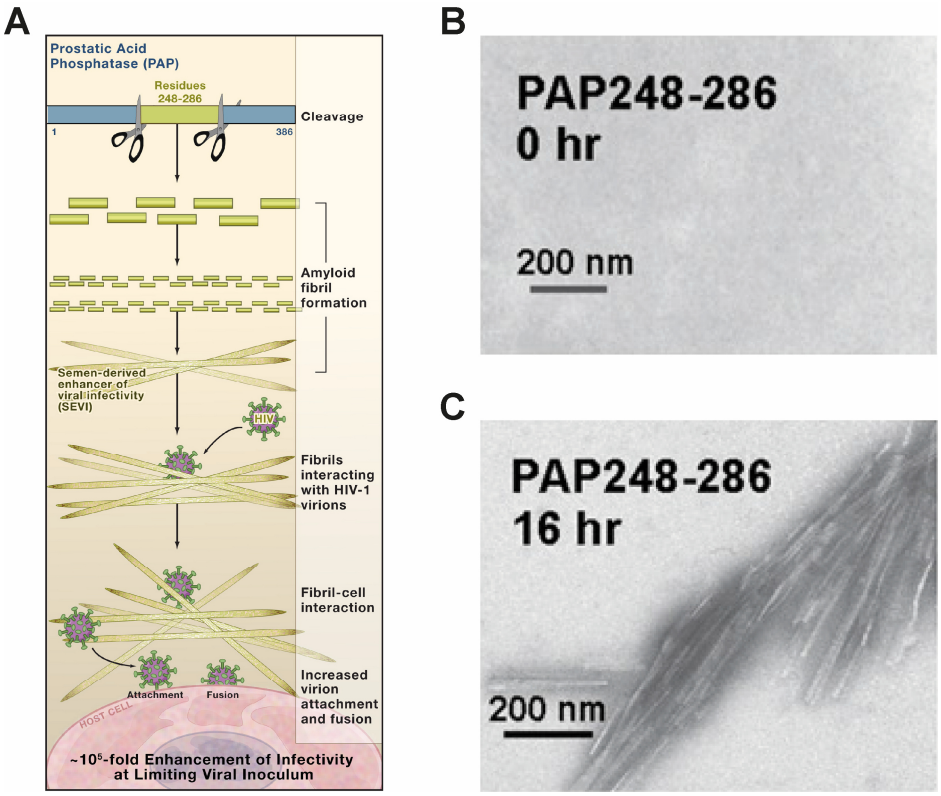

Figure 7: SEVI enhances HIV infection. (**A**) Schematic model of generation of SEVI (PAP248-286) from PAP and interaction of HIV with SEVI. This leads to increased virion fusion and subsequently enhanced infection. EM analysis of SEVI pre (**B**) and post agitation (**C**). Schematic from Roan and Greene, 2007 [82] (**A**) and EM images from Münch et al. [74] (**B+C**).

time points after ejaculation, which are the essential SEM peptide for amyloid fibril formation and in turn enhancement of HIV infection. Afterwards, this peptide is further degraded leading to a loss of the peptide and related infection enhancement after around 24h. In addition, kinetic analysis demonstrated a window of ~8 h post ejaculation for efficient HIV infection enhancement [83]. In contrast, other studies revealed that fragments derived from degradation of SEM and resulting cationic polypeptides can also have anti-HIV activity and block infection enhancement [84].

SEM1 amyloids as well as SEVI act synergistically with the extracellular matrix protein fibronectin. The latter, able to bind amyloid folds (also of the bacterial protein Curli), is known to inhibit HIV infection by blocking the gp120-CD4 interaction, but in this particular context was shown to boost SEVI- or SEM-dependent effects, possibly by facilitating interaction with HSPG on target cells [85]. Both SEVI and SEM amyloids have been demonstrated in the past to enhance sexually transmitted viruses other than HIV, including HSV (herpes simplex virus), CMV (cytomegalovirus) or Ebola [86-88]. Although, semen and the containing amyloids were shown to enhance infection of several viruses, infection with Zika virus seems to be inhibited in the presence of extracellular vesicles, of so far unknown nature, within ejaculates [89].

Unexpectedly, semen from HIV-infected men showed strongly reduced enhancing potential, apparently due to the presence of RANTES (CCL5), which can block infection with R5-tropic HI-viruses. Those semen samples contained also several proinflammatory cytokines (IL-1β, TNFα), indicating that HIV infection shapes a certain cytokine milieu in genital fluids that can affect transmission [90]. Semen also causes a proinflammatory response within the genital mucosa, leading to influx of immune cells and promoting conception as well as pregnancy, but also attracting HIV target cells. This is in part due to the presence of several proinflammatory cytokines in seminal plasma (also in healthy patients) that stimulate immune cells as well as epithelial cells within the female reproductive tract (FRT). As described by Münch et al. [74], seminal plasma can harm HIV target cells, e.g. through reactive oxygen species, which are toxic to cells and thereby exhibit antiviral activity. In addition, seminal plasma is able to down-regulate CD4 and CXCR4 expression on CD4 T cells, however, causing an upregulation of CCR5. Thus, semen tightly co-regulates proliferation and apoptosis of immune and epithelial cells. This is important for reproduction, yet sometimes beneficial or unfavorable to establish HIV infection [91-93].

After the finding that semen contains several amyloids and that even an evolutionary selection pressure on SEM proteins has been reported [94, 95], it was of course of interest, if these amyloids have a biological function, which explains their presence. Being only part of a degradation pathway hijacked by viruses seems unlikely given that there are several “functional amyloids” known to play important roles during reproduction. Characterized by a fast transition from monomer to mature amyloids, “functional amyloids” exhibit important roles for example during gametogenesis, germline specification, the acrosome reaction and maturation of the sperm as well as the structure of the zona pellucida of the egg [69]. Functional analysis of semen-derived amyloids revealed that especially SEVI and SEM amyloids, but not β-amyloid were able to entrap and immobilize sperm within semen, thereby enhancing phagocytosis by macrophages. The latter are responsible for clearance of spermatozoa from the FRT and seem to preferentially deplete damaged sperm, which can be further enhanced by the presence of semen amyloids (fibrils also target preferentially damaged spermatozoa). Due to dynamics of for example SEM amyloid levels in semen this amyloid-dependent sorting function of macrophages takes place early after ejaculation. Another interesting finding was that increasing concentrations of semen amyloids inhibited *in vitro* fertilization. Thus, semen amyloids together with macrophages seem to play an important role in the quality control of spermatozoa during reproduction [96].

Several attempts have been undertaken to inhibit formation of amyloid fibrils within the reproductive tract. For example, SEVI-mediated infection enhancement can be blocked by addition of anionic polymers, the aminoquinoline surfen or gallic acid, which inhibit the interaction between virus particles and the amyloid [67, 76, 97, 98]. Other ways to block the effect of semen

amyloids, are the inhibition of amyloid formation or the destruction of amyloid fibrils: the former can be achieved by for example non-natural amino acid (aa) inhibitors (computational design according to aa sequence of the amyloid) or D-amino acid peptide D3, known to treat Alzheimer's disease. Substances such as epigallocatechin-3-gallate - a component of green tea, can accomplish destruction and remodeling of amyloid fibrils [67, 99, 100]. All of these treatments seem to be promising, but have to be revised taking into account the findings described on non-pathological functions of semen/genital amyloids important during reproduction and clearance of bacteria from genital tract [96].

1.2.3 Human Papillomaviruses (HPV)

1.2.3.1 HPV facts

The family of *Papillomaviridiae* covers several genera, which can be found in humans, but also other mammals and birds [101]. In humans there are more than 207 different HPV types classified, most of which are represented by the sexually transmitted mucosa-related *alpha-papillomaviruses*, followed by the less abundant *beta-* and *gamma-papillomaviruses*, which have a cutaneous association [102, 103]. Human papillomaviruses are non-enveloped, icosahedral viruses that harbor a circular (episomal) double stranded (ds) DNA. The capsid is formed by pentameric capsomers (major capsid protein L1), which are connected inside of the particle by the minor capsid protein L2 (5:1 ratio L1 to L2), protecting the genome of 8 kb size encoding for the seven early genes (E1, E2, E4, E5, E6, E7, E8) and the two late genes (L1 and L2). In addition, the LCR (long control region) contains regulatory sequences for viral transcription and replication [103-105].

HPV is mainly transmitted through direct contact, and "HPV16 is the most prevalent sexually transmitted viral infection worldwide" [106], indicating the importance of HPV as an STD. As shown by Harald zur Hausen (awarded with the Nobel prize in 2008), and in context of many historical observations linking sexual intercourse, a persistent HPV infection and development of cervical cancer, HPV was identified as one of the main causes of cervical cancer (reviewed by zur Hausen [107]). This lead to further subdivision of *alpha-papillomaviruses* into genotypes that cause cancer and hence were termed "high-risk" HPV types (HR-HPV: 16, 18, 31, 33, 35, 39, 45, 51, 52, 56, 58, 68, 82). In contrast, genotypes causing anogenital warts or benign neoplasia, were called "low-risk" types (LR-HPV) [103]. Around 55% of cervical cancers can be attributed to HR-HPV HPV16, an additional 15% to HR-HPV HPV18 [108]. Development of cancer due to HPV infection is a rare event, since most of the frequently occurring transient HPV infections in the human body, but also CIN1 (cervical intraepithelial neoplasia) or LSIL (low-grade squamous intraepithelial lesion) pathologies, regress [109]. In rare cases, HPV infection can cause lesions of grade CIN2/3 or HSIL (high-grade SIL). Even these pre-cancerous stages regress in about 60% of cases [109], but can progress to cancer, if for example a failure

of clearance by the immune system takes place. Also, the vaginal microbiome of a suppressed immune system, like for example in HIV patients, can shift the balance towards cancer development [103].

HR-HPV can cause cancer in tissues other than cervix, including anus, penis, vagina or vulva, but also in the oropharyngeal tract, which is mainly due to sexual practices. *Beta-papillomaviruses* are present in the skin causing for example warts (hands) or verrucae (feet) and can cause cancer in immunocompromised patients [103]. In addition, *beta-* and *gamma-papillomaviruses* were reported to be present in the oral cavity [102]. Unrelated to a specific HPV type, recurrent respiratory papillomatosis (RRP) is causally linked to HPV infections [103, 110, 111].

To reduce the number of HPV-induced (cervix) carcinomas and warts several vaccines have been developed. In the past, a bivalent vaccine was used targeting HPV16/18 (Cervarix®), which was later on replaced by a quadrivalent vaccine, additionally targeting the LR-HPVs HPV6/11 (Gardasil®). Presently, the vaccine Gardasil®9 is used (https://www.msd. de/fileadmin/files/fachinformationen/gardasil_9.pdf), which targets several LR- and HR-HPV types (HPV6/11/16/18/31/33/45/52/58). All of these vaccines are based on HPV L1-based virus like particles (VLPs), which are obtained by overexpression of L1 proteins that in turn self-assemble into VLPs. Ongoing research tries to further increase the cross-reactivity of antibody responses elicited by vaccination. Thus, one approach is to create L1-fusion proteins that display highly immunogenic fragments of the minor capsid protein L2 on the surface of the VLPs, which causes broader immune responses. Finally, other epitopes, like the viral oncogenes E6/7 are in the focus as targets for therapeutic vaccines [103, 112-114].

1.2.3.2 HPV replication cycle

HPV enters the mucosa or skin mainly through lesions that allow access to the basal cell layer or by infection of the cells at the transition zone from ecto- to endocervix at the squamous cellular junction (**Fig. 8**). Here, the HPV major capsid protein L1 is thought to interact with HSPG on the cell surface, causing exposure of the *N-terminus* and cleavage of the minor capsid protein L2. This allows further binding to one of several secondary receptors like for example epidermal growth factor receptor (EGFR), integrins or laminins, which is followed by a micropinocytosis-like entry into the target cell [103, 104, 115].

Transport of the viral DNA occurs in a Golgi- as wells as tubulin-dependent fashion and entry into the nucleus happens through nuclear pores or collapse of the nuclear membrane during mitosis. Inside of the nucleus, the viral DNA co-localizes with PML (promyelocytic leukemia) bodies and the first phase of viral DNA replication takes place. After production of the viral transcription factors E1 and E2, which form heterodimers and bind to the early promoter within the LCR, low-level expression of HPV E6 and E7 proteins is induced. These two factors act cooperatively, tightly regulating cellular survival and viral genome maintenance by interaction

with several cellular factors. Of note, the integration of the DNA encoding for these two genes is the hallmark of progression from HPV-induced neoplasia to cancer. In parallel, E1/E2 induce the amplification of the episomal genomic DNA. Subsequently, resulting products are linked to host chromatin in an E2-dependent fashion can be passed to daughter cells. Another function of E2 is the suppression of expression of high amounts of viral proteins in the basal cell layer to avoid activation of the host immune defense. HPV DNA is present in differentiating keratinocytes (mid layers of the epithelium), and persistence of viral infection is mediated by E6/E7 (inhibition of apoptosis/ immune recognition and control of cell signaling/RNA

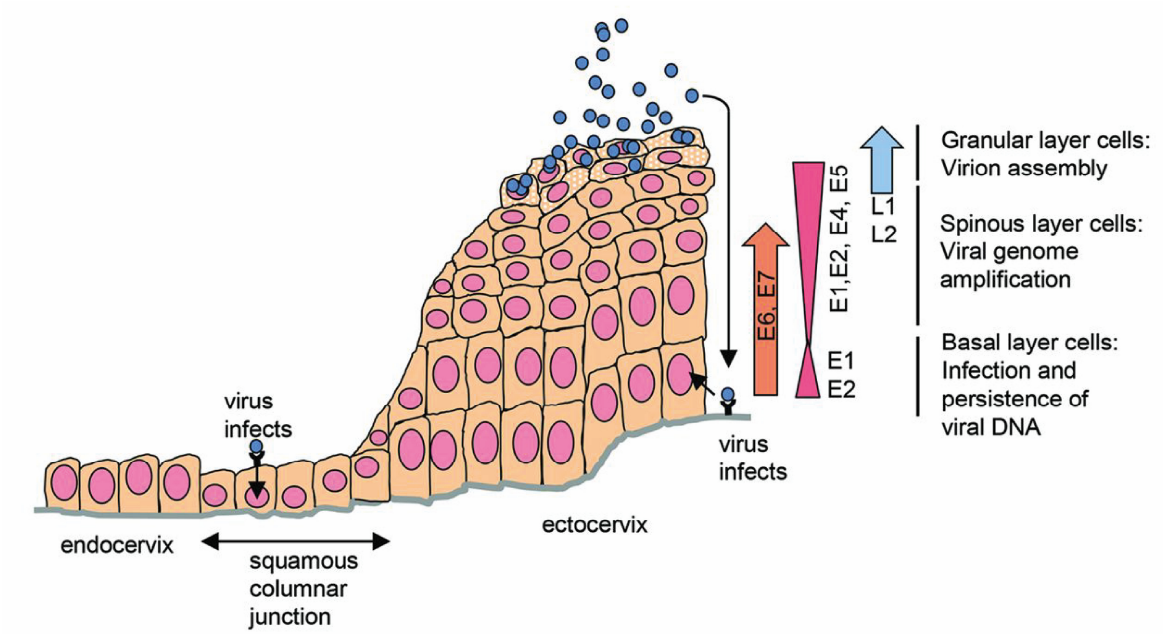

Figure 8: Entry and replication of HPV within the cervical mucosa. Shown are the different ways of entry as well as the expression levels of different HPV proteins during the differentiation of the keratinocytes. Also, the layer-specific steps of the viral replication cycle are indicated. Schematic taken from Graham [103].

polymerase II) (**Fig. 8**). In the late, vegetative phase of viral DNA replication HPV E1, E2, E4 and E5 have important functions in regulating viral gene expression as well as replication (rolling circle), DNA repair or cell division. Expression of the highly immunogenic capsid proteins L1 as well as L2 is suppressed until the upper layers of the epithelium to avoid recognition by the immune system and assembly of the capsid takes place in the nucleus (pre-assembly of pentameric L1 capsomers in the cytoplasm). Packaging of the viral DNA into the capsid is mediated by the L2 protein. As a final step of keratinocyte differentiation, a process called desquamation takes place, in which the cell looses the nucleus and dead cells are shed from the surface of the mucosa. This mode of cell death is used by HPV for the egress of viral

particles. Thus, papillomaviruses have perfectly adopted their replication cycle to the differentiation of the mucosal keratinocytes (**Fig. 8**) [103, 116, 117]. Interestingly, there are some reports that HPV may also be able to spread through aerosols between patients and that after infection is established also leukocytes can become infected, allowing spread of HPV through the blood stream [118].

1.2.3.3 HPV and HIV

There are several STDs, whose manifestations can lead to a reduction of the barrier function of the anogenital mucosa. In addition, a pre-existing HIV infection usually leads to a weakening of the host immune defense, which in turn allows survival of incoming pathogens. Putting this in the context of papillomavirus infection, HIV-induced immune suppression can support the development of HPV-induced cancer due to reduced clearance of HPV-infected cells [1, 9, 10, 119]. In contrast, it was also reported in epidemiological studies that for example an ongoing HSV-2 infection and the linked reduction of mucosal integrity can facilitate transmission of HIV [120]. Similar studies performed for papillomaviruses, most of them corrected for other STDs, showed that individuals especially infected with HR-HPV types exhibited an on average 3.3-fold (1.7- to 4.9-fold) increased risk to become infected with HIV [121-128]. Another finding was that the risk was dramatically increased, the more different HPV types were present within the anogenital tract [129]. This increase might have several reasons: besides the mucosal lesion, causing breakdown of the protective physical barrier, immune activation due to infection leads to influx of immune cells such as CD4 T cells, which are targets for HIV. Also, HIV infection can benefit from the pre-existing immune suppression associated with HPV infection [103, 130]. Finally, it was reported that HPV16 E7 can downregulate the expression of epithelial adhesion molecule E-cadherin inflicting an additional disturbance of the mucosal integrity [131].

1.2.3.4 The HPV E4 protein

In the context of amyloid-mediated enhancement of HIV infection [74-76, 80, 83], the HPV E4 protein may be of particular interest, since it is expressed at the anogenital mucosa and has the reported property to form amyloid fibrils [132, 133]. This protein is translated from an in frame splice RNA of exon one and four (E1^E4), of which the former contributes the five amino acids at the *N-terminus*. Although initially grouped to the early genes of HPV (lies within the early cassette of genes), its function is required for the late phases of the viral replication cycle. Comparison of E4 proteins from different HPV types reveals that while the amino acid sequence is largely different, it still shares structural similarities between the different types. In this way, the protein can be divided into *N-terminus* (helix), *loop* and *C-terminus* (β–sheet), of

which the latter can be further subdivided into *β-strand*, *multimerization* and *β-aggregation* domains [132, 134].

The E4 protein is expressed in the middle to upper layers of the epithelium (**Fig. 8**), stored in inclusion granulae with nuclear or cytoskeletal association [135], and can make up to 20 to 30% of the total protein content [132]. E4 has several important roles including stabilization of the E2 transcription factor, thus regulating HPV transcription [136]. In addition, E4 expression is able to arrest cells in the G2-phase of the cell cycle, which counteracts the E7-mediated G1- to S-phase transition [137, 138]. Also, processing of viral mRNA is thought to be co-regulated by E4 [139, 140]. The most important function thus far attributed to E4 is the rearrangement of the cytokeratin skeleton, which is believed to support virus egress [132, 135].

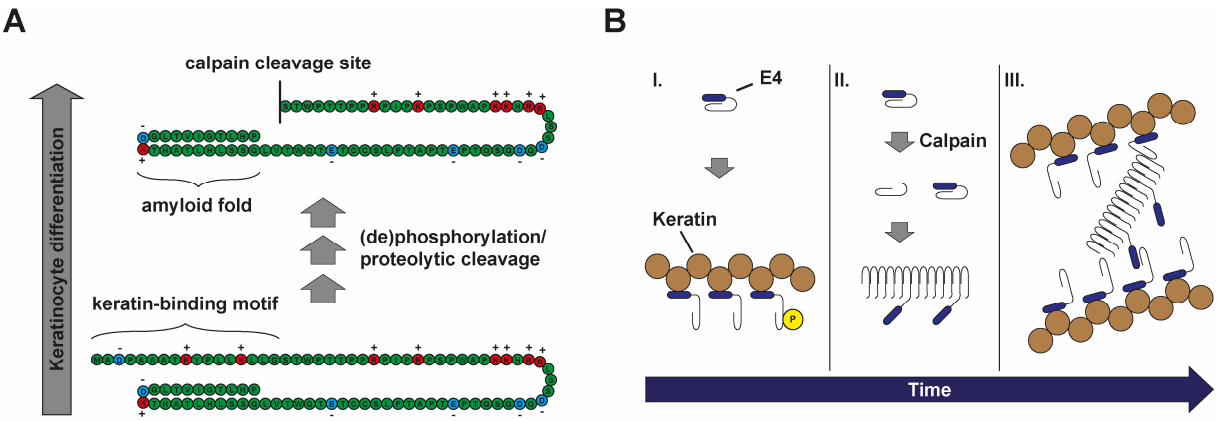

Figure 9: HPV E4 protein processing and mode of action. HPV E4 is expressed in middle to upper layers of the epithelium and is processed by several kinases and proteases. In the lower layers, E4 is mainly bound to cytokeratin, whereas in upper layers unbound E4 is cleaved by calpain, allowing multimerization (**A**). Schematic overview of (I) initial binding to keratin filaments, (II) multimerization of full length and *N-terminally* truncated E4 and (III) reorganization of cytoskeleton by crosslinking of keratin filaments (**B**). Schematics modified from Doorbar [132] (**A**) and Khan et al. [141] (**B**).

During the differentiation of keratinocytes a full-length E4 protein is expressed, which is present in the cytoplasm and further modified by phosphorylation and proteolytic removal of the *N-terminus* and the *C-terminus*. The full-length protein is rather short-lived and prone to bind to cytokeratin due to the presence of the *N-terminal* keratin-binding motif. Calpain cleavage in the upper layer of the epithelium causes removal of this domain (e.g. HPV16 ΔN1-17 E4), which shields the *C-terminus* (**Fig. 9A**). Next, multimerization can take place in a *C-terminus*-dependent fashion and stable amyloid fibrils are formed. Initially, full length E4 is bound to cytokeratin, thus preventing calpain cleavage, but accumulation of E4 in the cytoplasm of infected cells leads to E4, which is not bound to cytokeratin. These proteins can be *N-terminally* cleaved, hence allowing generation of E4 peptides that can lead to multimerization/ formation

of amyloids, composed of full length and truncated E4 peptides. In a next step, these aggregates can bind to cytokeratin and inhibit rearrangement of filaments due to crosslinking (**Fig. 9B**) [103, 132-135, 141].

1.2.4 Other amyloids and related pathogenesis

Beside amyloids derived from semen or papillomaviruses, also other classical amyloids like the brain-derived β-amyloids or α-synuclein, as well as the pancreatic islet amyloid polypeptide will be investigated in this study to gain a broader overview of the potency of amyloids potentially enhancing viral infection. The following paragraphs will give an overview about these candidates and related diseases (**Table 1**).

Alzheimer's disease (AD) is the most common neurodegenerative disorder and one of the main causes of dementia in patients older than 65 years. There are two main neuropathological characteristics for Alzheimer's disease (AD), the formation of extracellular plaques composed of β-amyloid (Aβ) and the microtubule binding protein tau in neurofibrillary tangles. Although Aβ and the precursor APP are present in healthy individuals, Aβ was shown to be involved in synaptic dysfunction, loss of neuronal connectivity and neuronal death. Imprecise processing of APP generates Aβ peptides of different length (e.g. Aβ40 consisting of 40 amino acids), which can aggregate and form plaques. The latter can be degraded by proteolytic cleavage, followed by clearance by macrophages or microglia. Nevertheless, a large amount of Aβ remains undegraded, but bi-directional transport of the peptide across the blood-brain-barrier can lead to further regulation of Aβ pools [142-144].

Another cause of dementia is Parkinson's disease (PD) and the related α-synuclein. Being the second common neurodegenerative disease leading to movement disorder, outbreak starts usually at the same age as AD and exhibits additional symptoms like bradykinesia, rigidity or resting tremor. There are several isoforms of α-synuclein produced by alternative splicing, of which the shorter proteins seem to be prone for aggregation. Formation of filaments in cytoplasmic inclusions can build so-called Lewy bodies, causing degeneration of subcortical structures especially dopaminergic neurons. In addition, posttranslational modifications like phosphorylation can lead to conformational changes of the protein, further supporting aggregation and formation of cytoplasmic inclusions [143, 145].

Diabetes mellitus (DM) is characterized by hyperglycemia, which causes damage to several organs, and is represented by either type 1 or type 2. Type 1 DM is caused by the lack of insulin, usually starts at the juvenile age and has an autoimmune background, which causes the destruction of the insulin-producing β-cells. In contrast, the onset of type 2 DM is typical for older people, developing an obesity-related insulin resistance. This is caused by a reduced sensitivity of insulin receptors in the periphery [146, 147]. Islet amyloid polypeptide (IAPP) aggregates have been reported to be associated with type 2 and possibly also type 1 DM.

IAPP is stored together with insulin (ratio 50:1-2) in secretory granules within pancreatic β-cells. Both insulin and IAPP are able to form insoluble amyloid fibrils, the β-chain of insulin being able to block the aggregation of IAPP. Amyloid fibrils derived from secreted IAPP can induce apoptosis of β-cells by for example blocking of autophagy, inflammasome activation or destruction of membrane integrity because of growing fibrils. In addition, inefficient processing of proIAPP can lead to ER stress, and thus also to apoptosis [148, 149]. Interestingly, epidemiological studies revealed an increased risk for patients suffering from DM in developing dementia and especially Alzheimer's disease. Of note, IAPP is able to cross the blood-brain-barrier and in *in vitro*-experiments, IAPP was able to seed the amyloid formation of β-amyloid [147, 148, 150].

Table 1: Overview of different other amyloids tested. Shown are different amyloids tested within this thesis, giving an overview on the related diseases and genes, whose mutation is related with disease. In addition, information on the life cycle of the different amyloids as well as their physiological function in healthy individuals are listed. Abbreviations: APP (amyloid progenitor protein), IAPP = islet amyloid polypeptide, IDE = insulin degrading enzyme, HSPG = heparan sulfate proteoglycan, PSEN1/2 = presenilin 1/2 (part of the catalytic subunit of γ-secretases). Table represents a summary of the following literature: Masters et al. [144], Murphy and LeVine [142], Goedert [143], Atik et al. [145], Ninomiya [147], Akter et al. [148], Westermark et al. [149], Ge et al. [150].

Disease	**Alzheimer's disease**		**Parkinson's disease**	**Diabetes mellitus**
Amyloid	**Aβ40**	**Aβ42**	**α-synuclein**	**IAPP**
Precursor	APP			preproIAPP → proIAPP
Related genes	APP, PSEN1/2		SCNA	
Processing	β- and γ-secretases			in Golgi apparatus
Tissue/ organ	brain		brain/ CSF/ plasma	pancreas
Localization	extracellular plaques/ vascular inclusion		cytoplasmic inclusions (Lewy bodies)	secretory granules in β-cells/ blood
Degradation	IDE (insulin can inhibit), neprilysin			IDE
Physiological function	synaptic function		• found in pre-synaptic nerve terminal • neurotransmission	• hormone • regulation of metabolism • glucose homeostasis • gastric emptying • regulation of satiety
Other	• abundancy: 80 to 90%	• abundancy: ~5 to 10% • hydrophobic, highly fibrillogenic	• binds to lipids (C-terminus) • aggregation is mediated by N-terminus • membrane-associated and cytoplasmic • membrane binding inhibits aggregation	• hydrophobic, positively charged • seeded after binding to anionic membranes/ HSPG
	• amyloid formation is nucleated by extracellular matrix/ on cell surfaces • large plaques serve as a reservoir for oligomeric forms			

1.3 Other viruses of neurotropic and respiratory origin

To characterize the potency of the different amyloid enhancers used in this study and to test for potential virus-specific differences, a panel of DNA and RNA viruses was chosen. Since many of the previously examined amyloid enhancers were of neurological origin, several viruses attacking the nervous system were picked also here. Additionally, also a family of non-enveloped virus was included to test the role of structural requirements necessary for infection enhancement. Below, a short overview of the structure, replication cycle, associated diseases as well as the use in research or the clinics, of members of this virus panel will be given.

Herpes simplex virus 1 (HSV-1) (**Table 2, Fig. 10A**) is known as a pathogen in the context of the oral mucosa and the eyes, where infection can lead to severe disease up to blindness. 90% of the adult human population is infected with HSV-1, which is far higher than the prevalence for HSV-2 (around 25%), which infects mainly the genital tract (Herpes genitalis). Transmission of HSV-1 occurs by direct contact with a virus-induced lesion or contaminated objects, leading to infection of epithelial cells or keratinocytes. Afterwards, latent infection of the peripheral nervous system (PNS) is established, where HSV spreads from a portal of entry in a retrograde fashion. Certain triggers, as for example stress or UV light can lead to recurrent reactivations, which initiate anterograde spread and hence formation of Herpes liabilis (cold sores). In rare cases, retrograde or antero-/retrograde spread can cause an infection of the central nervous system (CNS), resulting in an encephalitis. In addition, HSV has been reported to enhance susceptibility to co-infections such as HIV [151].

Rabies virus (RABV) (**Table 2, Fig. 10D**) has several hosts including human, bats, dogs, and foxes. The annual infection by RABV leads to around 55,000 deaths per year, due to lack of systematic vaccination in developing countries and high prevalence in particular in dogs [152]. Symptoms of rabies infection are initially fever, pruritus as well as paraesthesia and can later be divided in two subgroups - the furious and the paralytic rabies. The latter is characterized by drowsiness, whereas the furious outcome of RABV infection shows hyperactivity, confusion as well as agitation [153]. Rabid animals usually bite humans, thereby injecting virus particles into the muscle tissue, followed by entry of RABV into the PNS and retrograde spread. The variety of viruses studied comprises primary isolates, which are often referred to as “street viruses”, lab-adapted viruses and attenuated vaccination strains. Often, there are considerable discrepancies between viruses of these three origins, including cytotoxicity or neurotropism, making it essential to cover different isolates in study approaches [152].

Measles virus (MeV) (**Table 2, Fig. 10C**) is an exclusively human pathogen that arose from a zoonotic transmission. Before the introduction of a measles vaccine, MeV caused more than 2 million death per year. Symptoms of an ongoing MeV infection are skin rash, fever, cough, coryza, conjunctivitis and so-called Koplik spots. Due to a good vaccination coverage (usually

during childhood) and survivors of wild type infections, a strong herd immunity within the human population has been reached in many countries [154]. MeV is a highly contagious virus and is transmitted in chains between patients, mainly in an airborne fashion, but also by direct infection through contaminated objects. Within the host, this virus can infect several cell types of the immune system (macrophages, DCs, T and B cells), epithelial cells of the respiratory tract and neurons, the latter causing in rare cases measles' encephalitis [154, 155]. A key feature of acute MeV infection is a transient lymphopenia, which resolves soon after the clearance of infection. Nevertheless, a persistent impairment of the immune system that can last for several years, with an increased risk to secondary infections, can in some patients be created. This severe immunosuppression ("immune amnesia") in combination with a lifelong immunity against MeV is called "measles paradox" [154].

Table 2: Overview of DNA and RNA viruses tested. Shown is a comparative overview of the taxonomy, the particle properties, the tissue tropism and the replication cycle of the different viruses. Abbreviations: "-" = negative-stranded, CAR = coxsackievirus and adenovirus receptor, CD = cluster of differentiation, ds = double stranded), F = fusion protein, g or G = glycoprotein, H = hemagglutinin protein, HVEM = herpesvirus entry mediator (tumor necrosis factor receptor superfamily member 14 (TNFRSF14)), IR = inverted repeats, IGR = intergenic region, ITR = inverted terminal repeats, kb = kilobase pairs, L = RdRp (large RNA-dependent RNA polymerase), LATs = latency-associated transcripts, M = matrixprotein, N = nucleoprotein, nAChR = nicotinic acetylcholine receptor, NCAM = neural cell adhesion molecule, P = phosphoprotein, p75NTR = p75 neurotrophin receptor, Pol = polymerase, R = receptor, SLAM = signaling lymphocytic activation molecule, ss = single stranded, (p)TP = (precursor) terminal protein. Table represents a summary of the following literature: Kukhanova et al. [156], Kollias et al. [151], Su et al. [157]. Weller et al. [158], Albertini et al. [159], Ghanem and Conzelmann [152], Rota et al. [154], Bhattacharjee et al. [160], Delpeut et al. [155], Goncalves and de Vries [161], Ison and Hayden [162].

		Virus			
		Herpes simplex virus 1	**Adenovirus**	**Measles virus**	**Rabies virus**
Order		*Herpesvirales*		*Mononegavirales*	*Mononegavirales*
Family		*Herpesviridae*	*Adenoviridae*	*Paramyxoviridae*	*Rhabdoviridae*
Subfamily		*Alphaherpesvirinae*			
Genus			*Mastadenovirus*	*Morbillivirus*	*Lyssavirus*
Envelope		yes	no	yes	yes
Virion shape		spherical	icosahedral	round	bullet-like
Tissue		neuronal, genital	respiratory, anal, urinary	epithelial, neuronal, immune cells	neuronal
Genome	• **organization** • **size**	• dsDNA, linear, ITR/ IR, LATs • 150 kb	• dsDNA ITR, TP • 36 kb	• -ssRNA, non-segmented • 16 kb	• -ssRNA, non-segmented • 12 kb

Entry	• **viral R** • **cellular R** • **mode**	• gB/gC, gD, gB, gH/gL • nectin-1/-2, HVEM • fusion at the plasma membrane	• penton base/ fibre • CAR, CD46, CD80/86 • clathrin-mediated endocytosis, fusion in endosome	• H-/F-protein • SLAM (CD150), CD46, nectin-4 • fusion at the plasma membrane	• G-protein • nAChR, NCAM, p75NTR • clathrin-mediated endocytosis, fusion in endosome
Transport	**components** • **viral** • **cellular**	• Tegument • Microtubules	• Microtubules		
Replication	• **transcription** • **replication**	• hierarchic organization: α/β/γ-genes, by Pol II • circularization of genome (θ-type/ rolling-circle-type), by viral DNA Pol (U30)/ processivity factor (UL42)	• transcription of early and late genes in most cases by Pol II • pTP mediated initiation of replication of viral DNA		Negri bodies
				mode of transcription: "start-stop"-mode (genome organization + IGR), by L-P-complex, transcript a abundancy regulated by order of genes	
				• N>P>M>H>F>L • alternative ORF of P: accessory proteins V/C	• N>P>M>G>L
				genome amplification by L-P complex	
Assembly		• capsid: nucleus • virus particle: cytoplasm	assembly and maturation in the nucleus	RNP-formation (N/P/L proteins + viral RNA)	
				• M-protein mediated assembly (together with actin)	• M-protein-mediated packaging
Exit		exocytosis	lysis of infected cell	budding	budding
Specialties		latent persistence in PNS (circular genome, LATs)			• retrograde spread through transsynaptic transmission • "stealth mode"

Adenoviruses (AdV) (**Table 2, Fig. 10B**) are the only non-enveloped virus family within this thesis used to analyze amyloid-mediated enhancement of infection. Besides humans, other mammals and birds are hosts of this virus family [163]. Adenovirus transmission occurs by aerosols or direct contact and can lead to severe infections of the respiratory, urinary as well as anogenital tract, but also of the eye (conjunctivitis). As all adenoviruses have some sort of tissue specificity, the primary isolates used within this study, adenovirus serotype 2/5 (species C) as well as serotype 3/7 (species B), can both be found in the respiratory tract. The latter species was also reported to be present in the urinary tract [162].

Besides causing disease, several viruses within this panel are used as tools in the clinics or in laboratories. For example, treatment of cancer patients was achieved by using oncolytic viruses based on HSV-1, which was used to treat e.g. gliomas, glioblastomas, head and neck cancer, melanomas, pancreatic or breast cancer. Here, several properties of herpes simplex viruses are beneficial, like infecting replicating and non-replicating cells as well as a fast repli-

cation cycle, which leads to rapid lysis of tumor cells [164, 165]. MeV is also used as an oncolytic virus. In this context, especially CD46 as a receptor is interesting, since this molecule is overexpressed on many cancer cells [160]. To make the two described viruses even more efficient, viral receptors can be modified or viruses can be “armed” by delivering pro-inflammatory mediators, PAMPs (pathogen associated molecular patterns), or prodrug convertases [160, 164, 165]. AdV is widely used as vector in different settings and is applied for example to different vaccination studies for e.g. HIV, Ebola and other hemorrhagic fevers. Due to the long persistence of the virus in cells, lifelong correction of metabolic disorders has been achieved in some cases. Also, their role as oncolytic viruses in the context of cancer is studied [161, 162]. Rabies viruses can be used to analyze neuronal circuits. Depending on the virus modifications, transsynaptic or monosynaptic tracing can be done. The low cytotoxicity of RABV allows several rounds of replication within the brain of the respective animal, enabling mapping of huge areas, making RABV an interesting tool for neurosciences [152].

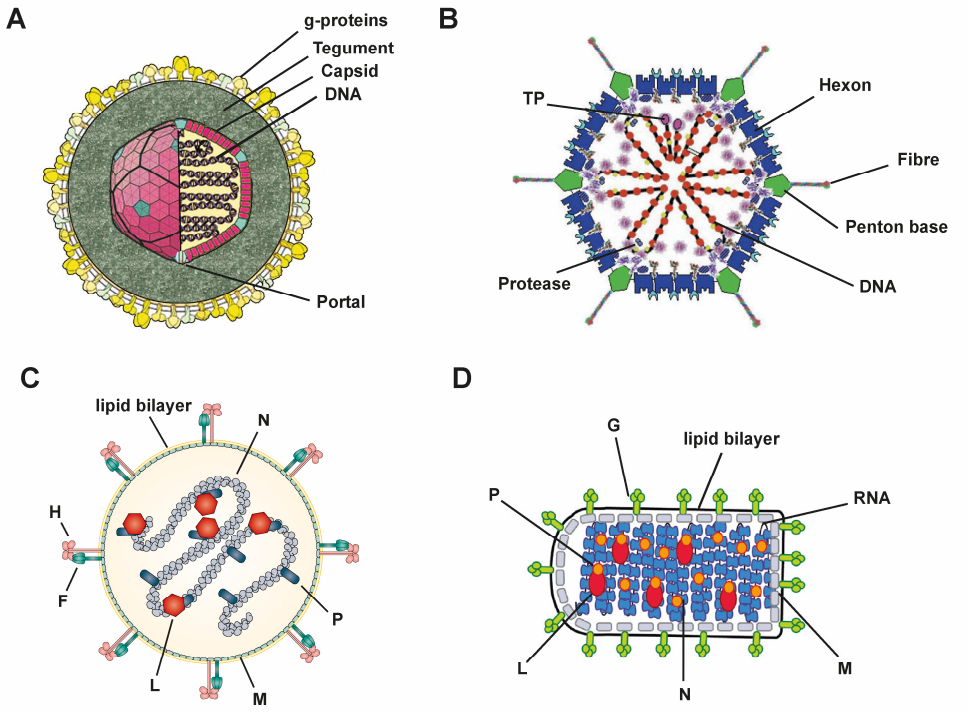

Figure 10: Virion structure of different neurotropic and respiratory viruses tested. (**A**) The HSV virus particle consist of a capsid, which encloses the viral dsDNA. Both are surrounded by the tegument, which fills the space in-between capsid and the glycoprotein-containing lipid bilayer. (**B**) Shown are different proteins forming the AdV capsid as well as the inner structural proteins of the virion. (**C**) Illustration of MeV particle: nucleoprotein covering viral -ssRNA, phosphoprotein, large RNA-dependent RNA polymerase (RdRp), matrix protein, hemagglutinin protein and fusion protein. (**D**) The bullet-shaped particle contains a 12 kb -ssRNA that forms together with N, P and L proteins the ribonucleoprotein (RNP). The latter is covered by a lipid bilayer envelope that contains the glycoprotein. The matrixprotein links trimeric G protein and RNP. Abbreviations are the same as in **Table 2**. Schematics taken from Kukhanova et al., 2014 [156], Albertini et al., 2011 [159], Rota et al., 2016 [154] and Russel, 2009 [166].

1.4 Aim of this study

HIV transmission in a relatively inefficient process (chapter 1.1.2), but recent studies underlined the role of semen-derived amyloids in enhancement of HIV infection and most likely also HIV transmission (chapter 1.2.2). Human *alpha-papillomaviruses* were in the past intensively studied in the context of their potential to induce cancer development in various tissues (chapter 1.2.3.1). In addition, several epidemiological studies highlighted the interplay between HIV and HPV infections, each facilitating subsequent acquisition of the other. Importantly, HPV seems to create a milieu at the transmission site, which is beneficial for HIV transmission (chapter 1.2.3.3). It has been reported that the HPV-derived E4 protein, which has several important functions during the viral replication cycle, is able to form amyloids (chapter 1.2.3.4). It is the aim of this study to characterize amyloids derived from the HPV E4 protein for their ability to modulate HIV infection *in vitro*. Furthermore, it will be elucidated at which step of the HIV replication cycle, this putative amyloid enhancer could be relevant. Moreover, experiments mimicking conditions present during HIV transmission will be used to investigate functionality of the E4-derived amyloids under physiological conditions. Also, the structural and physiochemical properties of this amyloidogenic peptide, eventually influencing HIV infection, will be studied. In addition, this thesis will try to get insight into the impact of this potential amyloid enhancer of infection on HIV therapy. Finally, the effect of amyloids derived from HPV E4 and other known amyloids (chapter 1.2.4) on infection with HIV and a panel of pathologically or structurally relevant viruses (HSV, RABV, MeV, AdV) (chapter 1.3), will be examined.

2 Material and Methods

2.1 Chemicals

Compound/Reagent	Company/Distributor
Agarose	Sigma-Aldrich, St. Louis, USA
Ampicillin sodium salt	Roth, Karlsruhe, Germany
Di-methylsulfoxid (DMSO)	Roth, Karlsruhe, Germany
Ethanol, 98-99% p.a.	Sigma-Aldrich, St. Louis, USA
Fetal calf serum (FCS)	Sigma-Aldrich, St. Louis, USA
Fluoroshield Mounting medium with DAPI	Sigma-Aldrich, St. Louis, USA
Glycine	Roth, Karlsruhe, Germany
Hydrochloric acid 37%	Roth, Karlsruhe, Germany
Isopropanol, p.a.	Sigma-Aldrich, St. Louis, USA
Kanamycin sulphate	Roth, Karlsruhe, Germany
Magnesium chloride	Sigma-Aldrich, St. Louis, USA
Mayer's haematoxylin solution	Roth, Karlsruhe, Germany
MS2 RNA (0.8 µg/µl)	Roche, Rotkreuz, Swizerland
Paraformaldehyde (PFA)	Applichem, Darmstadt, Germany
Perm/ Wash buffer	BD Biosciences, Franklin Lakes, USA
Phytohemagglutinin P (PHA-P)	Sigma-Aldrich, St. Louis, USA
Polyethylenimine (PEI)	Polysciences, Eppelheim
Potassium ferricyanide	Sigma-Aldrich, St. Louis, USA
Potassium ferrocyanide	Sigma-Aldrich, St. Louis, USA
Saponin	Sigma-Aldrich, St. Louis, USA
Sodium azide	Merck, Darmstadt, Germany
Sodium hydroxide pellets	Sigma-Aldrich, St. Louis, USA
Sucrose	Sigma-Aldrich, St. Louis, USA
SYBR Green, 10.000x	Invitrogen, Carlsbad, USA
SYBR Safe	Thermo Scientific, Waltham, USA
Ribolock	MBI Fermentas, St. Leon-Rot
Rotiphorese 50x TAE buffer	Roth, Karlsruhe, Germany
Thioflavin T	Sigma-Aldrich, St. Louis, USA
Tris	Roth, Karlsruhe, Germany
Triton X-100	Roth, Karlsruhe, Germany

Trypsin-EDTA (0.25%)	Biochrom, Berlin, Germany
Trypan blue	Roth, Karlsruhe, Germany
X-Gal	MBI Fermentas, St. Leon-Rot, Germany

Media and buffers (pre-casted)

CO_2-independent Medium	Thermo Scientific, Waltham, USA
DMEM, GlutaMAX™, pyruvate	Thermo Scientific, Waltham, USA
DMEM F-12 Medium, GlutaMAX™	Thermo Scientific, Waltham, USA
1x PBS (Phosphate buffered saline)	Thermo Scientific, Waltham, USA
10x PBS (Phosphate buffered saline)	Thermo Scientific, Waltham, USA
RPMI Medium 1640, GlutaMAX™	Thermo Scientific, Waltham, USA
LB-Medium	Roth, Karlsruhe, Germany
LB-Agar	Roth, Karlsruhe, Germany
TB-Medium	Roth, Karlsruhe, Germany

Peptides

E4 (mutants and variants)	Anaspec, Fremont, USA
SEVI and SEVI Ctrl	Anaspec, Fremont, USA
Beta-amyloid 40 (Aβ40)	Abcam, Cambridge, UK
Beta-amyloid 42 (Aβ42)	Abcam, Cambridge, UK
α-Synuclein	Abcam, Cambridge, UK
Diabetes associated peptide amide human (IAPP)	Sigma-Aldrich, St. Louis, USA

Drugs and inhibitors

AMD3100	Sigma-Aldrich, St. Louis, USA
Maraviroc	Sigma-Aldrich, St. Louis, USA
T20/ Enfuvirtide (Fuzeon)	Roche, Rotkreuz, Switzerland
anti-CD4 antibody (SK3)	Biolegend, San Diego, USA
Isotype IgG1 antibody (MPOC-21)	Biolegend, San Diego, USA
bNAbs/ NAbs	kindly provided by Prof. F. Klein Laboratory of experimental Immunology (Cologne, Germany)

Dyes and antibodies

anti-Adenovirus antibody (20/11)	Merck, Darmstadt, Germany
anti-p24 antibody KC57-FITC	Beckmann Coulter, Brea, USA
anti-E4 mouse monoclonal antibody (NA7-AA5) (immunogen bacterially expressed HPV16 E4)	Eurogentec, Lüttich, Belgium
goat anti-mouse Alexa Fluor 568	Thermo Scientific, Waltham, USA
goat anti-mouse Alexa Fluor 488	Thermo Scientific, Waltham, USA
CCF2	Thermo Scientific, Waltham, USA
Alexa Fluor 647 Phalloidin	Thermo Scientific, Waltham, USA
DAPI	Thermo Scientific, Waltham, USA

Other reagents

Vaginal fluid	Lee Biosolutions, Maryland Heights USA

Kits

LifeBLAzer FRET-B/G Loading Kit with CCF2-AM	Thermo Scientific, Waltham, USA
NucleoBond® Xtra Midi EF	Macherey-Nagel, Rölsdorf, Germany
One Shot™ Stbl3™ Chemically Competent E. coli	Thermo Scientific, Waltham, USA
RosetteSep™ Human CD4+ T Cell Enrichment Cocktail	Stemcell, Vancouver, Kanada

2.2 Machines

C1000/CFX96 Thermal Cycler	BioRad, Hercules, USA
CLARIOstar plate reader	BMG Labtech, Ortenberg
Eclipse Ti2 microscope + DS-Qi2 camera	Nikon, Tokyo, Japan
Eclipse Ts2 microscope	Nikon, Tokyo, Japan
FACS Lyric	BD Biosciences, Franklin Lakes, USA
TCS SP5 confocal microscope	Leica, Wetzlar, Germany

2.3 Buffers and reagents

2.3.1 General buffers and reagents

Antibiotics for the selection of bacteria: ampicillin/ kanamycin

Stock solutions of 50 mg/ml in Milli-Q water were prepared, sterile filtered (0.22 µm) and stored at -20°C.

Freezing medium

DMEM	300 ml
FCS	150 ml
DMSO	50 ml

4% Paraformaldehyde (PFA) solution

All working steps were performed under a chemical hood. First, 450 ml of Milli-Q water were heated to 60°C on a magnet stirrer, followed by addition of 20 g PFA (Applichem). Suspension was stirred for several minutes at constant temperature and then one pellet of NaOH was added. After cooling down to room temperature 50 ml of 10x PBS were added and pH was adjusted to 7.2 using HCl. Afterwards, the solution was filtered with a 0.22 µm Stericup (Millipore) to get rid of precipitates and stored at -20°C.

Polyethylenimine (PEI) transfection reagent (working solution)

To produce a 1 mg/ml stock solution, 250 ml Milli-Q water were heated to 70°C and 250 mg PEI (Polysciences, MW 25000) was added. Following cooling down to room temperature, pH was adjusted to 7 via HCl. Finally, the solution was sterile filtered (0.22 µm) and stored at -20°C.

2.3.2 Assay specific buffers and reagents

2.3.2.1 T cell activation

IL-2 (Biomol)

A stock of 200 µg/ml in 0.02 M acetic acid was prepared and stored at -20°C. For activation of primary CD4 T cells, a final concentration of 5.88 ng/ml was used.

PHA-P (Sigma-Aldrich)

A 1 mg/ml stock in 1x PBS was prepared and stored at store -20°C. To activate primary CD4 T cells, a final concentration of 2 µg/ml was used.

2.3.2.2 Blue Cell Assay

β-Gal reaction solution

in 1x PBS	
Potassium ferricyanide	3 mM
Potassium ferrocyanide	3 mM
$MgCl_2$	1 mM

X-Gal solution

X-Gal (Fermentas) was solved in di-methyl-formamide to prepare a stock solution of 20 mg/ml and store at -20°C, protected from light.

2.3.2.3 HIV-1 capsid (p24) ELISA

Special reagents

- Monoclonal anti-p24 antibody (mAb183, stock 0.5 mg/ml, obtained from Hans-Georg Kräusslich, Heidelberg, Germany) as catching antibody
- HIV-1 p24 capsid stock (Analytic Jena, #PR-1201) as standard
- Polyclonal rabbit anti-p24 antibody (rbαCA) as primary antibody
- anti-rabbit horseradish peroxidase (α-rb-PO) as secondary antibody
- TMB (10 mg/ml in DMSO, store at -20°C)

Buffers

ELISA washing buffer

1x PBS	
Tween 20	0.05%

ELISA blocking buffer

1x PBS	
Fetal calf serum (FCS)	10%

ELISA dilution buffer

1x PBS	
Tween 20	0.05%
TritonX-100	0.05%

Na-Acetat (NaAc) buffer

Stock solution was prepared by dissolving 4.1 g NaAc in 500 ml Milli-Q water and adjusting pH6 using acetic acid.

2.3.2.4 SG-PERT

Special reagents:

- pCHIV #528 virus supernatant as standard
- GoTaq Hot Start DNA polymerase
- MS2 RNA 0.8 µg/µl
- Ribolock 40 U/µl
- dNTP Set (Fermentas) 4x1 ml 100 mM each
- SYBR Green 500 µl 10,000x stock
- 100x BSA (NEB)

Primers:

RT-Assay-forward: TCCTGCTCAACTTCCTGTCGAG
RT-Assay-reverse: CACAGGTCAAACCTCCTAGGAATG

Buffers

2x SG-PERT lysis buffer

KCl	50 mM
Tris-HCl (pH 7.4)	100 mM
Glycerol	40%
TritonX-100	1%

10x PCR/ dilution buffer

$(NH_4)_2SO_4$	50 mM
KCl	200 mM
Tris-HCl (pH 8.3)	200 mM

2x Reaction buffer

1x PCR Buffer	
2x bovine serum albumin (BSA Fraktion IV, Carl Roth)	
1x SYBR Green	
$MgCl_2$	10 mM
dATP/ dTTP/ dGTP/ dCTP	400 µM (each)
RT-Assay-forward	1 pmol
RT-Assay-reverse	1 pmol
MS2 RNA	8 ng

2.3.2.5 Microscopy (Confocal)

Quenching buffer

1x PBS	
Glycine	25 mM

Permeabilization buffer

1x PBS	
TritonX-100	0.1%

Microscopy washing buffer

1x PBS	
BSA	1%

Microscopy blocking buffer

1x PBS	
Tween20	0.1%
BSA	1%
Horse serum	2.5%

2.4 Methods

2.4.1 Cell culture and production of virus stocks

2.4.1.1 Amplification of plasmid DNA

Proviral constructs and other plasmid DNAs (see **Table 3**) were amplified using different competent *E. coli* cells: Stbl2 for HIV-1 lab strain plasmids or Stbl3 One shot for HIV-1 T/F strain plasmids. First, an aliquot of bacteria was thawed on ice, then 1 µg of DNA was added and incubated for 30 min. Afterwards, heat shock was performed for 45 sec at 42°C followed by another 2 min incubation on ice. Next, 250 µl of pre-warmed SOC medium (Thermo Scientific, T/F plasmids) or 800 µl of pre-warmed LB medium (all other plasmids) were added and the bacteria were shaken for 1 h at 37°C, 800 rpm on a Thermoshaker. Following, cells were spun down for 20 sec at 20,000 x g in a tabletop centrifuge (5427R, Eppendorf) and plated on a LB agar plate with the corresponding antibiotic for selection: Ampicillin or kanamycin at a final concentration of 50 µg/ml. After 18 h to 24 h, single colonies were picked and added to 5 ml of TB medium with the corresponding antibiotic for selection (50 µg/ml), in a 15 ml reaction tube (pre-culture). Pre-cultures were shaken for 6 h to 8 h and then added to 400 ml of pre-warmed TB medium supplemented with the corresponding antibiotics (main culture). Main cultures were shaken for 18 h to 24 h. As a last step, cultures were spun down at 3,400 x g for 10 min (5920R, Eppendorf) and stored at -20°C until plasmid DNA isolation. Plasmid DNA isolation was performed using the NucleoBond® Xtra Midi EF Kit (Macherey Nagel). After isolation, plasmid DNA concentration was measured using the NanoDrop One (Thermo Scientific) and adjusted to 1 µg/µl.

2.4.1.2 Restriction digest of plasmid DNA and gel electrophoresis

Quality control of amplified plasmid DNA was done via a restriction digest using the FastDigest system (Thermo Scientific) according to manufacturer's instructions. Here, 2 µl of the restriction buffer (FastDigest Green Buffer) were mixed with 1 µl plasmid DNA, 1 µl of each restriction enzyme (see **Table 3** below) and the corresponding amount of water to reach a total volume of 20 µl. Next, mixes were incubated for 30 min at room temperature, followed by gel electrophoresis (Compact XS/S, Biometra, Analytik Jena) on a 1% Agarose gel. The Agarose gel was prepared in 1x TAE containing SYBR Safe (1:10,000). Gel was run at 120 V (Powerpac HC, BioRad) for 1 h and afterwards imaged with the UVP UV solo touch system (Analytik Jena). After comparing fragment sizes of input DNA and amplified DNA, correctly amplified plasmid DNA was stored at -20°C.

Table 3: DNA plasmids and properties.

Plasmid type	Name	Bacterial background	Antibiotic resistance	Restriction enzymes
HIV-1 lab strains	NL4-3	Stbl2	Ampicillin (Amp)	EcoRI/ HindIII
	NL4-3 ΔEnv		Amp	
	YU-2		Amp	EcoRI/ HindIII
	49.5		Amp	HindIII
	NL4-3 ΔNef GFP		Amp	EcoRI/ HindIII
	R7/3 GFP		Amp	HindIII
HIV-1 T/F strains	WITO	Stbl3	Kanamycin (Kana)	BamH1/ Not1
	CH040		Kana	BamH1/ Not1
	CH058		Kana	BamH1/ Not1
	CH077		Kana	EcoRI/ BamH1
	CH106		Kana	BamH1
	RHPA		Kana	EcoRI
	THRO		Kana	BamH1/ Not1
	TRJO		Amp	Xho1
other	BlaM-Vpr	Stbl2	Amp	
	eGFP-Vpr		Kana	

Proviral plasmids YU-2, WITO, CH040, CH058, CH077, CH106, RHPA, THRO and TRJO were obtained from the NIH AIDS reagent program. Other HIV-1 plasmids were derived from various origin: NL4-3 (Nathaniel Landau, Alexandria Center for Life Science, USA), NL4-3 ΔEnv (Oliver T. Fackler, Universitätsklinikum Heidelberg, Germany), 49.5, R7/3 GFP (Mark Goldsmith, UCSF, USA), NL4-3 ΔNef GFP (Frank Kirchhoff, Universitätsklinikum Ulm, Germany), BlaM-Vpr (D. von Laer, Medical University, Innsbruck, Austria) and eGFP-Vpr (Tom Hope, North-western University, USA).

2.4.1.3 Cell culture

All cell culture work was done under sterile conditions using a sterile hood (Safe2020, Thermo Scientific). Most of the adherent cells were cultured in DMEM plus 10% FCS and 1% Penicillin/Streptomycin (P/S, 10,000 U/ml, Biochrom), which will be referred to as “DMEM complete”. Suspension cells were cultivated in RPMI 1640 with 10% FCS and in the case of CD4 T cells

Table 4: Overview of used cell lines and primary cells.

Name	Description	Adherent (A)/ Suspension (S)	Cultivation medium
HEK293T cells	Human embryonic kidney cells, epithelial cell line	A	"DMEM complete"
TZM-bl cells	Hela cell-derived cell line containing HIV Tat-dependent expression cassettes for luciferase and β-galactosidase	A	"DMEM complete"
A549 cells	Adenocarcinoma cell line, Type II pneumocyte	A	"DMEM complete"
HFF	Human foreskin fibroblasts, primary cell line	A	"DMEM complete"
SH-SY5Y	Neuroblasts from neural tissue	A	DMEM F-12 Medium, 10% FCS, 1% non-essential amino acids, P/S
SupT1.CCR5 cells	Human T cell lymphoblastic lymphoma-derived cell line, stable overexpression of human CCR5	S	RPMI, 10 % FCS, Puromycin
Primary activated CD4 T cells	Purified from PBMCs from Healthy human blood donor	S	"RPMI complete" + IL-2

with 1% P/S ("RPMI complete") or 0.31 µg/ml puromycin in the case of SupT1.CCR5 cells (see **Table 4**). Cell lines were derived from various origin: TZM-bl cells (NIH AIDS reagent program), HEK293T, A549 and SH-SY5Y cells (ATCC), HFF cells (Barbara Adler, LMU Munich), and SupT1.CCR5 cells (Robert Doms, University of Pennsylvania).

2.4.1.4 Cultivation of cell lines

All cells were split according to the speed of cell growth 1-2 times per week. In case of adherent cells, cells were first washed with 1x PBS and then treated with Trypsin/EDTA (0.5%/ 0.2%, Biochrom). By pipetting, a single cell suspension was created and transferred into a new cell culture flask with fresh medium. Dilution of the cell suspension was chosen according to cell

type and growth speed. In case of suspension cells, cells were split 1:10 and resuspended in fresh medium.

2.4.1.5 Freezing and thawing of cell lines

Cell lines were frozen down at a density of 5 x 10^6 cells/ ml. Therefore, a single cells suspension was created if necessary. Next, cells were spun down (600 x g, 5 min room temperature) and resuspended in the adequate volume of freezing medium (for composition, please see general buffers and reagents). Aliquots of 1 ml were prepared in cryotubes (Sarstedt). The latter were put in a special cell freezing container (Cell Camper Mini) that allows constant cooling of 1°C per minute. Freezing was done by first putting the container for 24 h at -80°C and then transferring the tubes into a liquid nitrogen tank.

Thawing of cells in a 37°C water bath was performed by adding 1 ml of pre-warmed medium to avoid freeze/thaw effects. Finally, the cell suspension was added to 10 ml of fresh pre-warmed medium, followed by centrifugation (see above), resuspension in the cell type specific medium and plating according to cell properties.

2.4.1.6 Cultivation of primary cells

Blood cones (Terumo BCT leukocyte reduction system) containing red blood cells as well as enriched leukocytes were received from the Hospital of the University of Munich, Dept. of Immunohematology, infection screening and blood bank (ATMZH). Blood cells were derived exclusively from anonymized healthy donors in the age of 20 to 55 years. The ethics committee of the LMU München, Munich, Germany with the project No. 17-202-UE, approved usage of blood cones.

Primary CD4 T cells were isolated via the CD4 T cell enrichment Rosette Sep Kit (Stemcell) according to manufacturer's instructions. In brief, blood cones were flushed with 30 ml 1x PBS per cone into a 50 ml reaction tube (total volume of ~40 ml) and incubated with 2 ml of the antibody enrichment cocktail for 20 min at room temperature. During this time, the antibodies within the cocktail bind to all cell types except CD4 T cells and attach them to red blood cells. Afterwards, the antibody-blood mix was further diluted with 1x PBS, mounted on Biocoll (density 1,077 g/L, Biochrom) and spun at 700 x g for 35 min with slow acceleration and deceleration. As a result, the erythrocyte fraction can be found at the bottom of the tube, on top the Biocoll and at the phase border of Biocoll and plasma the thin layer of CD4 T cells. After removing most of the plasma, CD4 T cells were collected, washed twice with 1x PBS, and finally resuspended in RPMI containing 10% FCS, 1% P/S ("RPMI complete"). Cell number was determined using the Vi-Cell XR cell counter (Beckmann Coulter) and adjusted to 2 x 10^6 cells/ ml. To generate activated CD4 T cells, cells were cultured in medium supplemented with IL-2 (final concentration of 5.88 ng/ml) and PHA-P (final concentration of 2 µg/ml) for 3 to 4 days.

After this time cells were spun down at 500 x g for 5 min and kept in “RPMI complete” with IL-2 (concentration see above) for further experiments. For infection experiments, pools of 2 to 4 donors were created, where equal cell numbers/ volumes (2 x10^6 cells/ ml) of activated cells from different donors were mixed.

Primary human foreskin fibroblasts (HFF), isolated from circumcision-derived foreskins, were a kind gift of the Adler lab (Munich, Germany). Cells were cultivated in “DMEM complete” and split 1:4 once per week in fresh DMEM, the procedure was the same as for other adherent cell lines.

2.4.1.7 Production of HIV-1 lab strains and Transmitted/ Founder (T/F) strains on HEK293T cells

All work with HIV was done in a P3** or P3 laboratory. To produce HIV-1 by transfection of HEK293T cells, plating of the cells in a 15 cm dish at a density of 8 x 10^6 cells was required at one before manipulation. Next, the transfection mix had to be prepared: 1 ml of plain DMEM was mixed with the plasmid DNA (concentration 1 µg/µl) and PEI transfection reagent (see **Table 5** below). After 45 min, incubation at room temperature DNA-PEI-aggregates had been formed and 2.5 ml of transfection mix were applied to each cell culture plate.

Table 5: Overview of different transfection mixes.

	Normal Virus	Virus + BlaM-Vpr	Virus + eGFP-Vpr
DMEM	1 ml	1 ml	1 ml
proviral DNA	15 µg	15 µg	15 µg
BlaM-Vpr DNA		5 µg	
eGFP-Vpr DNA			1,5 µg
PEI	45 µg	60 µg	49,5 µg

48 h later, supernatants were collected and filtered with a 0.45 µm Stericup (Millipore) to remove floating dead cells as well as cellular fragments. In the next step, 28 ml of supernatant were mounted on 6 ml of sucrose (25% in 1x PBS) in a 35 ml ultracentrifuge tube. Purification of virus particles was done via centrifugation at 24,000 rpm at 4°C for 1.5 h (Sorvall WX+ Ultra series; rotor: SW32, Beckmann Coulter). Afterwards, the supernatant was discarded and pellets were resuspended in 100 µl 1x PBS per ultracentrifuge tube. As a final step, the contents of all tubes were pooled, aliquoted and frozen down at -80°C.

2.4.1.8 Expansion of HIV primary isolates

All work with HIV was done in a P3** or P3 laboratory. For the expansion of HIV-1 and HIV-2 primary isolates (see **Table 6**), virus isolates (provided by Josef Eberle, Max von Pettenkofer Institute, LMU Munich, Diagnostic and NRZ strain collection) were mixed with 5 to 10 x 10^6 primary activated CD4 T cells (four donor pool) and plated on a 6-well plate (total volume ~5 ml). After 2 to 4 days, the culture was transferred into a T75 flask and supplied with 4 x 10^7 primary activated CD4 T cells (total volume ~25 ml). Every 3 to 4 days supernatants were harvested and fresh cells were supplemented. In addition, ultracentrifugation was performed in the same way as for HIV labstrains (see chapter 2.4.1.7). Supernatants as well as concentrated viruses were aliquoted, stored at -80°C, ready to be used in different quantification methods of their virus titer and for infection experiments (see below).

Table 6: Overview of expanded HIV primary isolates.

Name	Tropism	Additional information
13127	CCR5 (R5)	HIV-1, group O
RW9	R5	HIV-1, group M
2044	CXCR4 (X4)	HIV-1, group M
2005	X4	HIV-1, group M
V1818215	X4	HIV-2, group A

2.4.1.9 Expansion of adenovirus (AdV) primary isolates and herpes simplex virus (HSV)-1 YFP

In the case of adenovirus primary isolates (obtained from Jindrich Cinatl, Uniklinikum Frankfurt) A549 cells and for the expansion of HSV-1 YFP (obtained from Barbara Adler, LMU München) HFF cells were used. Therefore, a confluent T175 cm flask of cells was split 1:2 in two new flasks with fresh medium. The next day, the corresponding virus was inoculated, and 24 h later YFP expression (HSV-1) and/or cytopathic effect (CPE, HSV-1 and AdV) were assessed via microscopy (Eclipse Ts2, Nikon). Detecting successful virus expansion, virus was harvested by freeze/thaw cycles. For HSV-1 YFP, in that way generated suspensions were collected, transferred into a 50 ml reaction tube and spun down at 3,400 x g, 4°C for 10 min. Thus cleaned up supernatants, were aliquoted and stored at -80°C. To process expansion of AdV primary isolates, freeze/thaw suspensions were first filtered using a 0.45 µm Stericup (Millipore) and then enriched via ultracentrifugation (24,000 rpm at 4°C for 1.5 h). Pellets were each resuspended in 100 µl 1x PBS, pooled, aliquoted and stored at -80°C.

2.4.2 Quantification of virus stocks

2.4.2.1 SG-PERT: Quantification of HIV RT activity

This method was published by Pizzato et al. [167] and uses the reverse transcriptase (RT) of HIV to transcribe a defined synthetic RNA template, the product of which is afterwards amplified by quantitative polymerase chain reaction (PCR). For composition of buffers, see buffers and reagents section. First, 20 µl of virus-containing supernatant were lysed via incubation with 20 µl of the 2x Lysis buffer (containing Ribolock 1:100), for 10 min at room temperature and then transferred outside of the P3 laboratory. Samples were stored until analysis at -80°C. For the quantification of RT activity, pCHIV #528 virus supernatant was used as a standard. The standard was prepared in a 1x PCR/ dilution buffer in dilution steps of 1:10, starting with the 1:10 dilution of the stock solution as highest concentration. Also, a non-target control (NTC, supernatant of untransfected HEK 293T cells) was used. Both standard and NTC were lysed in the same way as the samples before. During the lysis period, the pre-mixed 2x reaction buffer was supplemented with the GoTaq Hot Start DNA Polymerase (1:100) and 10 µl per well were plated in a 96-well PCR plate (BioRad). Next, 10 µl of standard, NTC and samples were added to the reaction buffer polymerase mix. All measurements were performed in duplicates. As a last step, plates were sealed and SG-PERT analysis was performed using the C1000/CFX96 system by BioRad (for protocol see **Fig. 11**). After the run, data was analyzed using the CFX Manager analysis software provided by BioRad. Starting dilution of the standard was set to 1.06 x 10^8 RT Units/ µl and based on the titration steps a standard curve was generated. The latter was used to estimate RT activity of the different samples. Data were plotted using GraphPad Prism.

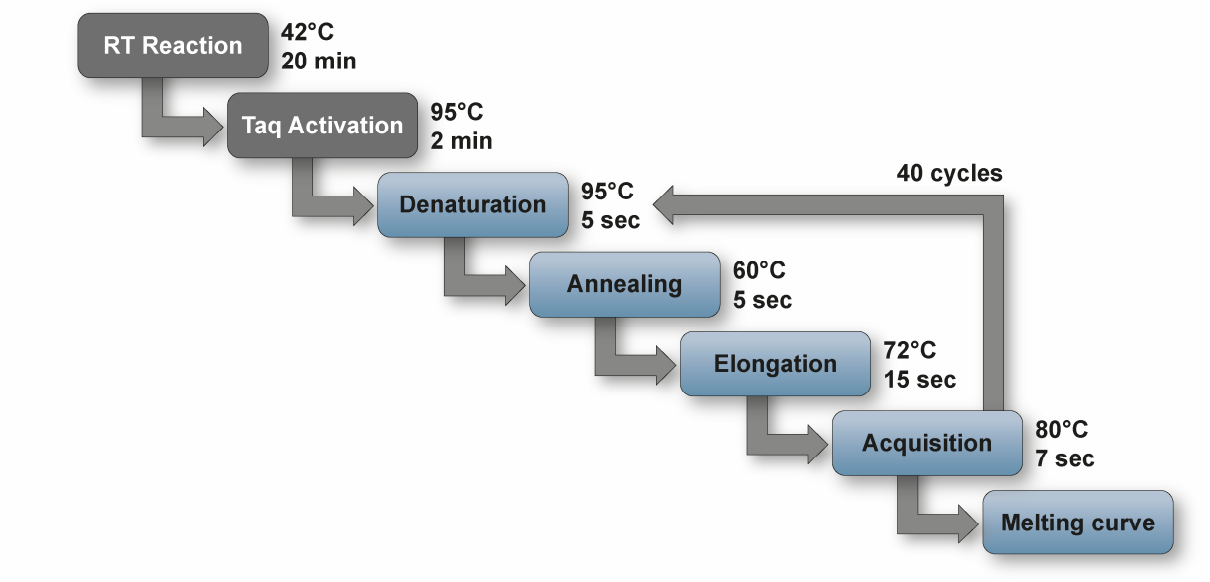

Figure 11: Running parameters SG-PERT.

2.4.2.2 Titration of HI-Viruses on the HIV reporter cell line TZM-bl

TZM-bl cells are a HIV reporter cell line that contains two reporter cassettes (β-galactosidase and firefly luciferase), which are HIV-Tat-dependent. For the following experiments, only the β-galactosidase cassette was used, which is expressed upon HIV infection and leads to cleavage of X-Gal, thereby forming a blue dye inside of the cells. First, cells were detached as described above, counted and plated in a density of 5 x 10^3 cells per well in volume of 100 µl in a 96-well flat bottom plate. Dilution series of different HIV strains were performed in "DMEM complete" in a 96-well round bottom plate (see **Fig. 12**). Next, the plating medium on the TZM-bl cells was removed and replaced with 100 µl of each dilution step. Infection experiments were performed in duplicates. 48 h post infection supernatants were removed and cells were fixed for 10 min with 4% paraformaldehyde (PFA). After removal of PFA, 100 µl of the "blue cell assay" (BCA) substrate solution (10 ml β-Gal reaction solution plus 100 µl X-Gal solution) were added. After 4 to 6 h incubation at 37°C, a blue staining of infected cells could be detected by light microscopy (Eclipse Ts2, Nikon). Wells of a dilution step with around 40 to 200 infected (blue) cells were counted and the mean was calculated. Due to the dilution procedure the dilution step (e.g. 10^4) was multiplied by ten and the calculated mean of infected cells per well. The results represent the infectious units per ml (IU/ ml) of the virus stock. Data were plotted using GraphPad Prism.

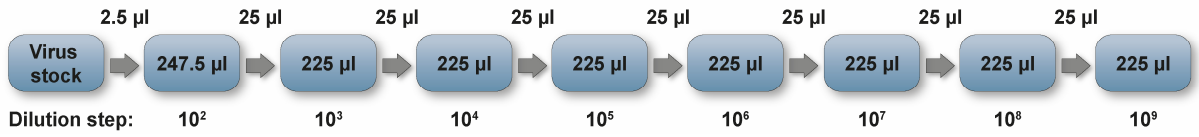

Figure 12: Dilution scheme used for the infection of TZM-bl cells.

2.4.2.3 Titration of HIV on primary CD4 T cells or the T cell line SupT1.CCR5

2.4.2.3.1 HIV infection assay

A pool of primary activated CD4 T cells or SupT1.CCR5 cells was plated at a density of 2 x 10^5 cells per well in a 96-well conical plate in a total volume of 90 µl of the corresponding medium (see above). Virus stocks were diluted in 1x PBS and then added in a volume of 10 µl to the cells. 4 h post infection, a medium change was performed. Cells were spun down at 600 x g for 5 min at room temperature and then resuspended in 200 µl of the respective medium. In experiments where only single-round infection or input virus were analyzed, the fusion inhibitor T20 (final concentration on cells: 50 µM) was added. 48 h post infection, cells were spun down as before, resuspended in 4% PFA/PBS. After 90 min fixation at room temperature in the dark, cells were spun down (1,000 x g, room temperature, 8 min) and washed once with 1x PBS. In the case of experiments, where productive virus infection lead

to expression of GFP in target cells, cells were directly resuspended in 120 µl 1x PBS and analyzed by flow cytometry. In infection experiments with viruses that carry no reporter gene, an antibody staining had to be performed (see section antibody stain of infected cells for flow cytometric analysis).

2.4.2.3.2 Virion-fusion assay

This assay determines fusion of viral particles to target cells as published by Cavrois et al. [168]. Virus particles, containing the HIV-1 Vpr protein fused to β-lactamase (BlaM), had to be produced (see paragraph virus production above). After fusion of these viral particles to target cells, the incorporated BlaM-Vpr fusion protein is released into the cytoplasm and is able to cleave the CCF2 dye. This leads to a shift of the dye's emission maximum from 520 nm to 447 nm, which can be measured by flow cytometry. Fusion experiments were performed in a similar way (cell types, cell numbers, medium volume, virus titrations) as infection experiments with the difference that after 4 h instead of a medium change a special staining procedure was performed. Cells were spun down (600 x g, 5 min, room temperature) and washed with 200 µl CO2-independent medium supplemented 10% FCS, a medium which allowed survival of cells outside of a CO2 incubator. Afterwards, cells were resuspended in 100 µl CCF2 staining solution (composition see **Table 7**), plates were wrapped into a wet tissue, and incubated over night in the dark at room temperature. The next day, 100 µl 1x PBS was added per well, cells were spun down and resuspended in 4% PFA/PBS. After 90 min fixation, cells were washed in 1x PBS, resuspended in 120 µl 1x PBS and virion fusion determined by flow cytometry (see section for flow cytometric analysis).

Table 7: Pipetting scheme for CCF2 staining solution.

Reagent	Volume
CO2-independent medium	1 ml
Solution B	8 µl
Probenecide	10 µl
CCF2 dye	2 µl

2.4.2.3.3 Virion-attachment assay

Measurement of binding/ attachment of virus particles to primary CD4 T cells requires production of GFP-carrying virus particles [169]. To generate these, a similar technique as for the virion-fusion assay was used: an eGFP-Vpr encoding plasmid was co-expressed during virus production. The administration of virus particles to the cells was done in a similar way as for infection and fusion experiments (cell types, cell numbers, medium volume, virus titrations)

but with the subsequent modifications. All steps (starting from virus production), were performed with as little light exposure as possible, to avoid bleaching of the viral particles. Another important parameter was the presence of the fusion inhibitor T20 in all conditions to block fusion of virus particles and arrest them at the binding stage. Cells plus fluorescent particles were incubated for 60 min at 20°C. Afterwards, 100 µl of 1x PBS was added, cells were spun down and washed one more time with 200 µl 1x PBS. After fixation (4% PFA/PBS), attachment was analyzed by flow cytometry.

2.4.2.4 Detection of HIV capsid (CA) protein: p24 CA ELISA (Enzyme linked immunosorbent assay)

Virus supernatants from virus production or infection experiments, which should be analyzed by p24 CA ELISA, were inactivated 1:10 (v/v) in 1x PBS containing TritonX-100 (final concentration 0.5%). Composition of all buffers can be found in the buffers and reagents section. Next, an ELISA plate had to be coated with the catching antibody. 10 ml 1x PBS were mixed with 10 µl of the mAb183 anti-p24 antibody (0.5 µg) and plated in a volume of 100 µl in a 96-well Nunc Immuno Plate (Maxi Sorp Surface). Plates were sealed with parafilm and incubated overnight in a wet chamber. The next day, plates were washed three times with washing buffer, followed by blocking of unspecific epitopes using 200 µl per well blocking buffer and incubating for 2 h at 37°C. Meanwhile, a p24 CA standard was prepared by serial dilution of the HIV-1 p24 CA stock (Analytic Jena) in stages of 1:2 using the ELISA standard dilution buffer. The first four dilution steps were discarded. Dilutions 5-11 were used in combination with a blank (only ELISA dilution buffer) on every plate for comparability between different plates (**Fig. 13**).

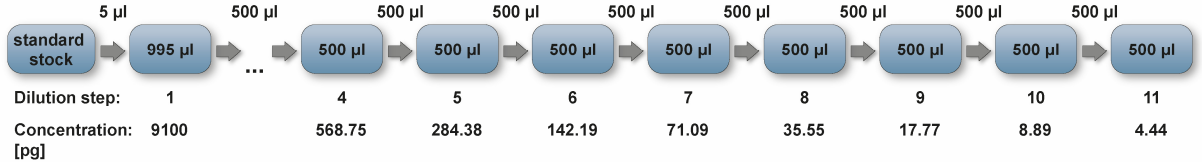

Figure 13: Schematic representation of serial dilution of the HIV-1 p24 CA standard.

Afterwards, the blocking buffer was removed from the ELISA plates and the latter were washed three times with washing buffer. Next, 50 µl of each dilution step of the standard were pipetted in duplicates on the ELISA plate. At the same time, inactivated samples were applied and further diluted in steps of 1:10 in ELISA dilution buffer (**Fig. 14**). Samples were pipetted in duplicates, except samples of TCID50 experiments (see section endpoint titration: TCID50 below), where each sample is already represented by a quadruplicate. Following overnight

incubation in a wet chamber at room temperature, plates were washed three times with washing buffer and 100 µl per well primary antibody solution (rbαCA, 1:1,000 in blocking buffer) were added. Detection of antigen was done by a 1 h-incubation at 37°C followed by extensive washing (as done before) and another 1 h incubation at 37°C with the secondary antibody solution (α-rb-PO). After three rounds of washing, first with washing buffer and then three rounds with distilled water the freshly prepared substrate solution (10 ml NaAc 0.1 M, 100 µl TMB, 2 µl H_2O_2) was added in a volume of 100 µl per well. Monitoring the standard, each ELISA plate was incubated until different stages of blue staining were visible. The reaction was stopped by addition of 50 µl of 0.5 M H_2SO_4 per well. Absorption measurement of the resulting yellowish staining was done using the CLARIOstar plate reader with two different filters. The 450 nm filter was used to measure the background and the 630 nm filter to measure the staining due to antigen-binding and resulting PO activity. In brief, gain adjustment and focal height were set according to the brightest sample. Then the absorbance was measured. As a final step, background (absorption at 450 nm) was subtracted and a standard curved was generated via linear regression. The latter was used to calculate absolute concentrations of p24 CA in sample wells. Data were plotted using GraphPad Prism.

	1	2	3	4	5	6	7	8	9	10	11	12
A	Std5		Sample 1	X	Sample 2	X	Sample 3	X	Sample 4	X	Sample 5	X
B	Std6			10		10		10		10		10
C	Std7			100		100		100		100		100
D	Std8			1000		1000		1000		1000		1000
E	Std9		Sample 6	X	Sample 7	X	Sample 8	X	Sample 9	X	Sample 10	X
F	Std10			10		10		10		10		10
G	Std11			100		100		100		100		100
H	Blank			1000		1000		1000		1000		1000

Figure 14: Plate scheme p24 CA ELISA.

2.4.2.5 Titration of AdV, HSV-1 YFP, rabies* and measles*

Similar to virus expansion, infection experiments with AdV were performed on A549 cells. For infection experiments using HSV-1 YFP, rabies* (ΔG, pseudotyped with the corresponding glycoprotein (G)) or measles* (attenuated) HEK293T and SH-SY5Y cells were chosen as target cells (see **Table 8**). The different cell types were plated at a density of 1 x 10^5 cells per

well in a 24-well flat bottom plate in a volume of 500 µl “DMEM complete”. The next day, medium was removed and replaced with 190 µl of the respective medium with low FCS (2% FCS, 1% P/S). Next, virus dilutions were performed in 1x PBS and added in a volume of 10 µl to the target cells. 2 h post infection, a medium change was performed (aspiration of old medium) and cells were supplemented with 500 µl of fresh medium containing 10% FCS. 18 h (AdV) or 20 h (HSV-1, measles*, rabies*) later, infection levels were checked via CPE (AdV) or YFP/GFP expression (HSV-1, measles*, rabies*) via light or fluorescent microcopy (Eclipse Ts2, Nikon). Subsequently, cells were detached by removal of the medium, addition of 150 µl of Trypsin/ EDTA and incubation of the cells for 5 min in the incubator. Afterwards, 100 µl 1x PBS was added, single cell suspension was created and transferred into a 96-well conical plate. Following centrifugation (600 x g) for 5 min at room temperatur, cells were resuspended in 200 µl 4% PFA/PBS and pipetted into a fresh 96-well conical plate. Infected cells were fixed for 90 min at room temperature in the dark, cells were spun down at 1,000 x g at room temperature for 8 min and for further procession washed with 1x PBS. Cells infected with reporter viruses (HSV-1, measles*, rabies*) were resuspended in 120 µl 1x PBS and analyzed via flow cytometry. For experiments with adenovirus, an antibody staining was performed (see section antibody staining of infected cells for flow cytometric analysis).

Table 8: Overview of used neurotropic and respiratory viruses.

Virus	Target cell	Reporter gene (Y/ N)	Additional information
Measles*	HEK 293T cells SH-SY5Y cells	Y (GFP)	Measles vac strain (attenuated)
HSV-1	HEK 293T cells SH-SY5Y cells	Y (YFP)	
Rabies*	HEK 293T cells SH-SY5Y cells	Y (GFP)	SAD L16 or N2C ΔGlycoprotein (G) viruses pseudotyped with SAD L16 or N2C G-protein respectively, (single-round)
Adenovirus	A549 cells	N	Used strains: AdV2/3/5/7

2.4.3 Characterization of amyloids

2.4.3.1 Preparation of amyloid stocks

HPV E4 from different HPV types as well HPV16 E4 mutants were synthesized by Anaspec after sequences obtained from the “PaVE” (https://pave.niaid.nih.gov/), which had been N-terminally truncated according to Doorbar et al. [132]. Reconstitution of peptides was done by adding 100 µl DMSO to 10 mg lyophilized peptide and further preparation of aliquots with a volume of 20 µl, which were stored at -20°C until usage. To prepare E4 peptide working solutions addition of 180 µl 1x PBS was necessary to create stocks of 10 mg/ml (1.2 mM).

SEVI was synthesized according to Münch et al. [74] also by Anaspec. Peptide powders were reconstituted in 1x PBS to a concentration of 10 mg/ml and stored at -20°C. Upon usage, stocks had to be further diluted in PBS to a final concentration of 2.5 mg/ml (549 µM) and shaken overnight at 37°C, 1,400 rpm on a thermoshaker until the solution was turbid.

Amyloid beta 1-40 (Aβ40) and amyloid beta 1-42 (Aβ42) were purchased from Abcam, dissolved in DMSO in a concentration for Aβ40 of 2.22 mM as well as for Aβ42 of 2.31 mM and frozen at -20°C. Before usage, stocks were further diluted in 1x PBS to a final concentration of 100µM and shaken for five days at 37°C, 1,400 rpm on a thermoshaker.

Islet amyloid polypeptide (Sigma Aldrich) was reconstituted in DMSO to a concentration of 1mM (storage at -20°C). To prepare working solutions stocks were further diluted in 1x PBS to a final concentration of 100 µM and shaken for five days at 25°C, 1,400 rpm on a thermoshaker.

Human α-synuclein was purchased from Sigma-Aldrich and shaken for five days at 37°C, 1,400 rpm on a thermoshaker after thawing. All thawed and finally prepared peptide stocks were kept at 4°C.

2.4.3.2 Quantification of amyloids

For staining and quantification of amyloids the Thioflavin T stain was used based on the methods used in Münch et al. [74]. The Thioflavin T dye intercalates into the amyloid fibrils and leads to an emission shift, which can be quantified. First, a 2.5 mM stock of Thioflavin T (Sigma Aldrich) in 1x PBS was prepared, aliquoted and stored at -20°C. Upon usage a 50 µM working solution was prepared in 1x PBS and equilibrated to room temperature. Amyloids were plated in a volume of 20 µl in a 384-blackwell plate (Corning) and mixed in a 1:1 ratio with the Thioflavin T working solution. Plates were spun down (3,400 x g, 5 min), shaken for 2 min on a Thermoshaker and fluorescence was measured at 483 nm on the CLARIOstar plate reader. Gain and focal height adjustments were performed as described in the p24 CA ELISA section.

2.4.3.3 Experiments using amyloid enhancers of infection

Previously described infection, fusion and attachment experiments were also performed in the presence of amyloid enhancers of infection. To facilitate a setup for maximum infection enhancement of infection, low multiplicities of infection (MOIs) were chosen. Identifying peptide concentrations for optimal infection enhancement, titrations of the different amyloid enhancers were performed as indicated (see exemplary pipetting scheme in **Table 9**). Amyloid concentrations were calculated relative to the final volume of medium on the cells. Virus stocks and different dilutions of amyloid enhancers were mixed and incubated for 10 min in the incubator prior to administration to cells. In cases where inhibitors were supposed to be effective already at the start of an experiment, the drug or antibody was added 1 h prior to infection to the cells. In experiments aimed at determining the thermo-stability and infectivity of viral particles, virus stocks were pre-incubated with different amyloid peptide or control solutions for the indicated periods. Afterwards, solutions were added to cells and a medium change was performed 4 h post infection with medium supplemented with T20, to restrict the infectivity readout to the first round of infection. Then the protocol of the corresponding assay was followed.

Table 9: Example of pipetting scheme for a HIV-1 amyloid enhancer experiment. Shown is a pipetting scheme for three technical replicates (each 10 µl) and an additional volume (5 µl). Indicated values are pipetted volumes (µl) of PBS, virus/peptide stock or the respective dilutions (dil.). Italic numbers represent volume of peptide stock, which was replaced by the respective dilution of the peptide (bold). Final concentrations [µM] on cells of each amyloid condition are indicated below the name of the peptide (E4/SEVI).

Pre-incubation (3.5-fold)	Virus	E4 0.12	E4 1.2	E4 6	E4 12	SEVI 0.22	SEVI 2.2	SEVI 11	SEVI 22
PBS	28	24.5	24.5	26.25	24.5	14	14	21	14
Virus: NL4-3	7	7	7	7	7	7	7	7	7
SEVI-Stock						*0.14*	*1.4*	**7**	**14**
E4-Stock		*0.035*	*0.35*	**1.75**	**3.5**				
E4 1:10 dil.			**3.5**						
E4 1:100 dil.		**3.5**							
SEVI 1:10 dil.							**14**		
SEVI 1:100 dil.						**14**			

2.4.3.4 Endpoint titration: TCID50

To asses changes of TCID50/ ml of an HIV stock in the presence of amyloid enhancers, a four donor pool of primary activated CD4 T cells was plated in a 96-well conical plate in a volume of 22.5 µl at a density of 1 x 10^5 cells/ well. Next, 2.5 µl of 1x PBS or the HPV16 E4 stock (corresponding to a final concentration on cells of 12 µM) were added. Subsequently, a dilution

series of different HIV-1 strains and isolates was performed in 1x PBS, starting as highest concentration with the original stock and going down in dilution factors of 3.3 for 15 steps (range: 10^{1} to 10^{-6}). 25 µl of each dilution were added to the previously plated cells, mixed and incubated for 3 h. The experiment was performed in quadruplicates. Afterwards, 225 µl of "RPMI complete" + IL-2 medium were added and plates were incubated further. After five days, cells were spun down (600 x g, 5 min, room temperature) and supernatants were transferred into a new 96-well conical plate. This procedure was repeated one more time to get rid of all cells. As a final step, supernatants were diluted 1:10 in 1x PBS containing 5% TritonX-100 (final concentration 0.5%). Inactivated samples were analyzed by p24 CA ELISA. HIV p24 CA-positive wells (with concentration >= 50 pg/ml) were counted and plotted against the differents dilution steps. Additionaly, TCID50/ ml values were calculated using an Excel makro TCID50 calculator (https://www.klinikum.uni-heidelberg.de/fileadmin/inst_hygiene/molekulare_virologie/Downloads/TCID50_calculator_v2_17-01-20_MB.xlsx). Fold changes of TCID50/ ml values were calculated using Excel. Data were plotted using GraphPad Prism.

2.4.3.5 Cell viability assay

Living cells reduce the dye resazurin to the fluorescent resorufin (emission max at 585 nm), as reviewed by Riss et al. [170], which can be measured via the CLARIOstar plate reader. To quantify the potential intrisic toxicity of amyloids, appropriate cell numbers (see **Table 10**) were plated in a volume of 29 µl medium in a 384-blackwell plate. Amyloid stock dilutions were added (in a volume of 3.2 to 9 µl, medium volume was adjusted). Besides a blank, containing only medium, also untreated cells were used as reference controls. In addition, DMSO controls, which correspond in their DMSO concentration to those in amyloid stock dilutions, were used. The same was done for the carrier of α-synuclein (0.0095% magnesium chloride, 0.316% Tris HCl, 0.58% sodium chloride, pH 7.5). Afterwards, cells were incubated for the same periods as in infection experiments (20 to 44h). Next, 6 µl of resazurin solution (0.15 µg/µl in 1x PBS) were added using the Mantis pipetting robot (Formulatrix), followed by 4 h incubation at 37°C. After adjustment of gain and focal height, emission at 590 +/- 8 nm was aquired. The blank value was substracted from the data of specific samples and subsequently, data were normalized to untreated cells, which were set as 100% viable cells. Data were plotted using GraphPad Prism.

Table 10: Overview of cell types used in cell viability assays.

Cell type	Cell density (x10^3)	Incubation time (h)
Primary activated CD4 T cells	50	44
SupT1.CCR5 cells	25	44
HEK293T cells	5	20
SH-SY5Y	5	20

2.4.4 Flow cytometry

2.4.4.1 Antibody staining of infected cells for flow cytometric analysis

To detect productively HIV-1 infected cells, a staining with a directly labelled anti-p24 CA antibody was used. To detect AdV antigen in AdV-infected cells a two-step staining procedure was performed, using a primary mouse antibody against AdV and a secondary goat anti-mouse Alexa Fluor 488 antibody. Fixed cells were spun down at 1,000 x g at 4°C for 5 min and washed with 1x PBS. Subsequently, cells were spun down at 1,000 x g at 4°C for 5 min (same parameters for all following centrifugation steps) and resuspended in 200 µl 1x BD Perm/Wash (P/W) buffer. After 15 min of permeabilization at 4°C in the dark, cells were spun down washed one time with 200 µl P/W buffer and resuspended in 50 µl primary antibody solution (AdV: anti-Adenovirus 1:500 in P/W buffer; HIV: anti-p24 KC57 FITC 1:100 in P/W buffer). After 30 min incubation in the dark, 150 µl P/W Buffer were added, cells spun down and washed again with 200 µl P/W buffer. Cells from HIV infection experiments were resuspended in 120 µl 1x PBS and used for flow cytometric analysis. A549 cells from adenovirus experiments were incubated in 50 µl secondary antibody solution (goat anti-mouse Alexa Fluor 488: 1:200 in P/W buffer) and processed further analogous to the staining with the primary antibody. As a final step, cells were resuspended in 120 µl 1x PBS and analyzed by flow cytometry.

2.4.4.2 Flow cytometric analysis

For analysis of infection, virion fusion and attachment the BD FACSLyric in combination with the FACSuite software were used. Therefore, the standard settings of the instrument had to be adjusted for the autofluorescence of the particular cell line and an experiment-specific gating strategy was developed. The principles of flow cytometry will not be explained in detail. The used FACSLyric (lasers: red (635 nm), blue (488 nm) and violet laser (405 nm)) allowed characterization of the cells in size (forward scatter, FSC) and granularity (side scatter, SSC) also enabling a preselection of live as well as single cells. In addition, this instrument allows detection of the presence of different fluorescent dyes, which can be directly bound to cellular structures as well as be present in the cytoplasm or nucleus. Finally, fluorochromes can be

linked to antibodies targeting different epitopes inside or outside of the cell, allowing a more specific analysis.

2.4.4.3 Analysis of infection levels and virus attachment by flow cytometry

For experiments with GFP expressing reporter viruses as well as GFP-fusion protein carrying viruses, uninfected cells were used to calibrate the flow cytometer. In other experiments where an antibody staining had been performed, uninfected cells with and without antibody staining had to be used as calibration controls. In a first step, the living cell population was defined by the FSC/SSC dot plot. After gating for single cells (FSC-A/FSC-H), a dot plot with FITC on the x-axis and APC as a reference channel on the y-axis was used to analyze infection or virus binding. The latter channel was chosen to correct for debris and autofluorescence. The gate defining cells as positive for HIV infection (GFP expressing or p24 CA positive cells) was set according to uninfected control cells. The background was set to be < 0.1%. After the measurement, FCS files were exported and analyzed by FlowJo software using the same gating strategy (**Fig. 15**). Data were plotted using GraphPad Prism.

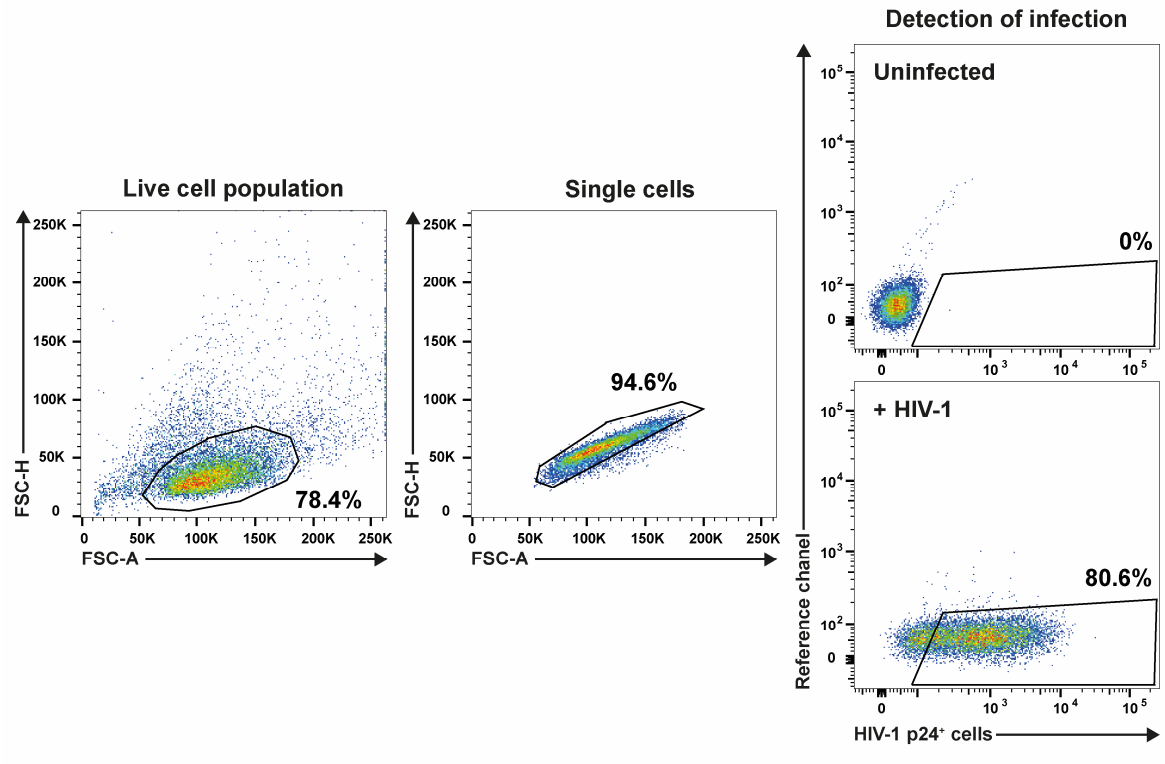

Figure 15: Gating strategy for HIV infection and virion-attachment experiments. Depicted are SupT1.CCR5 cells, gated for the “live cell population”, followed by “single cells”. This pre-selection allows subsequent gating for infected cells (using uninfected controls) and hence detection of HIV-positive cells in samples infected with HIV-1_{NL4-3}.

2.4.4.4 Analysis of virion fusion by flow cytometry

Adjustment of the flow cytometer for this assay requires uninfected controls with and without CCF2 dye treatment as calibration controls. Gating was performed analogous to infection experiments with the difference that fusion was detected by plotting the V500 (CCF2 uncleaved) against the V450 (CCF2 cleaved) channel. HIV fusion-positive cells were gated based on uninfected controls, T20 controls and, if necessary, cells treated with the respective amyloid. Background was set to be < 0.1%. After measurement, FCS files were exported and analyzed by FlowJo software using the same gating strategy (**Fig. 16**). Data were plotted using GraphPad Prism.

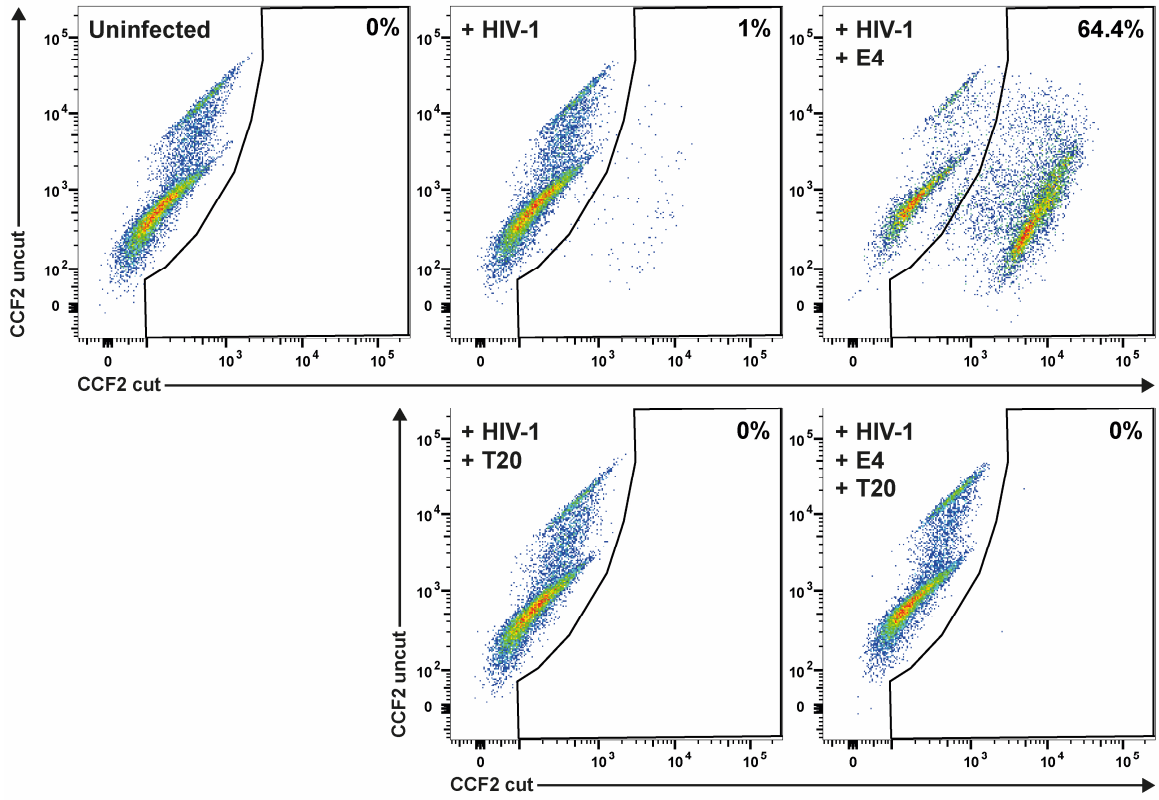

Figure 16: Gating strategy for HIV-1 virion-fusion experiments using appropriate controls. Depicted are in the upper panel uninfected CD4 T cells, cells challenged with BlaM-Vpr-carrying HIV-1_{NL4-3} pre-incubated with either PBS (+HIV-1), or HPV16 E4 (+HIV-1, +E4). In the lower panel the corresponding T20 (50 µM) controls are shown.

2.4.5 Microscopy

2.4.5.1 Visualization of HIV-1 attachment by confocal microscopy

To visualize attachment of HIV-1 eGFP-Vpr virions to E4 and cells, the identical virus particle preparations used in the virion-attachment assay were applied. First, round coverslips were coated with poly-L-lysine overnight at 37°C. Next, coverslips were washed with 1x PBS and

placed in a fresh 12-well plate. Then, 4 x 10^6 primary activated CD4 T cells (four donor pool) in a volume of 380 µl medium were added to each well and incubated for 1 h, allowing cells to adhere to the coated coverslips. Afterwards, 20 µl of virus stocks in combination with either PBS, E4 or control peptide, which had been treated as described above, were added to the wells (see **Table 11**).

Table 11: Pipetting scheme for HIV attachment experiments (microscopy). Shown is a pipetting scheme for two technical replicates (each 20 µl) and an additional volume (10 µl).

Pre-incubation (2.5-fold)	Virus	E4 100 µM	E4 scr. 100 µM	Uninfected
Virus: NL4-3 eGFP-Vpr	40 µl	40 µl	40 µl	
E4-stock		10 µl	10 µl	
PBS	10 µl			50 µl

Cells and different conditions (see table above) were incubated for 90 min at 37°C, followed by addition of 133 µl 16% PFA/PBS (final concentration 4%). After this initial fixation for 10 min in the dark, coverslips were transferred into a new 24-well plate with fresh 4% PFA/PBS and incubated for 80 min. All following incubation steps were performed at room temperature and in the dark to omit bleaching of fluorescent dyes. The buffer compositions can be found in the section “assay specific buffers and reagents”. After fixation, the PFA solution was removed and its activity was stopped by incubation for 5 min in 200 µl quenching buffer. Next, cells were permeabilized for 3 min by addition of 500 µl permeabilization buffer followed by washing three times with microscopy washing buffer. Staining was performed by addition of the different staining solutions (composition and incubation time see **Table 12**) followed by three times washing with the microscopy washing buffer. After the last staining step, coverslips were washed with Milli-Q water, followed by careful removal of the remaining liquid and mounting slides using the Prolong Diamond Antifade Mountant (Thermo Fisher Scientific). Finally, after drying overnight in the dark at room temperature, slides were stored at 4°C until imaging with the Leika confocal microscope (Leica TCS SP5). Acquired data were processed using the Imaris software and Adobe illustrator.

Table 12: Staining solutions for HIV attachment experiments.

	Antibody dilution in microscopy blocking buffer	Antibody	Target	Incubation time
Stain 1	1:40	Alexa Fluor 647 Phalloidin	F-actin	30 min
Stain 2	1:500	NA7-AA5 (mouse)	HPV16-E4	30 min
Stain 3	1:2,500	goat anti-mouse Alexa Fluor 568	mouse IgG	30 min
Stain 4	1:1,000	DAPI	chromatin	6 min

2.4.5.2 Visualization of virus infection by fluorescence microscopy

One way of visualizing HIV-1 infection of target cells was to use HIV-1 NL4-3 GFP reporter viruses. Here, $2x10^6$ SupT1.CCR5 cells per well were plated in a volume of 400 µl in a 12-well plate and infected with 20 µl of the different solutions indicated below (**Table 13**). 48 h after infection, cells were resuspended in the culture medium and 200 µl of this cell suspension were pipetted onto a round coverslip, which had previously been coated overnight with PEI (1 mg/ml). Following a 30 min incubation at 37°C that allowed sedimentation and binding of cells to coverslips, the latter were transferred into a new 24-well plate containing 1 ml of fresh 4% PFA/PBS. The remaining cells of each treatment were transferred to a 96-well conical plate, spun down (600 x g, 5 min, room temperature) and resuspended in 4% PFA/PBS. After 90 min fixation, coverslips were incubated for 5 min in 200 µl quenching buffer and subsequently washed once with 1 ml 1x PBS. Finally, coverslips were washed with Milli-Q water and mounted using Fluoroshield with DAPI mounting medium. Fixed cells in 96-well conical plates, were washed once with 1x PBS and then resuspended in 120 µl 1x PBS. Infection levels were determined by flow cytometry as described above for HIV reporter viruses.

Table 13: Pipetting scheme of HIV infection experiments (microscopy). Shown is a pipetting scheme for two technical replicates (each 20 µl) and an additional volume (10 µl).

Pre-incubation (2.5-fold)	Virus	E4 100 µM	E4 scr. 100 µM	Uninfected
Virus: NL4-3 eGFP	15 µl	15 µl	15 µl	
E4-Stock		10 µl	10 µl	
PBS	35 µl	25 µl	25 µl	50 µl

To visualize adenoviral infection, $1x10^5$ A549 cells were plated on poly-L-lysine-coated coverslips in a 24-well plate. Infection was performed at the indicated conditions for 18 h, followed by fixation (90 min, room temperature) of the samples with 4% PFA/PBS and storage in 1x PBS at 4°C. All staining steps were performed in the dark in a wet chamber at room temperature. 40 µl drops of AdV staining blocking buffer (1x PBS, 0.1% saponin, 1% horse serum) were placed on parafilm and coverslips were mounted upside down. Blocking was done for 30 min, followed by two times washing with AdV staining washing buffer (1x PBS, 0.1% saponin) and one time washing with 1x PBS. Afterwards, coverslips were mounted on drops (25 µl) of the primary antibody solution (anti-adenovirus antibody 1:500 in AdV staining blocking buffer). After 1 h of incubation, the washing procedure was repeated and coverslips were mounted on drops (40 µl) of the secondary antibody solution (goat anti-mouse Alexa Fluor 488 1:200 in AdV staining blocking buffer). Staining was done for 50 min, followed by washing of coverslips as described above, with an additional washing step in Milli-Q water. As a final step, coverslips were mounted using Fluoroshield with DAPI mounting medium. Slides were dried overnight at room temperature in the dark and analyzed using the Nikon Eclipse Ti2 fluorescence microscope. Fluorescent images were created using the DS-Qi2 (Nikon) camera.

3 Results

3.1 Basic characterization of HIV-1 strains and primary isolates in different T cell systems

To study HIV-1 replication *in vitro*, two different cell systems were used: primary activated CD4 T cells and the T cell line SupT1.CCR5. In all experiments, pools of primary activated CD4 T cells derived from two to four blood donors were used, which have the benefit that they are as primary cells more close to the *in vivo* scenario. Using pools of different donors helped to reduce the impact of donor variability and thus made the outcome of already a single experiment meaningful. Additionally, in many experiments the T cell lymphoma cell line SupT1.CCR5 was used. This cell line constantly overexpresses the HIV-1 co-receptor CCR5 on the cell surface, which facilitates entry of R5-tropic viruses. First, the behavior of HIV-1 in infecting these two cell systems was characterized. The standard X4-tropic lab strain HIV-1_{NL4-3} was titrated on primary activated CD4 T cells and the infection was stopped after either 24, 48, or 72 h (**Fig. 17A**, black symbols). Analysis of intracellular p24 levels of HIV-1 revealed ~4.1% positive cells after 24 h, 17.8% after 48 h and 48% after 72 h of infection. Addition of the fusion inhibitor T20, a peptidic drug targeting the formation of the six-helix-bundle of the HIV-1 Env protein during the fusion process [171], at the time point of medium change, restricted the infection to a single round, leading to 2.5% p24-positive cells 48 h post infection. This experiment showed how HIV-1 spreads within a cell culture system in the initial three days after infection and that, as already published [172], one round of HIV replication takes approximately 24 h. When investigating the behavior of HIV-1 in the context of transmission, the first rounds of infection are the most interesting that is why for most of the following experiments a time point of harvest of 48 h was chosen. Similar to primary CD4 T cells, also the performance of HIV-1 for infecting the T cell line SupT1.CCR5 was tested (**Fig. 17B**). HIV-1_{NL4-3} was titrated on SupT1.CCR5 cells and T20 was added after medium change 4 h post infection. After 48 h of infection, this resulted in a maximum infection of 42.9% in conditions where T20 was added (single-round infection), whereas in the absence of the drug (multiple rounds of infection) 79.9% infection was detected. These results were in line with the data of the experiments in activated CD4 T cells, showing that viral spread is possible in both systems. Comparing the two cell models, SupT1.CCR5 cells were generally more permissive to infection, reflected also by a bigger dynamic range. Primary activated CD4 T cells were less susceptible to HIV infection as well as related cytopathic effect of the virus and therefore often more robust as a cell system for infection.

Next, a broader virus panel of HIV-1 strains and primary isolates including various X4- and R5-tropic strains, was used to characterize infection kinetics in these two cell systems. Besides

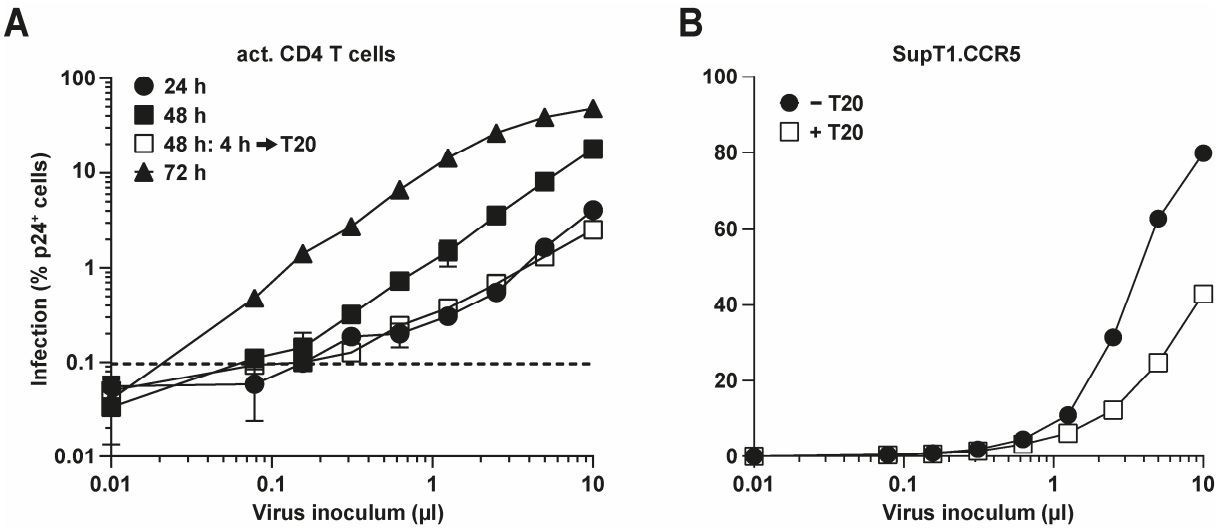

Figure 17: Titration and replication kinetic of HIV-1_{NL4-3} on primary activated CD4 T cells and the T cell line SupT1.CCR5. Evaluation of virus spread on different cell types. (**A**) A four donor pool of primary activated CD4 T cells was infected with increasing volumes of an HIV-1_{NL4-3} stock. Four hours post infection, a medium change was performed to synchronize infection. In the condition indicated, the fusion inhibitor T20 was added at medium change to inhibit virus spread (white squares). Infected cells were harvested at the indicated time points, fixed and stained for intracellular p24. Analysis of infection levels was done by flow cytometry. (**B**) SupT1.CCR5 cells were infected with HIV-1_{NL4-3}. A medium change was performed four hours post infection and cells were subsequently cultivated in medium with or without T20. 48 h post infection, intracellular p24 expression was determined by flow cytometry. Shown are the arithmetic mean and standard deviation of three technical replicates from one experiment.

classical HIV-1 lab strains and GFP expressing reporter viruses, also different Transmitted/ Founder (T/F) viruses were screened, each representing a consensus sequence of the different HIV-1 sequences isolated briefly after infection of one HIV patient. In the context of HIV transmission, these viruses are of great interest, because HIV-1 lab strains have often undergone adaptations by passaging on cell lines for several years. Access to the NRC collection for retrovirus samples, allowed testing of several HIV-1 primary isolates and one HIV-2 primary isolate. That way the virus panel covered not only several subtypes of HIV-1 group M, but also an HIV-1 group O virus and finally also an HIV-2 primary isolate, allowing us to investigate a broader spectrum of HIV diversity (**Fig. 18**).

HIV-1 lab strains, HIV-1 GFP expressing reporter viruses as well as HIV-1 T/F viruses were titrated on primary activated CD4 T cells and SupT1.CCR5 cells, whereas HIV-1 primary isolates were titrated only on CD4 T cells (**Fig. 19A-D, S1**). Overall the maximum degree of infection on primary activated CD4 T cells was lower than on SupT1.CCR5 cells (**Fig. 19A,B,D**). Levels of HIV-1 infected CD4 T cells at 48 h post infection ranged between ~1% (HIV-$1_{YU.2}$) to ~10% (HIV-1_{NL4-3}), when exposed to HIV-1 lab strains (**Fig. 19A, S1A-C**). HIV-1 GFP reporter viruses, HIV-1 T/F viruses and primary isolates fell into a similar range (**Fig. 19B-D, S1D-N**). Interestingly, the X4-tropic primary isolate HIV-1_{2005} represented with 10.6% p24-positive cells

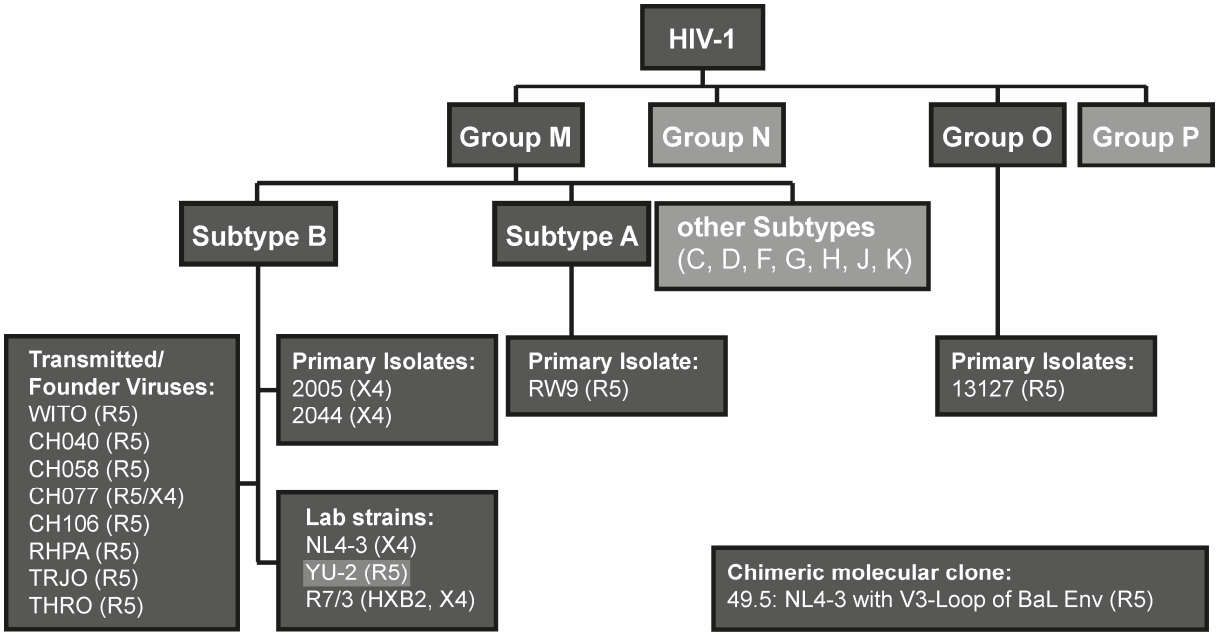

Figure 18: Overview of HIV-1 strains and isolates tested. Depicted is the simplified systematic overview of HIV-1 groups and subtypes. Within this thesis several lab strains, GFP reporter viruses and Transmitted/Founder viruses (T/F) of subtype B were used. The R5-tropic HIV-1_{YU-2} represents a special strain in this overview, since it was isolated from the brain of an HIV-infected patient and directly cloned into a proviral expression construct. Therefore, although often declared as a lab strain, is rather a primary isolate. In addition, primary isolates from patients infected with subtype A and B (both group M) as well as one group O isolate were used. To study the impact of co-receptor usage, the HIV-1_{NL4-3} isogenic virus 49.5 was applied. Tropism of viruses is indicated in brackets. Lab strains and GFP reporter viruses were produced by transfection of HEK293T cells with HIV-1 proviral constructs. Primary isolates were expanded on donor pools of primary activated CD4 T cells.

a highly potent virus on primary cells (**Fig. 19C, S1N**). SupT1.CCR5 cells covered with 9.4% (HIV-$1_{YU.2}$) to 51.1% (HIV-1_{NL4-3}) in the case of lab strains a much wider susceptibility range (**Fig. 19A, S1A-C**). While the GFP reporter viruses behaved similar, the T/F strains exhibited with 2.8% (HIV-1_{CH058}) to 19.1% (HIV-1_{CH077}) a lower infectivity on this cell line (**Fig. 19B-D, S1D-N**). In parallel, the different HIV-1 lab strains, GFP reporter viruses or T/F strains were characterized by p24 CA ELISA, SG-PERT (RT activity) assay or titrated on the HIV reporter cell line TZM-bl (BCA titer) (**Fig. S2A**). Although RT activity and p24 concentrations of HIV-1 stocks were typically comparable, their infectious titer varied considerably. Also, for HIV-1 primary isolates a disconnect of p24 concentrations and infectious titers was observed (**Fig. S2C**).

Unconcentrated supernatants of the HIV-2 primary isolate V1818215 (further called HIV-2_{V18}) were titrated on primary activated CD4 T cells. Here, only a low RT activity 72 h post infection could be observed (data not shown). However, the infectivity of the HIV-2 primary isolate stocks could be validated by examining the supernatants harvested at different time points

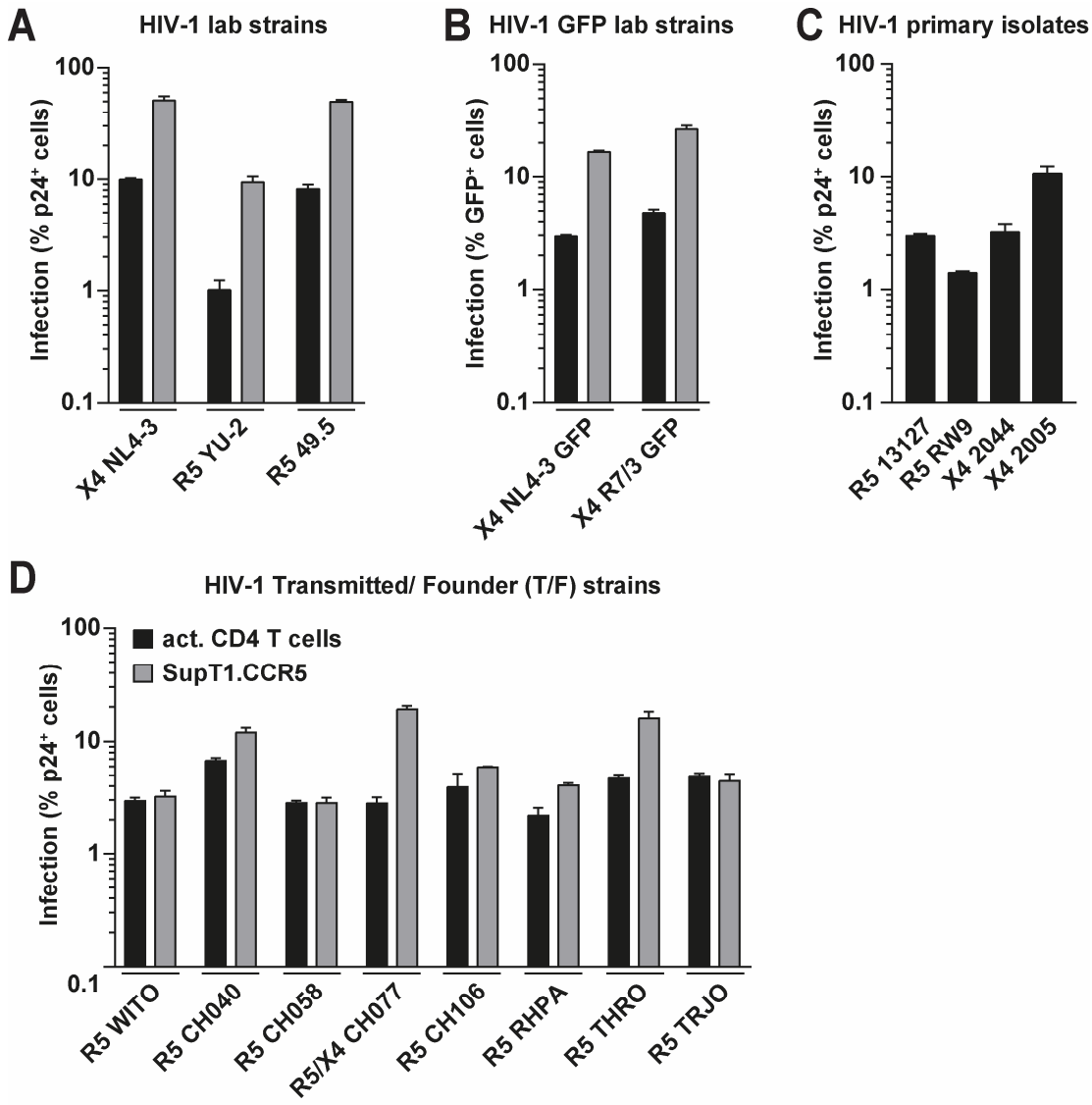

Figure 19: Infection of primary activated CD4 T cells and SupT1.CCR5 cells with different HIV strains and isolates. Four donor pools of primary activated CD4 T cells (black bars, **A-D**) or SupT1.CCR5 cells (grey bars, **A,B,D**) were infected for 48 h with increasing volumes of different HIV-1 lab strains (**A**), HIV-1 GFP-reporter viruses (**B**), HIV-1 primary isolates (**C**) and HIV-1 Transmitted/Founder viruses (**D**). For titration graphs of the different virus stocks, see **Fig. S1**. Identity of proviral plasmids was validated by restriction digest (**Fig. S2B**). Productive infection was scored either by GFP-expression, or intracellular p24 by flow cytometry. Shown are the maximum infection levels reached on indicated cell types. Depicted are the arithmetic mean and standard deviation of three technical replicates. Data shown represent either one experiment (**C**) or are representative data of two independent experiments (**A,B,D**).

during virus expansion. Presence of infectious virus in generated stocks was indicated by steadily increasing infectious titers (from $1x10^4$ to $1.1x10^6$ IU/ml) as measured on the HIV reporter cell line TZM-bl (**Fig. S3A**). In addition, the RT activity was also constantly increasing during virus expansion ($3.9x10^4$ to $5.9x10^6$) (**Fig. S3B**). Taken together, these results show that primary CD4 T cells supported infection of all HIV strains or primary isolates tested and

that SupT1.CCR5 cells could be used in experiments where a bigger dynamic range of infection was required.

3.2 The *N-terminally* truncated E4 peptide from HPV16 can enhance HIV infection

As described in the introduction, HPV16 *ΔN*1-17 E4 (HPV16 E4) has been reported to form large aggregates [132, 133], which led to the hypothesis that this peptide might cause similar effects as the already published Semen-derived enhancer of virus infection (SEVI) [74]. In contrast to SEVI, E4 spontaneously forms aggregates, which can be detected by an increased turbidity of the solution. To test the ability of E4 to enhance HIV-1 infection, different dilutions of E4 were first incubated with a low volume of HIV-1_{NL4-3} stock and the mixes then added to primary activated CD4 T cells (**Fig. 20**). Analysis of infection levels revealed a concentration-dependent enhancement of HIV-1 infection by the HPV-derived E4 with a maximum enhancement of infection of 81.6-fold (**Fig. 20A**) at a concentration of 12 µM. A similar degree of infection enhancement (82-fold) was observed for SEVI peaking in this experiment at a concentration of 5.5 µM (**Fig. 20B**). Both peptides were completely non-toxic (**Fig. S4**). To analyze the phenotype of enhanced infection levels in more detail, HIV-1-positive cells were scored in parallel by microscopy and flow cytometry (**Fig. 20C,D**). SupT1.CCR5 cells were infected with a low virus inoculum of the reporter virus HIV-1_{NL4-3}GFP, which had been pre-incubated with PBS or HPV16 E4 (12 µM). In this experiment, 3.3% HIV-positive cells were found in the absence of E4 and 30.4% in the presence of the amyloid enhancer. As an important control, the same concentration of a peptide was used, which consisted of the same amino acids as HPV16 E4, but in a scrambled order. This so-called “E4 scrambled” (E4 scr.) peptide had no or only a minor effect on HIV infection enhancement.

Further validation of specificity of infection enhancement included drugs, which target different steps of the replication cycle. As it was possible that the peptidic aggregates might affect the first steps of virus-cell interaction, a panel of binding and entry inhibitors was evaluated. This included anti-CD4 receptor antibodies, the co-receptor antagonizing drugs AMD3100 (CXCR4), Maraviroc (MVC, CCR5), as well as the fusion inhibitor T20. Primary activated CD4 T cells were treated with these inhibitors before being exposed to HIV-1_{NL4-3} pre-incubated with either PBS, E4 or E4 scrambled. Two days post infection, a 128-fold increase of HIV-1-positive cells in the presence of E4 was observed, compared to PBS controls. Treatment with E4 scr. did not enhance HIV infection (**Fig. 21**). The anti-CD4 receptor antibodies blocked infection in all three scenarios (PBS, E4, E4 scr.), whereas the isotype control antibodies had no effect. To elucidate the role of co-receptor usage, two co-receptor blocking drugs were used. The HIV strain used in this experiment was X4-tropic and, expectedly, only AMD3100 was able to block infection, whereas MVC-pretreated cells showed infection levels comparable to untreated controls. Of note, E4 or E4 scr. had no effect on autofluorescence of cells (**Fig. 21A**, left panel).

The same experimental setup (n=2) was performed using SupT1.CCR5 cells obtaining similar results (data not shown).

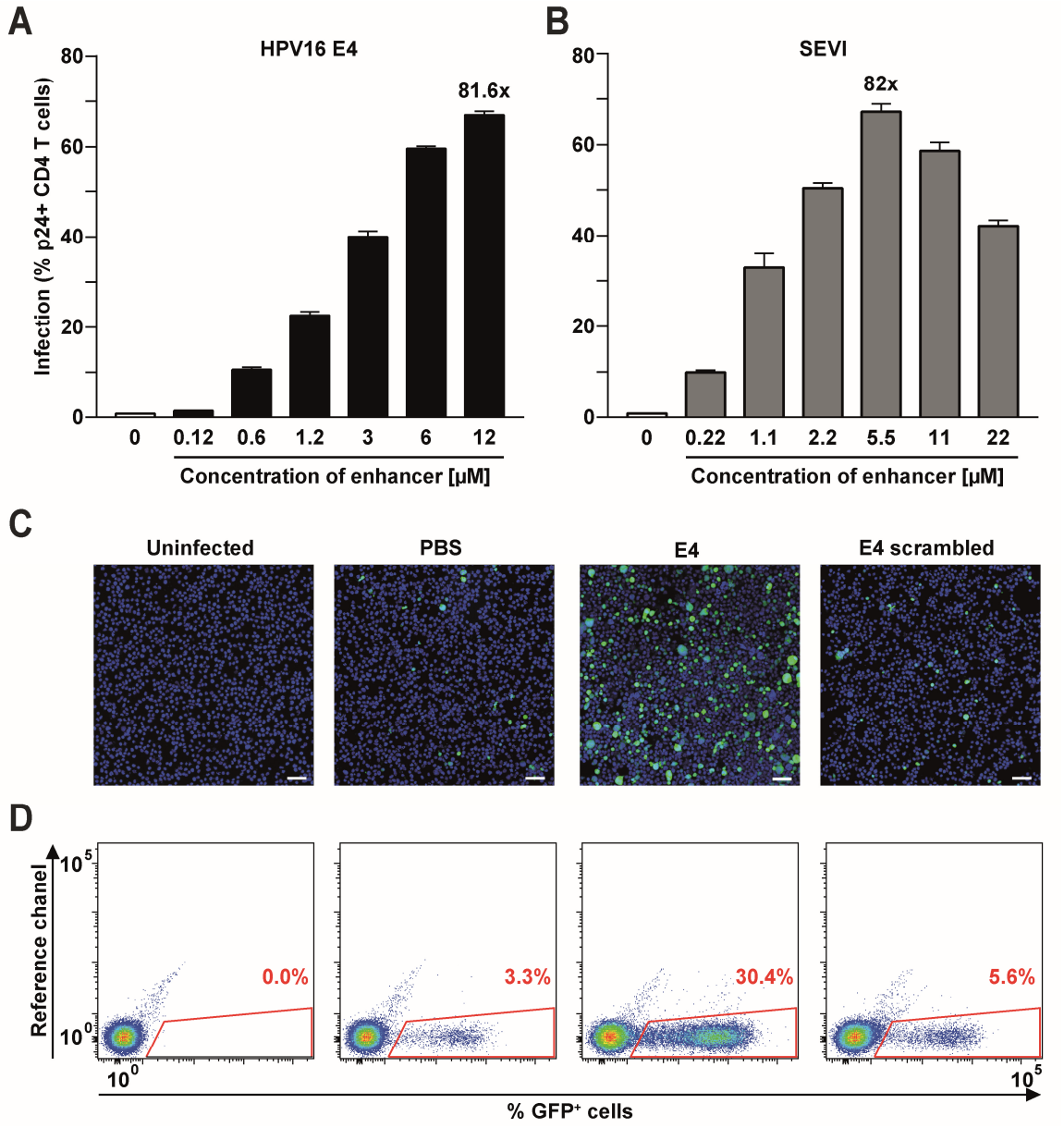

Figure 20: HPV16 E4 enhances HIV-1_{NL4-3} infection to a comparable degree as Semen-derived enhancer of virus infection (SEVI). HIV-1_{NL4-3} particles were incubated with increasing concentrations of HPV16 E4 (**A**) or SEVI (**B**). Next, primary activated CD4 T cells (donor pool) were challenged and intracellular p24 levels were measured by flow cytometry. Depicted are the arithmetic mean and standard deviation of three technical replicates. Data shown are representative data of 11 experiments. The factor of enhancement of infection is indicated on top of the histogram bars with the highest infection. (**C,D**) Visualization and quantification of HIV infection by microscopy and flow cytometry. SupT1.CCR5 cells were infected with HIV-1_{NL4-3} GFP alone, in the presence of HPV16 E4 (12 µM final concentration on cells) or the corresponding control peptide (E4 scrambled). 48 h post infection, cells were either processed for microscopy (**C**), or GFP expression was analyzed by flow cytometry (**D**). (**C**) Cells were loaded on PEI-coated coverslips and mounted with DAPI-containing medium. Scale bars represent 50 µm. Data shown are representative data of two experiments.

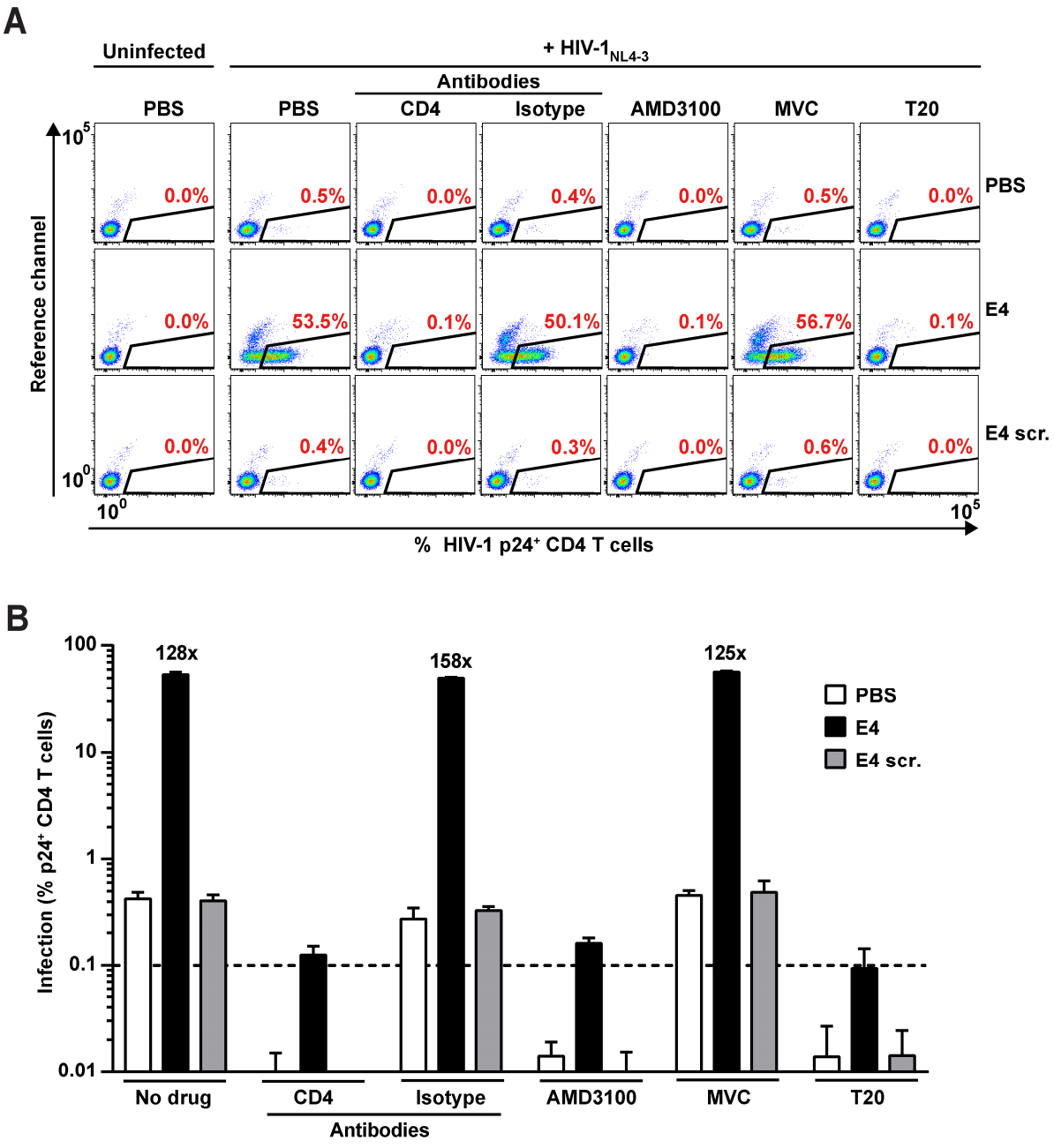

Figure 21: HPV16 E4-enhanced infection of primary activated CD4 T cells with HIV-1$_{NL4-3}$ can be blocked by specific binding and entry inhibitors. Primary activated CD4 T cells (four donor pool) were infected with HIV-1$_{NL4-3}$ in the absence (PBS/ white bars) or presence of E4 (black bars) or E4 scrambled (E4 scr., grey bars). Cells were pre-treated with different binding and entry inhibitors: primary HIV receptor-blocking anti-CD4 antibodies and corresponding isotype control antibodies (100 µg/ml), the co-receptor antagonizing AMD3100 (20 µM, CXCR4) or Maraviroc (MVC, 20 µM, CCR5) or the fusion inhibitor T20 (50 µM). Infection levels were analyzed 48 h post infection by intracellular p24 staining and subsequent flow cytometric analysis. Depicted are representative dot plots of flow cytometric measurements (**A**) and corresponding summary of analysis (**B**) from one experiment. The factor of enhancement of infection is indicated on top of each histogram bar. Shown are the arithmetic mean and standard deviation of three technical replicates.

After describing that HPV16 E4 can specifically enhance HIV-1 infection, the next step was to check the potency of the two amyloid enhancers, E4 and SEVI, for infection enhancement of

a panel of HIV strains and isolates. Analogous to the above described experimental setup, a low virus inoculum of HIV-1 lab strains, HIV-1 GFP reporter viruses, HIV-1 primary isolates, HIV-1 T/F viruses as well as the HIV-2_{V18} primary isolate was pre-incubated with increasing concentrations of E4 or SEVI and used to infect primary activated CD4 T cells. In general, the infection of all HIV strains and isolates tested could be enhanced, albeit to varying degrees (titration data see **Fig. S5, S6**; maximum factor of enhancement **Fig. 22**). For HIV-1 lab strains (**Fig. 22A, S5A-C**), the X4-tropic HIV-1_{NL4-3} reached the highest factors of increase, i.e. 98-fold for E4 and 118-fold for SEVI. The R5-tropic lab strains displayed lower factors of infection enhancement ranging from 10-fold for HIV-1_{YU-2} to 20-fold for HIV-$1_{49.5}$. The latter represents an HIV-1_{NL4-3} isogenic virus, what means that only the V3 loop of HIV-1_{NL4-3} has been replaced with the V3 loop of R5 HIV-1_{BaL}. Together, this demonstrated that peptidic infection enhancement was independent of co-receptor usage. HIV-1 GFP reporter viruses showed infection enhancements in the order of 10- to 20-fold (**Fig. 22B, S5D,E**). Analysis of the different HIV-1 primary isolates revealed that R5-tropic viruses (HIV-1_{13127} and HIV-1_{RW9}) displayed lower absolute infection levels in the presence of amyloids (~18 to 31%) compared to X4-tropic isolates (HIV-1_{2044} and HIV-1_{2005}, ~46 to 77%). Overall, infection with X4-tropic viruses was boosted to a lower degree than infection with R5-tropic strains (**Fig. 22C, S5N-Q**). Evaluation of maximum enhancement levels of infection of T/F viruses showed a range from 6- to 55-fold (**Fig. 22D, S5F-M**). Remarkably, the dual-tropic HIV-1_{CH077} T/F virus reached infection levels of 40 to 70% in CD4 T cells in the presence of amyloid enhancers, which was comparable to HIV-1_{NL4-3}.

To investigate E4-/SEVI-mediated infection enhancement of the HIV-2_{V18} primary isolate changes in RT activity of culture supernatants at the time of medium change (4 h input) and the time of harvest (“72 h p. i.") were analyzed by SG-PERT (**Fig. 22E, S6**). Also here, a concentration-dependent enhancement of RT activity was found, reflecting release of HIV-2 particles: 724-fold for E4 (12 µM) and 3821-fold for SEVI (22 µM, **Fig. 22E, S6B,C**). Interestingly, E4 and SEVI both seemed to clear free virus from the supernatant, because the presence of amyloid enhancer dropped the RT activity in the “4 h input” samples in a concentration-dependent manner **(Fig. S6A,C**). This decrease (~5- to 10-fold) is, however, considerably smaller than the detected enhancement of RT activity at “72 h p. i.” **(Fig. S6C**). The specificity of the enhancement of RT activity was validated using CD4 blocking antibodies. The presence of the anti-CD4 antibodies dramatically reduced RT activity in culture supernatants, whereas the isotype control antibodies had no significant effect (**Fig. 22E**). As a control, neither the CD4 blocking antibodies nor the isotype control antibodies had an effect on RT activity in the “4 h input” samples (**Fig. S6A**). Taken together, the infection of a broad range of different HIV-1 strains and primary isolates as well as one HIV-2 primary isolate tested

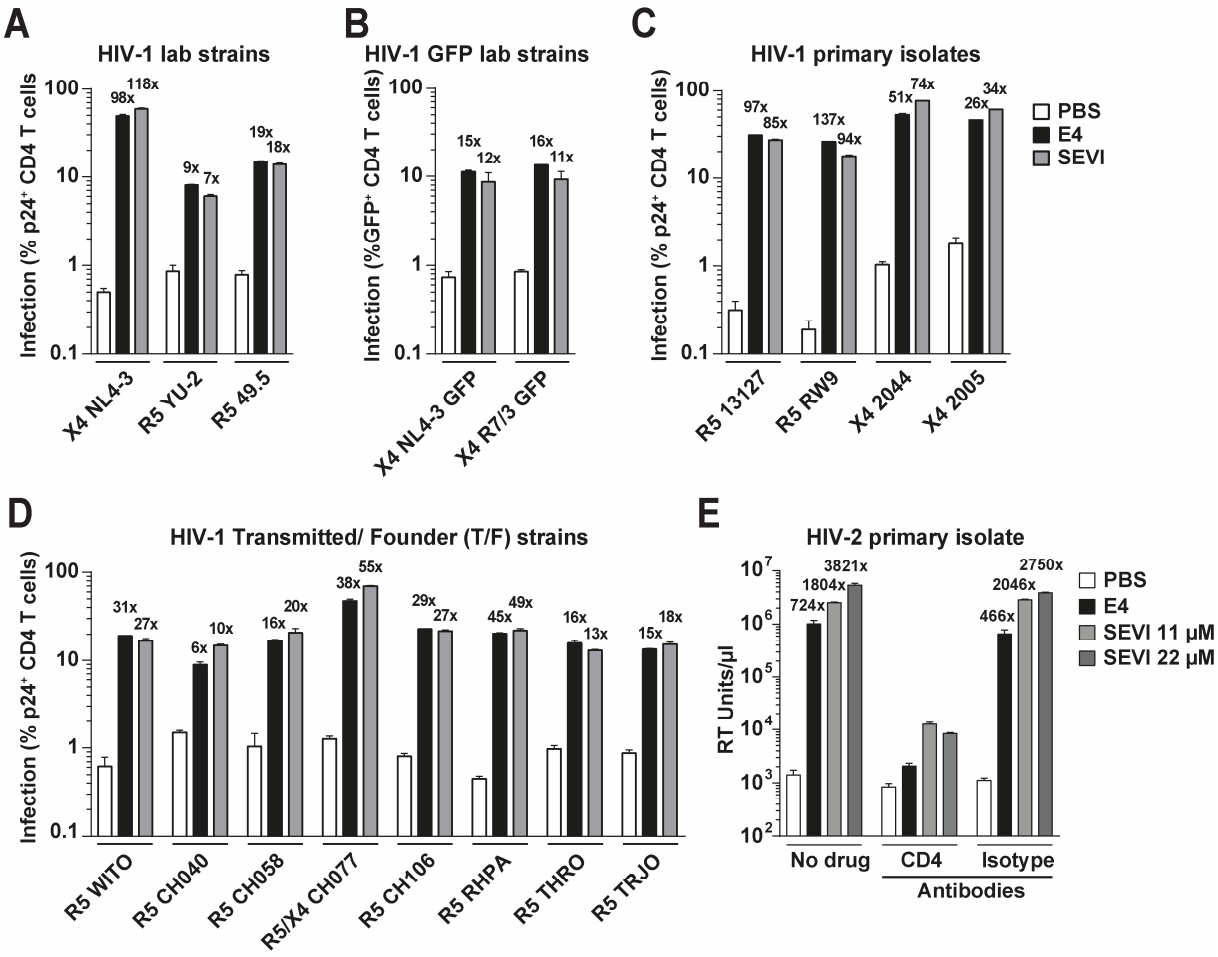

Figure 22: Effect of amyloid enhancers on infection of primary activated CD4 T cells with various HIV strains and isolates. Four donor pools of primary activated CD4 T cells were infected with a constant inoculum of the indicated HIV-1 strains or isolates as well as HIV-2_{V18} isolate in the absence (white bars) or presence of increasing concentrations of HPV16 E4 (black bars) or SEVI (grey bars). Infection enhancement was evaluated for different HIV-1 lab strains (**A**), HIV-1 GFP reporter viruses (**B**), HIV-1 primary isolates (**C**), HIV-1 T/F viruses (**D**) or HIV-2_{V18} primary isolate (**E**). Viruses were pre-incubated with PBS or one of the two amyloid enhancers for 10 min at 37°C before addition to cells. Shown are the maximum infection levels from titration experiments (for titration see **Fig. S5**). Medium change was performed four hours post infection, and infection levels (GFP-expression/ intracellular p24 levels) were measured 48 h later by flow cytometry. The factor of increase of infection is depicted on top of each histogram bar. (**E**) A donor pool of activated CD4 T cells was pre-treated with either no inhibitor, CD4 blocking antibodies, or corresponding isotype control antibodies for the highest enhancer concentrations. Next, the HIV-2_{V18} primary isolate was incubated with either PBS, E4, or SEVI, followed by challenging cells with the different solutions. 72 h post infection, supernatants were harvested and analyzed for RT activity. Depicted are the highest RT activities measured, for titrations and further controls see **Fig. S6**. The factor of enhancement of RT activity is indicated on top of each histogram bar. Depicted are the arithmetic mean and standard deviation of three technical replicates. Data shown represent either one experiment (**E**) or are representative data of two experiments (**A-D**).

were enhanced by amyloids in a concentration-dependent manner. In addition, the concentrations for optimal infection enhancement of most of the HIV-1 strains and isolates was determined: the optimum concentration for E4 was typically 12 µM and for SEVI typically 11 µM.

An observation during the testing of different HIV strains and isolates was that the absolute infection levels that could be reached in the presence of amyloids were often comparable, but the factor of enhancement varied dramatically. Assessing the infection levels in the absence of enhancing amyloids, revealed a marked variability in the basal infectivity of different strains and isolates. To further investigate this phenomenon, the X4-tropic HIV-1_{NL4-3} and the R5-tropic HIV-1_{YU-2} were chosen. Infection of primary activated CD4 T cells was performed using two different volumes of virus inoculum, which were each incubated with either PBS or constant concentrations of E4 or SEVI. This infection experiment was performed in parallel as a "normal" infection (no spin) and as a "spinoculation" (spin). In the "normal" infection condition, cells were exposed to the different infection solutions and incubated for 48 h. The "spinoculation" protocol

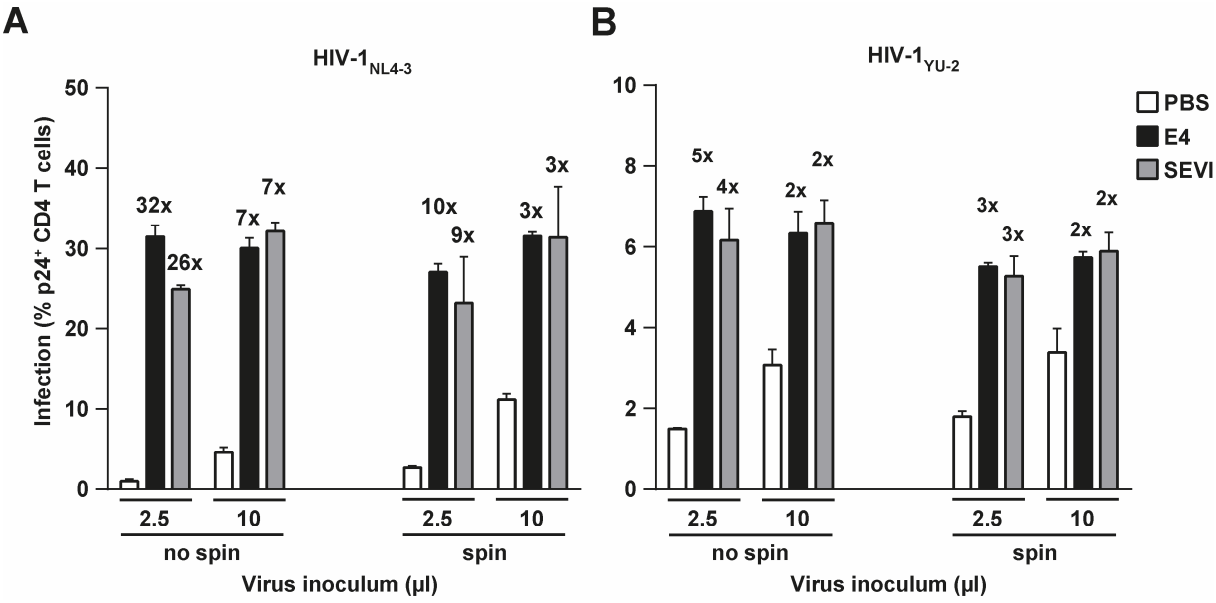

Figure 23: HPV16 E4-mediated infection enhancement is virus- and context-dependent. A donor pool of primary activated CD4 T cells was infected with two different volumes of HIV-1_{NL4-3} (**A**) and HIV-1_{YU-2} (**B**) in absence (white bar) or presence of E4 (black bar, 12 µM final concentration on cells) or SEVI (grey bar, 11 µM final concentration on cells). In parallel, normal infection (no spin) or "spinoculation" (spin) at 300 x g, 1.5 h, 37°C was performed. After a medium change four hours post infection, cells were incubated for in total 48 h, fixed and stained for intracellular p24. Flow cytometric analysis was performed. The factor of enhancement of infection is indicated on top of each histogram bar. Shown are arithmetic mean and standard deviation or three technical replicates from one experiment.

included an additional centrifugation ("spinning") step (90 min at 37°C) within the first four hours of incubation, which is supposed to facilitate HIV infection as published by Guo et al. [173] (**Fig. 23**).

Analysis of the data revealed that the infection of both viruses incubated with PBS alone (**Fig. 23**, white bars) could be markedly enhanced by "spinoculation", although the degree of spinning-induced infection enhancement was larger for HIV-1_{NL4-3} (**Fig. 23A**) than for

HIV-1_{YU-2} (**Fig. 23B**). Surprisingly, in the presence of E4 or SEVI no further infection enhancement of absolute levels of infection by "spinoculation" was visible. Additionally, infection levels seemed to saturate at a certain "virus-specific" percentage, irrespective of the initial virus inoculum or mode of infection. For HIV-1_{NL4-3}, this was in the range of 20 to 40% (**Fig. 23A**) and for HIV-1_{YU-2} in the range of 5 to 8% (**Fig. 23B**) cells positive for intracellular p24 antigen. Comparing effects that could be attributed to the virus input, differences in amyloid-mediated infection enhancement were larger for HIV-1_{NL4-3}, where an increase of MOI resulted in a ~4-fold reduced level of infection enhancement (**Fig. 23A**). For HIV-1_{YU-2}, infection enhancement was attenuated at most by 2.5-fold (**Fig. 23B**). This experiment mirrors the phenotype observed in the larger HIV panel, where an inverse correlation between the basal infection level of a strain or isolate and the magnitude of infection enhancement was observed.

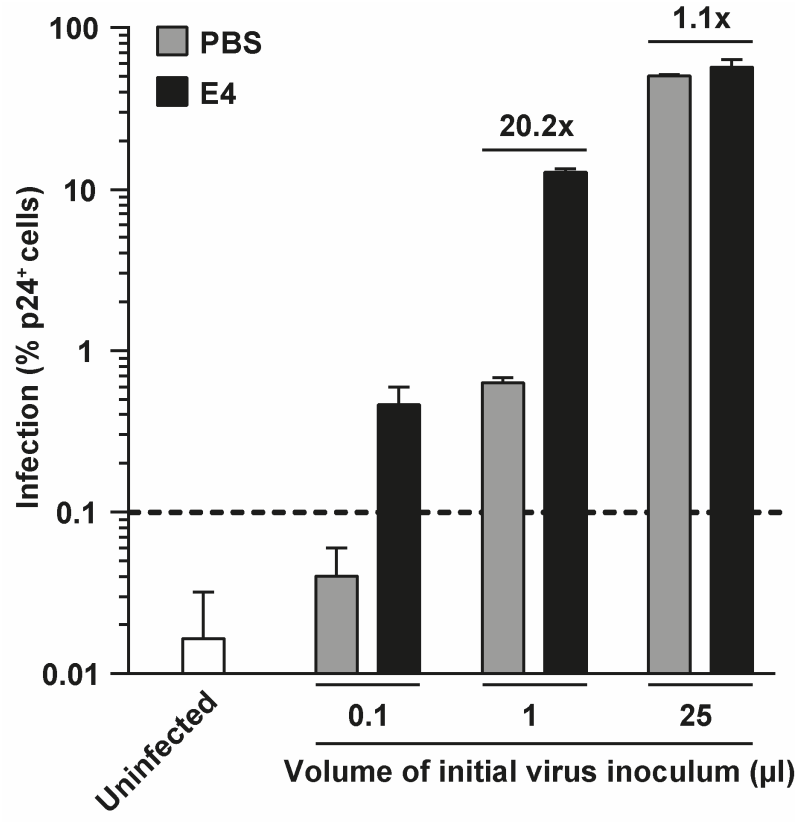

Figure 24: HPV16 E4 potentiates HIV-1 infection and spread in cell culture in an inoculum-dependent manner. The indicated volumes of HIV-1_{NL4-3} were pre-incubated with (black) or without HPV16 E4 (grey), added to SupT1.CCR5 cells and cells kept as described in material and methods section (chapter 2.4.1.8) for expansion of HIV-1 primary isolates. Five days post infection, cell aliquots of each treatment were collected, fixed, stained and analyzed for intracellular p24 levels by flow cytometry. Depicted are arithmetic mean and standard deviation of four technical replicates from one experiment. The factor of enhancement is depicted on top of the respective histogram bar.

After studying early time points of infection, it was interesting to test whether amyloid enhancers could support also a spreading HIV-1 infection. Hence, an experiment mimicking virus expansion was performed. Different volumes of HIV-1_{NL4-3} inoculum were applied, of which one was thought to be sub-infectious, one to establish a low-level infection and one a high-level infection in the absence of amyloids. These virus inocula were pre-incubated with either PBS or E4, then added to SupT1.CCR5 cells and five days later infection levels were determined (**Fig. 24**).

Experimental conditions without amyloid enhancer gave either no (<0.1%), low (0.6%) or high (56.8%) levels of infection (grey bars). In the presence of E4, the percentage of HIV-1-positive cells could be enhanced ~20-fold at initially low infection levels in the absence of the amyloid enhancer. Consistent with the previous observations, under conditions of maximal viral infection, no infection enhancement was achieved by E4 addition (**Fig. 24**). Interestingly, the presence of E4 facilitated the establishment of a productive infection, where virus alone was not infectious (0.1µl inoculum, **Fig. 24**). These data also support that amyloids could be an important experimental and diagnostic tool to allow more efficient isolation of viruses from patient with low viral loads.

To gain deeper insight into the potency of HPV16 E4 in the context of spreading infection, an endpoint titration experiment was performed (**Fig. 25**). In brief, serial dilutions of HIV-1 were added to primary activated CD4 T cells, which had been incubated with a constant concentration E4 (12 µM) or the corresponding volume of PBS. Five days later, the supernatant of each quadruplicate was analyzed for presence of p24 by ELISA and used to calculate TCID50 per ml as well as the factor of change of this value (PBS vs. E4 condition).

As reflected by images of the p24-ELISA plates (**Fig. 25A,B**) and quantified by colorimetric readout, the infectivity of the HIV-1_{13127} primary isolate could be dramatically increased, when cells had been challenged with the inoculum dilution in the presence of E4 (**Fig. 25C**). In the absence of E4, particle release (p24-positive wells, defined as ≥ 35pg/ml p24) was detectable until a virus dilution of 0.033 µl of stock, whereas in the presence of amyloid enhancer still one well was still positive for p24 at a virus inoculum of 0.00033 µl of stock. Analysis of the factor of change of TCID50/ml based on the colorimetric readout of the plates supported this, showing a 161-fold increase for the E4-exposed cells. The same experiment was performed for other HIV-1 strains and isolates (**Fig. 25D, S7**). Also here, marked changes of the TCID50/ml were observed: for the HIV-1_{NL4-3} lab strain (**Fig. 25D, S7A,B,G**) 89-fold, for the HIV-1_{CH058} T/F strain (**Fig. 25D, S7C,D,H**) 49-fold and for the HIV-1_{2005} primary isolate (**Fig. 25D, S7E,F,I**) 66-fold. Taken together, E4 did not only lead to infection enhancement in experiments investigating early time points after inoculation, but also increased spreading of different HIV-1 strains and isolates, allowing otherwise sub-infectious inocula to establish infection.

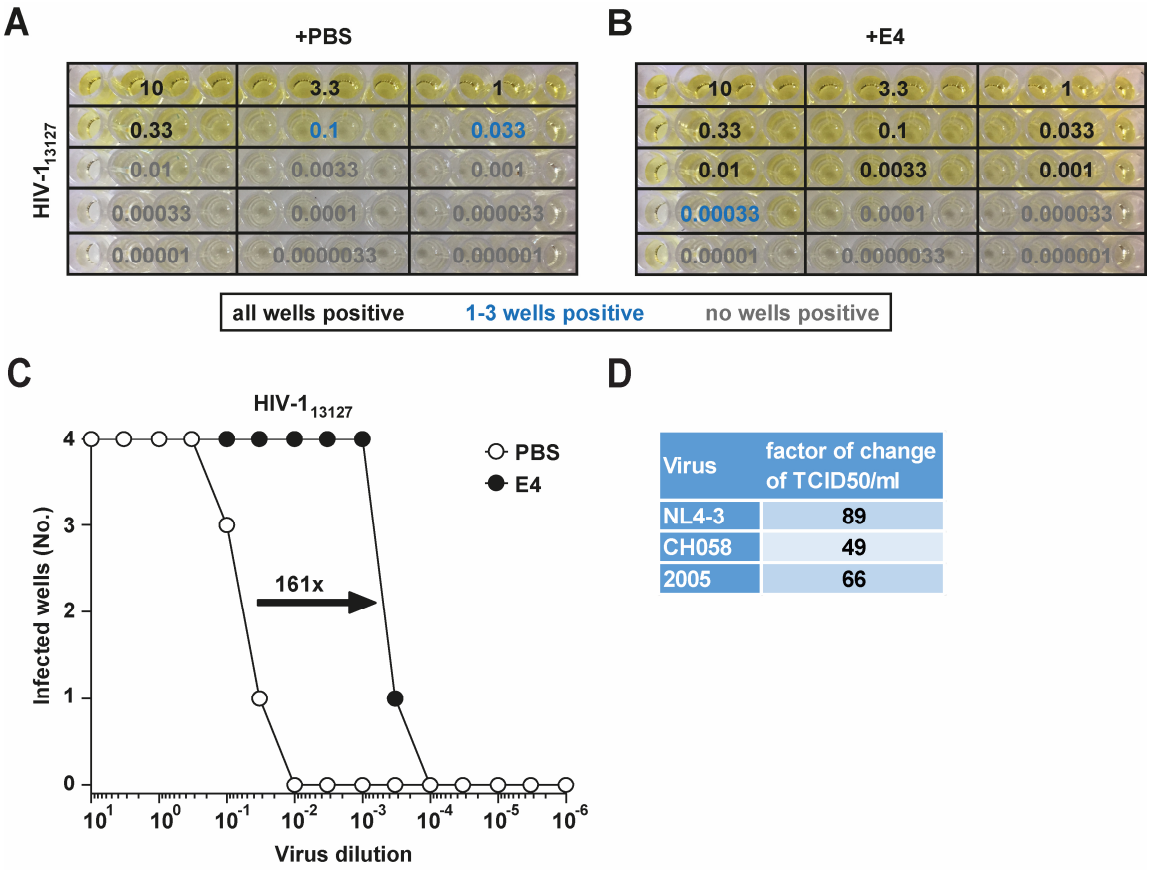

Figure 25: HPV16 E4 drastically increases HIV-1 infection in endpoint titration experiments. Primary activated CD4 T cells (four donor pool) were plated and mixed with a constant concentration of HPV16 E4 (12 µM) or the corresponding volume of PBS. Serial dilutions of HIV-1_{13127} primary isolate (other viruses see **Fig. S7**) were added and incubated for five days. The infection experiment was performed in quadruplicates. The number of HIV-1 p24-positive wells was evaluated by p24 CA ELISA. Images depict ELISA plates analyzing supernatants of the infection in presence of PBS (**A**) or E4 (**B**). A color code, based on the colorimetric readout of the plate, defines virus concentrations at which either all wells were positive (numbers in black), one to three wells were positive (numbers in blue) or no wells were positive (numbers in grey). (**C**) Number of p24-positive wells was determined by p24 CA ELISA and plotted against the dilutions of the inoculum. Based on these data TCID50/ml values and factors of change of TCID50/ml comparing PBS- and E4-treated cells were determined (**D**).

3.3 E4 peptides derived from different HPV types can enhance HIV-1 infection

After showing that: (i) HPV16 E4 mediated infection enhancement of a broad panel of different HI-viruses, (ii) each virus had an individual infection plateau to which it could be enhanced, and (iii) infection enhancement could be seen at early time points after infection as well as in spreading infection, it was important to study whether E4 peptides from other HPV types had similar properties. HPV16 belongs to the group of human *alpha-papillomaviruses*, consisting of 64 members (**Fig. 26A**), of which around 40 are known to be present at anogenital mucosa [103]. Hence, a broad panel of E4 *ΔN* (*N-terminally* truncated) peptides from different HPV types was chosen, covering HR-HPV (“high-risk”-HPV) and LR-HPV (“low-risk”-HPV) types in the context of cervix carcinoma.

Analogous to previous experiments (e.g. **Fig. 22, S5**), a titration of the different HPV E4 variants (**Fig. S8A-M**) as well as SEVI (**Fig. S8N**) was performed. Primary activated CD4 T cells were infected with different MOIs of HIV-1_{NL4-3} (0.4, 1.3 and 13) of which the lowest was used to test the concentration-dependent enhancement of infection after incubation with the different E4 peptides. Analysis of the maximum infection levels demonstrated that E4 variants derived from both HR-HPV (red) as well as LR-HPV (blue) could enhance HIV-1 infection, with different efficiencies ranging from 2- to 184-fold (**Fig. 26B**). Next, we wondered whether these variations are dependent on the physiochemical properties of the different E4 peptides. To this end, the "ProtParam" tool was employed (**Fig. S9**, used variants marked with black bars and bigger labelling). Comparing the number of amino acids (**Fig. S9A**), the isoelectric point (**Fig. S9B**), the number of negatively (**Fig. S9C**) or positively (**Fig. S9D**) charged amino acid, the resulting net charge (**Fig. S9E**) and other parameters (instability index, aliphatic index, grand average of hydropathy (GRAVY), **Fig. S9F-G**), no apparent correlation with the different infection

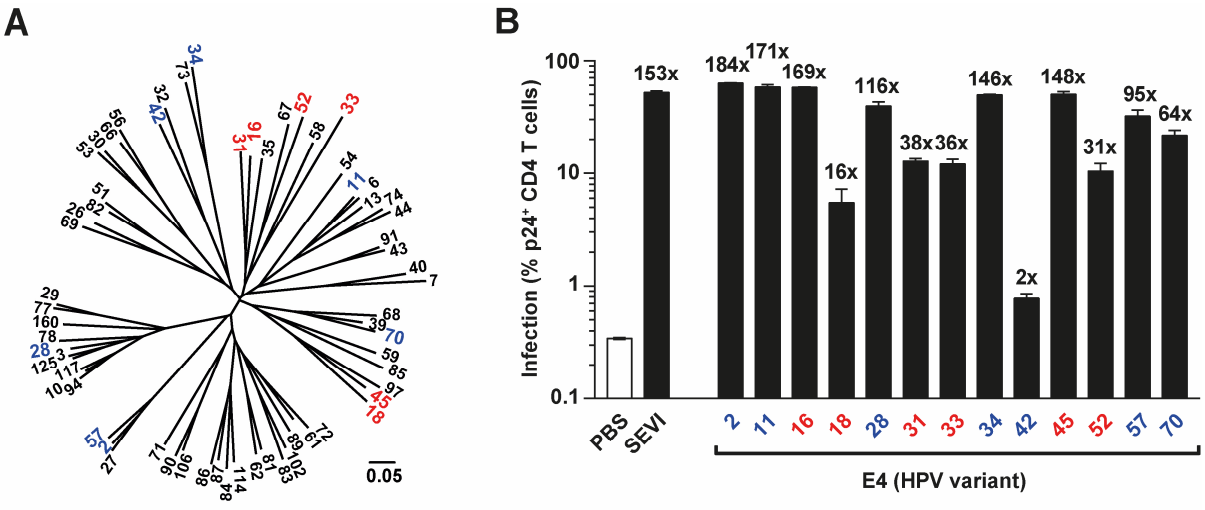

Figure 26: Enhancement of HIV-1 infection is a conserved function of HPV E4 proteins. (**A**) Overview of all human *alpha-papillomaviruses*, of which HPV variants used in this study are colored. Cervix carcinoma "high-risk" HPV (HR-HPV) variants are marked in red and "low-risk" (LR-HPV) types in blue. HPV E4 amino acid sequences were obtained from the collection database: "PaVE: the papillomavirus knowledge source" (https://pave.niaid.nih.gov/) and truncated based on John Doorbar [132]. Sequences were aligned using Clustal omega and tree files were plotted using TreeFig v1.4.3. (**B**) Primary activated CD4 T cells (four donor pool) were challenged with HIV-1_{NL4-3} at different MOIs (depicted is the lowest MOI of 0.4), of which the lowest MOI was pre-incubated with either PBS (white bar), or increasing concentrations of HPV E4 from different variants or SEVI. 48 h later, infections levels were quantified by intracellular p24 staining and subsequent flow cytometric analysis. HPV variants used for infection enhancement experiments are marked in the same color code as in (**A**). Shown are the highest infection levels reached for each peptide, for titrations and other MOIs see **Fig. S8**. Depicted are the arithmetic mean and standard deviation of three technical replicates. Data are representative of two experiments. The factor of enhancement of infection is plotted on top of each histogram bar.

enhancement properties was observed. Comparing the amino acid heterogeneity of several proteins of the different HPV types showed no striking differences between either full-length (**Fig. S10A**) or *N-terminally* truncated (**Fig. S10B**) E4 peptides. The highest conservation of amino acid sequence was found within HPV L1 (**Fig. S10C**) and HPV L2 proteins (**Fig. S10D**), with the latter displaying a slightly higher heterogeneity. Both HPV L1 and L2 are by far more conserved than HPV E4 proteins. Strikingly, although all these data suggest a huge variation between the different E4 proteins tested, they still exhibited a similar HIV infection enhancement function.

Additionally, most of the E4 peptides (HPV 2, 11, 18, 31, 33, 34, 45, 52) saturated infection enhancement at a similar concentration as HPV16 (~10 µM), whereas HPV 28, 57 and 70 saturated at a 10-fold lower concentration (**Fig. S8**). Comparing the maximal E4-enhanced infection levels to the highest used MOI of 13 in the absence of amyloid enhancer, which contained a 32.5-fold higher virus inoculum, in most of the cases, a higher infection level was reached with the low MOI of 0.4 plus E4 (HPV2, 11, 16, 28, 34, 45, 57). For some E4 variants a similar magnitude of infection (HPV31, 33, 52, 70) and only for HPV18 an infection level lower than the highest MOI was reached. Of note, the E4 peptide derived from HPV42 was able to enhance infection by only 2-fold, and thus to a far lesser degree than the other tested variants (**Fig. S8I**). The decline of infection enhancement in the case of HPV28 at the highest concentration was observed in two independent experiments (data not shown) and might be explained by a concentration-dependent decrease of vital cells due to higher rates of infection. SEVI, analyzed in parallel, peaked in these experiments at a concentration of 2.2 µM and at infection levels higher than achieved with the MOI of 13. Agitation of SEVI is dependent on many factors (e.g. synthesis specific differences, plastic, etc.) and therefore can result in stocks of varying potential to enhance HIV infection. In conclusion, the phenotype of HIV-1 infection enhancement is not restricted to the E4 *ΔN* peptide from HPV 16, but is a conserved characteristic of *N-terminally* truncated E4 from *alpha-papillomaviruses*.

3.4 Characterization of the initial interaction of virus, cell, and infection enhancers

The potency of E4 and SEVI has in this thesis thus far been primarily studied at the level of productive infection of cells. Here, we wanted to characterize the earliest steps of the interaction of virus and amyloid enhancers with target cells. In a first approach, we sought to visualize this early interaction. To this end, HIV-1 particles carrying eGFP-Vpr [169], generating green fluorescent virions, were produced. These particles were pre-incubated with either PBS, E4, or E4 scrambled, before adding them to a donor pool of primary activated CD4 T cells. After short-time incubation, cells were fixed and stained for actin, chromatin as well as E4. Analysis of the merged images showed, that E4 locally accumulated together with large amounts of

virus particles (**Fig. 27**). In the condition where virus was pre-incubated with PBS or the E4 scrambled control peptide, this phenomenon was not detectable (**Fig. 27, S11**). When comparing the signals for E4 and HIV-1 eGFP-Vpr (**Fig. S11**) a frequent co-localization is apparent. Cells appeared to closely interact with the E4-virus-clusters. E4 aggregates seemed to locally concentrate HIV-1 particles, looking almost like the latter could be presented to target cells.

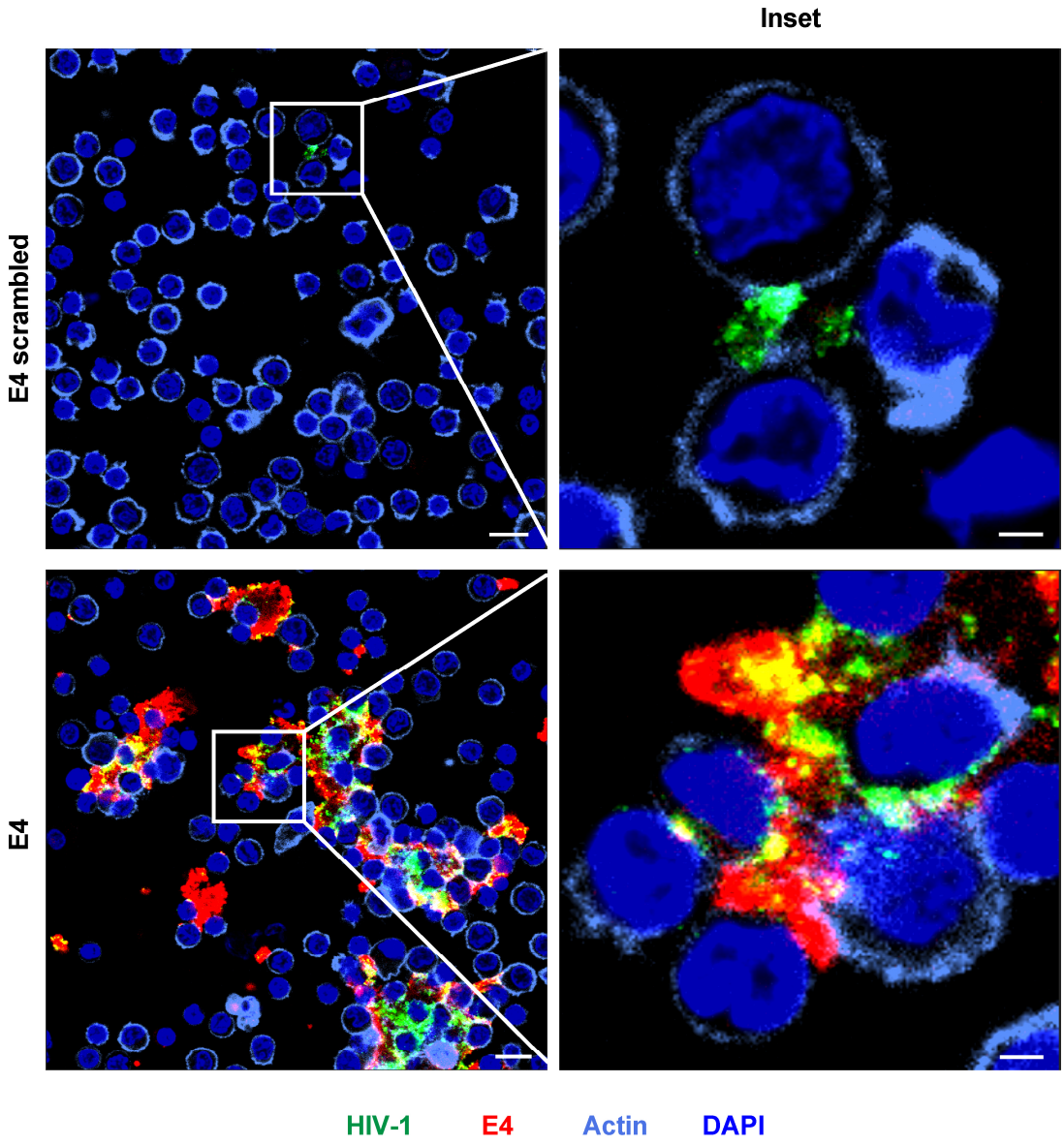

Figure 27: HPV16 E4 is able to concentrate HIV-1 particles locally. Cells of a donor pool of primary activated CD4 T cells were plated on poly-L-lysine-coated coverslips and incubated for 90 min with eGFP-Vpr-carrying HIV-1_{NL4-3} particles, which were pre-treated with either PBS, E4, or E4 scrambled (12 µM final concentration on cells). After fixation, cells were stained on the coverslips for actin (light blue, Alexa Fluor 647 Phalloidin), E4 (red, anti-E4 NA7-AA5 plus goat anti-mouse Alexa Fluor 568) and chromatin (dark blue, DAPI). Shown are the conditions with E4 scr. (upper panel) or E4 (lower panel). Right columns show a magnification of the inset marked in the left columns. Other conditions are shown in **Fig. S11**. Scale bars: 10 µm (inset: 2 µm).

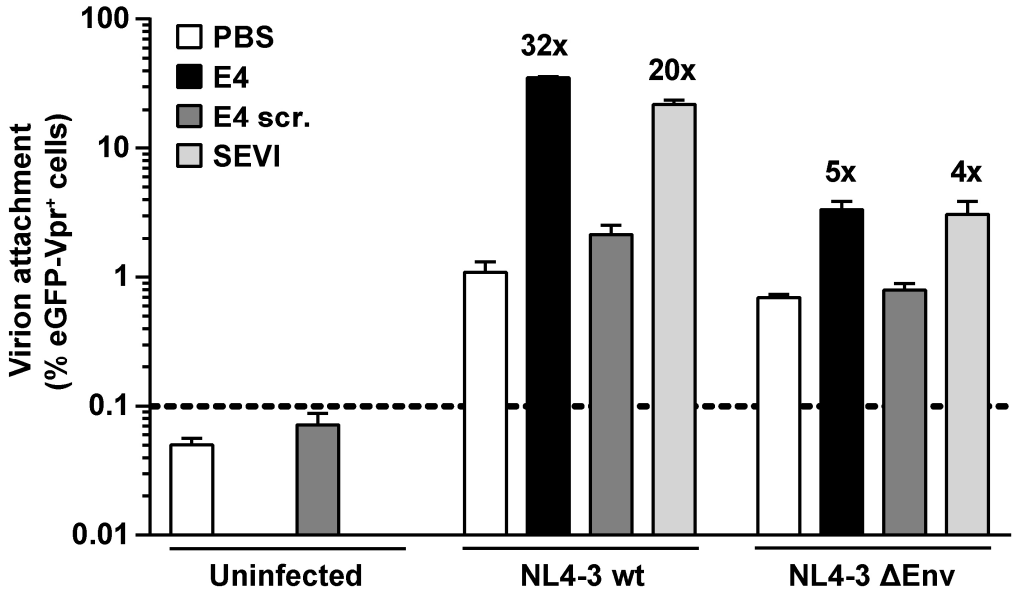

Figure 28: Peptidic enhancers of infection increase attachment of HIV-1 virions to target cells. Attachment of viral particles is partially Env-dependent. A donor pool of primary activated CD4 T cells was incubated for 1 h with eGFP-Vpr-carrying HIV-1_{NL4-3}wt and HIV-1_{NL4-3}ΔEnv particles pre-treated with either PBS, 12 µM E4/ E4scr., or 2.2 µM SEVI (final concentration on cells). Incubation of viruses with cells was carried out in the presence of T20 (50 µM) and at 20°C. Depicted are the arithmetic mean and standard deviation of three technical replicates of one representative experiment. The factor of enhancement of eGFP-Vpr-positive cells is indicated on top of the respective histogram bar.

First binding of viruses to cells can occur via heparansulfate proteoglycans (HSPG) or in a virus receptor-dependent fashion, both being dependent on Env. To further evaluate the data obtained by microscopy, a virion-attachment assay using either HIV-1_{NL4-3}wt or HIV-1_{NL4-3}ΔEnv was performed. The two viruses were incubated with E4 or SEVI, with PBS and E4 scr. serving as negative controls. Both in the absence of amyloid enhancers E4/SEVI or in the presence of the control peptide, virus particles were able to bind to target cells. Attachment of HIV-1_{NL4-3}wt was enhanced after incubation with E4 by 32-fold, whereas binding of HIV-1_{NL4-3}ΔEnv was boosted by ~5-fold (**Fig. 28**). The enhancement of HIV-1_{NL4-3}wt virion binding in the presence of 11 µM SEVI was ~80-fold (data not shown). For better comparison, the concentration of SEVI (2.2 µM) leading to a similar magnitude of attachment (20-fold) as E4, is depicted. Here, the same phenotype as for E4 was visible when comparing HIV-1_{NL4-3}wt and HIV-1_{NL4-3}ΔEnv, suggesting that the loss of Env allowed only a reduced, but still significant increase of virion binding. Of note, if higher concentrations of SEVI (11 µM) were applied differences between HIV-1_{NL4-3}wt and HIV-1_{NL4-3}ΔEnv in the numbers of eGFP-Vpr-positive primary activated CD4 T cells could no longer be detected (data not shown). Similar observations were made using SupT1.CCR5 cells, where absolute levels of attachment for Env-deficient particles were low for low SEVI concentrations, but not when high concentrations of SEVI were used (data not shown).

Next, a larger panel of HIV-1 strains was used to assess enhancement of virion attachment in the presence of HPV16 E4: besides HIV-1_{NL4-3}wt and HIV-1_{NL4-3}ΔEnv these included HIV-1_{YU-2} and the T/F strains HIV-1_{CH058} as well as HIV-1_{CH077}. These eGFP-Vpr-carrying viruses were also characterized for infectivity (**Fig. S12A,C**) and presence of p24 antigen in virus stocks (**Fig. S12B**), demonstrating that all viruses, but HIV-1_{NL4-3}ΔEnv, were infectious. Incubating increasing volumes of either HIV-1_{NL4-3}wt (**Fig. S13A**), HIV-1_{NL4-3}ΔEnv (**Fig. S13B**), HIV-1_{YU-2} (**Fig. S13C**), HIV-1_{CH058} (**Fig. S13D**) and HIV-1_{CH077} (**Fig. S13E**) with either PBS, E4, or E4scr., revealed that E4 could specifically enhance virion attachment. The degree of attachment in most scenarios depended on the MOI. For HIV-1_{NL4-3}, it is likely that this experimental system was already saturated and therefore not MOI-dependent. For HIV-1_{YU-2} (**Fig. S13C**), virus only or in presence of the control peptide, no virion attachment was detectable. In contrast, the presence of E4 led to a detectable binding of virus particles, whose degree was dependent on the virus input. Taken together, these results indicate that HPV16 E4-mediated enhancement of virion attachment is partially dependent on the envelope glycoprotein. For SEVI, Env dependency was overcome by higher concentrations of the seminal peptide.

As the next step in the replication cycle of HIV following attachment is the fusion of the virus particle with the target cell, we investigated whether HPV16 E4 enhanced this process. Thus, a virion-fusion assay was employed, in which a fusion protein of the HIV-1 Vpr protein and a beta-lactamase (BlaM) was incorporated into virus particles during production in HEK293T cells [168]. After fusion of HI-viruses carrying BlaM-Vpr to the cells, the latter were incubated with the CCF2 dye, whose BlaM-dependent cleavage can be measured by flow cytometry (**Fig. S14A**). T20 served as a specificity control, since it efficiently inhibits gp41-dependent fusion of HIV-1. Virion fusion was assessed for the following HIV-1 strains: HIV-1_{NL4-3}BlaM, HIV-1_{YU-2}BlaM, HIV-1_{CH058}BlaM and HIV-1_{CH077}BlaM.

First, we characterized their fusion to primary activated CD4 T cells and to SupT1.CCR5 cells. Maximum virion fusion levels for the X4-tropic HIV-1_{NL4-3}BlaM, reached 11% for CD4 T cells and 59% for SupT1.CCR5 cells (**Fig. S14B**). The fusion rate of the R5-tropic lab strain HIV-1_{YU-2}BlaM (**Fig. S14C**) was generally low (10% at maximum on SupT1.CCR5 cells). Interestingly, the T/F strains HIV-1_{CH058}BlaM (R5-tropic, **Fig. S14D**) and HIV-1_{CH077}BlaM (dual-tropic, **Fig. S14E**) showed maximum fusion levels of ~75 to 91% on SupT1.CCR5 cells. Of note, BlaM-Vpr-carrying viruses displayed strongly reduced infectivity, as seen e.g. for HIV-1_{NL4-3} and HIV-1_{YU-2}, resulting in maximum infection levels of 0.1% on primary activated CD4 T cells and of 0.5% on SupT1.CCR5 cells (data not shown). This was also reflected by lowered titers on the HIV reporter cell line TZM-bl (BCA titer) (**Fig. S14F**).

To determine whether virion fusion of these strains could also be altered by amyloids, increasing concentrations of E4 or SEVI were incubated with BlaM-Vpr-carrying HIV-1_{NL4-3}, HIV-1_{YU-2}, HIV-1_{CH058} or HIV-1_{CH077}. Similar to infection experiments (**Fig. 22**), also fusion of virions to

primary activated CD4 T cells was markedly enhanced in a concentration-dependent manner. Analyses demonstrated for HIV-1_{NL4-3}BlaM ~42- to 64-fold (**Fig. S15A**), for HIV-1_{YU-2}BlaM ~33- to 43-fold (**Fig. S15B**), for HIV-1_{CH058}BlaM ~15- to 18-fold (**Fig. S15C**), and for HIV-1_{CH077}BlaM ~32- to 35-fold (**Fig. S15D**) increase in the percentage of fusion-positive cells.

After basic characterization these reporter virions, they were employed in an enhancer-inhibitor experiment using primary activated CD4 T cells, which had been pre-treated with the previously used panel of binding and entry inhibitors: anti-CD4 antibodies, isotype control antibodies, AMD3100, MVC, or T20 (**Fig. 29, S16**). A constant concentration of E4 or E4 scr. (**Fig. 29A,C, S16A,C**) as well as SEVI or SEVI control (SEVI Ctrl) (**Fig. 29B,D, S16B,D**) was

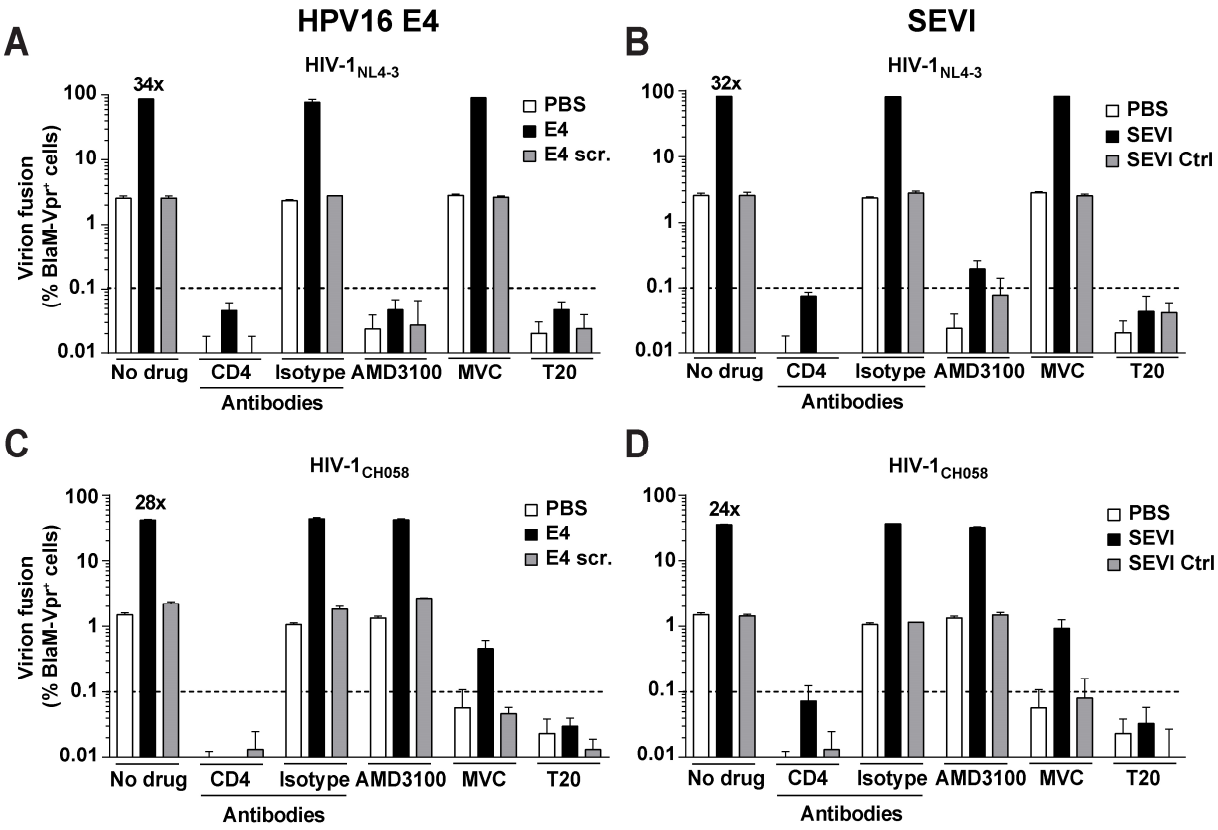

Figure 29: Enhancers of infection potentiate virion fusion of particles from different HIV-1 strains to target cells in a receptor-dependent manner. HIV-1_{NL4-3} (**A,B**) or HIV-1_{CH058} (**C,D**) virions carrying BlaM-Vpr were pre-incubated in the presence or absence of HPV16 E4/ E4scr (12 µM) (**A,C**) or SEVI (11 µM)/ SEVI Ctrl (25.9 µM) (**B,D**) and then used to infect primary activated CD4 T cells. These peptide concentrations represent final concentrations on cells. For other viruses used, see **Fig. S16**. Cells were pre-treated with different binding and entry inhibitors: anti-CD4 antibodies and corresponding isotype control antibodies (100 µg/ml), AMD3100 (20 µM, CXCR4 antagonist) or Maraviroc (MVC, 20 µM, CCR5 antagonist) or the fusion inhibitor T20 (50 µM). Four hours later, cells were washed and incubated with the CCF2 staining solution. After overnight incubation, cells were fixed and BlaM-Vpr-dependent cleavage of CCF2 in infected cells was quantified by flow cytometry. Depicted are the arithmetic mean and standard deviation of three technical replicates from one experiment. Data represent one experiment (**C,D**) or are representative of two experiments (**A,B**) The factor of enhancement of virion fusion is indicated on top of the histogram bar of the no drug condition.

incubated with HIV-1_{NL4-3}, HIV-1_{YU-2}, HIV-1_{CH058} or HIV-1_{CH077} all carrying BlaM-Vpr. SEVI Ctrl, (PAP267-282) represents a shorter peptide fragment of PAP, which is unable to form amyloids and has been shown by Münch et al. [74] to not enhance infection. Fusion of all viruses could be enhanced by E4 and SEVI up to ~40-fold, whereas the respective control peptides had no effect (**Fig. S16E**). More detailed analysis revealed that for X4 HIV-1_{NL4-3} (**Fig. 29A,B**) E4 and SEVI increased fusion by ~30-fold, which could be specifically blocked by either CD4 blocking antibodies, AMD3100 or T20. The respective controls (isotype antibodies and MVC) did not alter the fusion efficiency. The R5 T/F strain HIV-1_{CH058} (**Fig. 29C,D**) and the lab strain HIV-1_{YU-2} (**Fig. S16A,B**) showed enhanced fusion in the range of 24- to 28- fold in the presence of amyloid enhancers. All drugs, apart from the co-receptor targeting ones, behaved as seen for HIV-1_{NL4-3}. Due to the CCR5 tropism of these two viruses AMD3100 had no effect, whereas MVC specifically blocked infection. As a side note, MVC was not as potent as AMD3100 in the presence of amyloid enhancers for their respective viruses, still allowing 0.5 to 0.6% fusion. Studying tropism-dependent effects was most interesting for HIV-1_{CH077} carrying BlaM-Vpr (**Fig. S16C,D**), an isolate described to be dual-tropic [174]. In line with this, neither AMD3100 nor MVC blocked infection efficiently. Only the anti-CD4 antibodies and T20 were able to completely suppress virion fusion of this isolate to primary activated CD4 T cells. Taken together these data indicated that (i) E4 and SEVI can enhance fusion of viral particles to target cells, (ii) the enhancement is independent of co-receptor tropism but (iii) can be blocked using specific binding and entry inhibitors of HIV infection.

3.5 Elucidation of the interplay of HPV16 E4 and HIV and of HPV16 E4 and SEVI

HPV E4 is present at HIV transmission sites [3, 103, 115] and can be found in HPV-induced lesions of cervix (**Fig. 30A**), anus (**Fig. 30B**) and penis (**Fig. 30C**), where keratinocytes at the epithelial surface as well as the lower regions contain large amounts of E4 protein, as shown by immunohistochemistry. Data were obtained in collaboration with Prof. M. Dürst (Department of Gynecology, Jena University Hospital – Friedrich Schiller University, Jena, Germany) and Prof. N. Brockmeyer, (Department of Dermatology, St. Josef-Hospital, Ruhr-University Bochum, Bochum, Germany). Further characterization by multi-epitope ligand cartography (MELC), which allowed staining of a large number of different epitopes on the same tissue slide, revealed close proximity of HIV target cells (CD4 T cells and macrophages) and HPV E4 within a CIN lesion (data obtained in collaboration with Prof. A. Baur, Department of Dermatology, University Hospital Erlangen, Erlangen, Germany) (**Fig. 30D,E**). Taken together, these data demonstrated that within HPV-induced lesions of the anogenital mucosa, which represent potential HIV transmission sites, both desquamating keratinocytes expressing large amounts of E4 as well as infiltrating HIV target cells could be monitored.

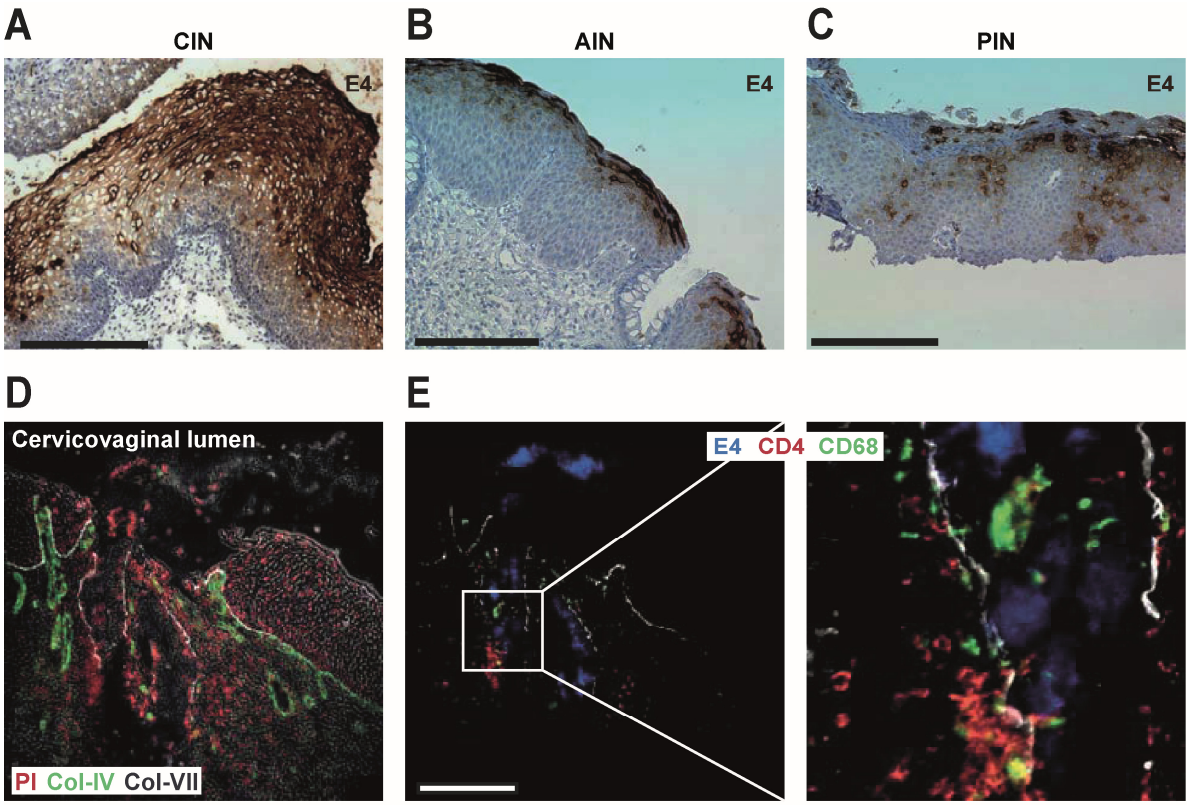

Figure 30: Immunocharacterization of E4 expression in HPV-positive lesions in anogenital tissue. (A-C) Detection of E4 (brown staining) by immunohistochemistry (IHC) in epithelial biopsy samples, previously characterized as HPV DNA-positive CIN (**A**), AIN (**B**) and PIN (**C**) lesions. (**D+E**) Analysis of protein expression and distribution of immune cells in a frozen section of a HPV16-positive CIN lesion by multi epitope ligand cartography (MELC). Images represent overlays of the indicated epitopes/markers for the identical position of the tissue section: (**D**) Propidium iodide (PI, nuclei), Collagen-IV (Col-IV/ collagen in basal lamina), Collagen-VII (Col-VII/ collagen in basement membrane); (**E**) HPV-E4 (E4), CD4 (primarily CD4-positive T cells), CD68 (macrophages). Scale bars: 200 µm. IHC data were generated in collaboration with Prof. M. Dürst (Department of Gynecology, Jena University Hospital – Friedrich Schiller University, Jena, Germany) and Prof. N. Brockmeyer (Department of Dermatology, St. Josef-Hospital, Ruhr-University Bochum, Bochum, Germany) and MELC data in collaboration with Prof. A. Baur (Department of Dermatology, University Hospital Erlangen, Erlangen, Germany).

The results shown so far indicate that E4 is able to locally concentrate HIV particles and in that way serve as a platform for target cells to get exposed to virus and then infected. *In vivo*, the time-span until free infectious virus particles encounter conceivably a target cell can vary considerably. The same is true for the time until a cell binds to E4-virus-clusters, what led to the question whether the amyloid enhancer could alter the “infectious half-life” of HI-viruses. To investigate this, a thermostability assay was conducted, in which HIV-1_{NL4-3} virions were incubated at 37°C for increasing time periods (0 to 48 h) with PBS alone or in the presence of E4 or E4 scrambled. In parallel, a “high MOI” reference condition was used, which contained ~15-fold more virus in the absence of amyloid enhancer. SupT1.CCR5 cells were challenged

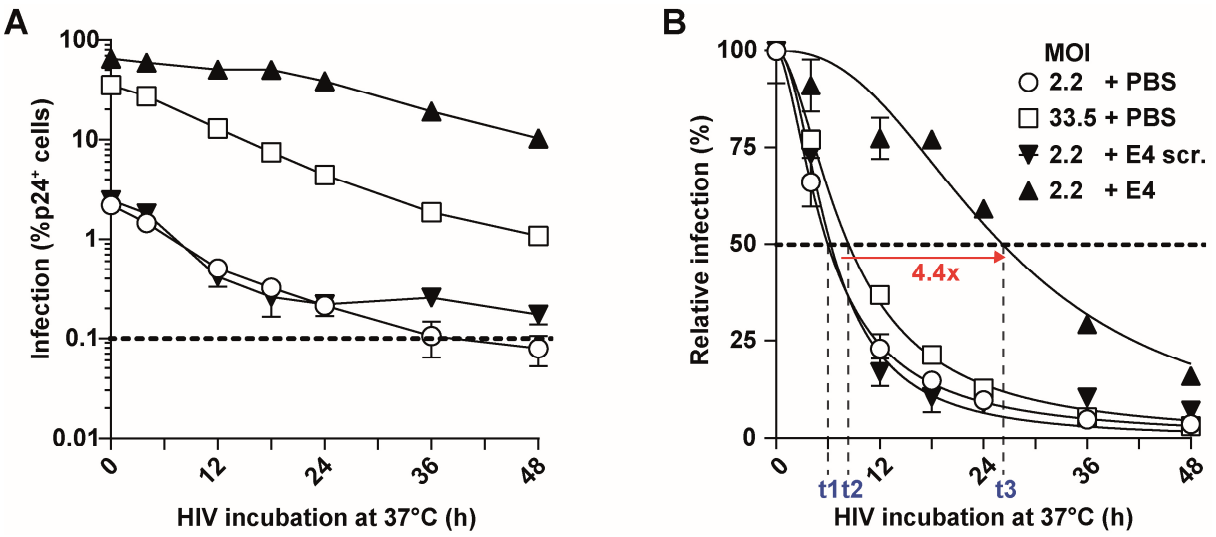

Figure 31: HPV16 E4 increases the temperature stability of HIV-1 particles. A "low MOI" (2.2) of HIV-1_{NL4-3} particles was incubated with PBS, E4/ E4 scr. (12 µM final concentration on cells) for the indicated time periods (0 to 48 h) at 37°C. Also a "high MOI" (33.5) reference control incubated with PBS was used. SupT1.CCR5 cells were exposed to the different solutions and, four hours later, a medium change was performed. Subsequently, cells were supplied with fresh medium containing the fusion inhibitor T20 (50 µM). Infection levels, as shown in (**A**), were determined 48 h post infection by flow cytometric analysis of intracellular p24 levels. Data were normalized and using GraphPad Prism fitting to a non-linear dose response curve allowed calculation of the different half-lifes, t1-t3 (**B**). Depicted are the arithmetic mean and standard deviation of three technical replicates from one experiment.

with the different conditions and four hours later, cells were supplied with fresh medium containing T20, allowing the assessment of the infectivity of solely the input virus. Infection levels were determined and data were normalized, allowing comparison of the half-lifes of virion infectivity for the different conditions. Prolonged incubation (>24 h) of HIV-1_{NL4-3} at an MOI of 2.2 at 37°C with PBS or E4 scr. dropped infectivity almost to background levels (**Fig. 31**). For MOI 33.5, infectivity dropped by 32.6-fold. Interestingly, after 48 h of incubation at 37°C, the high virus inoculum still allowed for a productive infection of ~1% of CD4 T cells. Most remarkably, the "low MOI" in combination with E4 led at all time points of pre-incubation at 37°C to a higher level of infection than the "high MOI" reference, and only a 6.3-fold loss of infection was noted at 48 h. The fact that after 48 h of incubation of HIV-1_{NL4-3} with E4, virus could still lead to an infection of 10.3% was outstanding, since this level was ~10-fold higher than for the "high MOI" condition and ~60-fold higher than the "low MOI" together with E4 scrambled. The "low MOI" plus PBS, resulted in ~100-fold lower numbers of p24-positive T cells than in the presence of E4 (**Fig. 31A**). This experiment was also performed for primary activated CD4 T cells, but without the addition of T20, with similar effects being observed (data not shown). The "low MOI" condition incubated with PBS or E4 scr. displayed a half-life of ~6 h (t1), the "high MOI" condition of 8.4 h (t2) (**Fig. 31B**). The presence of E4 increased the half-life of virus particles

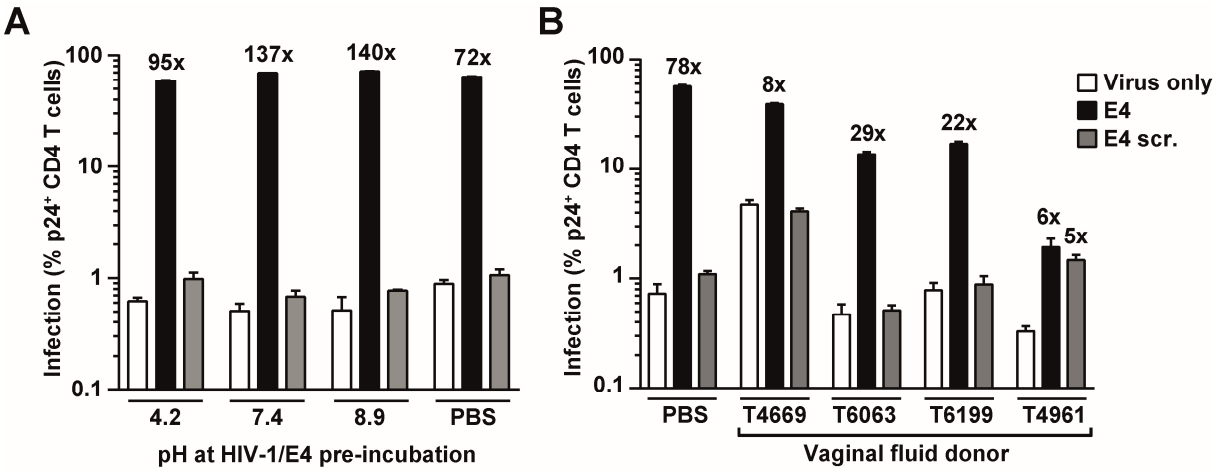

Figure 32: An infection-enhancing interaction of HPV16 E4 and HIV-1_{NL4-3} is possible in a wide range of pH environments and in vaginal fluid. (**A**) Effect of pH on interaction between HIV-1 and E4. HIV-1_{NL4-3} was pre-incubated in the absence or presence of HPV16 E4/ E4 scr. (12 µM final concentration on cells) in PBS or RPMI with the indicated pH values (4.2, 7.4, 8.9). (**B**) Effect of vaginal fluid on the E4-mediated enhancement of HIV-1 infection. HIV-1_{NL4-3} was pre-incubated alone or together with HPV16 E4/ E4 scr. (12 µM final concentration on cells) in PBS or vaginal fluid from four different donors. Afterwards, a donor pool of primary activated CD4 T cells was challenged for 48 h with the different mixes from (**A,B**). A medium change was performed four hours post challenge to synchronize infection. Infection levels were analyzed by intracellular p24 staining followed by flow cytometry. Depicted are the arithmetic mean and standard deviation of three technical replicates. Data represent one experiment (**A**) or are representative of three experiments (**B**). Factor of enhancement of infection is indicated on top of each histogram bar.

at “low MOI” by ~4.4-fold (t3=26.2 h). Thus, the presence of HPV16 E4 can markedly prolong the infectivity of HIV-1 particles.

In the context of sexual transmission, virus particles may have to resist different pH environments: whereas the vaginal pH is rather acidic (~4.5) [175], it is more or less neutralized if semen is present (semen has a pH of 7.2 to 8.2 [176]) , and the anal pH is slightly basic (7.9) [177]. Since pH can affect folding and in that way, also the structure of proteins, the next step was to study, whether the interaction between HIV-1 and E4 and the resulting infection enhancement could be altered by pH (**Fig. 32A**). To test this, HIV-1_{NL4-3} was pre-incubated for 10 min either alone or with E4/E4 scr., in either PBS or in RPMI medium with pH values adjusted to either 4.2, 7.4 or 8.9. Mixes were then used to challenge primary activated CD4 T cells. E4 and virus incubated in PBS led to a 72-fold enhancement of infection. In line with previous experiments, the E4 scr. control peptide did not enhance infection. The different pH exposures did not markedly alter the degree of infection enhancement, which was in the range of 95- to 137-fold. Also, absolute infection levels under different pH environments in the presence of E4 showed only small variations.

To further investigate whether the infection-enhancing E4-HIV interaction could take place under physiological conditions, the interaction was allowed to occur in vaginal fluid of several

donors. HIV-1_{NL4-3} was incubated alone or with E4/ E4 scr. either in PBS or in vaginal (**Fig. 32B**). Again, enhanced infection of primary activated CD4 T cells was visible at all treatments where E4 was present, with 78-fold enhancement of infection in the PBS reference control. Incubation in vaginal fluid resulted in an overall reduction in absolute infection levels in the presence of E4 (~1.5- to 29.4-fold lower levels of p24-positive cells), still allowing infection enhancement of ~6- to 29-fold. Moreover, the percentage of p24-positive cells was modulated by incubation with vaginal fluid when virus was used either alone or pre-treated with E4 scrambled. Interestingly, in the case of donor T4669 infection in both control scenarios was elevated by ~6-fold compared to the PBS control, indicating the presence of other factors in vaginal fluid that can modulate the susceptibility of cells to HIV infection. In line with this, vaginal fluid of donor T4961 caused a reduction of infection in the virus only condition and an increased infection when E4 scr. was present. Interestingly, for some donors the infection enhancement capability varied for samples taken on different time points (data not shown). Taken together, these data suggested that interactions between HPV16 E4 and HIV-1 that can lead to enhanced infection, can take place at acidic, neutral and basic pH as well as in vaginal fluid.

Given the fact that semen is the main vector for transmission of HIV [73], that SEVI requires seeding to be active [74] and that E4 forms aggregates in aqueous solution spontaneously, it was of interest, whether E4 could facilitate the amyloid fibril formation of SEVI. This kind of cross-peptide-species seeding is also known from other amyloids, as e.g. the diabetes-associated islet amyloid peptide (IAPP) can seed β-amyloid implicated in Alzheimer's disease [150]. As a note, co-administration of E4 and SEVI in infection experiments was neither reducing enhancement nor causing synergistic effects (data not shown). As described above, amyloid formation of SEVI in a lab environment requires seeding and agitation by overnight shaking at 37°C. To investigate E4-mediated seeding of SEVI, an experimental setup was designed, in which low concentrations of E4, E4 scr. or the respective volume of PBS were spiked into a large volume of a non-seeded SEVI solution. A titration of E4 and the control peptide (0.024 to 0.6 µM), was performed to test for concentration dependency and mixes were incubated overnight without shaking at 37°C (**Fig. 33A**). The highest E4 concentration was chosen based on previous titrations, with the aim to reach a low but significant infection enhancement. Next, HIV-1_{NL4-3} was incubated with the different seeding mixes, and primary activated CD4 T cells were challenged. Analysis of infection two days post challenge showed that the highest concentration of E4 (0.6 µM) incubated with PBS led to a small but significant, 4-fold infection enhancement, whereas all lower E4 concentrations did not show increased infection (grey bars). Remarkably, seeding of SEVI was titratable, as seen by E4 concentration-dependent enhancement of infection (**Fig. 33A**). At the lowest E4 concentration, no infection enhancement was observed, but 0.12 µM of E4 increased infection already by 3.5-fold and 0.6 µM of

E4 by even 27.7-fold. Comparing the infection levels of different E4 concentrations spiked into SEVI to the same E4 concentrations spiked into PBS, only the highest E4 concentration resulted in a significant increase (p=0.0084). In the presence of SEVI, this was 6.9-fold higher. The control E4 scr. did neither enhance infection (grey bars) nor induce any

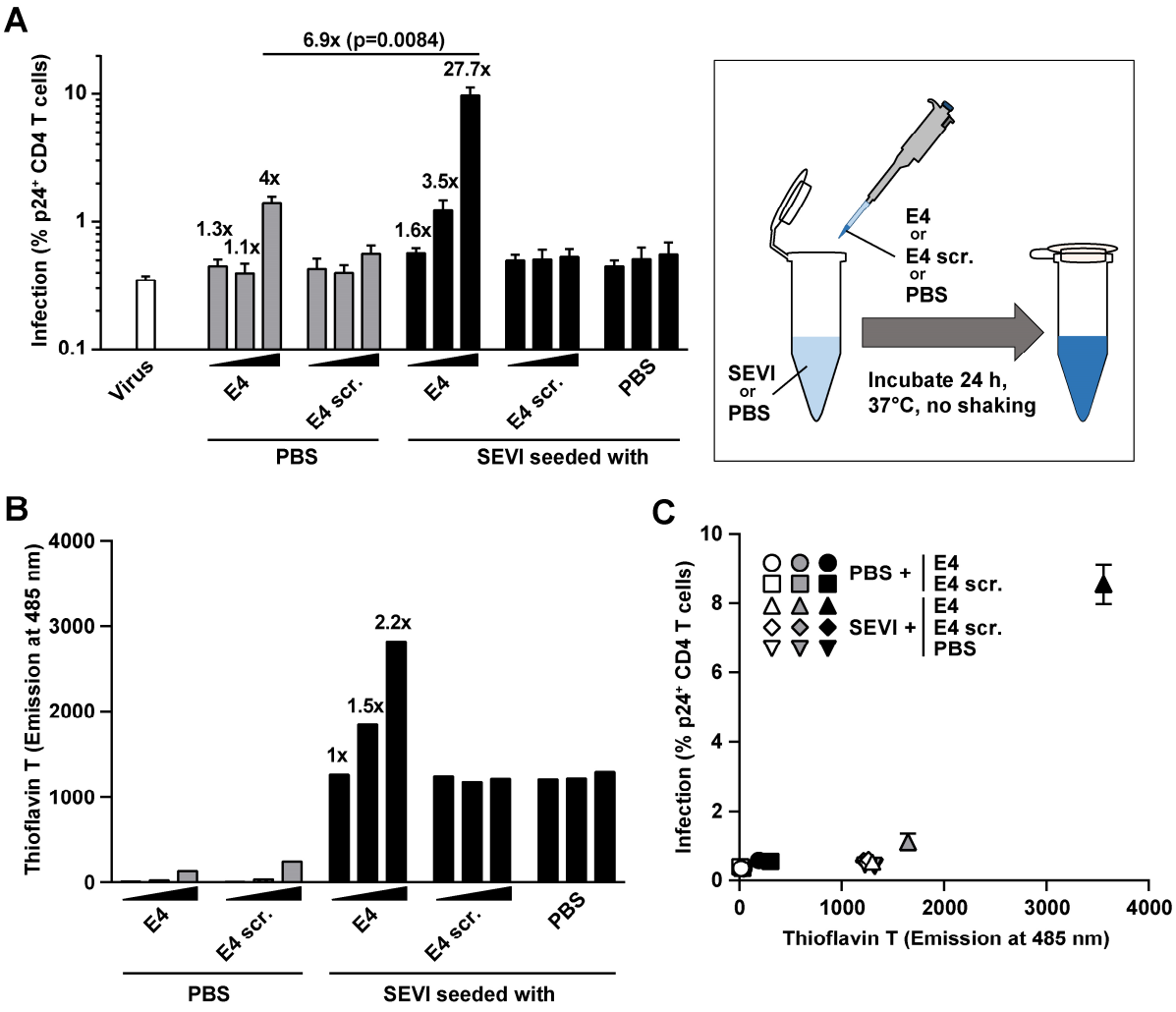

Figure 33: HPV16 E4 can initiate seeding of SEVI in a concentration-dependent manner. (**A**) Increasing concentrations of E4/ E4 scr. (final concentration on cells: 0.024 µM, 0.12 µM, 0.6 µM) or the corresponding volume of PBS were spiked into a large volume of SEVI or PBS and incubated overnight at 37°C without shaking (see schematic). Next, HIV-1_{NL4-3} was incubated with the different mixes (SEVI concentration of 11 µM). Afterwards, primary activated CD4 T cells were challenged with the different conditions. 48 h post challenge, intracellular p24 staining was performed and infection levels were determined by flow cytometry. Depicted are the arithmetic mean and standard deviation of three technical replicates from one experiment. Data shown are representative of three experiments. The factor of enhancement of infection is indicated on top of each histogram bar. (**B**) In parallel, amyloid formation in different solutions was measured by Thioflavin T staining. Data shown are representative of two experiments. Factor of increase of Thioflavin T staining is plotted on top of the respective histogram bars. (**C**) Representative data of infection levels plotted against Thioflavin T staining. Different PBS/E4/E4scr. concentrations are indicated through color code (white = 0.024 µM, grey = 0.12 µM, black = 0.6 µM).

enhancement in the presence of non-seeded SEVI (black bars, **Fig. 33A**). Addition of the respective volumes of PBS to unseeded SEVI did also not alter infection levels.
In parallel, a staining with Thioflavin T, a dye that intercalates into certain types of amyloids and thereby changes its fluorescence [178], was performed (**Fig. 33B**). Here, a concentration-dependent effect was seen for E4-mediated seeding of SEVI with a maximum increase of emission at OD 485 nm of 2.2-fold. Again, controls showed no alteration of SEVI seeding, and E4 as well as E4 scr. alone indicated at the concentrations used a very low intrinsic Thioflavin T staining. When plotting Thioflavin T (ThT) fluorescence against infection levels, two major groups can be observed: conditions with large volumes of PBS with small volumes of E4/E4 scr. (very left group) and large volumes of SEVI together with PBS/E4 scrambled. Both groups displayed similarly low infection levels. A slight shift to the right of the group where SEVI was present, was likely due to higher basal ThT staining of SEVI (**Fig. 33C**). The lowest concentration of E4 (0.024 µM) spiked into SEVI grouped with the other SEVI controls, whereas the medium E4 concentration (0.12 µM) showed a slight increase in HIV-1 infection as well as in ThT fluorescence. The highest E4 concentration (0.6 µM) led to the strongest increase of HIV-1 infection and ThT staining.
In parallel, also the effect of pH on the E4-mediated seeding of SEVI was assessed. Here, only minor pH-dependent effects (4.2, 7.2, and 8.7) on HIV-1 infection as well a ThT staining were observed (data not shown). In conclusion, a 20-fold lower E4 concentration as generally used in infection enhancer experiments was able to induce amyloid formation of non-seeded SEVI, adding a new potential mode of action to the spectrum of HPV-mediated HIV infection enhancement.

3.6 Analysis of infection enhancement potential of HPV16 E4 protein mutants as well as different HPV E4 variants

As described in the introduction, the HPV E4 protein consists of several domains. Moreover, during the differentiation of keratinocytes, E4 is processed by calpain, which causes removal of almost the whole *N-terminal* domain of the protein [132]. To further analyze, which parts of this *N-terminally* truncated peptide are responsible for the characterized HIV-1 infection enhancement, several mutants with combinations of different domains (*N-terminus*, *loop*, *β-strand*, *multimerization* and *β-aggregation*) were generated based on a structural model proposed by John Doorbar [132]. Since the net charge of E4 is cationic and it was known from SEVI that the positive charge may have functional relevance [76], also alanine (Ala) mutants neutralizing the positive charge were created. In addition, the E4 scrambled control peptide was included into this analysis (**Fig. 34A**).
To assess their functional potency, HIV-1_{NL4-3} was pre-incubated with the different mutants and, subsequently, solutions were used to infect primary activated CD4 T cells. Infection data

were collected (**Fig. S17**) and normalized to the PBS control (**Fig. 34B**). An infection enhancement of 175-fold was observed for the *N-terminally* truncated E4 peptide (aa position 18-92), whereas the E4 scrambled control peptide did not significantly affect infection levels. The deletion of the *β-aggregation* (aa position 18-81) domain led to a ~7-fold reduction of infection enhancement, while the additional removal of the *multimerization* (aa position 18-70) domain did not further affect the infection increase. Further deletion of the *β-strand* (aa position 18-62) domain, as well as the *loop* domain (aa position 26-60) or the *N-terminus* (aa position 18-25) domain alone, completely abolished infection enhancement (**Fig. 34B**). These data, indicating the importance of the *C-terminus*, were supported by the fact that peptides consisting of the

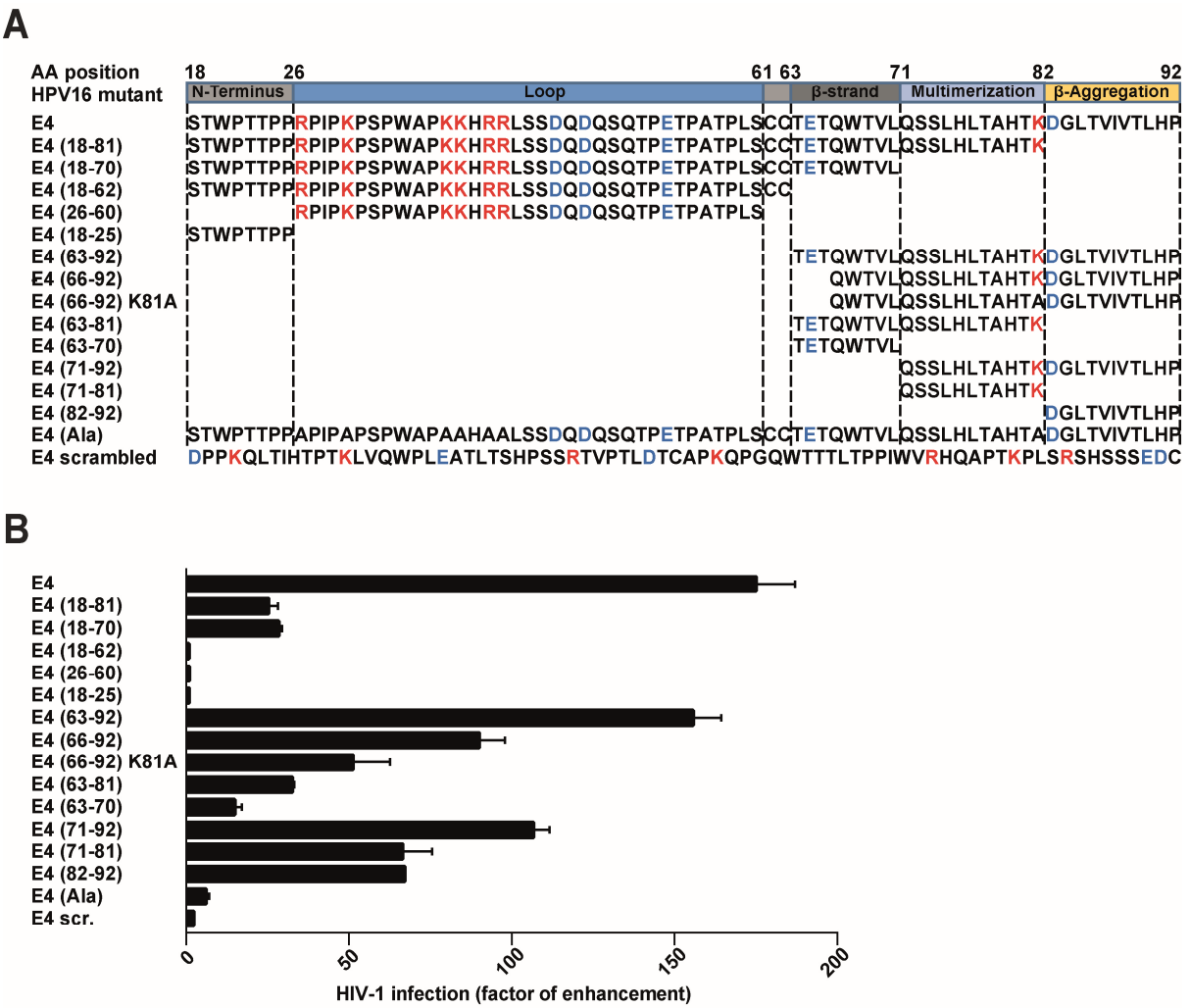

Figure 34: HPV16 E4-mediated HIV-1 infection enhancement is mainly determined by the *C-terminal* domain. (**A**) Different domain and charge mutants of the calpain-cleaved (*N-terminally* truncated) HPV16 E4 peptide were created. (**B**) HIV-1_{NL4-3} was pre-incubated with the different peptides at a concentration of 1 mg/ml (100 µg/ml final concentration on cells). Primary activated CD4 T cells (four donor pools) were challenged with the different virus-peptide mixes and intracellular p24 levels were measured 48 h post infection by flow cytometry to score infection (see **Fig. S17**). Shown is the calculated factor of enhancement of infection. Depicted are the arithmetic mean and standard deviation of three technical replicates from one experiment. Data shown are representative of two experiments.

C-terminus alone, which consists of the three domains *β-strand*, *multimerization* and *β-aggregation*, led to an infection enhancement of about 156-fold. The partial (aa position 66-92) or the complete deletion (aa position 71-92) of the *β-strand* from the *C-terminus* slightly reduced the enhancement of infection by 1.9- or 1.6-fold, respectively. The *β-strand* (aa position 63-70) domain alone enhanced infection by ~15-fold, which is an 11.7-fold reduction compared to the *N-terminally* truncated E4 peptide (aa position 18-92). In contrast, the removal of the *β-aggregation* (aa position 63-81) domain from the *C-term* dropped enhancement of infection by 5.4-fold, while addition of the *β-aggregation* domain alone (aa position 82-92) led to a 67-fold infection enhancement (2.6-fold reduction from maximum), implying the importance of this domain. Similarly, the *multimerization* domain alone (aa position 71-81) increased infection by 66.5-fold (2.6-fold reduction from maximum). Interestingly, when looking at the data described before, the *multimerization* (aa position 71-81) and *β-aggregation* (aa position 82-92) domain together (aa position 71-92) showed almost an additive functional effect (107-fold). Of note, deletion of the positive charge from the *N-terminally* truncated E4 (E4 (Ala)) allowed only a 6-fold enhancement of infection (28.7-fold reduction compared to E4) indicating the overall importance of charge for infection enhancement. A not as drastic reduction due to removal of a single positive charge was observed when using an alanine mutant of the *C-terminus* peptide (aa position 66-92 K81A), which still led to a 51-fold increase of infection. This represents a reduction of 3.4-fold compared to the *N-terminally* truncated E4 and of 1.8- to 3-fold (aa position 66-92 K81A and 63-92, respectively) compared to the *C-terminus*. Taken together, the *C-terminus* as well as, in part, the positive charge are crucial for the capacity of HPV E4 to enhance HIV-1 infection.

In a next step, the amyloid structure of the different HPV16 E4 mutants as well as HPV variants was characterized in a collaboration with Dr. M. Neßling and Dr. K. Richter (Core Facility Electron Microscopy, W230, German Cancer Research Center (DKFZ), Heidelberg, Germany) by electron microscopy (EM). This analysis revealed an amyloid-like phenotype for most of the peptides imaged, which were grouped according to their morphological structure irrespective of knowledge of their potency to influence HIV infection (**Fig. 35A**). This unbiased approach allowed classification of five major ultrastructural morphotypes: starting with amyloid-unrelated protein aggregations (EM morphotype 0), over intermediate stages of amyloidogenesis (EM morphotypes I to III) and ending with mature amyloid fibrils (EM morphotype IV). The HPV variants found to be enhancing in infection experiments (**Fig. 35B**) mainly grouped with the intermediate morphotypes (II+III), only HPV2 and HPV33 showed a less amyloid-like structure. The different domain mutants of HPV16 E4 grouped within all five morphotypes (**Fig. 35C**): The super dense mature amyloid fibrils (IV) were found only if the *β-strand*, the *loop* domain or the peptide with the deleted *C-terminus* (aa position 18-62) were present. The intermediate morphotype stage III was covered by the peptides of the *multimerization* domain alone or E4

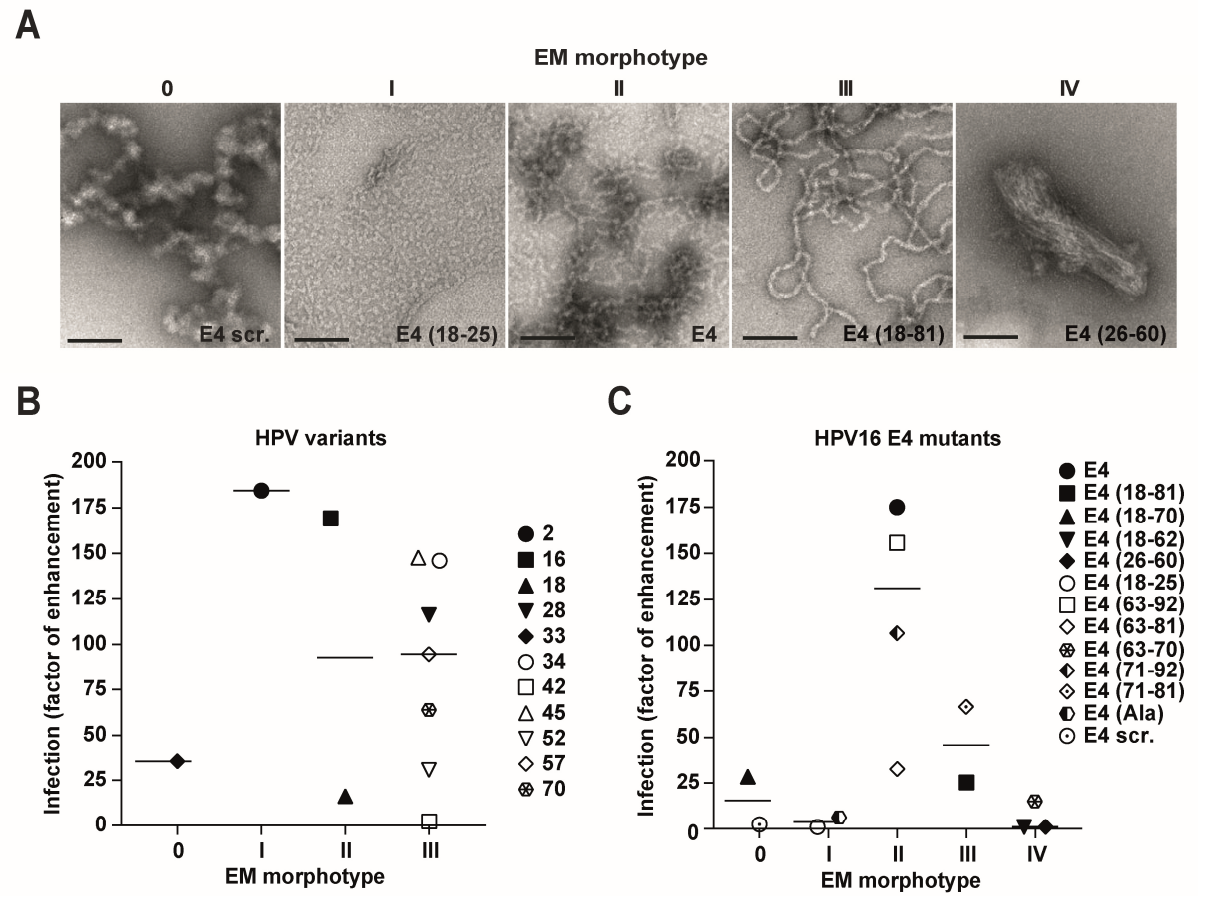

Figure 35: Intermediate stage of amyloid formation is associated with enhancing potential of HPV E4 variants and HPV16 E4 mutants. (**A**) Data obtained from a collaboration with Dr. M. Neßling and Dr. K. Richter (Core Facility Electron Microscopy, W230, German Cancer Research Center (DKFZ), Heidelberg, Germany). HPV E4 variants as wells as HPV16 E4 mutants were imaged by EM and randomly assigned to different morphotypes of amyloid formation. Shown are representative images of the found morphotypes analyzing the mutants of HPV16-E4, 0: Amyloid-unrelated protein aggregation; I: Monotypic background or early side products of amyloidogenesis; II: "A-type" short, tube-like amyloid fibrils; III: "B-type" long, conglomerated amyloid fibrils, and IV: Mature amyloid fibrils. Scale bar: 100 nm. (**B,C**) Correlation of EM morphotype and HIV-1_{NL4-3} factor of enhancement of infection for HPV E4 variants from Fig. 13 (**B**) and HPV16 E4 mutants from Fig 17 (**C**).

lacking the *β-aggregation* domain and the intermediate stage II was represented by the *N-terminally* truncated E4 (aa position 18-92), the *C-terminus* as well as the *C-terminus* lacking either the *β-strand* or the *β-aggregation* domain. The *N-terminus* alone or the E4 (Ala) mutant exhibited the lowest stage of amyloidogenesis (I), whereas the deletion of *multimerization* and *β-aggregation* domain (aa position 18-70) as well as the E4 scrambled peptides showed protein aggregation, which was not amyloid-related (0). Correlating factor of enhancement of HIV-1 infection of the different mutants to the EM morphotypes demonstrated that mainly morphotype II and III were associated with enhancement. These peptides mainly represented mutants of the *C-terminus*. This implies that the structure provided by the *C-terminus* is critical and that the minimum requirement for infection enhancement lies in the *multimerization* and/or

β-aggregation domain of E4. The deletion of charge (E4 (Ala)) and the destruction of the original sequence (E4 scr.) resulted in low or no amyloidogenesis. Since all HPV variants were enhancing infection to some degree no such comparison was possible, but the fact that the majority grouped within EM morphotype II and III underlined the finding that amyloids of intermediate density mediate HIV infection enhancement (**Fig. 35B**). Taken together, these data support that (i) the *C-terminus* of HPV16 E4 is crucial for the infection enhancement, (ii) that functional E4 forms amyloids of intermediate density, and (iii) that not only charge, but also the folding structure of the peptides is important.

In summary, this study has thus far extensively characterized HPV E4 as a new amyloid enhancer of HIV infection, reflected by the breadth across HIV isolates/strains and E4 peptides derived from different HPV types. Enhancement of infection was observed for early virus-cell interaction events, but also for spreading infection. Imaging suggested a model, in which aggregated E4 can bind and concentrate viral particles and enhance attachment by serving as a presentation platform for viruses to target cells. The increased virion fusion is dependent on HIV-specific cellular receptors, while HIV-1 Env is only partially required for enhancement of attachment. In the context of an anogenital transmission scenario, the presence of E4 at mucosal surfaces was monitored in tissue samples and the potency of low concentrations of E4 to seed amyloid formation of SEVI was revealed. In addition, it was shown, that E4 can stabilize viral particles and prolong their infectivity. The functional interaction of E4 and HIV particles is possible at different pH as well as in vaginal fluid. Finally, the *C-terminal* domain of E4 and positive charge together with intermediately densely packed amyloid structure are important for the observed enhancement of HIV infection.

3.7 Effect of amyloid enhancers of HIV infection on therapeutic approaches

So far it was demonstrated that HPV E4 as wells as SEVI can massively increase the infectivity of a low virus inoculum. Since development of new drugs always includes the stage of determining optimal concentrations in a relevant cell system and since it was already published, that SEVI was able to alter the efficiency of certain antiviral drugs [179], it was of interest whether HPV E4 might have a similar effect. Broadly neutralizing antibodies (bNAbs) against HIV represent a new treatment approach, which has been studied in different animal models as well as in clinical trials (see chapter 1.1.7).

In a first experiment the efficiency of a panel of bNAbs and neutralizing antibodies (NAbs), targeting different epitopes on Env were tested for their neutralizing capacity: the variable loops V2 and V3, the CD4 binding site (CD4bs), MPER, gp41 as well as gp41/gp120 bridging. Here, a panel of different HIV-1 strains was used: the lab strains X4 HIV-1_{NL4-3}, R5 HIV-$1_{49.5}$, the R5 virus HIV-1_{YU-2} cloned directly from the brain of an AIDS patient, and the two T/F strains R5

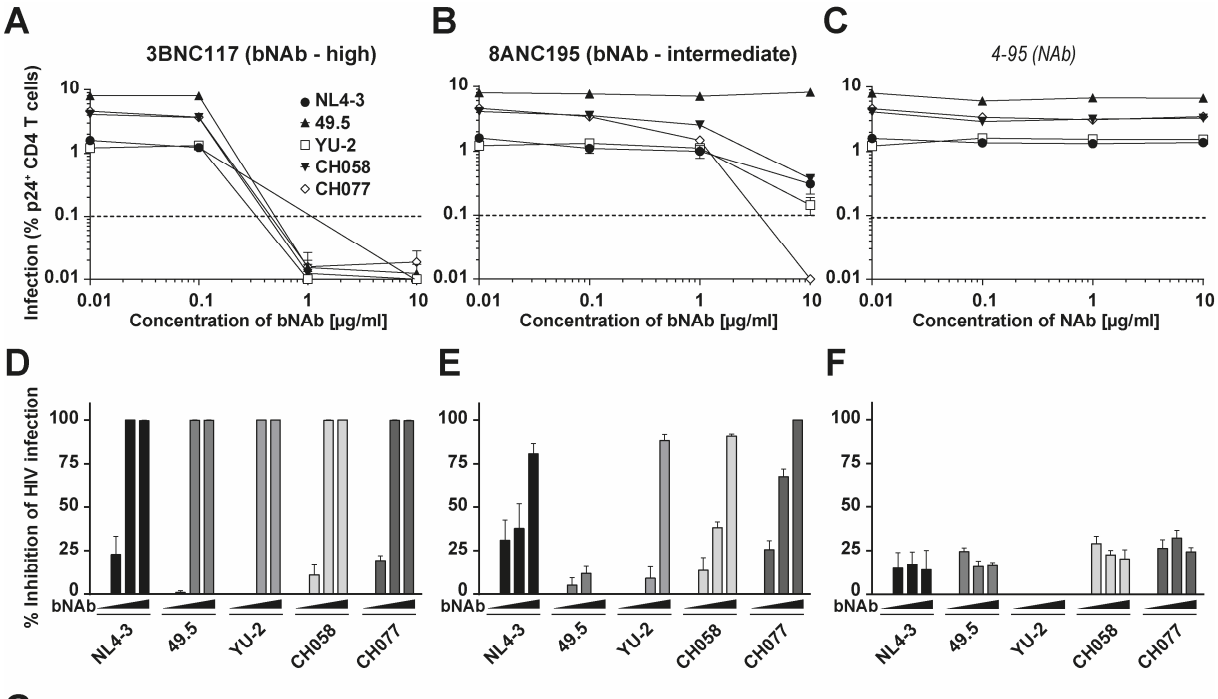

G

(b)NAb			NL4-3	49.5	YU-2	CH058	CH077
Epitope		Name					
Variable loops	V2	PG16	+	++	+	-	++
	V3	10-1074	-	+++	+++	+++	+
	V3	PGT128	-	+++	++	+++	++
	V3	*1-79*	-	-	-	-	-
	V3	*10-188*	-	-	-	-	-
	V3	*4-150*	-	-	-	-	-
CD4bs		3BNC117	+++	+++	+++	+++	+++
		VRC01	+++	+++	+++	+++	+++
		11-989	++	-	-	-	-
Epitope spanning	gp41/gp120 bridging	8ANC195	++	-	++	++	+++
	gp41/gp120 Interface	PGT151	++	++	-	-	-
other	MPER	10E8	+++	+++	-	++	++
	gp41	*4-95*	-	-	-	-	-

Legend [inhibition]:
<50% = -
50% - 75% = +
75% - 99% = ++
>99% = +++

Figure 36: Screening for neutralization capacity of different broadly neutralizing antibodies (bNAbs) and neutralizing antibodies (NAb) on different HIV-1 lab strains, a primary molecular clone and Transmitted/ Founder strains. For the evaluation of the neutralization behavior of the (b)NAb panel (kindly provided by the lab of Prof. F. Klein, Laboratory of experimental Immunology, Cologne, Germany), a high virus inoculum was used in combination with increasing concentrations of bNAbs (bold) and NAbs (italic). Therefore, HIV-1_{NL4-3}, HIV-$1_{49.5}$, HIV-1_{YU-2}, HIV-1_{CH058} and HIV-1_{CH077} were pre-incubated with different dilutions of antibodies before addition to primary activated CD4 T cells (four donor pool). 48 h later, infection levels were quantified by intracellular p24 staining and subsequent flow cytometric analysis (**A-C**). (**D-F**) Graphs display the percent inhibition of HIV infection, as it was calculated from (**A-C**). Shown are examples for different neutralization capacity: the highly and broadly neutralizing 3BNC117 (**A,D**), the intermediate neutralizing bNAb 8ANC195 (**B,E**) and the control NAb 4-95 (**C,F**). Depicted are the arithmetic mean and standard deviation of three technical replicates from one experiment. (**G**) Overview of bNAbs (bold)/NAbs (italic) and HIV-1 strains screened including the efficiency of neutralization. The degree of inhibition/neutralization is indicated by symbols: <50% = -, 50%-75% = +, 75%-99% = ++, >99% = +++.

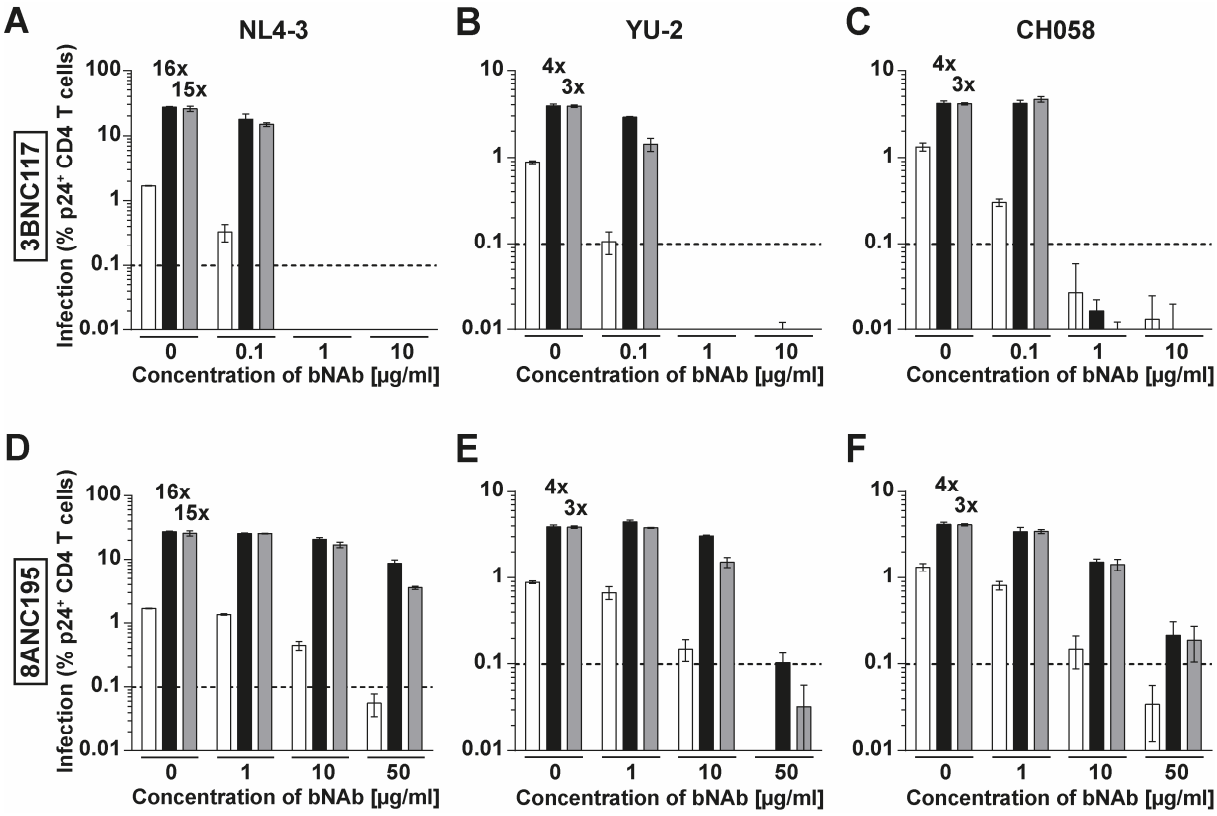

Figure 37: Presence of amyloid enhancers can alter the potency of bNAbs in an epitope-dependent manner. HIV-1_{NL4-3} (**A,D**), HIV-1_{YU-2} (**B,E**) and HIV-1_{CH058} (**C,F**) were first pre-incubated with HPV16 E4 (12 µM, black bars), SEVI (11 µM, grey bars) or PBS (white bars), followed by incubation with the indicated dilutions of different bNAbs. Shown is the CD4 binding site (CD4bs) antibody 3BNC117 (**A-C**) and the epitope spanning antibody 8ANC195 (**D-F**). Please see **Fig. S18**, for the other CD4bs antibody VRC01 and the NAb 4-95. Depicted are the arithmetic mean and standard deviation of three technical replicates from one experiment. The factor of enhancement of infection is indicated on top of each histogram bar at no antibody condition.

HIV-1_{CH058} and R5/X4 HIV-1_{CH077} (**Fig. 36**). A virus concentration aiming to yield ~1 to 10% infected T cells was chosen and virus was incubated with increasing concentrations of the different antibodies before adding them to primary activated CD4 T cells. Analysis of the data revealed that it was possible to define three groups: highly neutralizing bNAbs (**Fig. 36A,D**), bNAbs with intermediate efficiency (**Fig. 36B,E**) and NAbs with low or no neutralizing activity (**Fig. 36C,F**). bNAbs targeting the CD4bs were all highly neutralizing (+++), whereas all other bNAbs targeting the variable loops, gp41, MPER as well as the gp41/gp120 epitope spanning antibodies showed rather variable and often intermediate neutralizing capacity. Most of the tested NAbs had a neutralizing capacity of less than 50% and only the CD4bs antibody 11-989 displayed an efficiency of 75 to 99% in the context of HIV-1_{NL4-3} (**Fig. 36G**). Interestingly, the antibodies 10-1074 and PGT128 targeting the V3 loop, which determines the co-receptor tropism of HIV, seemed to be less efficient for the X4-tropic HIV-1_{NL4-3} and the dual-tropic HIV-1_{CH077}. Another observation was that the PGT151 antibody, targeting the gp41/gp120 interface,

seemed to be efficient only for HIV-1_{NL4-3} and its isogenic counterpart HIV-$1_{49.5}$, which has the same Env except for an exchange of the V3 loop, derived from HIV-1_{BaL}. Additionally, the gp41 and gp120 epitope bridging antibody 8ANC195, was severely impaired in its neutralizing activity in the context of infection with the chimeric HIV-$1_{49.5}$.

The next step, was to combine amyloid enhancers and (b)NAbs in one experiment, to examine whether the amyloids can alter the antibody efficiency. To test this, a constant volume of either HIV-1_{NL4-3} (**Fig. 37A,D, S18A,D**), HIV-1_{YU-2} (**Fig. 37B,E, S18B,E**), or HIV-1_{CH058} (**Fig. 37C,F, S18C,F**) was first incubated with a constant concentration of E4, SEVI or the corresponding volume of PBS. Subsequently, increasing concentrations of different bNAbs were added: the two CD4bs antibodies 3BNC117 (**Fig. 37A-C**) or VRC01 (**Fig. S18A-C**) or the gp41/gp120 targeting antibody 8ANC195 (**Fig. 37D-F**). The gp41-targeting NAb 4-95 (**Fig. S18D-F**) was used as a control. Next, primary activated CD4 T cells were challenged with these mixes. In absence or presence of amyloid enhancers, all bNAbs were able to modulate infection, but to varying degrees, whereas NAb 4-95 had no effect (**Fig. 37, S18**). Comparing the CD4bs to the gp41/gp120 bridging antibody showed that the latter was much less efficient. In the PBS condition, CD4bs antibodies dropped the infection of all viruses tested to background levels at a concentration of 1 µg/ml, whereas for 8ANC195 a 50-fold higher antibody concentration (50 µg/ml) was required to achieve the same effect (**Fig. 37, S18A-C**).

Analysis of the infection conditions at which amyloid enhancers were present, revealed a more diverse picture: 3BNC117 was able to block infection for all viruses at a concentration of 1 µg/ml (**Fig. 37A-C**), while VRC01 only reached this efficiency for HIV-1_{YU-2}; for HIV-1_{NL4-3} and HIV-1_{CH058} a 10-fold higher concentration of antibody was required (**Fig. S18A-C**). A similar observation was made for 8ANC195, where the maximum antibody concentration of 50 µg/ml was able to neutralize infection only for HIV-1_{YU-2} in the presence of E4 or SEVI. Neither HIV-1_{NL4-3} nor HIV-1_{CH058} infection could be blocked by 8ANC195 completely in the presence of amyloids (**Fig. 37D-F**). Calculation of a factor of change of IC50 values based on four data points revealed only minor differences in the context of HIV-1_{NL4-3} and HIV-1_{YU-2}, but for the T/F virus HIV-1_{CH058} an overall increase of IC50 in the range of 4.4- to 16.1-fold (**Fig. S19A**). Further analyses of loss of neutralization capacity in the presence of amyloids were performed, by calculating the factors of infection increase in the presence of amyloid enhancers, when infection levels of the “virus alone” condition were reduced by the antibodies by at least 50% (**Fig. S19B-D**). Interestingly, a ~7-fold (HIV-1_{CH058}/VRC01) to 54-fold (HIV-1_{NL4-3}/3BNC117) higher infection was still possible in the presence of E4. For SEVI a ~8-fold (HIV-1_{CH058}/VRC01) to 45-fold (HIV-1_{NL4-3}/3BNC117) higher infection was possible. An analogous titration experiment was performed for the binding and entry inhibitors (AMD3100, MVC, anti-CD4 antibodies, T20) previously used in this study, where a 10- to 100-fold higher concentration of inhibitors had been required to block infection of primary activated CD4 T cells with HIV-1_{NL4-3} or HIV-

1_{YU-2} in the presence of E4 or SEVI (data not shown). Taken together, these data indicate that amyloid enhancers can dramatically increase in most cases the concentration of drugs or bNAbs necessary to neutralize infection with HIV-1.

3.8 Characterization of different naturally occurring amyloids in the context of HIV-1 infection

Based on literature analysis potentially interesting amyloids were identified, which were mainly of neurological origin, including β-amyloid (Aβ) [142], but also the pancreatic islet amyloid polypeptide (IAPP) [149]. The potential of β-amyloid to enhance infection of cell lines with pseudotyped viruses was studied in the past by Münch et al. [74] and Wojtowicz et al. [75]. In contrast, IAPP is not a candidate known to have physiological relevance in the context of HIV infection. Here, HIV was used as virus for an initial screening approach, since the virus appears to be very sensitive to amyloid-mediated infection enhancement.

In a pilot experiment it was tested whether Aβ42, which is known to be strongly amyloidogenic [142], and IAPP can enhance HIV-1 infection. Primary activated CD4 T cells were challenged with a low virus inoculum of HIV-1_{NL4-3} carrying BlaM-Vpr or HIV-1_{NL4-3}, which had been pre-incubated with increasing concentrations of either E4, SEVI, Aβ42, or IAPP. Virion fusion or infection levels, respectively, were determined, revealing that virion fusion of HIV particles was enhanced by ~41-fold for (12 µM) or SEVI (11 µM) and by ~28-fold at the highest concentration of Aβ42 (10 µM). The Diabetes mellitus-associated IAPP (10 µM) showed a maximum increase of virion fusion of 3.3-fold (**Fig. 38A**). Analysis of infection enhancement displayed a ~300-fold increase for E4 (12 µM) and Aβ42 (10 µM), and 186-fold for SEVI (11 µM). Similar to effects seen for virion fusion, the presence of IAPP (10 µM) elevated infection levels only to a lower degree of ~30-fold (**Fig. 38B**).

After this initial observation, the amyloid panel was broadened, covering now with Aβ40 and Aβ42 the most relevant amyloids in the context of Alzheimer's disease [142]. Also, another amyloid with neurological association, the Parkinson's disease-related α-synuclein [145], was included. Titrating theses amyloids in infection experiments, in which primary activated CD4 T cells were infected with HIV-1_{NL4-3} (**Fig. 38C**) and SupT1.CCR5 cells with HIV-1_{NL4-3}GFP (**Fig. 38D**), it was possible to define two groups of amyloids according to their infection enhancement potency. The first group, consisting of E4 (12 µM), SEVI (11 µM), Aβ40 (10 µM) as well as Aβ42 (10 µM) led to an HIV-1 infection enhancement of 128- to 140-fold on CD4 T cells and of 11- to 32-fold on the T cell line, respectively. In contrast, the second group, comprised of α-synuclein and IAPP increased infection levels on primary CD4 T cells by only 15- to 21-fold and on SupT1.CCR5 cells by 3- to 7-fold (**Fig. 38E**). These data were in line with the described observation [74] that enhancement of infection potency of amyloids correlated in

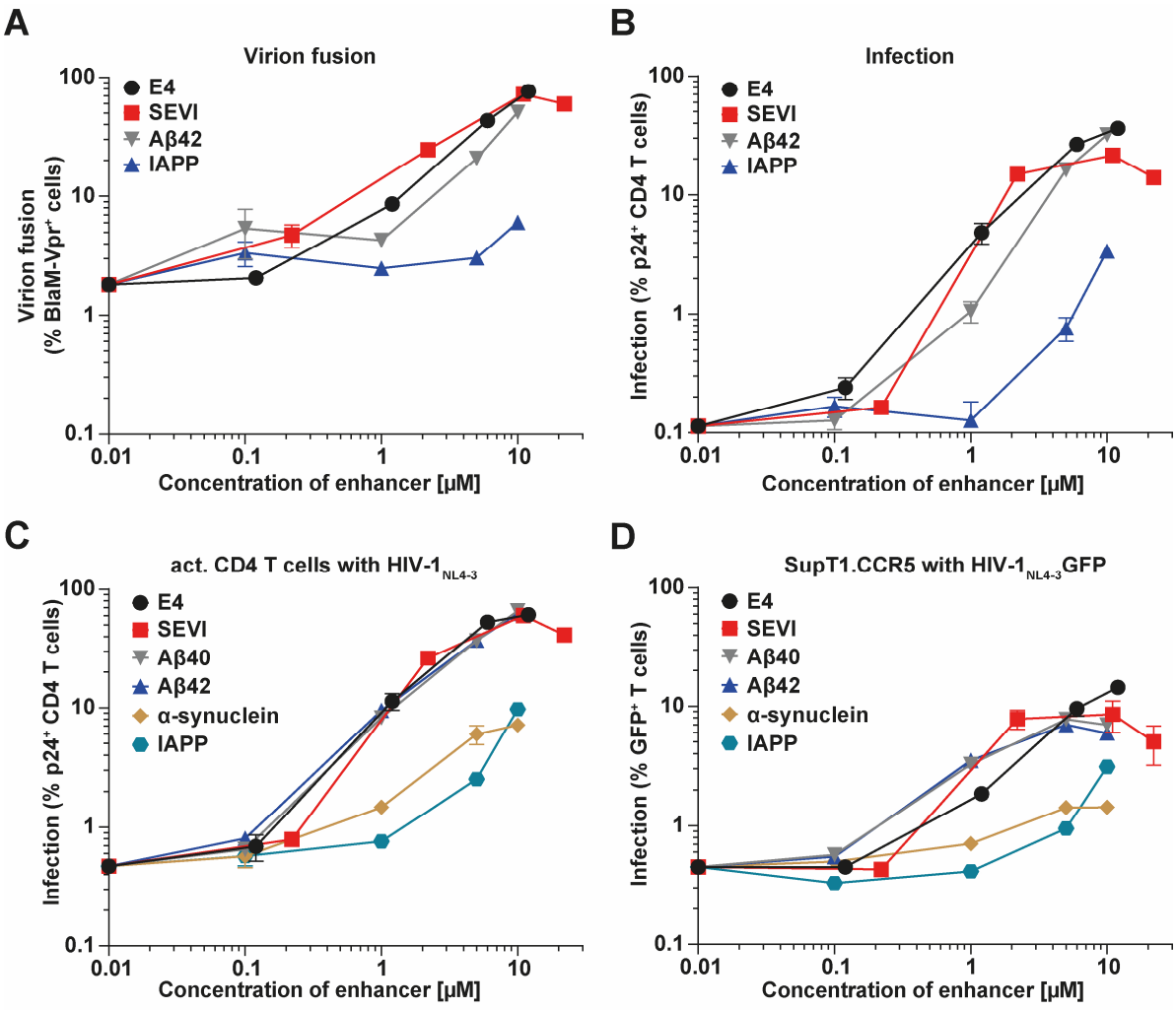

E

Amyloid	max. factor of enhancement	
	act. CD4 T cells	SupT1.CCR5
E4	128	11
SEVI	130	32
Aβ40	140	17
Aβ42	136	16
α-synuclein	15	3
IAPP	21	7

Figure 38: Different amyloids are able to enhance HIV-1 virion fusion to and infection of T cells. HIV-1_{NL4-3} carrying BlaM-Vpr (**A**) or HIV-1_{NL4-3} (**B**) were pre-incubated with the indicated concentration of HPV16 E4, SEVI, Aβ42, or IAPP and mixes used to challenge primary activated CD4 T cells (donor pool). Virion fusion (**A**) and infection (**B**) were determined as described above by flow cytometry. Depicted are the arithmetic mean and standard deviation of three technical replicates from one experiment. HIV-1_{NL4-3} (**C**) or HIV-1_{NL4-3} GFP (**D**) were pre-incubated with increasing concentrations of HPV16 E4, SEVI, Aβ40, Aβ42, α-synuclein or IAPP and used to infect a four donor pool of primary activated CD4 T cells (**C**) or SupT1.CCR5 cells (**D**). Infection levels (GFP or intracellular p24 expression) were measured by flow cytometry. Depicted are the arithmetic mean and standard deviation of three technical replicates from one experiment. Data shown represent one experiment (**C,D**) or are representative of three experiments (**A,B**). (**E**) Overview of maximum factor of enhancement of infection from (**C**) and (**D**).

part with turbidity of the peptide dissolved in aqueous solution, since β-amyloids were comparable in this regard to E4 and SEVI. The stock of α-synuclein was only slightly turbid and IAPP stocks were rather transparent (data not shown). The observed infection enhancement was not caused by any toxic effects of the amyloids that may have made the cells more permissive to infection, since all concentrations used did not alter viability (>85% viable cells) (**Fig. S20A,B**). The apparent reduction of viability in SupT1.CCR5 cells exposed to high concentrations of IAPP is likely due to an increased sensitivity of this cell type to DMSO solvent concentration of 1% (**Fig. S20E**). Together, also amyloids (β-amyloids, α-synuclein and IAPP) other than E4 and SEVI enhanced HIV-1 infection of human CD4 T cells, although, the degree of infection enhancement varied considerably.

3.9 Characterization of the amyloid panel in the context of neurotropic viruses

Many of the previously used amyloids have a neurological background. Therefore, we next screened several neuro-associated viruses (HSV-1, measles and rabies) for the ability of amyloids to enhance their infection. To study herpes virus infection, a HSV-1 VP26-YFP reporter virus was used, for measles, an attenuated vaccination strain (Measles vac GFP reporter virus/ measles*) was employed. Finally, for rabies two different virus isolates were used: the SAD (Street Alabama Dufferin) L16 strain, which is an attenuated vaccination strain, and the N2C strain, which represents a lab-adapted strain that is more neurotropic, but less cytotoxic than SAD L16. Both replication-incompetent viruses were GFP reporter viruses, which had been deleted for the glycoprotein G gene (replaced by GFP) and rescued by ectopic expression of G-proteins of either SAD L16 or N2C, respectively (rabies*). Measles* and rabies* viruses were kind gifts of Max Eizinger and Alexandru Hennrich (AG Conzelmann).

To get a first impression of the behavior of these viruses, HEK293T cells were chosen and HSV-1, measles* as well as rabies* viruses were titrated to determine the optimal inoculum to study subsequent enhancement of infection (data not shown). Afterwards, the four reporter viruses were incubated with increasing concentrations of the six amyloids and infection of HEK293T cells was analyzed 20 h post challenge (**Fig. 39**). Interestingly, in many of the different virus-enhancer combinations an infection enhancement in the range of 2.1- to 6.2-fold was observed (**Fig. 39E**). The optimal concentration of amyloids for infection enhancement of these viruses was more diverse compared to HIV (typically ~10 µM), ranging from 1 to 10 µM. Infection of HSV-1 YFP (**Fig. 39A,E**) was increased by all amyloid enhancers by 4- to 6-fold, except for α-synuclein (1.3-fold). This is in line with a previous report that seminal amyloids can enhance HSV-1 infection [87]. Also for measles vac GFP (**Fig. 39B,E**), amyloids enhanced infection by 2- (IAPP) to 6.1-fold (E4). Analysis of rabies* virus infection experiments revealed less pronounced effects, given that N2C (**Fig. 39C,E**) allowed infection enhancement

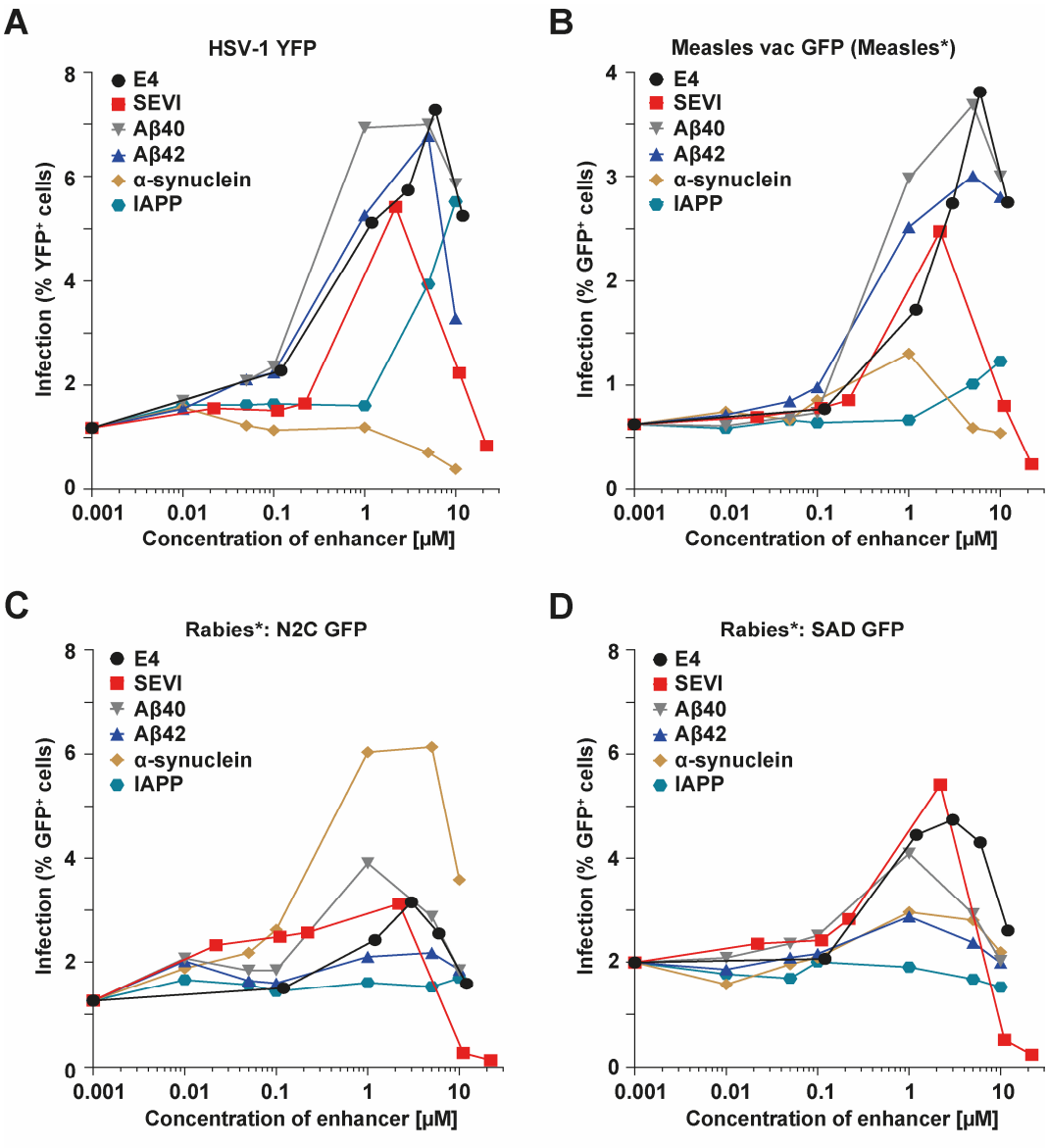

E

Amyloid	max. factor of enhancement of			
	HSV-1	Measles*	Rabies*: N2C GFP	Rabies*: SAD GFP
E4	6.2	6.1	2.5	2.4
SEVI	4.6	4	2.5	1.4
Aβ40	5.9	5.9	3.1	2.1
Aβ42	5.7	4.8	1.7	1.4
α-synuclein	1.3	2.1	4.9	1.5
IAPP	4.7	2	-	-

Figure 39: Different amyloids enhance infection of HEK293T cells with neurotropic viruses. HSV-1 YFP (**A**), measles vac GFP (measles*) (**B**) and the two rabies* strains, SAD L16ΔG GFP + SAD L16-G (**C**) and N2CΔG GFP + N2C-G (**D**), were pre-incubated with increasing concentrations of HPV16 E4, SEVI, Aβ40, Aβ42, α-synuclein, or IAPP. Subsequently, HEK293T cells were infected with the different mixes. 20 h post challenge, cells were harvested, fixed and infection levels (YFP/ GFP expression) were analyzed by flow cytometry. Data shown represent the arithmetic mean of two technical replicates from one experiment. (**E**) Summary of maximum factor of infection enhancement from panels (**A-D**).

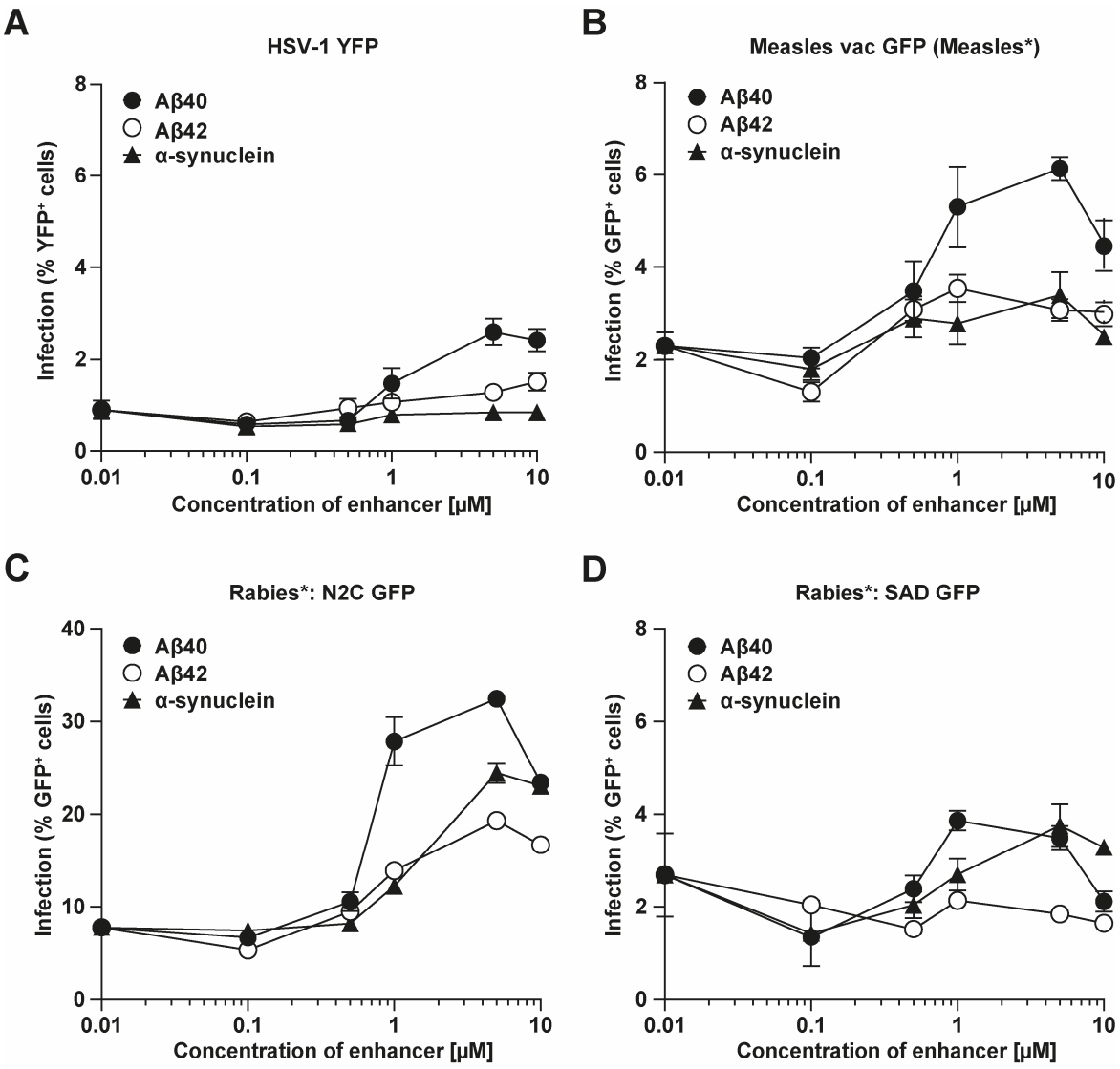

E

Amyloid	max. factor of enhancement of			
	HSV-1	Measles*	Rabies*: N2C GFP	Rabies*: SAD GFP
Aβ40	2.9	2.7	4.2	1.4
Aβ42	1.7	1.5	2.5	-
α-synuclein	-	1.5	3.2	1.4

Figure 40: The enhancing efficiency of brain-related amyloids on infection of SH-SY5Y cells with different neurotropic viruses depends on the specific virus-amyloid combination. Increasing concentrations of Aβ40, Aβ42, or α-synuclein were pre-incubated with HSV-1 YFP (**A**), measles vac GFP (measles*) (**B**) and the two rabies* strains, SAD L16ΔG GFP + SAD L16-G (**C**) or N2CΔG GFP + N2C-G (**D**). Next, SH-SY5Y cells were challenged with the different mixes. 20 h post challenge, YFP/ GFP expression of viable cells was analyzed by flow cytometry. Depicted are the arithmetic mean and standard deviation of three technical replicates from one experiment. (**E**) Overview of maximum factor of infection enhancement from panels (**A-D**).

by 1.7- (Aβ42) to 4.9-fold (α-synuclein) and SAD L16 (**Fig. 39D,E**) by 1.4- (SEVI and Aβ42) to 2.4-fold (E4). For both rabies* strains the Diabetes mellitus-associated IAPP showed no infection enhancement. All peptides within the amyloid panel were non-toxic to HEK293T cells, which were more than 85% viable at all concentrations used (**Fig. S20C,E**). Of note, the decrease of the infection rate at higher amyloid concentrations was not due to higher levels of dying cells, as assessed by flow cytometry (data not shown). Taken together, not only E4 and SEVI, but also the β-amyloid peptides, α-synuclein and IAPP enhanced infection of HEK293T cells with HSV-1 and measles* virus, and to a lesser extent also of rabies* virus.

The thus far examined HEK293T cells are a widely used cell system to study various biological effects, e.g. effects of protein overexpression, protein-protein interactions. SH-SY5Y cells are a cell line derived from a neuroblastoma and therefore more similar to the *in vivo* targets of neurotropic viruses than epithelial kidney cells. Next, viruses were incubated with increasing concentrations of either one of the two β-amyloids (Aβ40 and Aβ42) or α-synuclein, and used to challenge SH-SY5Y cells (**Fig. 40**). Also for these experiments, the optimal enhancing concentration of amyloids was much more variable (~1 µM to 5 µM) than seen for HIV. This neuro-associated amyloid panel had a low to intermediate enhancing effect on infection with measles* or HSV-1 (**Fig. 40A,B,E**), ranging from ~1.5- to 2.9-fold enhancement, with the exception that α-synuclein had no detectable effect on HSV-1 infection. The most interesting virus in this preliminary set-up turned out to be the rabies* strain N2C (**Fig. 40C,E**), for which all amyloids increased infection by 2.5- (Aβ42), 3.2-fold (α-synuclein) to 4.2-fold (Aβ40). In contrast, the panel had almost no effect on the infection levels of rabies* strain SAD L16 (**Fig. 40D,E**). The neuro-associated amyloid panel was not toxic to SH-SY5Y cells at all concentrations used (**Fig. S20D,E**). As seen for HEK293T cells, decreasing percentages of infected cells at high amyloid concentrations were not due to a general loss of cells in the culture, as determined by flow cytometry (data not shown). Thus, also viruses other than HIV can be increased in their infectivity using amyloid enhancers of different origin, although to a less pronounced degree.

3.10 Enhancement of adenoviral infection by amyloids

While the so far used viruses largely differed in their target cell and tissue tropism, they were all surrounded by a lipid bilayer, which contains the viral envelope glycoproteins. Different from these so-called enveloped viruses are the non-enveloped viruses, represented e.g. by the family of adenoviruses (AdV). These viruses are of mainly respiratory origin and their target cells in the conducted experiments were A549 cells derived from type II pneumocytes.

Several primary AdV isolates (AdV2/3/5/7) were incubated with increasing concentrations of E4 or SEVI prior to infection of A549 cells for 18 h. We observed a maximum infection enhancement of 8.1-fold for E4 (1.8 µM) and 3.9-fold for SEVI (1.1 µM). For the other AdV strains (inset table, AdV3/5/7) tested, a similar observation was made, with E4 resulting in 2.7- to 3.3-

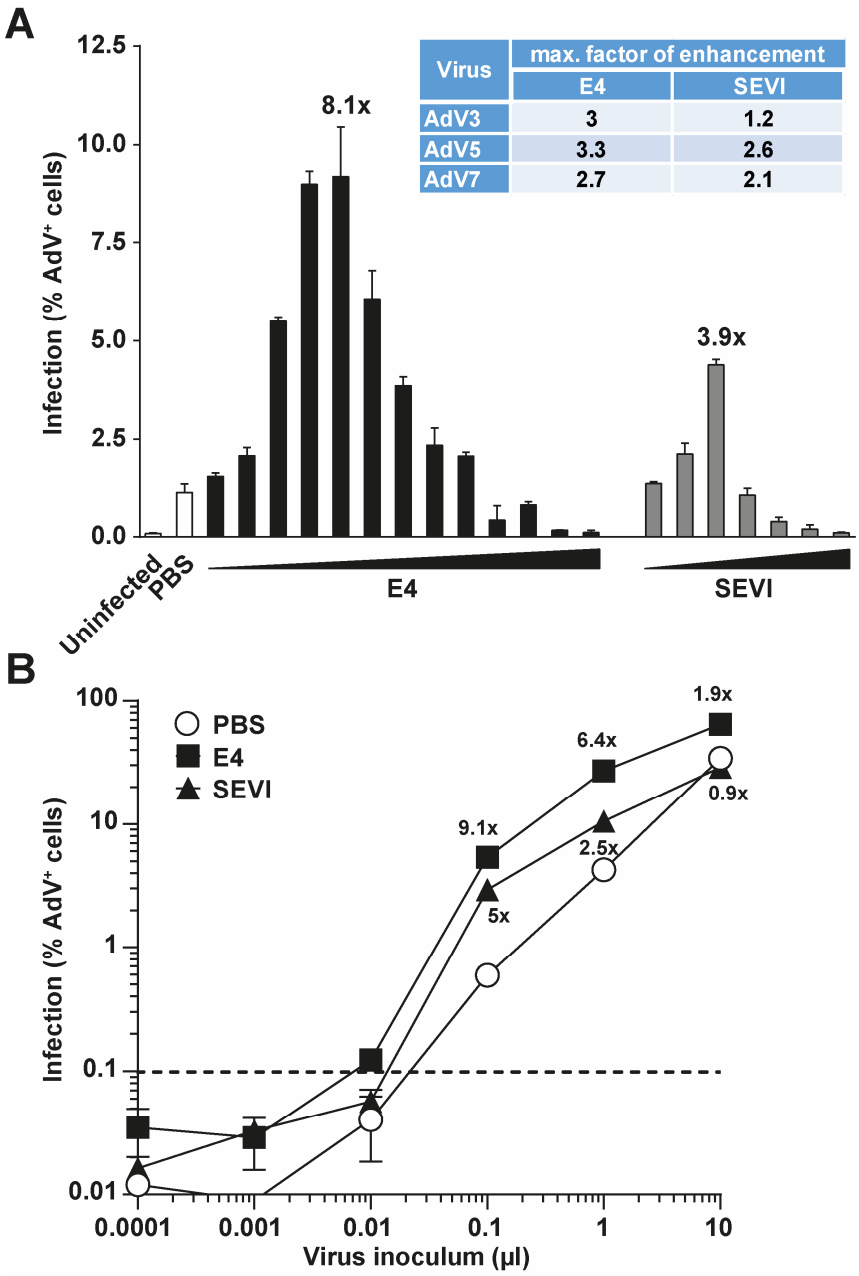

Figure 41: E4- and SEVI-mediated enhancement of adenoviral infection. (**A**) Adenovirus (AdV) primary isolate AdV2 was pre-incubated with increasing concentrations of HPV16 E4 (0.012, 0.06, 0.6, 1.2, 1.8, 2.4, 3, 3.6, 4.2, 5.4, 6, 12, 24 µM) or SEVI (0.022, 0.11, 1.1, 2.2, 4.4, 6.6, 11 µM) and afterwards used to infect A549 cells. 18 h post infection, cells were harvested, fixed and stained with a primary monoclonal mouse anti-AdV antibody followed by a secondary goat anti-mouse Alexa Fluor 488 antibody. Infection levels were determined by flow cytometry. Maximum factor of enhancement is depicted on top of the respective histogram bar. Inset table shows maximum factor of enhancement of other adenoviral isolates (AdV3/5/7) tested. Depicted are the arithmetic mean and standard deviation of three technical replicates from one representative experiment. Shown are representative experiments of AdV2 (n=4), AdV3 (n=1), AdV5 (n=2), AdV7 (n=1). (**B**) Increasing volumes of virus inoculum were pre-incubated with a constant amount of PBS, HPV16 E4 (1.8 µM) of SEVI (1.1 µM) and then used to challenge A549 cells. 18 h post infection, cells were treated as described before and infection levels were determined by flow cytometry. The factor of enhancement of infection is indicated by numbers above the respective data points. Depicted are the arithmetic mean and standard deviation of three technical replicates from one experiment.

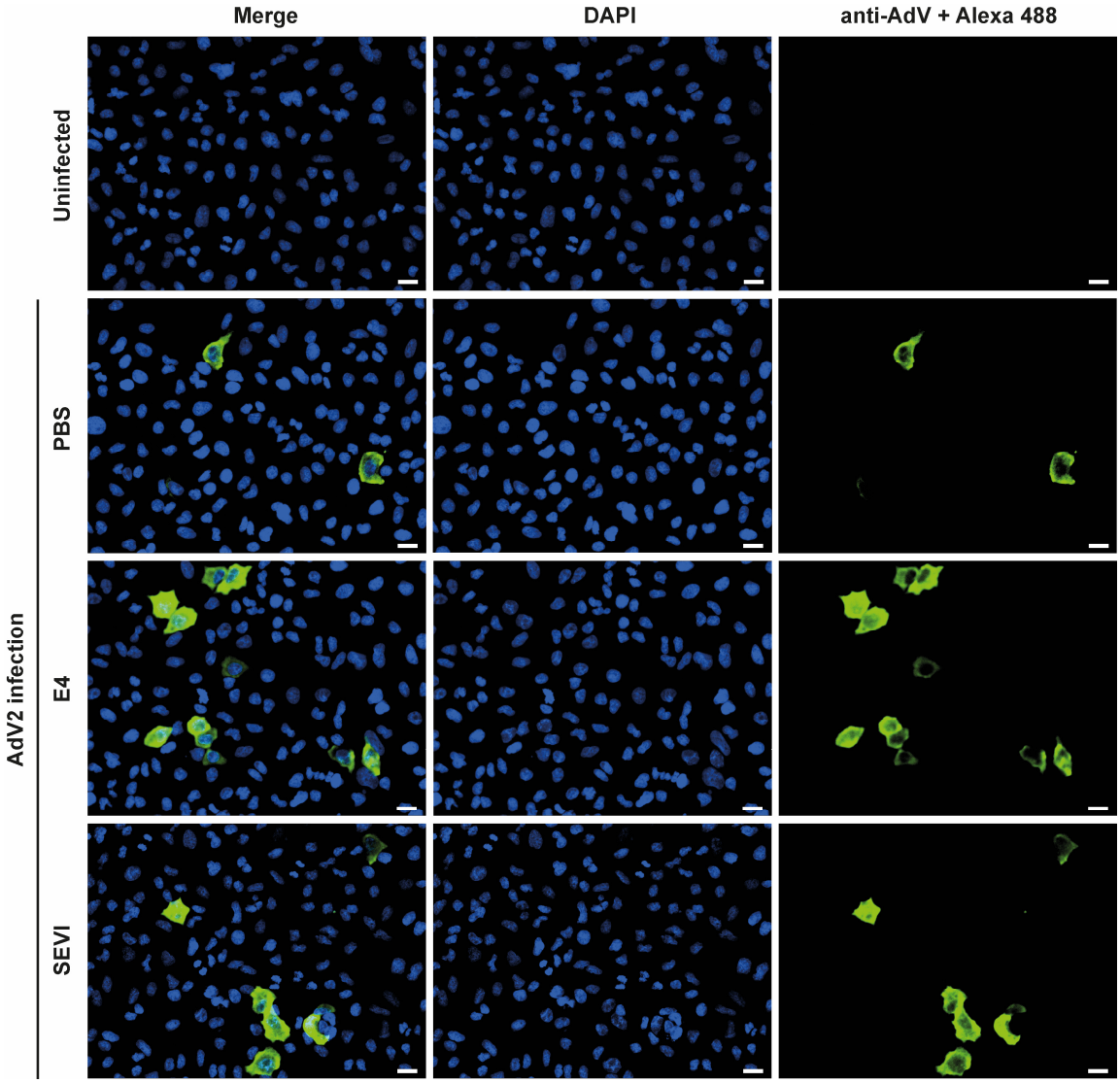

Figure 42: Visualization of enhancement of adenoviral infection. Microscopy pictures showing infection of A549 cells with AdV2, which was pre-incubated with either PBS, HPV16 E4 (1.8 µM), or SEVI (1.1 µM). Cells were grown overnight on poly-L-lysine-coated coverslips. After fixation of cells 18 h post infection, a staining with a primary mouse monoclonal anti-AdV antibody and a secondary goat anti-mouse Alexa Fluor 488 antibody was performed. Coverslips were mounted in DAPI-containing medium. Virus-infected cells in green, nuclei in blue. Shown are the merge as well as the single channels for DAPI and Alexa Fluor 488. Scale bar: 20 µm.

fold and SEVI in 1.2- to 2.6-fold infection enhancement, respectively (**Fig. 41A**). Typically, the titration of amyloids in experiments of adenoviral infection resulted in a “bell-shaped” picture, of increasing infection to a certain degree, followed by a stepwise loss of productively infected cells at higher amyloid concentrations. This decrease was not due to reduced viability of the cells as assessed by flow cytometry (data not shown).

After defining optimal enhancing amyloid concentrations at one MOI, it was tested, whether enhancement of infection could be boosted depending on the input virus concentration. Hence,

in a follow-up experiment AdV2 was titrated alone (PBS) or together with a constant concentration of E4 (1.8 µM) or SEVI (1.1 µM), and infection of A549 cells was performed (**Fig. 41B**). Here, a ~9-fold infection enhancement by E4 and a ~5-fold infection enhancement by SEVI was found at the optimal amyloid-virus combination. In addition, this experiment confirmed a phenotype observed in HIV experiments, where the factor of enhancement decreased with increasing MOI. Here, for E4 a 4.8-fold and for SEVI a 5.9-fold reduction of infection enhancement was measured for the highest virus inoculum compared to optimal amyloid-virus combination. Of note, at the highest MOI SEVI was not able to further enhance infection, whereas E4 still boosted by 1.9-fold. The same experiment was performed for the AdV5 strain, giving similar results, where E4 was able to lead to a 4.4-fold infection enhancement and SEVI did no longer enhance at highest MOI (data not shown).

Finally, E4- and SEVI-mediated infection enhancement for AdV was visualized by fluorescent microscopy. A549 cells were infected with the combination of optimal inoculum of AdV2 and either E4 or SEVI, determined in the previous infection experiments (**Fig. 42**). Also here, a comparable degree of infection enhancement was visible: E4 lead to a ~5.5-fold infection increase and SEVI to a ~3-fold increase of AdV-infected cells (green). Taken together, enveloped as well as non-enveloped viruses can be enhanced in their infectivity in the presence of appropriate concentrations of amyloidic peptides.

4 Discussion

4.1 The *N-terminally* truncated HPV E4 enhances HIV infection *in vitro*

Although HIV itself is no longer among the "global top 10 causes of death", several AIDS-defining as well as non-AIDS-defining, HIV-associated diseases are still found within this list. Thus, research not only for better understanding of the HIV replication cycle including cellular restriction factors, accessory viral proteins, drug targets, but also on extracellular factors that can modulate viral entry, is crucial for an optimized treatment or future cure of HIV infection. Mucosal surfaces represent an effective barrier against invading pathogens at transmission sites, which require chemical, biological or mechanical disruption to overcome them [3, 4, 6]. Human papillomaviruses have been identified as a confounding risk factor during epidemiological studies indicating that a pre-existing HPV infection can increase the risk to acquire an HIV infection by 1.7- to 4.9-fold (see chapter 1.2.3.3). So far, it is believed that this enhanced susceptibility of HIV is mainly due to HPV-derived lesions, which cause inflammation and disruption of the mucosal barrier. Consequently, HIV is able to invade the protective mucosa and infiltrating immune cells may serve as HIV targets [125, 180].

Data published by the lab of John Doorbar [103, 132, 135, 141] identify HPV E4, a protein involved in the regulation of the cell cycle and cytokeratin rearrangement, as being able to form amyloidic structures. Up to date there are several studies showing that semen-derived (SEM-amyloids, SEVI), but also other amyloids (e.g. β-amyloid), are able to enhance HIV infection [74, 75, 78, 80, 83]. We hypothesized that HPV E4 could be another candidate exhibiting such a potential. Within this thesis, the role of HPV E4 as a potential enhancer of viral infection was characterized in detail.

Testing the effect of HPV16 E4 and SEVI on HIV infection revealed similar enhancing potential of the two peptides in the range of ~100-fold (**Fig. 20A,B**). The specificity of the E4-mediated enhancement of infection was verified using inhibitors targeting HIV entry (anti-CD4 antibodies/ co-receptor-antagonizing AMD3100/ fusion inhibitor T20) (**Fig. 21**). Screening of a broad panel of HIV-1 lab, T/F strains as well as both HIV-1 and HIV-2 primary isolates revealed that neither lab adaption, nor differences between T/F and chronic viruses significantly affected their potential to be enhanced by amyloids. Covering R5-, X4- and dual-tropic HIV strains as well as primary isolates, a possible restriction of enhancement related to co-receptor usage could be excluded. Besides variations between the different HIV-1 viruses concerning maximum infection and amyloid-mediated enhancement levels (**Fig. 22A-D**), titration of E4 and SEVI amyloids revealed individual characteristics for each strain/isolate (**Fig. S5**). Of note, within this screen infection enhancement levels of up to 137-fold for HIV-1 and of up to 3821-fold for HIV-2 (**Fig. 22, S6**) were observed. Another observation of the screening is the inverse correlation of

virus input and the degree of infection enhancement by amyloids. Likely, this is due to the limited fraction of cells that are infectable within such a culture. This is in particular true for primary cells, which do not allow infection of the entire culture. Experiments using “spinoculation” could only increase infection without amyloid enhancers, whereas enhancers led in most cases to infection of all susceptible cells independent of “spinoculation” (**Fig. 23**). In addition, these data suggest a maximum level of infection, which is defined by the cell type and HIV strain used. This plateau cannot be altered by the addition of E4 or SEVI.

Critical for establishing infection in a new host is the viral load within the transmission fluid. Amyloid enhancers of viral infection like SEVI are thought to serve as some sort of catalyzers enabling sub-infectious virus loads to cause a productive infection [74]. In spreading infection experiments performed herein, HPV E4 was able to mediate this function and its potency was quantified by an endpoint titration/ TCID50 assay on primary activated CD4 T cells (**Fig. 24, 25, S7**). Using a panel of HIV-1 strains and primary isolates (HIV-1_{NL4-3}, HIV-1_{CH058}, HIV-1_{13127}, HIV-1_{2005}) an increase of the TCID50 of up to 161-fold was detected. In addition, the endpoint titration assays showed that the E4-mediated increase of infection does not require pre-incubation of the amyloid with the virus before adding to cells. This is in contrast to semen or seminal plasma, where small volume pre-incubation followed by dilution is essential to avoid toxicity effects [74]. Of note, also the conducted experiments benefited from this approach, because the small pre-incubation volume makes virus-enhancer interaction more efficient.

All experiments discussed so far, had been performed with E4 peptide derived from HPV16, which is the most extensively studied type since it accounts for around 55% of cervical cancers [108]. To test the potential of E4 peptides derived from other *alpha-papillomaviruses* to enhance HIV infection an E4 peptide panel containing HR (“high risk”)- and LR (“low risk”)-HPV types was designed. Here, all variants tested were able to enhance HIV-1 infection in a range of 2- to 184-fold, independent of their related cancer risk (**Fig. 26**). This is interesting, as it has been reported that the presence of several HPV types at transmission sites correlated with an increased risk of acquiring HIV [129, 181, 182]. Previous studies showed that administration of semen amyloids and SIV/HIV at anogenital sites without mucosal disruption failed to enhance transmission [78, 79]. This may indicate that the quality of the lesion, the related inflammation, and influx of immune cells could differ dependent on the plethora of consequences inflicted by HPV type infections at transmission sites. Titration of the different HPV E4 variants provided additional insight into the dynamics of infection enhancement, with saturation of enhanced infection for some types (HPV 28, 57 and 70) occurring already at much lower peptide concentrations as observed for HPV16 (**Fig. S8**). In addition, the different variants were also analyzed for their physiochemical properties showing no apparent rule or correlation of infection enhancement with any of the evaluated parameters (**Fig. S9**). Specifically, although E4 is

cationic (based on the theoretical pI, **Fig. S9B**), no correlation between higher cationicity and infection enhancement, as found for semen-derived amyloids, could be detected. Nevertheless, the positive net charge is likely to be important to overcome the repulsion forces imposed by the negatively charged target cell as well as virus membranes [76]. Remarkably, E4 proteins of the different HPV types display a large heterogeneity concerning their amino acid (aa) sequence (**Fig. S10**), but are still all able to enhance HIV infection. This is likely due to the fact that all of them are composed of aa-sequence-independent, conserved domains, which mediate this functionality (**Fig. 34A**) [132]. The fact that several HPV types may be present at transmission sites, could result in an additive infection-enhancing effect of E4 proteins derived from several HPV types. Interestingly, reflecting a scenario potentially occurring during *in vivo* transmission, co-administration of E4 and SEVI *in vitro* had neither inhibiting nor synergistic, but additive effects, reflecting rather the absolute concentration of amyloid critical for the observed infection enhancement (data not shown). Further studies combining E4 proteins from different HPV types could still reveal combinations, which act differently in their infection-modulating characteristics.

Trying to elucidate the amyloid's mode of action in more detail, confocal microscopy showed that E4 efficiently binds free HIV particles (carrying eGFP-Vpr) in a "sponge"-like fashion likely mediating an efficient presentation to HIV target cells, thereby increasing the likelihood of virus-cell interaction (**Fig. 27, 43, S11**). Further assessment of the E4-mediated increase of virion binding/attachment to primary activated CD4 T cells revealed that HIV Env (HIV-1_{NL4-3} wt vs. ΔEnv) is of partial importance (**Fig. 28**). In previous infection experiments, E4 and SEVI showed optimal enhancement of infection at a concentration of ~10 µM. Here, SEVI-mediated virion binding behaved completely different, saturating at this concentration independent of Env. However, at a lower amyloid concentration (2.2 µM) also for SEVI a reduced enhancement in the absence of HIV Env was detected (data not shown). Thus, similar Env-dependent effects could be observed for both amyloids. This suggests that the initial facilitating steps of the two amyloid enhancers may be different, but create a similar functional outcome. Enhancement of virion attachment was also observed for other HIV strains tested (HIV-1_{NL4-3}, HIV-1_{YU-2}, HIV-1_{CH058}, HIV-1_{CH077}, **Fig. S13**).

To further analyze the effect of amyloids on HIV entry, enhancement of virion fusion by either E4 or SEVI was analyzed using HIV-1 particles containing BlaM-Vpr (same set of strains as for the virion attachment assay). At the conditions chosen, a ~30-fold increase of virion fusion was detected. In addition, inhibitors targeting CD4 (anti-CD4 antibodies), the HIV co-receptors (MVC/ AMD3100) and fusion (T20) (**Fig. 29, S16**) were included, confirming the tropism of the different HIV-1 strains tested and the dependence of infection enhancement on canonical

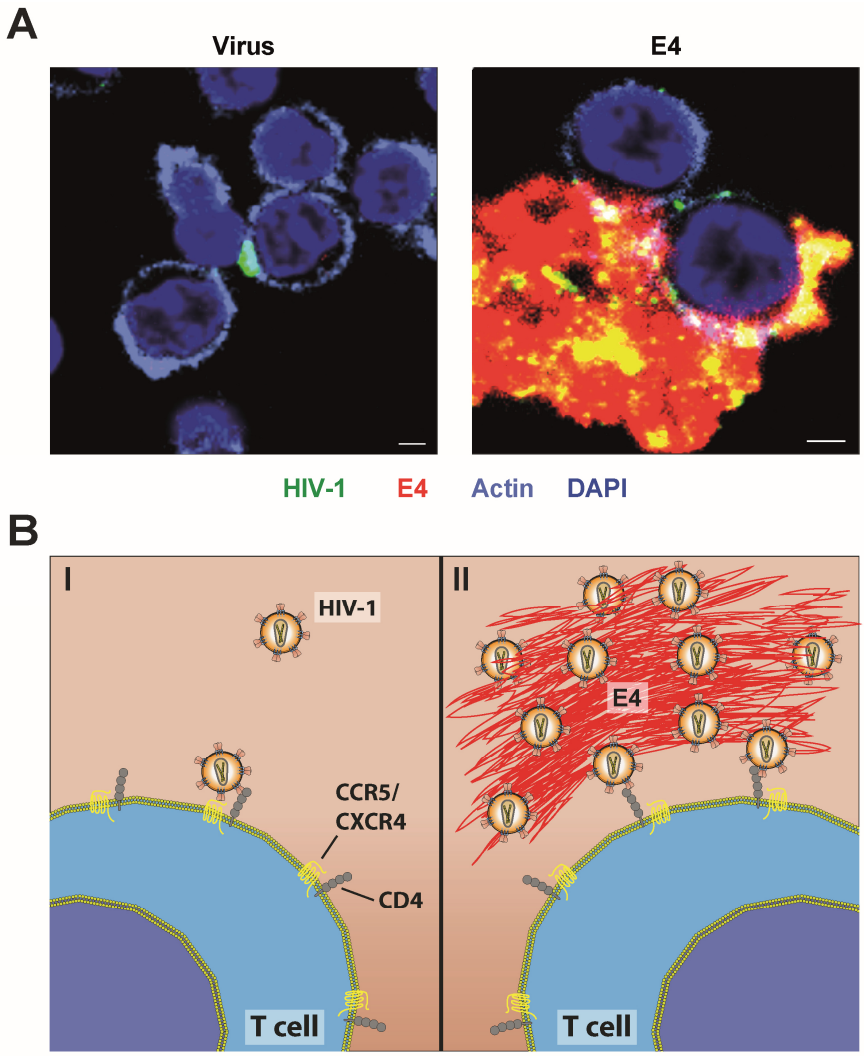

Figure 43: Model of HPV E4-bound HIV particles and infection enhancement. (**A**) Confocal images of primary activated CD4 T cells incubated with HIV-1_{NL4-3} eGFP-Vpr alone or pre-treated with HPV16 E4 (for detailed information see **Fig. 27, S11**). (**B**) Proposed model of HPV E4-mediated infection enhancement effect with (i) reflecting the virus alone scenario, with few virus particles reaching the cellular membrane which are often unable to attach, because of repulsion forces and low receptor density. In contrast, (ii) showing the virus pre-treated with E4 condition, where a huge E4 aggregate concentrates a large amount of virus particles and subsequently mediates efficient presentation to target cells. Conceivably, negatively charged virus and cell membrane are forced to interact, thereby overcoming repulsion forces.

steps of the virion entry process within this assay. Together with the data from experiments monitoring the effect of amyloid enhancers on infection levels in the presence of these inhibitors (**Fig. 21**), these results indicate that infection in the presence of amyloids does not occur using an alternative entry pathway (CD4-independent, alternative co-receptors, endocytosis, etc.). Furthermore, these experiments showed that only blockage of CD4 binding or fusion (T20) completely inhibited fusion of amyloid-exposed viruses. The co-receptor-blocking drugs failed in most cases to inhibit virion fusion completely in the presence of amyloid enhancers.

However, the low remaining virion fusion/infection is negligible in comparison to the high virion fusion/infection (~40-/130-fold higher, respectively) in the absence of inhibitor (**Fig. 21, 29, S16**). The issue of targeting the co-receptors to prevent infection becomes even more relevant when looking at the dual-tropic T/F virus HIV-1_{CH077} used in this study, indicating that these kind of receptor antagonists are less efficient tools to treat or prevent HIV infection. This is contrast to the results published by Zirafi et al. [179], which suggested MVC as the only fully effective drug in the presence of semen-derived amyloids, when analyzing changes of IC50 values. Thus, also in the presence of amyloid enhancers, binding and entry inhibitors can effectively block both virion fusion and infection. This further supports the observation of an at least partial requirement of Env for enhancement of virus attachment and largely excludes alternative entry pathways for the infection of primary activated CD4 T cells.

In the context of virion entry, two other points could play important roles for the infection enhancement mediated by the amyloids used. As described in chapter 1.1.6, HIV Env is not a static molecule that only undergoes structural changes after receptor engagement [36] and conformational changes at initial steps of virus-cell interaction could probably switch back. Following this idea, one may hypothesize, that the Env molecule itself with its bridging-sheet β-sheet structures [32] could be stabilized by the β-sheets of the amyloids, thereby supporting co-receptor engagement and subsequent fusion.

Finally, besides all assays within this thesis focusing on the effect of HPV E4 on infection with cell-free virus, in earlier experiments, colleagues examined the impact of this amyloid enhancer on cell-to-cell transmission. These experiments revealed enhanced transfer of virus particles from DC or LC to CD4 T cells, but not between T cells (data not shown). According to literature, virological synapse (VS) formation during cell-to-cell transmission (infected T cell to uninfected T cell), or infectious synapse (IS) formation (uninfected DC/LC, harboring HIV particles attached to the cell surface in crypt-like structures, to uninfected T cell), can lead to enhancement of infection [8, 32]. Interestingly, when comparing these two infection models to the proposed mode of action of amyloid enhancers, some parallels can be observed. All three scenarios cause (i) a locally high concentration of virus particles, which is (ii) protected from the surrounding cells, creating a microenvironment and which (iii) forces viruses and cells to interact. This is further reflected by the observation that in VS, IS, and amyloid-containing scenarios RT inhibitors and integrase inhibitors are dramatically reduced in their efficiency. This might be due to multiple virus particles infecting one cell overrunning of the block imposed by the drug [8] (data for amyloids not shown).

4.2 Relevance of E4-mediated enhancement of HIV infection under *in vivo*-like conditions

Human papillomaviruses have adapted their replication cycle to the differentiation of keratinocytes and use the final step, the desquamation of the keratinocytes from the mucosa, for the egress of viral particles. HPV-infected keratinocytes contain large amounts of E4 protein (up to 30% of total protein) [132], most likely creating a scenario with dead cells and cellular fragments covered with E4 at the mucosal surface, conceivably allowing interaction with incoming pathogens like HIV. Subsequently, accumulation of virus particles, with efficient presentation to target cells could take place. Indeed, the crosslinking of cytokeratin with E4 (chapter 1.2.3.4), important for the release of HPV particles, could serve as a scaffold, supporting the formation of large aggregates in an environment "protected" from extracellular proteases. This scenario seems plausible and argues against potential concerns that HPV E4 is not actively secreted. Another interesting finding is that although both viruses were found to infect the cervical mucosa at several places, HIV as well as HPV seem to preferentially infect their targets at the transition zone from ecto- to endocervix [3, 115]. Whether similar preferences exist within other mucosal tissues has to be evaluated by future studies. Further relevance of this model was added by IHC as well as MELC images, obtained from collaborations with Prof. M. Dürst/ Prof. N. Brockmeyer, and Prof. A. Baur, respectively. These data showed not only the presence of large amounts of E4 at different transmission sites, but also proximity of HIV target cells and E4 within an HPV-induced lesion (**Fig. 30, 44**).

During transmission of HIV, several parameters can potentially influence the infectivity of viral particles. In a thermostability assay, the "infectious half-life" of HIV particles incubated at 37°C was assessed. Here, HPV E4 was able to prolong the infectivity of a small virus inoculum by 4.4-fold and resulting after 48 h of incubation still in a 10-fold higher infection rate than the untreated control with a 15-fold higher MOI ("high MOI" reference) (**Fig. 31**). These data are of great interest, because in that way the time span, during which HIV is able to establish infection may be dramatically increased. Under *in vivo* conditions, the E4-mediated increase of particle's "infectious half-life" might be different due to the presence of other factors, including proteases. The large E4 amyloids are probably able to withstand degradation, allowing infection enhancement. In this context, it would be also interesting, which infection levels could be achieved upon incubating different MOIs at 37°C for different time spans, and afterwards trying to boost their infectious potency with amyloid enhancers. Such experiments could give additional insight into the mechanisms of how E4 stabilizes virus particles but also enhances infection in general.

Another factor of potential importance during HIV transmission is the pH within the different transmission fluids at the mucosae, e.g. an acidic pH in the vagina, a rather neutral pH in semen and a slightly basic pH at the anorectal mucosa [175-177]. The performed experiments

showed infection enhancement (72- to 140-fold) at all three pre-incubation pH conditions (pH 4.2, 7.4, 8.9), with neutral and basic pH showing a slightly higher infection enhancement than

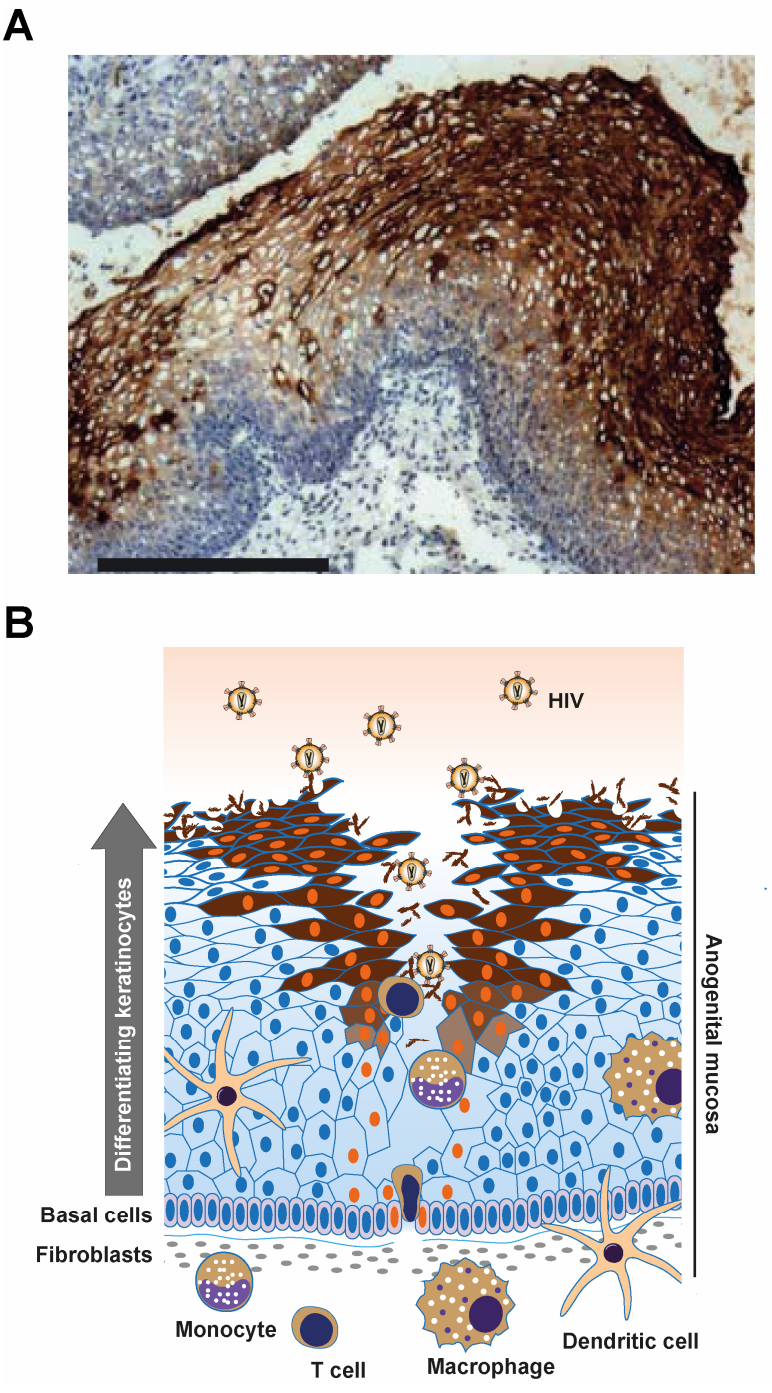

Figure 44: Model of HPV E4-mediated effect at transmission sites. (**A**) Immunohistochemical analysis of an HPV DNA-positive CIN lesion for the presence of E4 (brown staining). Data obtained in a collaboration with Prof. M. Dürst. For more detailed information, see **Fig. 30**. (**B**) Model of the mucosa with desquamating keratinocytes and an HPV-induced lesion with infiltrating HIV targets cells, E4 (brown cells/ extracellular aggregates) as well as incoming HIV particles. HPV E4 concentrates HIV particles in a “sponge”-like fashion and subsequently presents them to target cells, thereby increasing the likelihood to establish infection in the new host.

acidic pH (**Fig. 32A**). Notably, the different pH conditions apparently did not cause irreversible conformational changes, either to HPV E4 aggregates or to HIV particles. This hypothesis is based on the observation that the infection was carried out in RPMI medium, which neutralizes the pH previously used for pre-incubation of virus and E4, during the subsequent cell infection. The most physiological *in vitro* experiment for HIV transmission performed within this thesis was the pre-incubation of HPV16 E4 and HIV-1_{NL4-3} in the presence of vaginal fluid derived from different donors (**Fig. 32B**). This experiment combines several aspects: (thermo) stability of HIV particles in the presence of a transmission fluid, which likely contains proteases, immune mediators (e.g. cytokines/ chemokines/ antimicrobial peptides) as well as potentially other pathogens, and a physiological pH. Furthermore, the vaginal mucus could influence the interaction between HIV and HPV E4, since it was shown to entrap HIV particles thereby preventing infection [6]. In most tested donor fluids, amyloid-mediated enhancement of HIV infection was possible. For one donor two longitudinal samples were available, of which one allowed infection enhancement and the other did not, potentially indicating a different composition of the fluid, which could be due to one of the above listed parameters or also a factor related to the stage of the menstruation cycle. Few donor fluids did not support infection enhancement. Unfortunately, it was not possible to study details of the composition (e.g. by ELISA/ PCR to check for immune mediators/ pathogens) of the vaginal fluids, because of the small sample size. Concerning pH-dependent effects on infection enhancement, these experiments provided further information, since the pH indicator within the medium displayed an acidic pH (yellow staining of the medium), which was present from the step of adding the pre-incubation mix to the cell suspension until harvest of the experiment two days later. This suggests that not only E4/HIV pre-incubation can take place at acidic pH, but also the later steps of infection of target cells, still allowing enhancement. As in many previous experiments, differences in absolute infection as well as the starting infection were observed (comparing the different vaginal fluid donors) and are the cause of the variation in enhancement of infection levels. Thus, usage of these vaginal fluid samples is a very interesting tool, because they represent a relevant approach to mimic some of the conditions during transmission *in vitro*, but handling of these samples is generally difficult and permits no replicates due to limited sample volumes.

As mentioned above, in experiments applying co-administration of E4 and agitated SEVI, only the total concentration of amyloid was important for the degree of infection enhancement, indicating no obvious synergistic effect of the effective amyloids on each other. Interestingly, small amounts of E4 aggregates were able to seed SEVI amyloid formation in a dose-dependent manner and caused increased infection (around 28-fold) (**Fig. 33**). Experimentally, these observations were made without shaking, which is likely more physiological and stands in contrast to the usual way of SEVI agitation. This type of “cross-seeding” has already been described in the literature, e.g. for IAPP being able to seed Aβ, or bacterial Curli, which can

initiated the amyloid formation of SEVI [67, 150]. The data of this study, together with the reported observations, indicate the importance of pathogen-associated amyloids, maybe also of other so far unknown ones, both directly and indirectly, e.g. by seeding of seminal amyloids, enhancing HIV infection at transmission sites. In addition, the genital tract itself contains several amyloids, termed “functional amyloids”, which play important roles during reproduction, e.g. gametogenesis or maturation of sperm [69]. These “functional amyloids” are characterized by a fast transition from monomer to mature amyloids (see chapter 1.2.2), and potentially also support seeding of SEVI or pathogen-associated amyloids.

Concerning amyloids at transmission sites, several other aspects might be interesting for future studies: for example, during “compartmentalized” replication of HIV at the mucosa [4] of the infected host, the presence of HPV E4 may lead to a higher viral load in the transmission fluid. Such a scenario could increase the likelihood of establishing a HIV infection in the new host, and would probably be boosted further by the presence of cellular debris and immune mediators, due to the high local virus replication. Another interesting point is raised by the recently published data on semen amyloids and their function during reproduction in helping to immobilize and clear damaged sperm from the ejaculate, with the help of macrophages [96]. In the context of “functional amyloids”, it would be interesting whether E4 aggregates, with their preferential location at the cervix, could also participate within the described selection process during reproduction. Of note, amyloids within the anogenital tract can play somewhat controversial roles, with for example SEM amyloids exhibiting bivalent functions. Here, certain cleavage products have been reported to be antiviral, whereas others are able to enhance HIV infection [80, 83, 84]. Approaches trying to lower the amyloid load within the genital tract by applying inhibitors of amyloid formation or amyloid breakers [66-68] with the aim to reduce the risk of amyloid-related increase of HIV transmission have to be considered with care. Not least because, besides many pathogen-associated amyloids, also the diverse set of “functional amyloids” could be harmed, and hence might interfere with the fine-tuned functions as well as homeostasis of the anogenital tract environment. Based on the current study, a “broader” HPV vaccine would be beneficial, because it allows the specific abrogation of infection by HPV [103, 112, 114], thereby lowering the abundance of E4 at transmission sites, without any side effects on the physiological amyloids.

4.3 HPV E4’s structural requirement for infection enhancement

The amino acid sequences of the E4 proteins from different HPV types show large variations, but share structural similarities, which are supposed to mediate the functions required during HPV replication. Generation of several structural as well as charge mutants, aimed at narrowing down the residues relevant for HIV infection enhancement, allowed identification of the *C*-

terminus. The minimal requirement could be linked to a mutant containing, with the *multimerization* and the *β-aggregation* domain, the 22 *C-terminal* amino acids of the HPV16 E4 protein (**Fig. 34, 45, S17**). In addition, the importance of charge for the E4-mediated enhancement of infection was supported by the use of alanine mutants. The role of positive/cationic net charge in enhancing HIV infection was already studied by the Roan et al., which analyzed semen amyloids and could block infection enhancement effects using anions [76]. Within this thesis

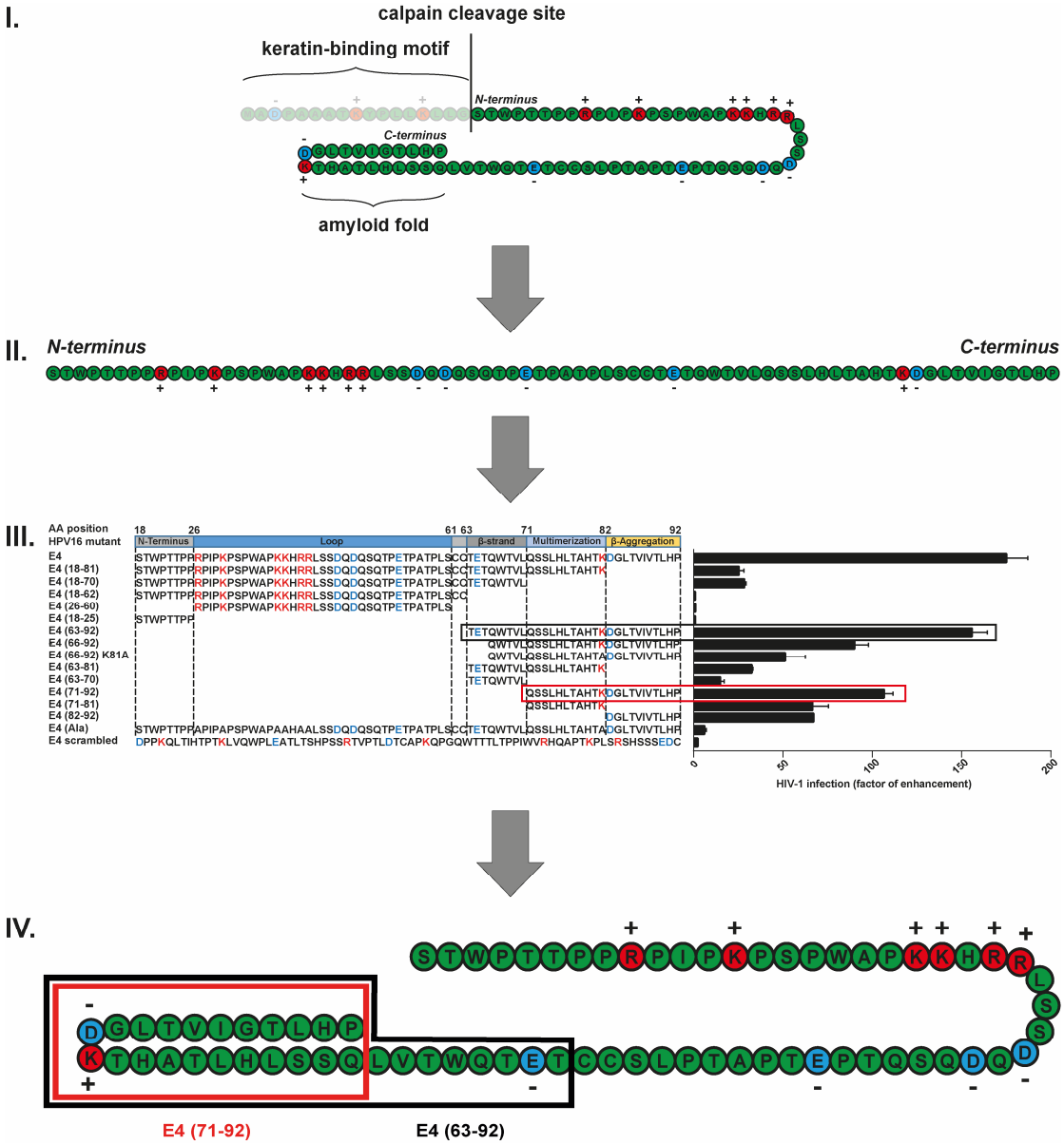

Figure 45: HPV E4-mediated enhancement of HIV infection is dependent on E4's *C-terminus*. E4 is processed during keratinocyte differentiation (I.), which results in the deletion of almost the complete *N-terminal* keratin-binding motif (grey shading). Based on the *N-terminally* truncated E4 protein (II.) a set of mutants (III.) was created to study the relevance of the different structural domains in the context of infection enhancement. Enhancement of HIV infection is dependent on the *C-terminus* (III.) and can be mapped within the region of the amyloid fold (IV.). Schematics in (I.) and (IV.) are modified from Doorbar [132].

similar experiments were conducted, but due to the fact that anions interfere with HIV infection even in the absence of amyloid enhancers, were not included and will require further studies. A caveat of the current experimental setup was the usage of the same weight per volume of the peptides within the HPV16 E4 mutant panel in this screening. This might over- or underestimate the HIV infection enhancement in some cases, due to the variable length of the different mutants resulting in different molarities. Further studies will have to include this point, but the fact of gradual *C-terminal* deletion causing stepwise abrogation of infection enhancement and only specific subunits (or combinations) of the *C-terminus* leading to enhancement, supports the importance of this part of the peptide for E4's function. Finally, the amino acid sequence-related structural organization of E4 plays an important role, which is indicated by the loss of infection enhancement in the E4 scrambled peptide (and in part the E4 Ala mutant). The importance of structure in addition to charge was supported by EM studies (data obtained in collaboration with Dr. M. Neßling and Dr. K. Richter (Core Facility Electron Microscopy, DKFZ, Heidelberg, Germany)) of the different HPV E4 variants and HPV16 E4 mutants. These data revealed a requirement of intermediately packaged amyloid structures, referred to as morphotype II and III, which correlated with HIV infection enhancement (**Fig. 35**).

Taken together, the data discussed so far suggest that the HPV E4-mediated enhancement causes accumulation of HIV particles, which requires defined amyloid structure of the peptide, and is to some degree dependent on charge. This leads to enhanced attachment and fusion of viral particles, through the classical HIV entry pathway. Moreover, HPV E4 is able to increase the duration of particle infectivity, can mediate enhancement of infection under different pH conditions as well as in vaginal fluid and induce amyloid formation of SEVI.

4.4 HPV E4 as a potential tool for research

HPV E4 was shown to potently enhance HIV infection, which could also be an interesting tool for research. For example, enhancement of retroviral infection during spreading infection (**Fig. 24, 25**), could be beneficial for cell-culture virus propagation assays. Moreover, amyloids could be useful for the isolation of viruses from serum/plasma or other body fluids. In particular, a more efficient isolation from transmission fluids may be possible, since the activity of HPV E4 was shown also in vaginal fluid (**Fig. 32B**). Incubation of patient samples with amyloids like E4, followed by spinning of the sample and subsequent addition to target cells could help to isolate otherwise "sub-infectious" virus loads. For most experiments performed within this study, virus-amyloid incubation was performed in a small volume, to make the interaction more efficient. In case of bigger volumes of body fluids, interaction between virus and amyloid can be facilitated by shaking the sample during pre-incubation, as performed for infection enhancement experiments using cell culture supernatants of the HIV-2_{V18} primary isolate (**Fig. 22E**). Another interesting application of amyloid enhancers of infection could be their application in

viral outgrowth assays, where co-culture of target cells with leukocytes of an HIV-infected host could boost infection and thereby make the read out more sensitive.
The E4 peptides used within this thesis were synthesized, and due to their length, were rather complicated and expensive. Here, the much shorter mutants HPV16 E4 (71-92) and E4 (63-92) could be the solution, since those were also able to enhance HIV infection efficiently. As shown by previous studies for synthetic nanofibrils [183], such short peptidic fragments can be used in different experimental approaches, requiring for example enhancement of lentiviral transduction.

4.5 Amyloid enhancers might alter the efficiency of therapeutic approaches

Up to date there is still no potent active vaccine available but initial clinical studies using bNAbs (broadly neutralizing antibodies) to treat HIV-infected patients seem to be promising as a passive immunization approach (see chapter 1.1.7). HPV E4 is abundantly expressed at transmission sites, potentially increasing HIV loads in the transmission fluid of donors. In a worst-case scenario, additional HPV infections in the recipient could subsequently also increase the transmission rates. In the context of PrEP, PEP, ART or passive immunization with bNAbs such altered conditions could be of great importance [1, 9, 63-65]. Within this study, (b)NAbs were kindly provided by the lab of Prof. F. Klein (Laboratory of experimental Immunology, Cologne, Germany) and tested with a small panel of different HIV-1 strains (HIV-1_{NL4-3}, HIV-1_{YU-2}, HIV-$1_{49.5}$, HIV-1_{CH058}, HIV-1_{CH077}) to validate their functionality. Analyzing the general neutralization capacity of this bNAb panel in a pre-screen without amyloid enhancer demonstrated large differences in neutralization potency dependent on the targeted epitope, with antibodies targeting the CD4 binding site (CD4bs, 3BNC117/ VRC01) being the most potent ones (**Fig. 36**).
In the presence of the amyloid enhancers E4 and SEVI, still CD4bs antibodies were much more potent than the gp41/gp120 bridging antibody 8ANC195 (**Fig. 37, S18**). The latter allowed no complete neutralization of infection with HIV-1_{NL4-3} and HIV-1_{CH058} at the highest antibody concentration (5-fold higher than the highest concentration used of CD4bs antibodies) when E4 or SEVI were present. The overall potency of CD4bs antibodies reflects the importance of the initial CD4-Env interaction during HIV entry, which is supported by the previously described data, using antibodies causing neutralization of CD4 on the target cell. According to the literature, 8ANC195 preferentially binds to closed Env trimers (leads to a stabilization of this conformation), but it could also interact with several other Env conformations. Interestingly, it was described that this bNAb could also bind Env molecules, which are already bound to CD4, which “partially recloses the trimer or captures and stabilizes a pre-existing conformation” [53, 184]. Accordingly, there are at least two possible explanations for the observed phenomenon: (i) shielding of the 8ANC195 epitope or (ii) stabilization of an altered conformation by the amyloid enhancers, which does no longer allow efficient antibody binding.

The latter could be due to high mobility of the Env trimer also in absence of CD4 and the potential stabilization of the Env bridging sheet [32, 36]. Specificity of the data obtained was supported by the 4-95 NAb, which had no effects.

More detailed analysis of the data and calculating simplified IC50 values, revealed the most dramatic changes for the T/F virus HIV-1_{CH058} (4.2- to 16.1-fold, **Fig. S19A**) in the presence of amyloid enhancers. This is interesting, since current translational approaches also propose applicability of bNAbs in the context of PrEP. This preliminary finding suggests the need to include more T/F viruses in future bNAb screening projects. Experiments titrating the previously used binding and entry inhibitors in combination with the lab strains HIV-1_{NL4-3} and HIV-1_{YU-2} showed comparable tendencies, requiring 10- to 100-fold higher inhibitor concentrations to block infection in the presence of amyloid enhancers (data not shown). Another way of evaluating potency of bNAbs in the presence of amyloid enhancers was to calculate the factors of infection increase in the presence of amyloids, when infection levels of the “virus alone” condition were reduced by at least 50%. This analysis highlighted the potency of the amyloid enhancers used, since for E4 up to 54-fold and for SEVI up to 45-fold higher infection was observed (**Fig. S19B-D**). Unfortunately, this way of analysis has a certain caveat. The concentration of antibodies targeting the CD4bs (0.1 µg/ml) was 100-fold lower than for the 8ANC195 antibodies (10 µg/ml). Even though this underlines the high efficiency of bNAbs targeting the CD4bs, it makes a direct comparison to 8ANC195 more difficult.

Taken together, these data demonstrate that higher concentrations of bNAbs as well as binding and entry inhibitors are required in the presence of amyloid enhancers like HPV E4 or SEVI. These data are of importance for future *in vitro* screening trials analyzing the potency of new drugs and bNAbs. Consequently, such data should be included when choosing for example bNAb panels for clinical studies. In addition, theses enhancers of viral infection could, due to more efficient replication of HI-viruses, potentially cause faster viral escape, supplying another important argument for applying combined therapies using antibodies targeting several epitopes on Env (bi-/tri-mix) [49, 61, 63]. Future studies with broader panels of bNAbs will enhance our understanding of the mechanisms involved in both viral entry and functionality of amyloid enhancers of viral infection.

4.6 Amyloids of various origin enhance infection with HIV, neurotropic and respiratory viruses

Besides the anogenital tract, amyloids can play important roles within other tissues, frequently having regulatory functions, but can become pathologic under certain conditions (chapter 1.2.1/1.2.2/1.2.4). After studying extensively the effect of E4 and SEVI on HIV infection, this last section will discuss results obtained from experiments using different neuro-associated amyloids (Aβ, α-synuclein) as well as the pancreatic IAPP. HIV-1 with its great sensitivity to

amyloid-mediated enhancement of infection was chosen for the initial screening, revealing increased infection for all amyloids tested (**Fig. 38**). Interestingly, E4, SEVI as well as β-amyloids led to a comparable degree of enhancement of HIV infection (around 130-fold on primary activated CD4 T cells), whereas the amyloids of α-synuclein and IAPP displayed a lower degree of infection enhancement (15- to 21-fold).

Although HIV was primarily used as a sensitive experimental tool in this context, it is also known that HIV can enter the brain, which usually happens quite early after transmission, where it can infect a set of cell types. Among these, microglia are believed to play the most important role, but also astrocytes and oligodendrocytes have been shown to be susceptible to HIV infection. HIV replication in the brain has been reported to be associated with stroke, neurocognitive impairment and dementia. This might be caused by infection of the above cell types or the HIV-related endothelial dysfunction [9, 185]. Hence, extracellular aggregates of Aβ could support the HIV infection of different cells in the brain, thereby contributing to the described pathologies and potentially helping to establish the HIV reservoir in this compartment [186]. Another interesting hypothesis could be related to the beta and gamma HPV types present in the oral cavity [102], which could lead to increased replication of HIV in oral lymphatic tissue, thereby increasing spread and systemic viral loads. Whether amyloid networks enhancing viral loads locally exist, and which viruses can benefit from them *in vivo* has to be evaluated by further studies. Also the less potent α-synuclein, which is not actively secreted, but might be set free by dying cells, could be of importance in this context, either by cross-seeding of other amyloids or by increasing with its presence the local total amyloid concentration.

For the Alzheimer's disease-associated Aβ peptides and the Parkinson's disease-related α-synuclein several mechanisms of causing these diseases have been proposed [142-145]. A so far underestimated role in this regard could play neuro-associated viruses like HSV-1, HHV6/7 or MeV, which are so far mainly known to cause encephalitis [151, 154, 155, 187, 188]. Analysis of infection data generated on HEK293T cells (up to 6.2-fold) and the neuronal cell line SH-SY5Y (up to 2.9-fold) exhibited much lower levels of infection enhancement when using these viruses than observed for HIV. Nevertheless, these results may be of physiological relevance, because the former viruses are more cytopathic aggressive in infection than HIV (**Fig. 39, 40 each A,B,E**). Interestingly, it was reported that HSV-1 and Aβ peptides seem to have an interplay during Alzheimer's disease. Stress-induced HSV-1 reactivation was demonstrated to cause accumulation of Aβ and brain damage. Other reports have indicated an antiviral role for β-amyloid [189, 190]. A typical observation, made for many of the viruses other that HIV used in this thesis is a "bell"-shaped pattern of infection enhancement in response to amyloid concentrations, exhibiting a distinct loss of infection enhancement when exceeding a certain amyloid concentration. This phenomenon is most likely not due to cytotoxicity (based

on not shown flow cytometry data) and might be a sign of virus entrapment within larger aggregates. One can hypothesize a scenario in which an initially low virus infection, *in vivo* leads to a self-propagating interplay of virus replication and Aβ deposition. The resulting high amyloid concentrations could cause inhibition of further virus infection. Similar self-perpetuating mechanisms could be factor in the development of encephalitis caused by HSV-1 or MeV infection of the brain. Local presence of amyloids may in part explain reduced efficiency of antiviral therapies, as seen for HIV. Besides HSV-1, also other herpes viruses have been shown to be associated with neurological disorders (also epilepsy), including HHV6/7, and should be included in future studies. The same is true for CMV, which is able to induce HSV reactivation by causing immune dysregulation, and whose enhanced infection in the presence of semen amyloids has been reported [86, 189].

As described by others, pancreatic IAPP is associated with the loss of β-cells in diabetes type 2, but could be also one of the missing links causing depletion of those very cells leading to diabetes type 1 [148, 149]. There are several reports indicating the presence of HHV6b but also enteroviruses in the pancreas of patients with diabetes [191-194]. Infection and replication of these viruses could be facilitated by the presence of IAPP, leading to the described tissue destruction. Neuro-associated amyloids could also play an important role in the pathogenesis of RABV infection, which could fuel the infection and damage of the brain after the retrograde transport. In this context, this thesis provided interesting findings revealing an up to 4.9-fold (α-synuclein) infection enhancement on HEK293T cells, and up to 4.2-fold (Aβ40) on the neuronal cell line SH-SY5Y, using the lab-adapted rabies virus* strain N2C. The attenuated rabies virus* strain SAD L16 showed lower increase of infection on both cell lines (maximum 2.4-fold) (**Fig. 39, 40 each C-E**). Whether these data may suggest a preferential effect of specific amyloids depending on the virus has to be elucidated by future studies.

The potential of these amyloids to enhance viral infections or transductions has to be taken into account, since both HSV and MeV are used in the clinic as therapeutic oncolytic viruses [160, 164, 165]. In addition, the usage of RABV to trace neuronal connections under lab conditions has to consider these data also during experimental design and interpretation of data. Furthermore, E4 and SEVI could play important roles in the transmission (oral/sexual) and local replication of HSV-1/-2.

Finally, E4 and SEVI amyloids were capable of enhancing also adenoviral infection up to 8.1-fold, when applying AdV2 in combination with E4 (**Fig. 41A, 42**). Besides recapitulating the previously described “bell”-shaped infection enhancement pattern, the experiments suggested a saturation of infection (E4) or an entrapping of virus particles (SEVI)-phenotype (**Fig. 41B**). The potential entrapment of viral particles may be important for viruses other than HIV. This notion is based on the observation that the amyloid concentrations leading to the strongest infection enhancement are often lower for these viruses than for HIV. The actual reason for

this observation has to be examined in future studies. Although mechanistically interesting, since adenoviruses represent the only non-enveloped virus in this study, enhancement of infection for this virus family may be of relevance in the respiratory tract. HPV has been reported to be present in the respiratory tract examining for example lung cancer or recurrent respiratory papillomatosis (RRP). *Beta-papillomaviruses* replicating in the oral cavity supplying desquamating cells with large amounts of E4 may support infection in the respiratory tract by other viruses (see chapter 1.2.3.1) [102, 110, 118]. Preliminary data, excluded from this thesis, imply the presence of HPV E4 in respiratory samples (BAL, sputum, etc.), but have to be validated by more detailed studies. Taken together, the amyloid panel used in this thesis enhanced infection of viruses studied, covering a broad spectrum of diseases, in a dose-dependent manner.

4.7 Outlook

The present thesis intensively characterized properties of HPV E4 proteins as enhancers of HIV infection under *in vitro* as well as *ex vivo* conditions. HPV E4 was shown to increase attachment and fusion of HIV particles to target cells, which resulted in enhanced productive infection *in vitro*. Moreover, HPV E4 was able to mediate infection enhancement within a broad range of pHs, impair efficacy of bNAbs and induce seeding of non-agitated SEVI. Structural analysis revealed the 22 *C-terminal* residues of E4 to be crucial for HIV infection enhancement. Experiments performed in this thesis and by others show that E4-mediated infection enhancement works also in more complex *ex vivo* systems, e.g. incubation of virus and HPV E4 in the presence of vaginal fluid prior to infection of target cells, or incubation of HIV and E4 prior to infection of HLAC (human lymphocyte aggregate culture), respectively. These *ex vivo* models, trying to mimic the complex milieu at transmission sites, are inevitable to validate *in vitro* data. Still, these models are unable to recapitulate the complexity of events involved in HIV transmission. As reported for SEVI [74, 78, 79], there are unfortunately currently no appropriate *in vivo* models available, which would allow the validation of the obtained *in vitro* and *ex vivo* data on the HPV-mediated HIV infection enhancement. Here, longitudinal follow-up studies such as the “HISIS (HIV superinfection study) cohort” consisting of HIV-negative female bar workers, which were regularly checked for their HIV/ STD status by vaginal swaps, may increase our understanding. Retrospective correlative analyses of HIV status and vaginal co-infections such as HPV, will provide interesting insight into the potential cross-talk of STIs causing disease [195].

Besides providing a new perspective on possible limitations of current preventive and therapeutic approaches for HIV, this thesis gives an overview on the potential of amyloids of anogenital (E4/ SEVI), neuronal (Aβ40/Aβ42/α-synuclein) and pancreatic (IAPP) origin to increase infection of different viruses. This encompasses HIV, HSV, MeV, RABV and AdV, which all

can target multiple organs and are the causative agents of important diseases placing a considerable burden on the human population. Their effect on viral infection together with the fact of many of the amyloids studied cause diseases likely on their own, underlines the importance of finding ways to eliminate accumulations of such amyloids. However, despite their pathological role many of these amyloids also have distinct physiological functions, making their overall depletion difficult. In contrast, the HPV vaccine (Gardasil®9), which is at the current stage able to target nine different HPV types (oncogenic and non-oncogenic, see chapter 1.2.3.1), offers in this context a promising tool, due to its potential of specifically preventing HPV infections, thereby also lowering the abundance of E4-derived aggregates at mucosal surfaces. Based on our study the development of new vaccination regimens with the goal of targeting the more than 40 genitally transmitted HPV types (https://www.cancer.gov/about-cancer/causes-prevention/risk/infectious-agents/hpv-vaccine-fact-sheet) should be supported. Ongoing studies could provide a big step in this direction by generating more broadly acting vaccines containing fusion peptides of L1, which self-assembles into VLPs, and highly immunogenic fragments of the minor capsid protein L2 [112, 114]. Interesting in this context, will be the outcome of HPV vaccination on the potential decline of the HIV pandemic in retrospective field studies in sub-Saharan Africa.

The effect of the different amyloid enhancers analyzed in this study, will be of importance for future screening approaches as well as the subsequent design of clinical studies evaluating the potency of new drugs against transmission of HIV, but also other pathogens. In addition, viral outgrowth assays as well as isolation of new virus strains from patient material will be likely more sensitive when using amyloid enhancers. Further, the data on infection enhancement of viruses than HIV could help to understand so far poorly understood pathologies. Here, the role of neuro-associated amyloids in combination with MeV and herpesviruses, supporting the progression of encephalitis, dementia as well as epilepsy, will have to be studied in more detail. Also, a better understanding of the impact of IAPP, with regard to viral (herpesvirus and enterovirus) infections, on the development of diabetes has to be elucidated. Finally, screening studies uncovering additional amyloids either originating from the host or pathogens (e.g. bacterial Curli) as well as deciphering potential network functions of different amyloids are required, and will potentially allow an improved treatment of different diseases.

5 Supplemental figures

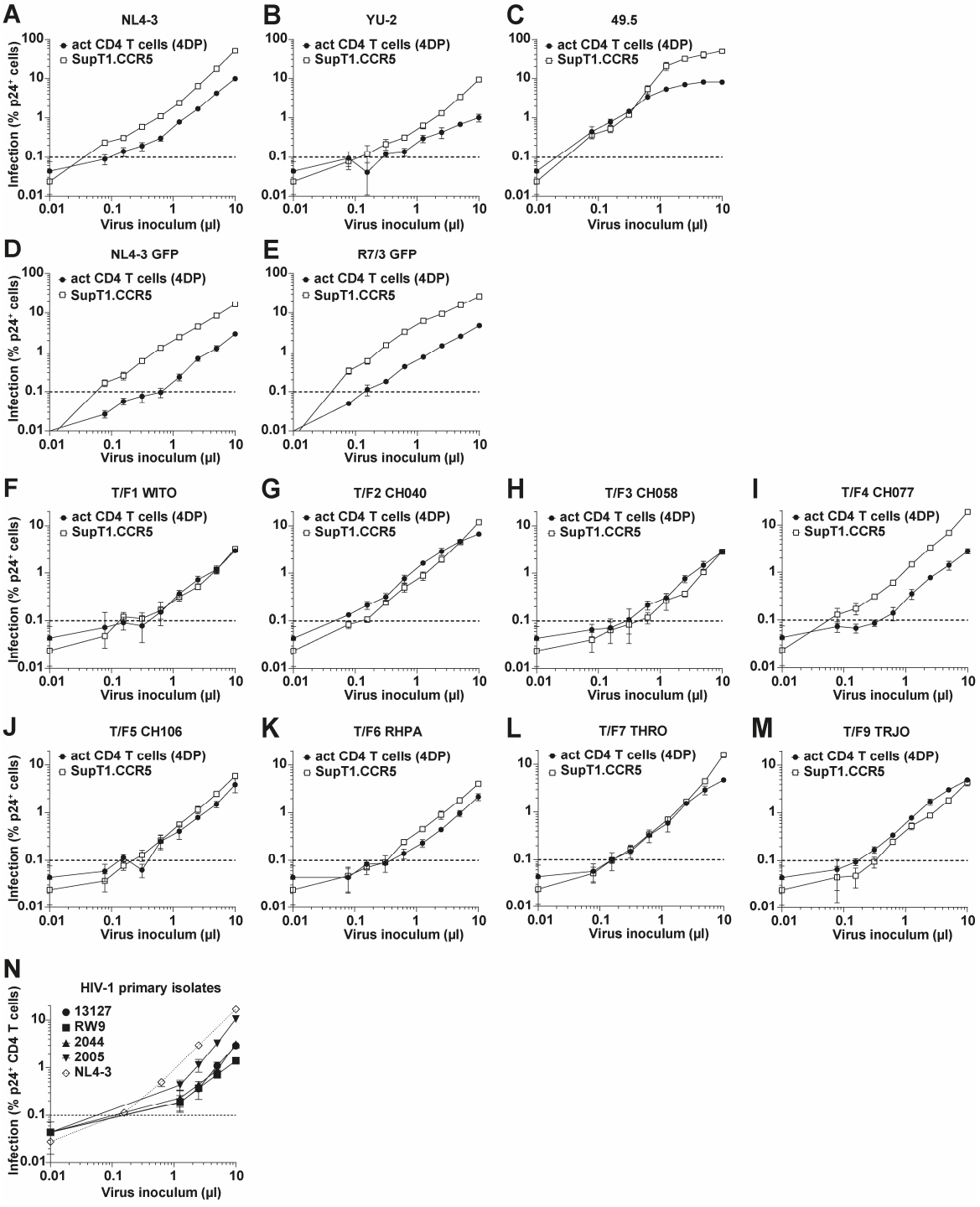

Figure S1: Overview of titrations of different HIV-1 lab strains, T/F strains and primary isolates. Donor pools of primary activated CD4 T cells (**A-N**) or SupT1.CCR5 cells (**A-M**) were infected with increasing virus inoculum of different HIV-1 lab strains (**A-E**), T/F strains (**F-M**) or primary isolates (**N**). 48 h post challenge, infection levels were determined by measuring intracellular p24 (**A-C, F-N**) or GFP expression (**D+E**) by flow cytometry. Depicted are the arithmetic mean and standard deviation of three technical replicates. Data shown represent either one experiment (**N**), or are representative of two experiments (**A-M**). Supplementary figure for **Fig. 19**.

A

Virus	BCA Titer [x10^8 IU/ml]	SG-PERT [x10^9 RT Units/µl]	p24 ELISA [ng/ml]
NL4-3	2.3 - 5.4	3.38	2309.07
YU-2	0.21 - 0.3	3.4	2125.16
49.5	5.72	9.87	5607.92
NL4-3 GFP	0.6	2.47	792.46
R7/3 GFP	1.6	10.6	989.40
WITO (T/F1)	0.037 - 0.043	6.65	5025.54
CH040 (T/F2)	0.97 - 3.9	9.55	2833.97
CH058 (T/F3)	0.19 - 0.48	3.01	2263.09
CH077 (T/F4)	0.52 - 0.64	0.73	2494.25
CH106 (T/F5)	0.57 - 0.61	1.44	2146.15
RHPA (T/F6)	0.062 - 0.085	4.22	4462.36
THRO (T/F7)	0.098 - 0.29	2.68	2298.49
TRJO (T/F9)	0.11 - 0.29	2.08	1379.10

B

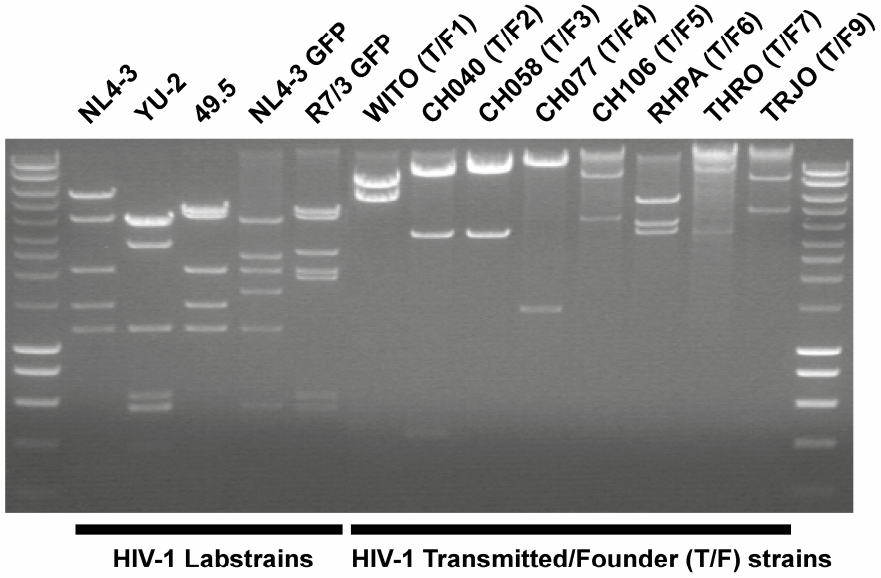

C

Virus	p24 ELISA [ng/ml]	BCA titer [IU/ml]
13127	1262.16	0.85 x 10^6
RW9	2946.13	0.68 x 10^8
2044	3987.04	0.64 x 10^6
2005	4015.29	5.2 x 10

Figure S2: Characterization of HIV-1 lab strains, T/F strains and primary isolates. (**A**) The stocks of the different HIV-1 lab strains and T/F strains were characterized with different assays: HIV reporter cell assay (TZM-bl cells, BCA titer), measurement of RT activity (SG-PERT) and p24 CA ELISA were performed. (**B**) Restriction digest of the proviral plasmids used to produce viruses characterized in (**A**). For restriction enzymes, see chapter 2.4.1.2. (**C**) p24 CA ELISA and HIV-1 reporter cell assay of virus stocks of HIV-1 primary isolates. Supplementary figure for **Fig. 19**.

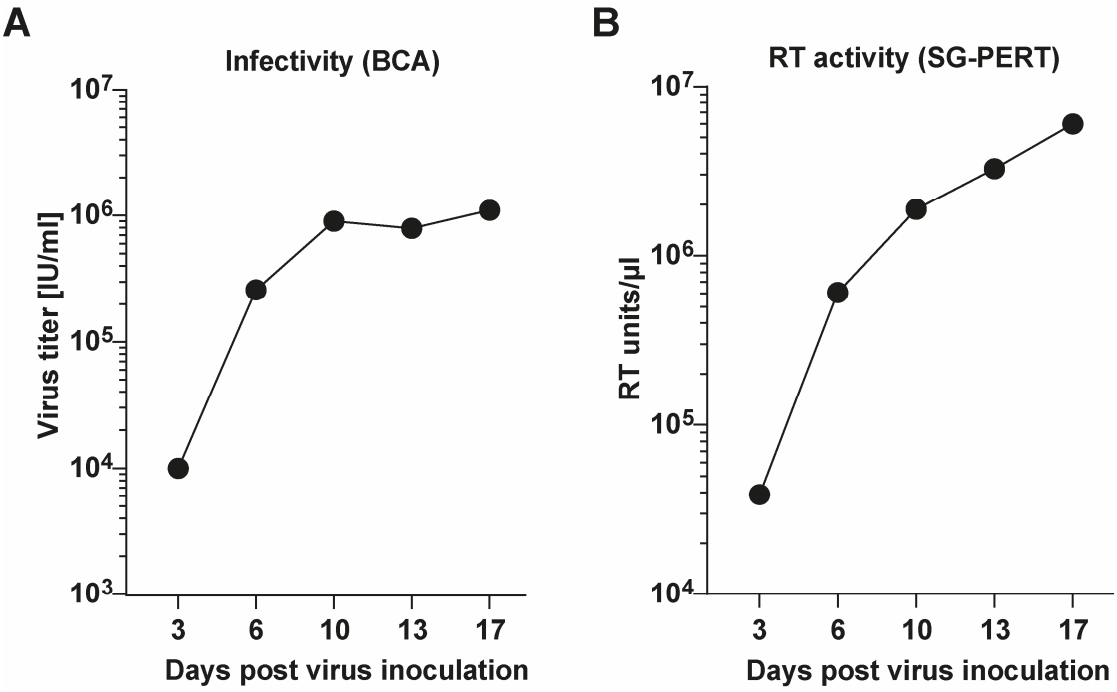

Figure S3: Infectivity and RT activity of the HIV-2$_{V18}$ primary isolate stock. Expansion of the HIV-2$_{V18}$ primary isolate was performed using donor pools of primary activated CD4 T cells. At the indicated time points post inoculation, virus-containing supernatants were harvested and fresh target cells were added. Virus-containing supernatants were aliquoted and stored at -80°C. All collected virus-containing supernatants were characterized for their infectious titer (**A**) and RT activity (**B**).

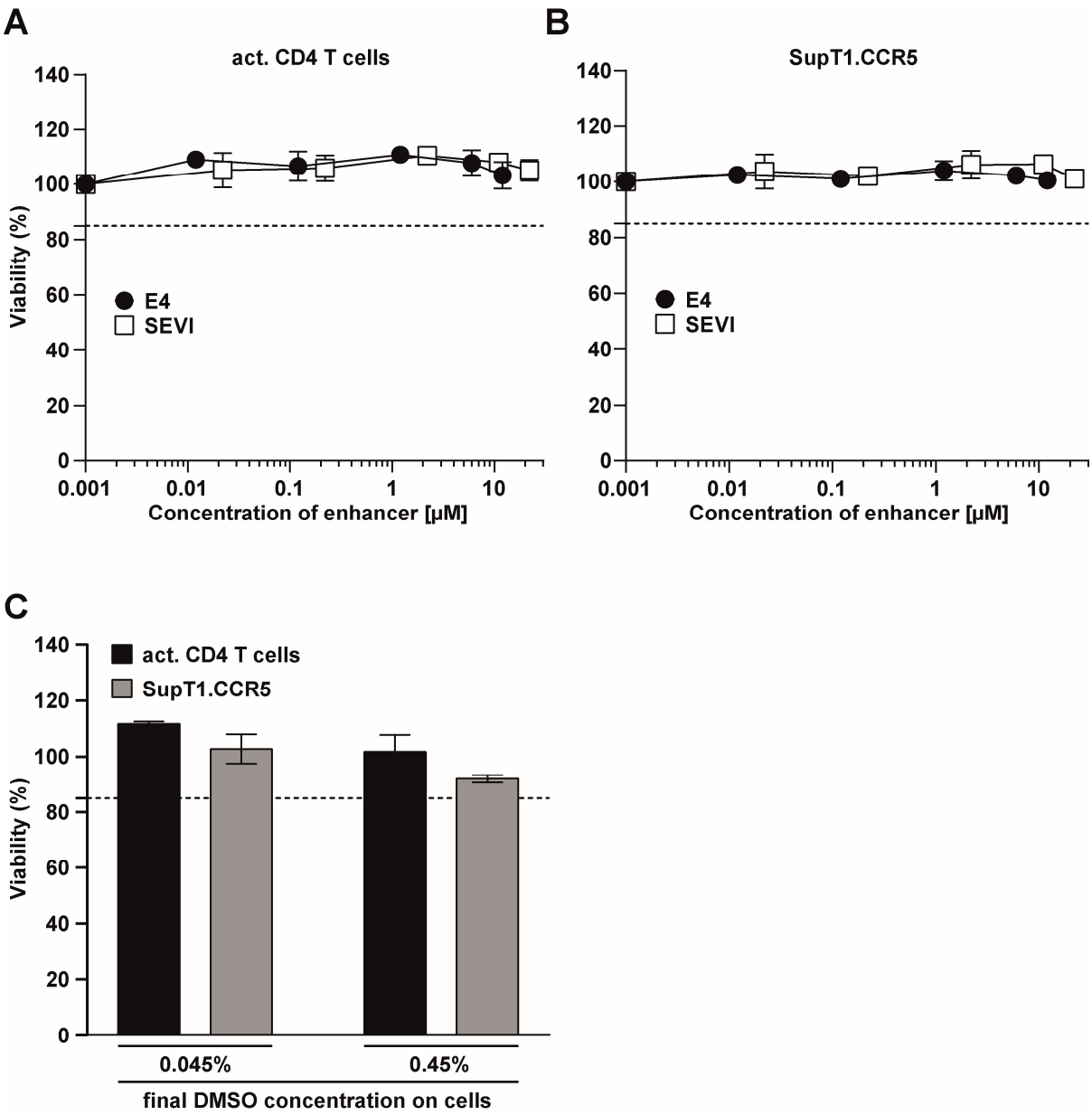

Figure S4: HPV16 E4 and SEVI are not cytotoxic to primary activated CD4 T cells and SupT1.CCR5 cells. A three donor pool of primary activated CD4 T cells (**A**) or SupT1.CCR5 cells (**B**) were incubated for 44 h with increasing concentrations of either HPV16 E4, or SEVI. Solvent controls were used (**C**). Next, Resazurin was added to cell suspension at a final concentration of 24 µg/ml followed by incubation for four hours in the dark in a cell culture incubator. Fluorescence was measured using the Clariostar plate reader. Background was subtracted and data were normalized to untreated cells, which were set to be 100% viable. Depicted are the arithmetic mean and standard deviation of three technical replicates. Data shown represent one experiment (**C**) or are representative of two experiments (**A,B**). Supplementary figure for **Fig. 20**.

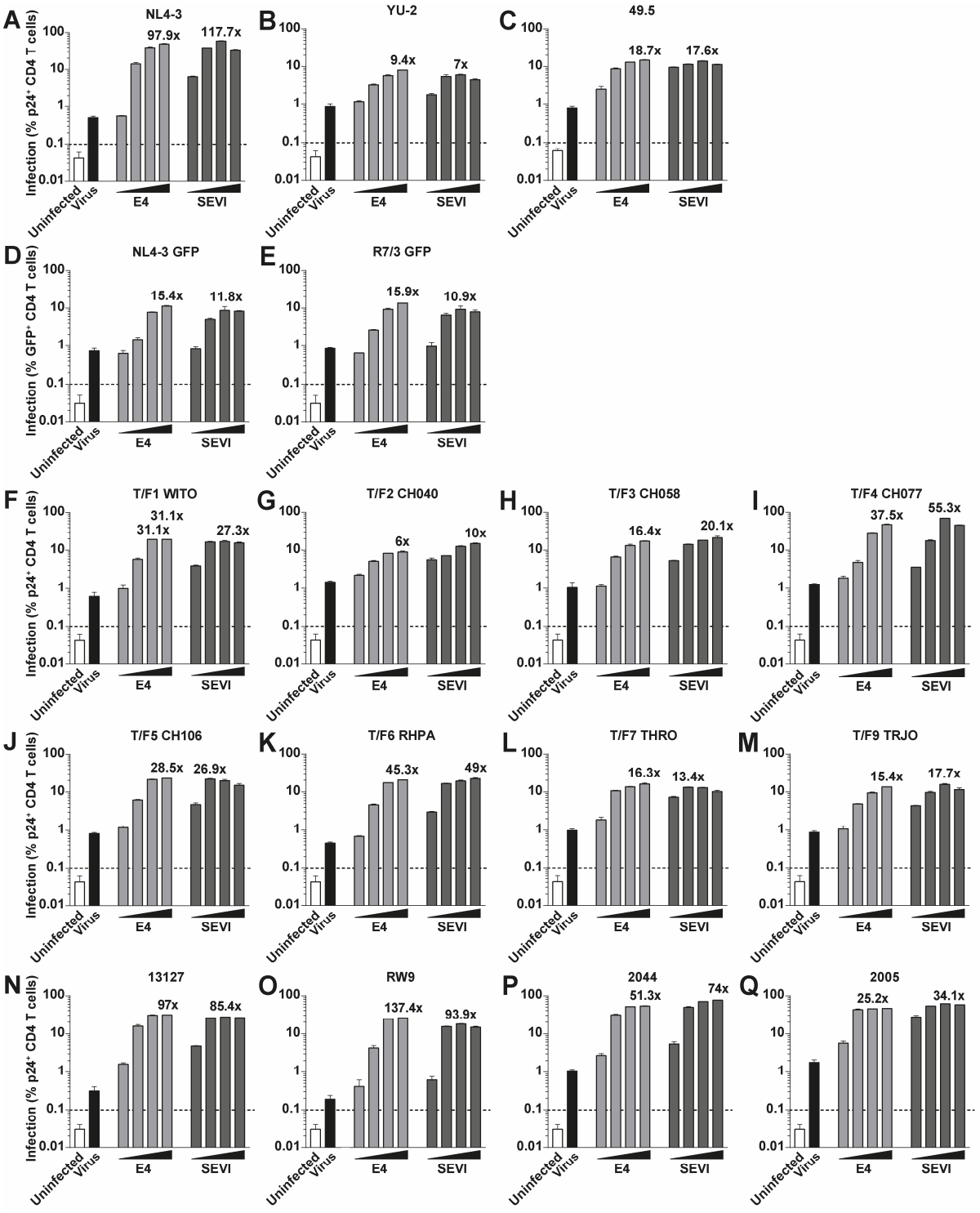

Figure S5: Overview of concentration-dependent effect of HPV16 E4 and SEVI on enhancement of infection with HIV-1 lab strains, T/F strains and primary isolates. A low virus inoculum of different HIV-1 lab strains (**A-E**), T/F strains (**F-M**) or primary isolates (**N-Q**) was pre-incubated with either PBS (black bar), a titration of HPV16 E4 (0.12, 1.2, 6, 12 µM, light grey bars), or SEVI (0.22, 2.2, 11, 22 µM, dark grey bars). Next, donor pools of primary activated CD4 T cells were challenged for 48 h. Infection was quantified by flow cytometry by either intracellular p24 (**A-C, F-Q**), or GFP expression (**D+E**). As a reference, uninfected cells are shown (white bar). Depicted are the arithmetic mean and standard deviation of three technical replicates. Data shown represent either one experiment (**N-Q**), or are representative of two experiments (**A-M**). Supplementary figure for **Fig. 22**.

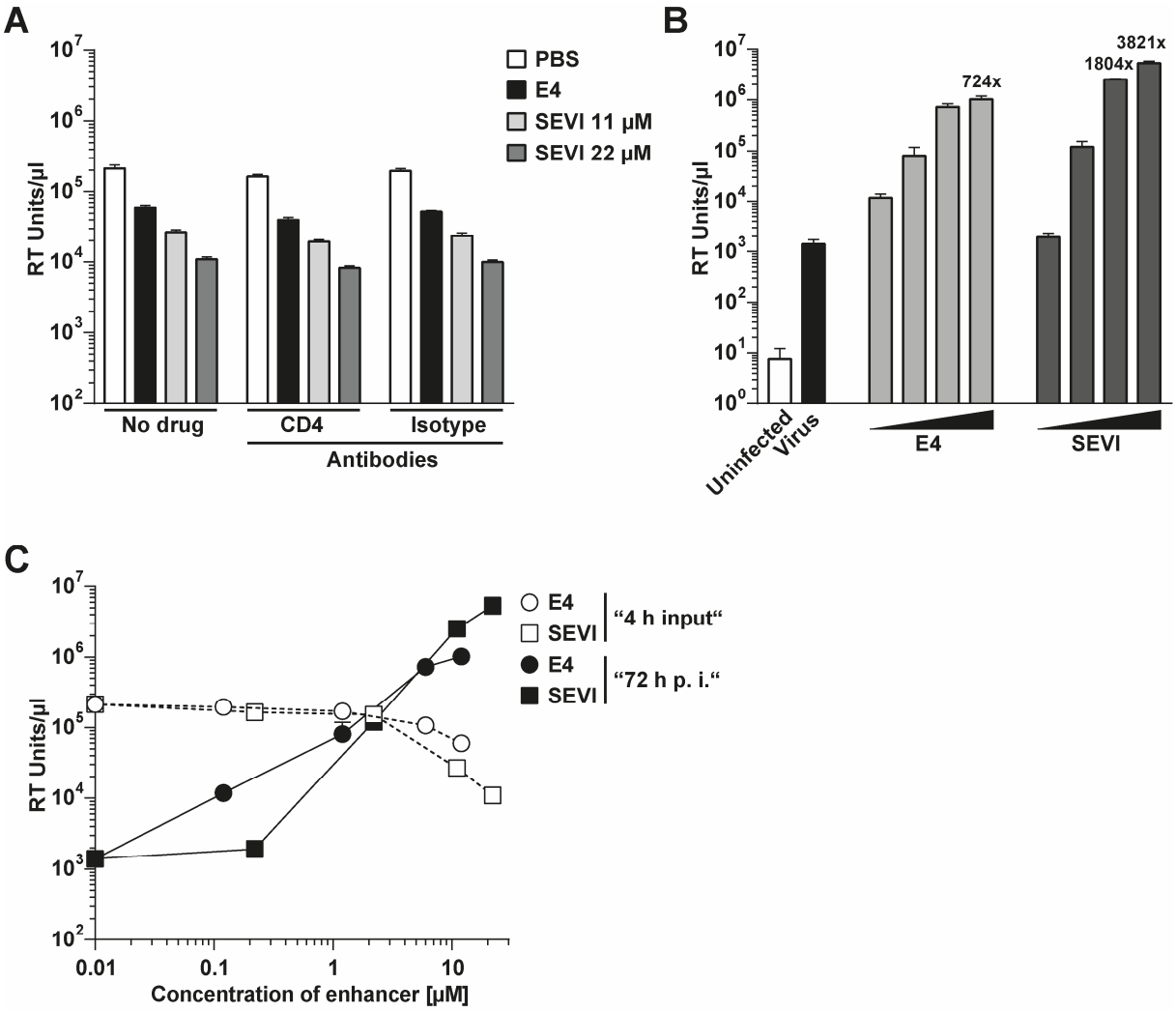

Figure S6: Effect of amyloid enhancers on infection of primary activated CD4 T cells with HIV-2_{V18} primary isolate. A donor pool of primary activated CD4 T cells was pre-treated with either no drug, CD4 blocking antibodies (100µg/ml), or isotype control antibodies for highest enhancer concentrations. Next, the HIV-2_{V18} primary isolate was incubated with either PBS, E4 (0.12, 1.2, 6, 12 µM), or SEVI (0.22, 2.2, 11, 22 µM) and then cells were challenged with the different mixes. Four hours post infection, a medium change was performed, of which the virus-containing medium was kept for analysis ("4 h input"). 72 h post infection ("72 h p. i."), supernatants were harvested. "4 h input" and "72 h p. i." samples were analyzed for RT activity. (**A**) Analysis of "4 h input" samples by SG-PERT. HIV-2_{V18} primary isolate was pre-incubated with either E4 (12 µM), or SEVI (11 µM or 22 µM) previously to infection of a donor pool of primary activated CD4 T cells. Cells were treated with either PBS, anti-CD4 antibodies, or isotype control antibodies prior to infection. (**B**) SG-PERT analysis of the "72 h p. i." samples, showing RT activity of the virus alone (black bar) and in the presence of increasing concentrations of E4 (light grey) or SEVI (dark grey). Also, the background of the assay is shown (white bar). The factor of enhancement of infection is depicted on top of the respective histogram bar. (**C**) Overlay of SG-PERT data from "4 h input" (white symbols) and "72 h p. i." (black symbols) samples. Depicted is the effect of E4 (circles) and SEVI (squares) titrations on infection of primary activated CD4 T cells with HIV-2_{V18}. Shown are the arithmetic mean and standard deviation of three technical replicates. Supplementary figure for **Fig. 22**.

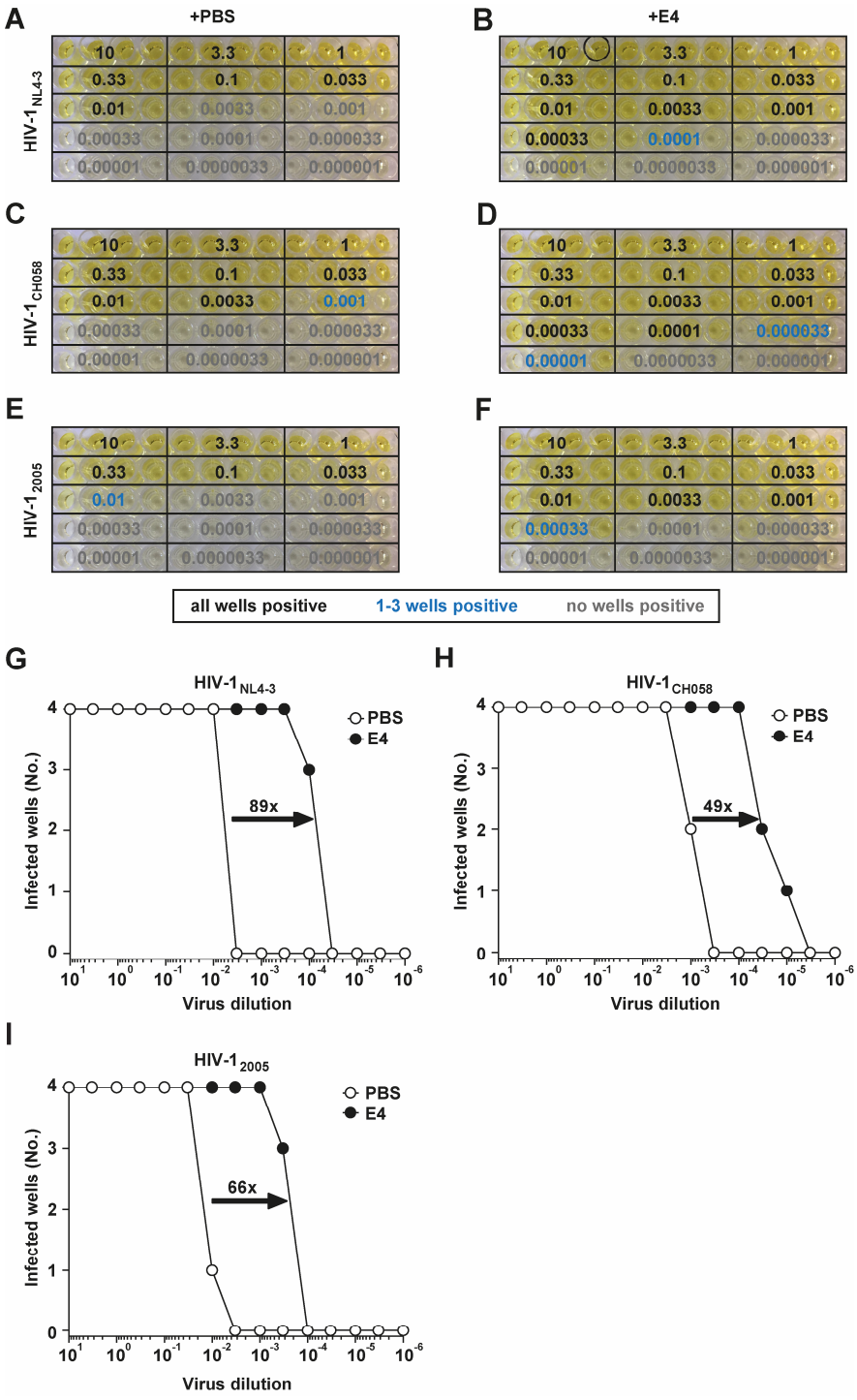

Figure S7: Effect of amyloid enhancers in endpoint titration experiments of an HIV-1 lab strain, a T/F strain and a primary isolate. Images of ELISA plates before absorption measurement (**A-F**) and analyzed data sets (**G-H**). Primary activated CD4 T cells were incubated with either PBS, or HPV16 E4 (12 µM final concentration on cells). Next, decreasing concentrations of the lab strain HIV-1_{NL4-3} (**A,B,G**), the T/F strain HIV-1_{CH058} (**C,D,H**) or the primary isolate HIV-1_{2005} (**E,F,I**) were added. Infection experiment was performed in quadruplicates. Five days post challenge, supernatants were harvested and p24 positive wells were determined by p24 CA ELISA. Number of positive wells was plotted against the different dilutions (**G-H**). TCID50/ ml and subsequently factor of change of TCID50/ml comparing PBS- and E4-treated cells (indicated on top of the arrow in each graph) were calculated. Supplementary figure for **Fig. 25**.

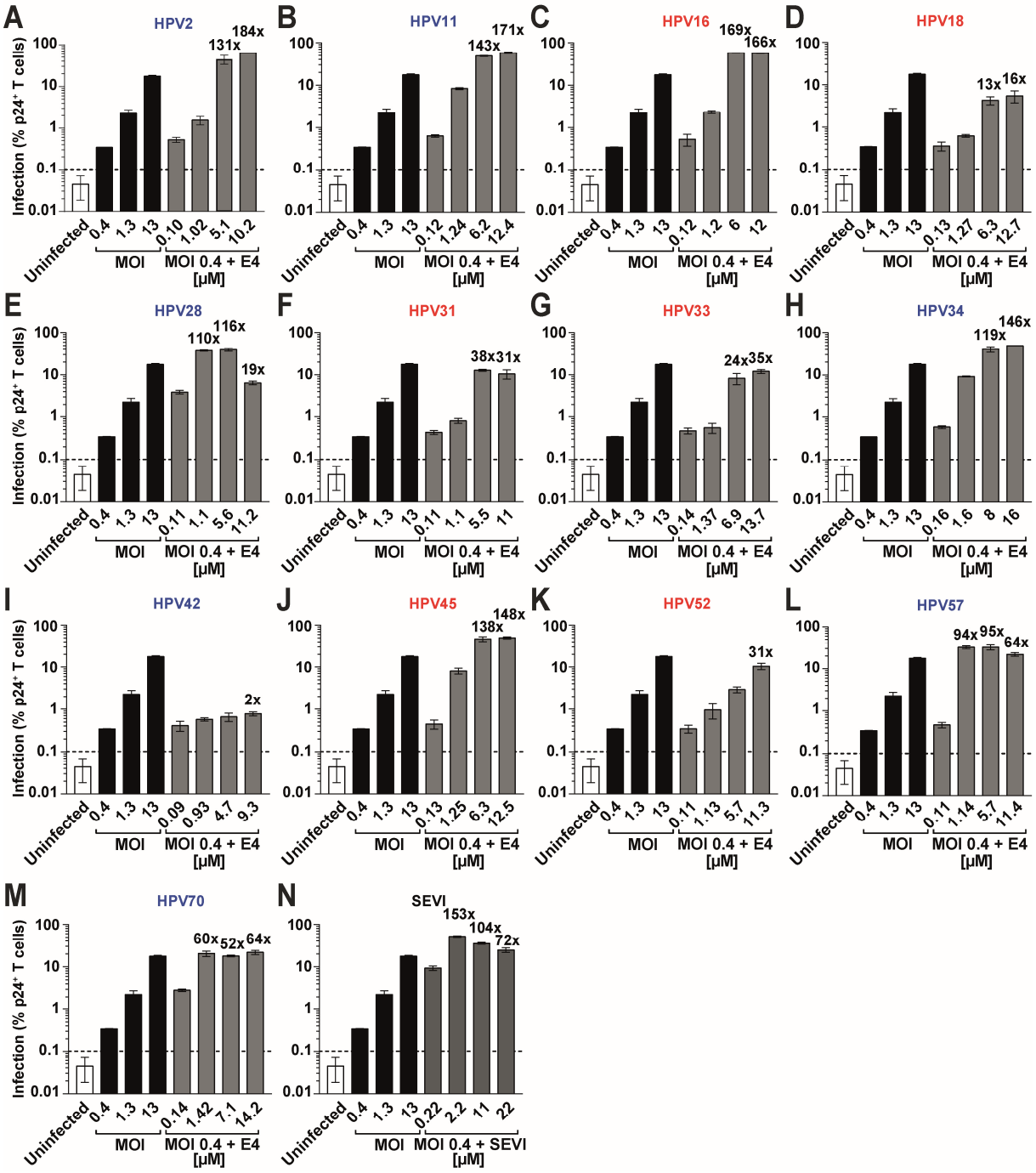

Figure S8: Enhancement of infection with HIV-1 is not restricted to HPV16 E4. (**A-N**) Primary activated CD4 T cells (four donor pool) were challenged with HIV-1_{NL4-3} at different MOIs (0.4, 1.3, 13). In parallel, the lowest MOI of 0.4 was pre-incubated with either PBS, increasing concentrations of HPV E4 from different variants (**A-M**), or SEVI (**N**) and used to infect the cells. 48 h post challenge, intracellular p24 staining was performed and infections levels were assessed by flow cytometry. Depicted are the arithmetic mean and standard deviation of three technical replicates. Data are representative of two experiments. Factor of enhancement of infection is plotted on top of respective histogram bars. Supplementary figure for **Fig. 26**.

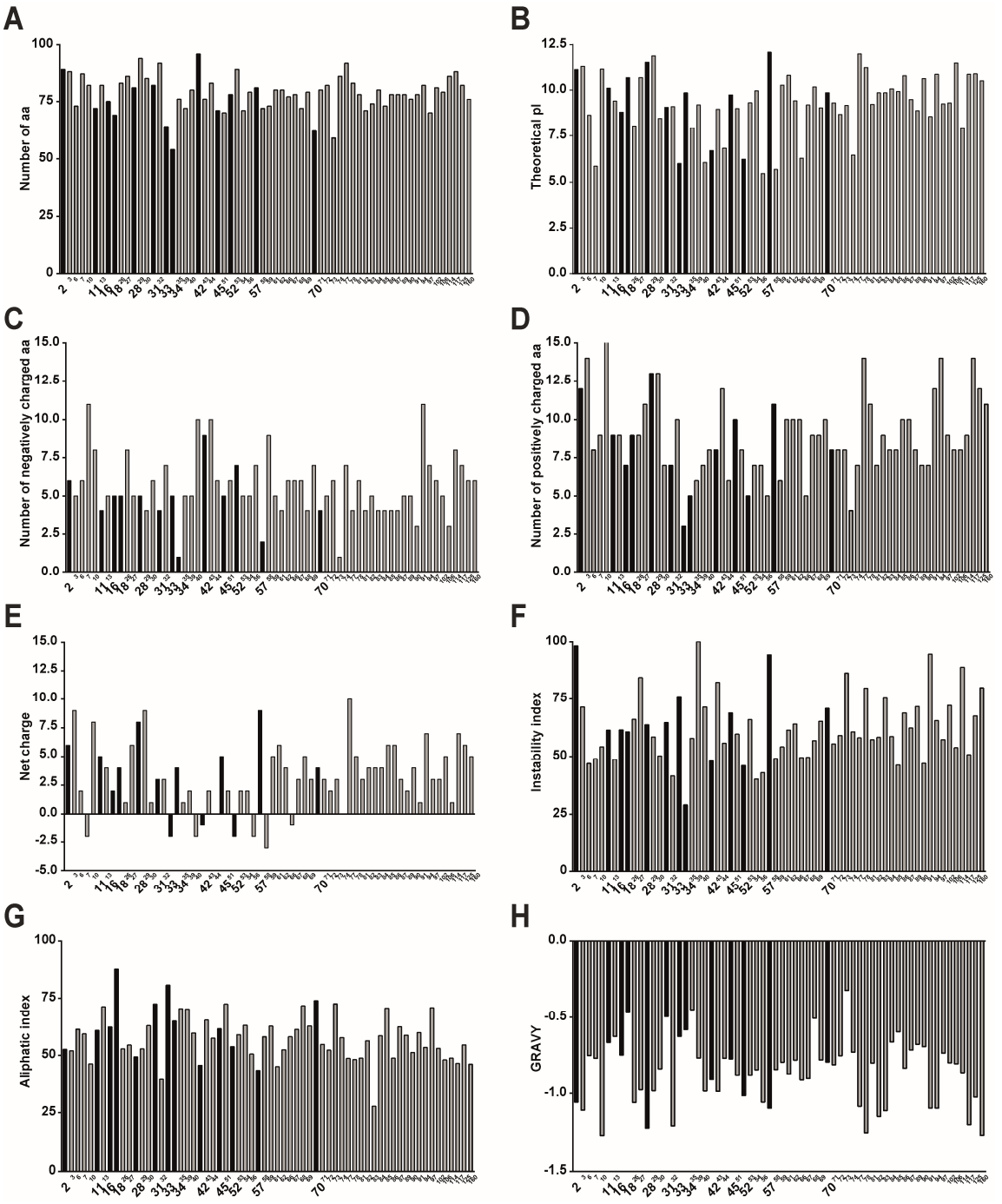

Figure S9. Physiochemical data on the *N-terminally* truncated E4 proteins of all human alpha-papillomaviruses. E4 (E1^E4) amino acid sequence files were retrieved from the collection database "PaVE: the papillomavirus knowledge source" (https://pave.niaid.nih.gov/) and truncated based on literature by John Doorbar [132]. Physiochemical analysis was done using the ProtParam Tool (therapuetical). Depicted are the number of amino acids (aa, **A**), theoretical isoelectric point (pI, **B**), number of negatively (**C**) and positively (**D**) charged aa, net charge (**E**), instability index (**F**), aliphatic index (**G**) and the grand average of hydropathy (GRAVY, **H**). Marked with bigger letters and black graphs are E4 peptides of HPV variants used in infection enhancement experiments. Supplementary figure for **Fig. 26**.

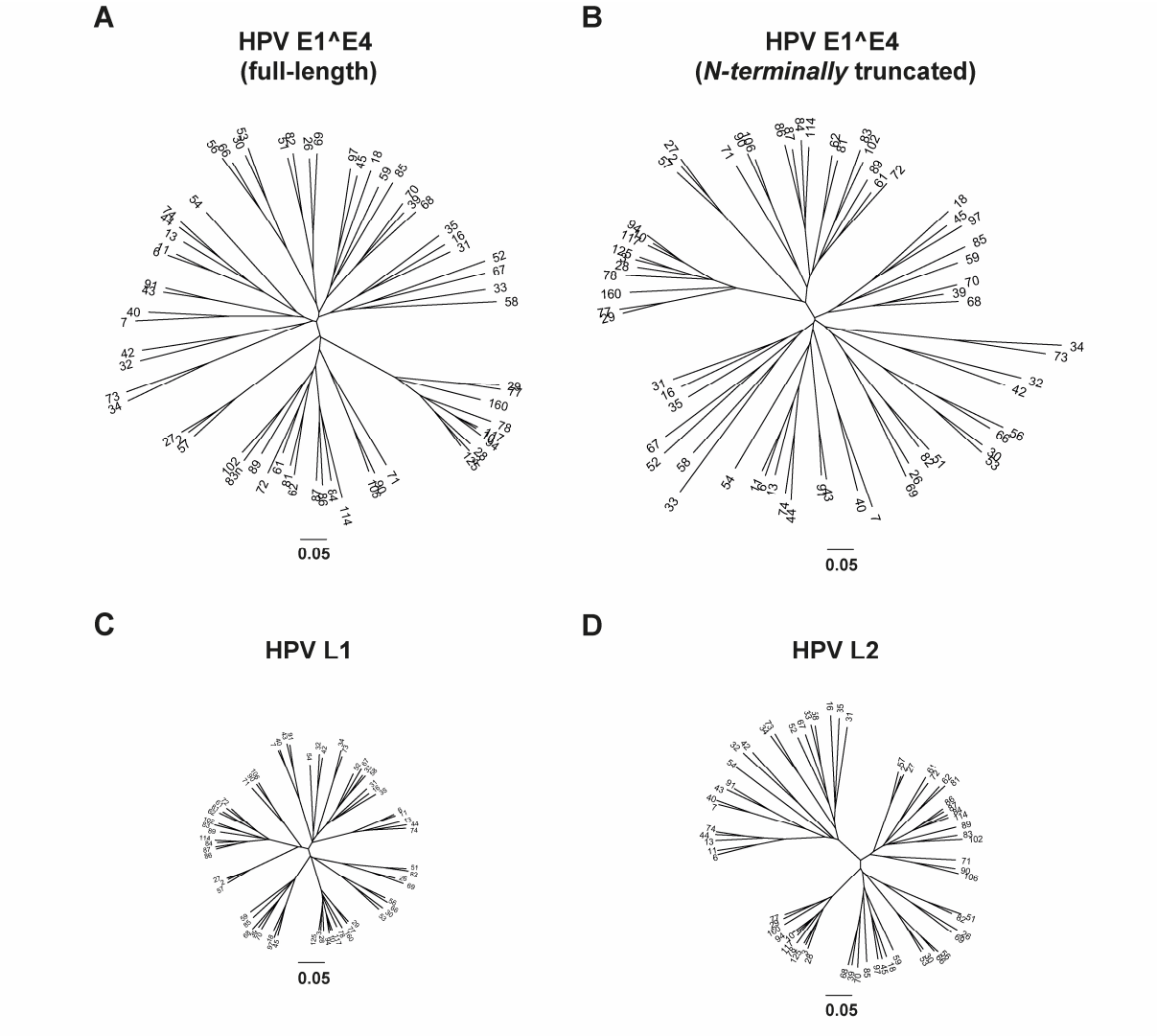

Figure S10. Phylogenetic comparison of amino acid sequences of HPV E4 (E1^E4), L1 and L2 proteins of human alpha-papillomaviruses. Comparison of heterogeneity of amino acid sequences of HPV E4 (E1^E4), L1 and L2 proteins of human alpha-papillomaviruses. Sequences were obtained from PaVe (see above), aligned using Clustal Omega and trees drawn using TreeFig v1.4.3. Shown are the phylogenetic trees of full-length E4 (**A**), *N-terminally* truncated E4 (**B**), L1 (**C**) and L2 (**C**) proteins. Scales were matched in size. Supplementary figure for **Fig. 26**.

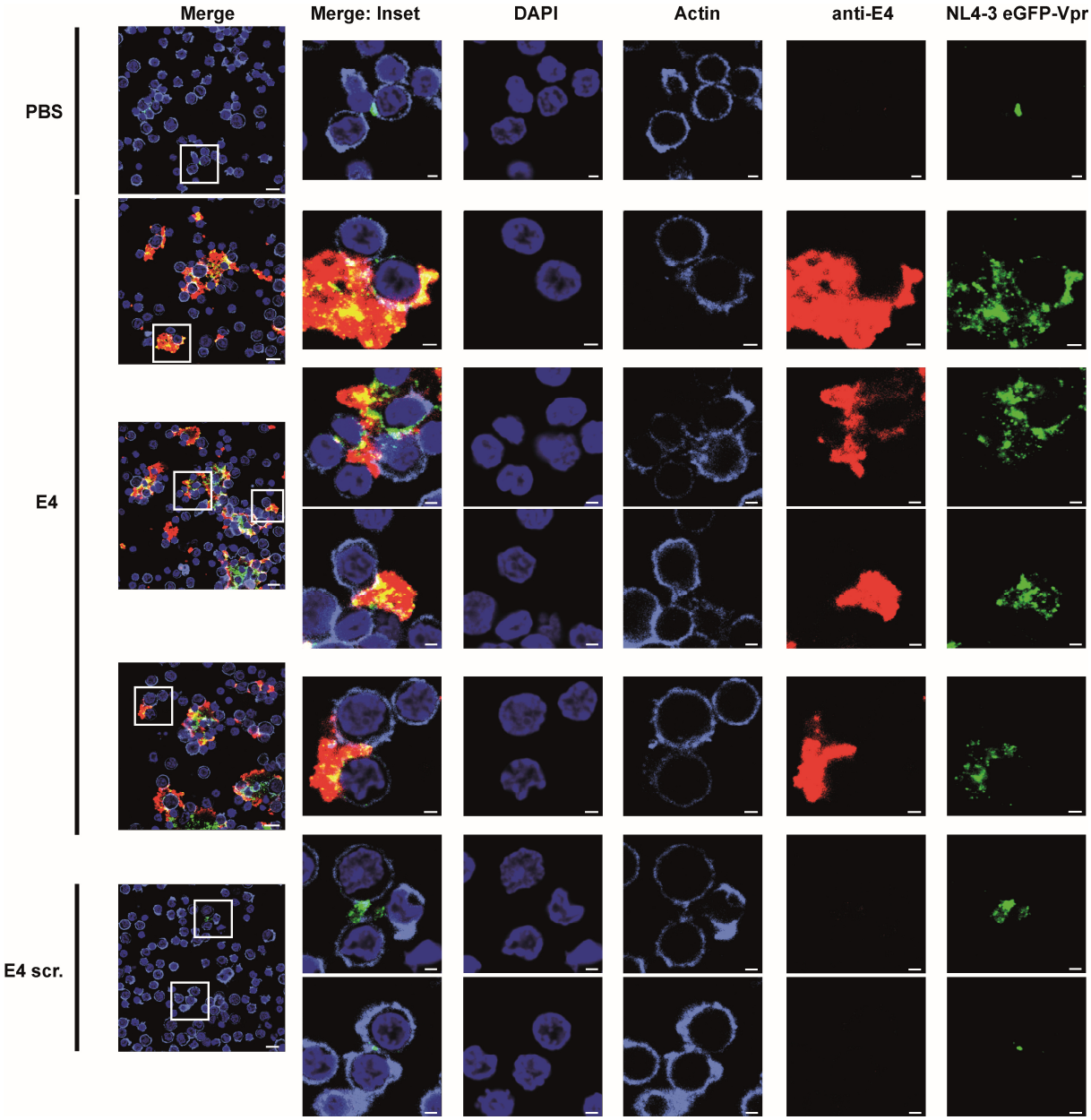

Figure S11: HPV16 E4 is able to concentrate HIV-1 particles locally. Cells of a donor pool of primary activated CD4 T cells were placed on poly-L-lysine-coated coverslips and incubated with eGFP-Vpr-carrying HIV-1_{NL4-3} particles, which were pre-incubated either with PBS, E4, or E4 scrambled (12 µM final concentration on cells). After fixation, cells were stained on the coverslips for actin (light blue, Alexa Fluor 647 Phalloidin), E4 (red, anti-E4 NA7-AA5 + goat anti-mouse Alexa Fluor 568) and chromatin (dark blue, DAPI). Shown are the conditions with PBS (Virus only), E4 and E4 scrambled. The very left column shows the merge and directly next to it the higher magnification of the marked inset (Merge: Inset). Right to the two merge columns the different single channels for DAPI, actin, anti-E4 and NL4-3 eGFP-Vpr of the magnified inset are depicted. Scale bars: 10 µm (inset: 2 µm). Supplementary figure for **Fig. 27**.

A

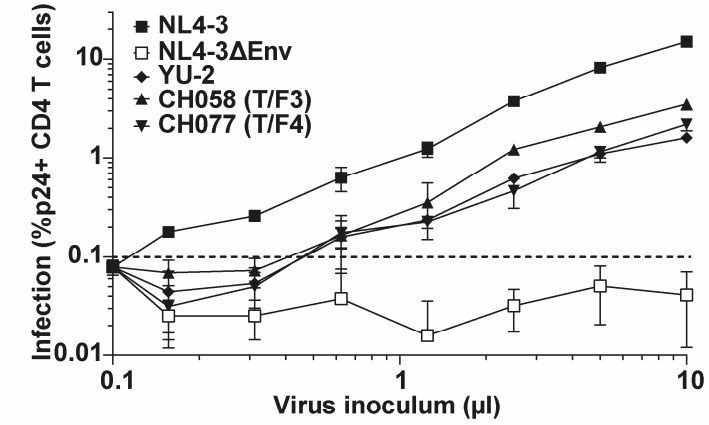

B

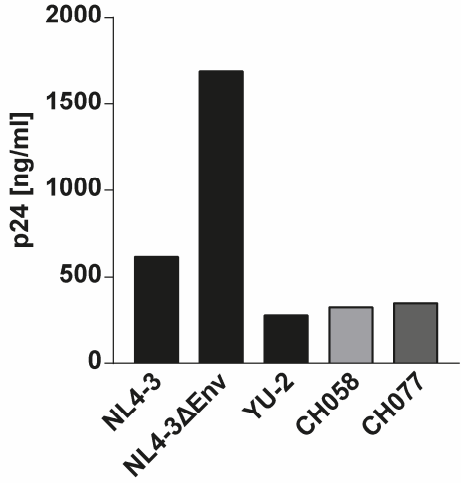

C

Virus	BCA titer [TZM-bl IU/ml]
NL4-3	3.45×10^8
NL4-3ΔEnv	0
YU-2	1.65×10^7
CH058	0.56×10^7
CH077	0.54×10^7

Figure S12: Characterization of eGFP-Vpr-carrying HIV-1 particles. Different HIV-1 lab strains (HIV-1_{NL4-3}wt, HIV-1_{YU-2}), a mutant (HIV-1_{NL4-3}ΔEnv) and T/F strains (HIV-1_{CH058}, HIV-1_{CH077}), all carrying eGFP-Vpr, were checked for their infectivity on a three donor pool of primary activated CD4 T cells (**A**) and the HIV reporter cell line TZM-bl (**C,** BCA titer). Depicted are the arithmetic mean and standard deviation of three technical replicates (**A**). p24 CA ELISA was performed to check for the presence of HIV-1 capsid protein in virus stocks (**B**). Supplementary figure for **Fig. 28**.

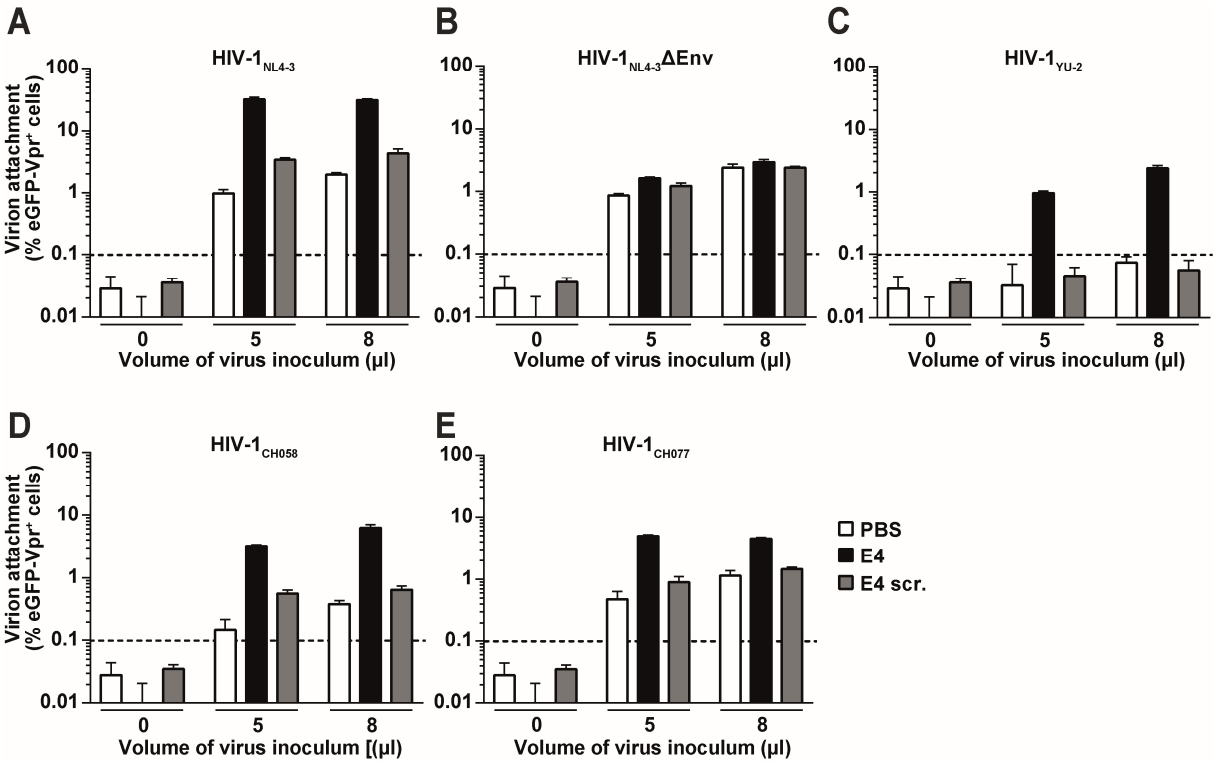

Figure S13: HPV16 E4 leads to enhanced virion attachment of different HIV-1 strains to primary activated CD4 T cells. Primary activated CD4 T cells were incubated with eGFP-Vpr-carrying HIV-1_{NL4-3}wt (**A**), HIV-1_{NL4-3}ΔEnv (**B**), HIV-1_{YU-2} (**C**), HIV-1_{CH058} (**D**), HIV-1_{CH077} (**E**) pre-incubated with either PBS, HPV16 E4, or E4scr. (12 µM final concentration on cells). Indicated volumes of virus were used. Incubation of viruses with cells was done in the presence of T20 (50 µM) and at 20°C. After fixation, virion attachment was quantified by flow cytometry. Depicted are the arithmetic mean and standard deviation of three technical replicates. Supplementary figure for **Fig. 28**.

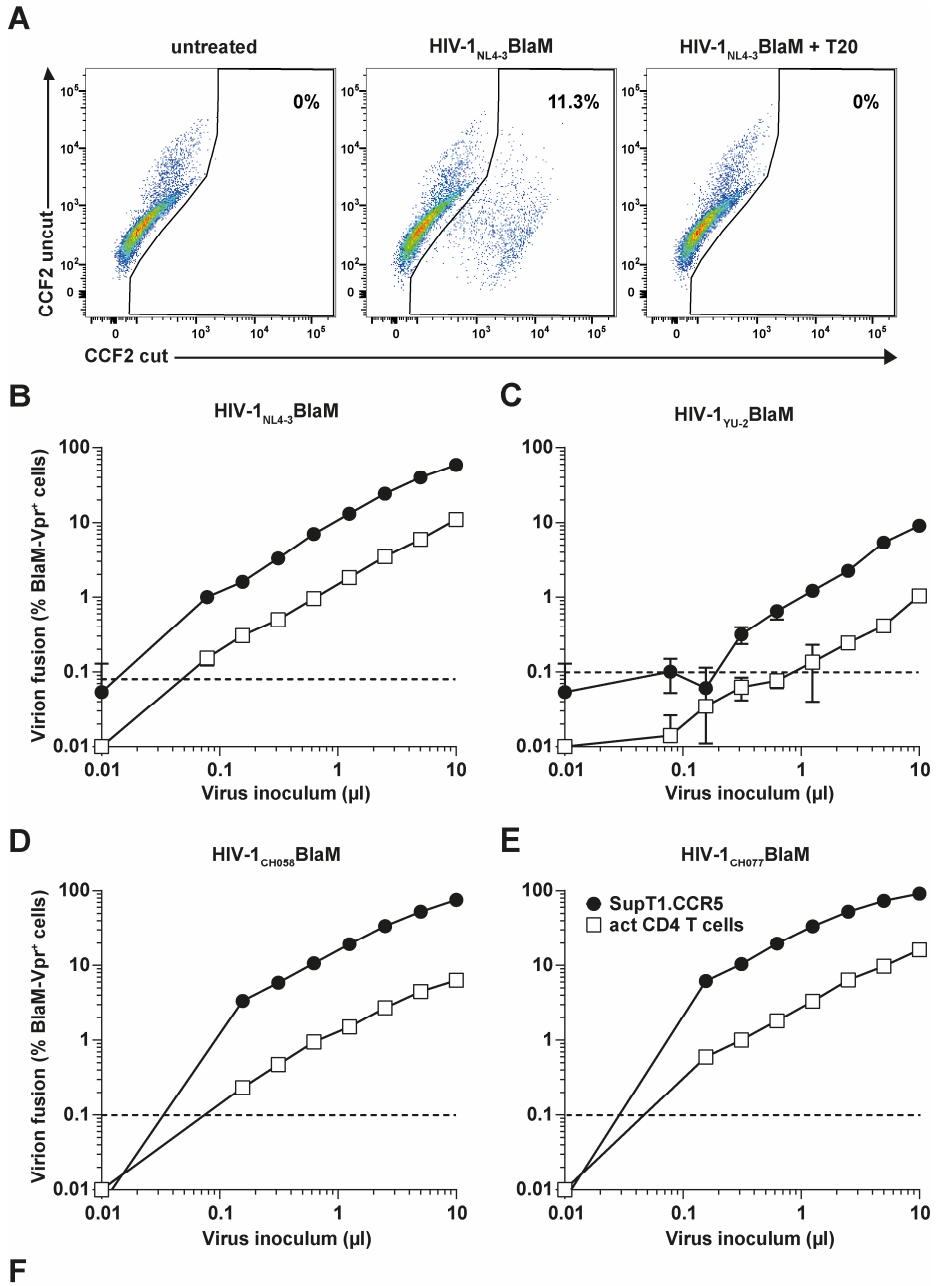

F

Virus	BCA Titer [x10^7 IU/ml]
NL4-3$_{BlaM}$	0.78
YU-2$_{BlaM}$	0.21
CH058$_{BlaM}$	0.51
CH077$_{BlaM}$	0.33

Figure S14: Characterization of BlaM-Vpr-carrying HIV-1 particles. (**A**) Gating strategy of the virion-fusion assay for virion fusion-positive cells. For detailed description, see chapter 2.4.4.4. Shown are primary activated CD4 T cells (four donor pool), challenged for four hours with either PBS, or HIV-1$_{NL4-3}$BlaM. As control, cells were pre-treated with the fusion inhibitor T20 (50 µM) before infection with BlaM-Vpr-carrying HIV-1$_{NL4-3}$. Depicted are titrations of BlaM-Vpr-carrying HIV-1$_{NL4-3}$ (**B**), HIV-1$_{YU-2}$ (**C**), HIV-1$_{CH058}$ (**D**) and HIV-1$_{CH077}$ (**E**) on primary activated CD4 T cells and SupT1.CCR5 cells. Virion fusion was quantified by flow cytometry. Depicted are the arithmetic mean and standard deviation of three technical replicates. (**F**) Infectivity of BlaM-Vpr-carrying HIV-1 lab strains and T/F strains on the HIV report cell line TZM-bl (BCA titer). Supplementary figure for **Fig. 29**.

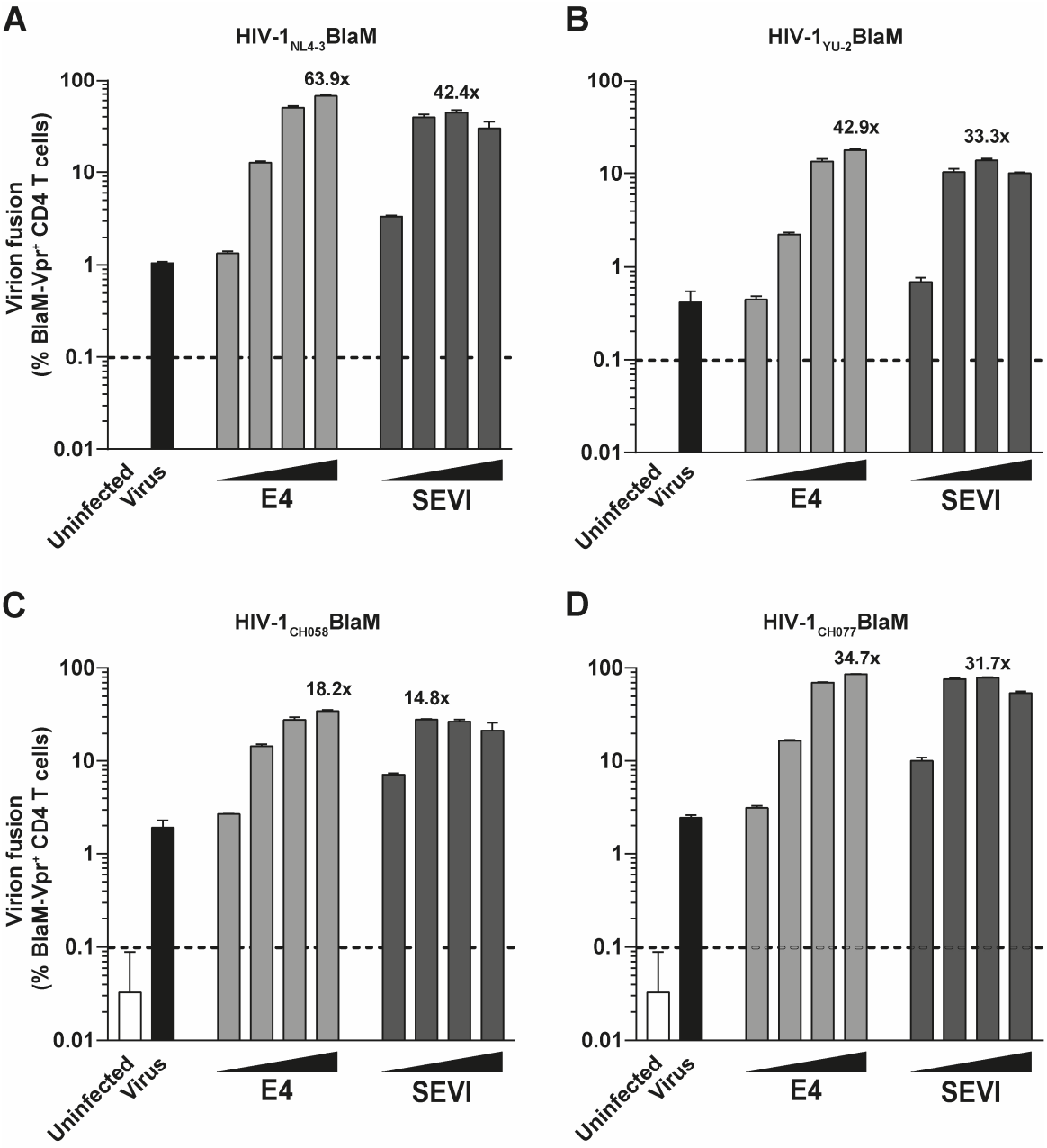

Figure S15: Amyloid enhancers increase virion fusion of different BlaM-Vpr-carrying HIV-1 lab strains and T/F strains. A low inoculum of the HIV-1 lab strains HIV-1_{NL4-3} (**A**) and HIV-1_{YU-2} (**B**) as well as the T/F strains HIV-1_{CH058} (**C**) and HIV-1_{CH077} (**D**), all carrying BlaM-Vpr, was pre-incubated with either PBS (black bar), a titration of HPV16 E4 (0.12, 1.2, 6, 12 µM, light grey bars), or SEVI (0.22, 2.2, 11, 22 µM, dark grey bars). Next, primary activated CD4 T cells (four donor pool) were challenged for four hours and virion fusion was analyzed by flow cytometry. As a reference, untreated cells are shown (white bar). Depicted are the arithmetic mean and standard deviation of three technical replicates. Data are representative of two experiments. Highest factor of enhancement of infection is indicated on top of the respective histogram bar. Supplementary figure for **Fig. 29**.

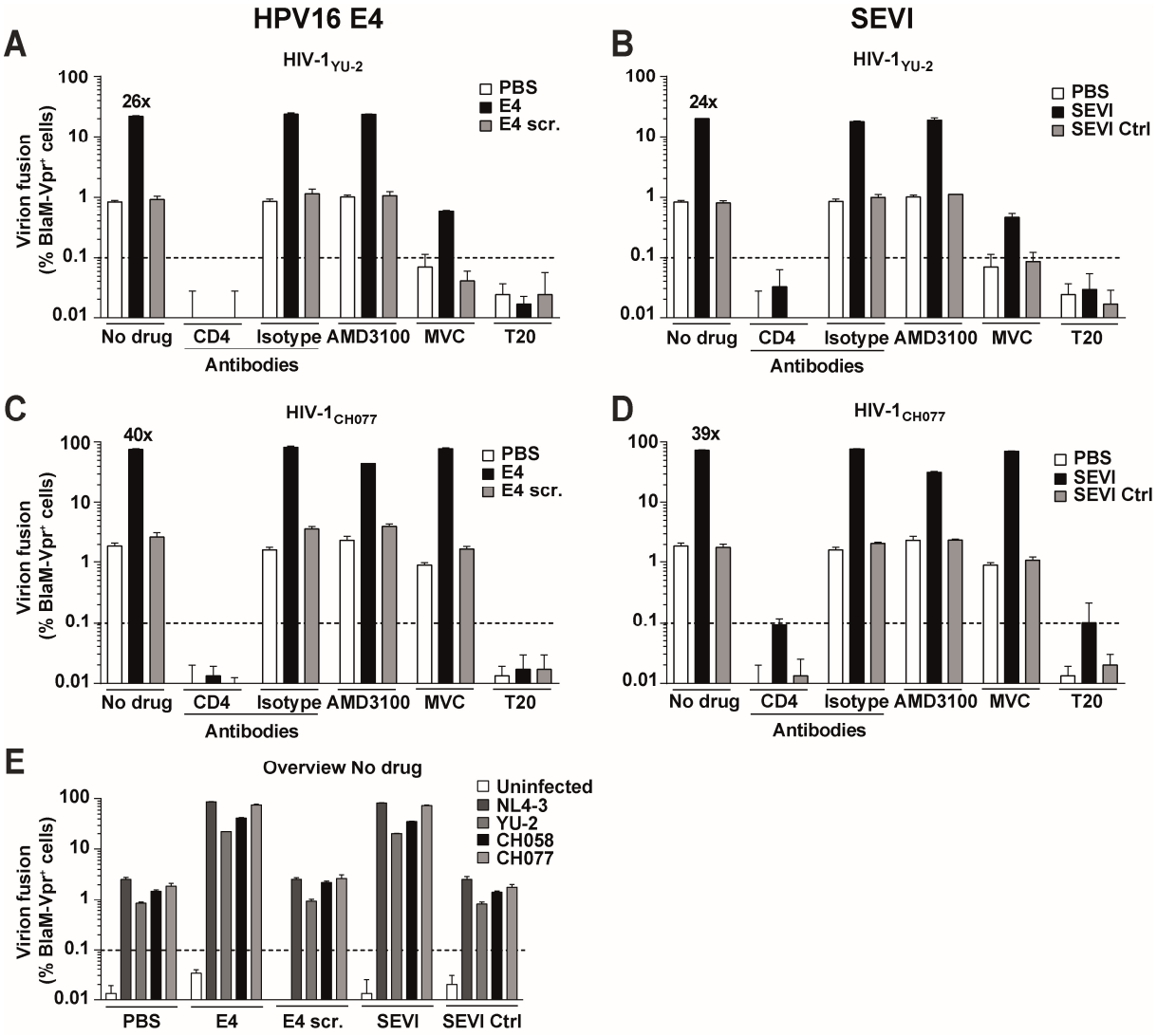

Figure S16: Binding and entry inhibitors can block enhancing effect of amyloids on virion fusion of HIV-1 particles. Primary activated CD4 T cells (four donor pool) were pre-treated with different binding and entry inhibitors: anti-CD4 antibodies and isotype control antibodies (100 µg/ml), AMD3100 (20 µM), Maraviroc (MVC, 20 µM), or the fusion inhibitor T20 (50 µM). BlaM-Vpr-carrying HIV-1_{YU-2} (**A+B**) or HIV-1_{CH077} (**C+D**) were pre-incubated with either PBS, HPV16 E4/ E4 scr. (12 µM) (**A+C**), or SEVI (11 µM)/ SEVI Ctrl (25.9 µM) (**B+D**). Subsequently, mixes were used to infect the pre-treated cells. Indicated concentrations represent final concentration on cells. Virion fusion was quantified by flow cytometry. Factor of enhancement of infection is indicated on top of the no drug condition. Depicted are the arithmetic mean and standard deviation of three technical replicates from one experiment. Data represent one experiment (**C,D**) of are representative of two experiments (**A,B**). (**E**) Shows an overview of virion fusion of the no drug condition of viruses used in **Fig. 29A-D** and supplementary **Fig. S15A-D**. Supplementary figure for **Fig. 29**.

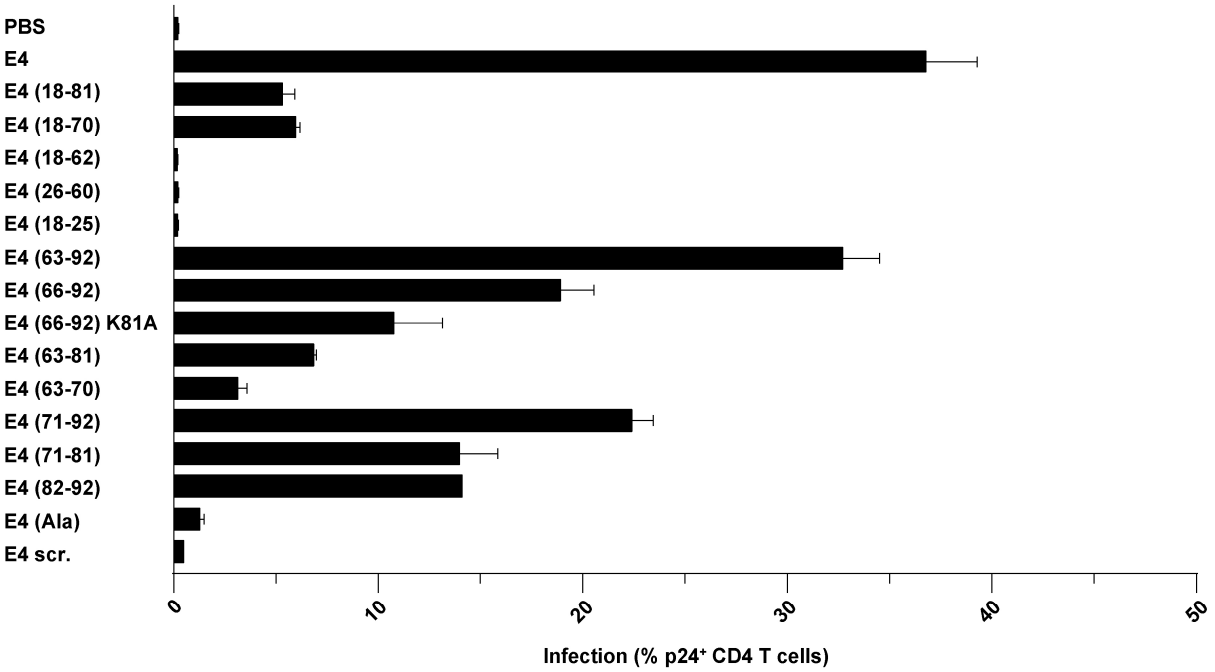

Figure S17: HPV16 E4-mediated HIV infection enhancement is mainly restricted to the *C-terminus* of the *N-terminally* truncated peptide. HIV-1_{NL4-3} was pre-incubated with the different mutants of the *N-terminally* truncated HPV16 E4 peptide at a concentration of 1 mg/ml (100 µg/ml final concentration on cells). Primary activated CD4 T cells were challenged with the different conditions and intracellular p24 levels were quantified 48 h post infection by flow cytometry. Data are representative of two experiments. Depicted are the arithmetic mean and standard deviation of three technical replicates. Supplementary figure for **Fig. 34**.

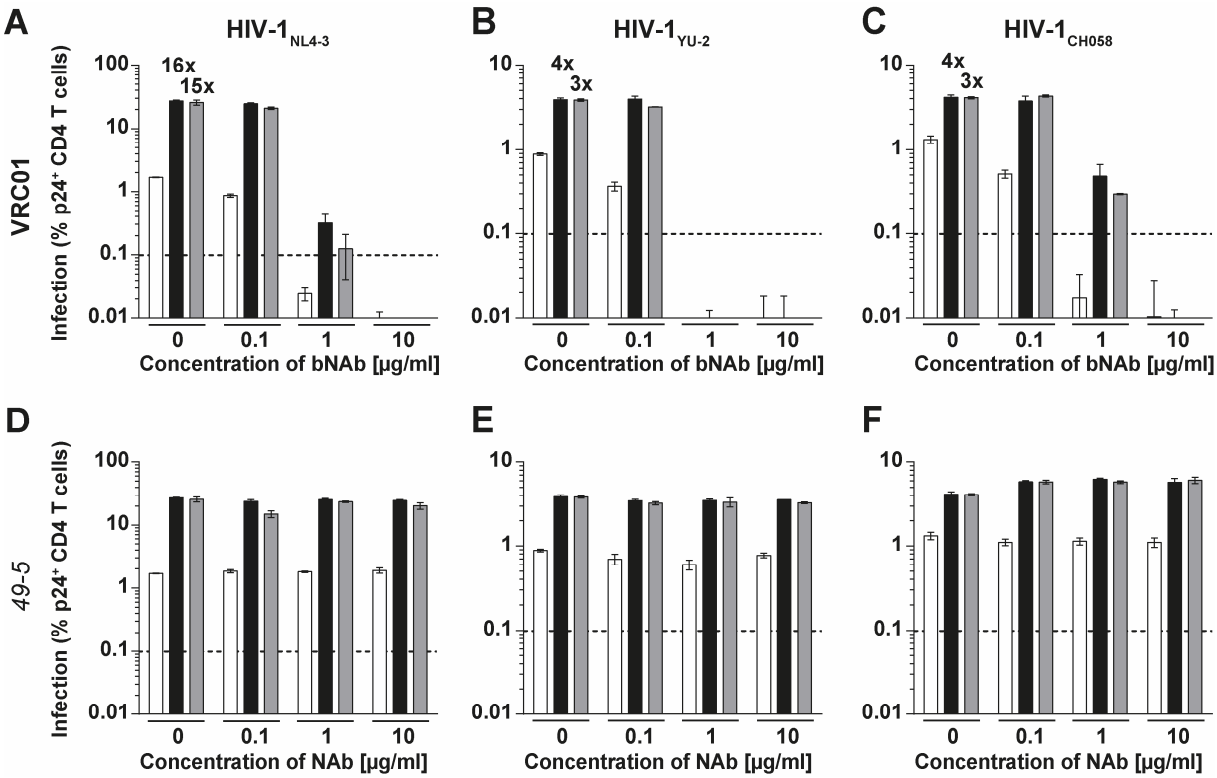

Figure S18: Presence of amyloid enhancers can alter the potency of bNAbs in an epitope-dependent manner. A low volume of either HIV-1_{NL4-3} (**A,D**), HIV-1_{YU-2} (**B,E**), or HIV-1_{CH058} (**C,F**) was first pre-incubated with a constant amount of either HPV16 E4 (12 µM, black), SEVI (11 µM, grey) or PBS (white), followed by incubation with the indicated dilutions of different bNAbs/ NAbs. Shown is the CD4 binding site (CD4bs) bNAb VRC01 (**A-C**) and the NAb 4-95 as control (**D-F**). Depicted are the arithmetic mean and standard deviation of three technical replicates. Factor of enhancement of infection is indicated on top of respective histogram bars at no antibody condition. Supplementary figure for **Fig. 37**.

A

	bNAb	X4 NL4-3		R5 YU-2		R5 CH058	
		E4	SEVI	E4	SEVI	E4	SEVI
gp120/gp41 bridging	8ANC195	>11.7	3.1	4.1	2.8	5.3	4.4
CD4bs	VRC01	2.1	1.6	2.7	1.4	4.2	8.9
CD4bs	3BNC117	1.9	1.8	2.6	2	8.3	16.1

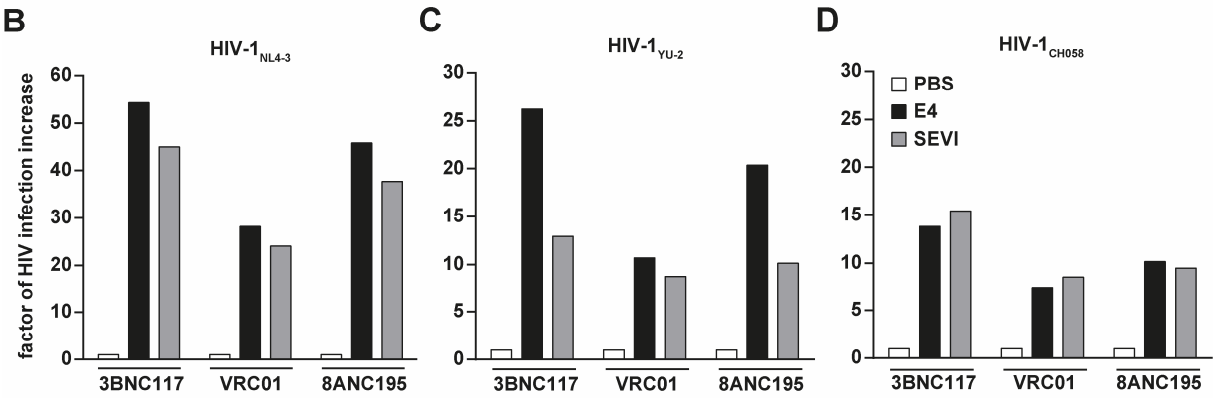

Figure S19: Factors of change of IC50 values and factors of infection increase in the presence of amyloid enhancers when virus only condition is reduced by at least 50%. (**A**) Factors of change of IC50 values of the indicated bNAb-virus combinations in the presence of E4 or SEVI. Infection data were normalized and IC50 values based on four data points were calculated using non-linear curve fitting (GraphPad Prism). Based on this, factors of change of IC50 values were calculated. (**B-D**) Shown are the factors of infection increase of HIV-1_{NL4-3} (**B**), HIV-1_{YU-2} (**C**) and HIV-1_{CH058} (**D**) in the presence of amyloid enhancers when infection levels in virus only conditions were reduced by the antibodies by at least 50% (from **Fig. 37**). For the CD4bs antibodies 3BNC117 and VRC01 this was reached at a concentration of 0.1 µg/ml, for 8ANC195 at a concentration of 10 µg/ml. Supplementary figure for **Fig. 37**.

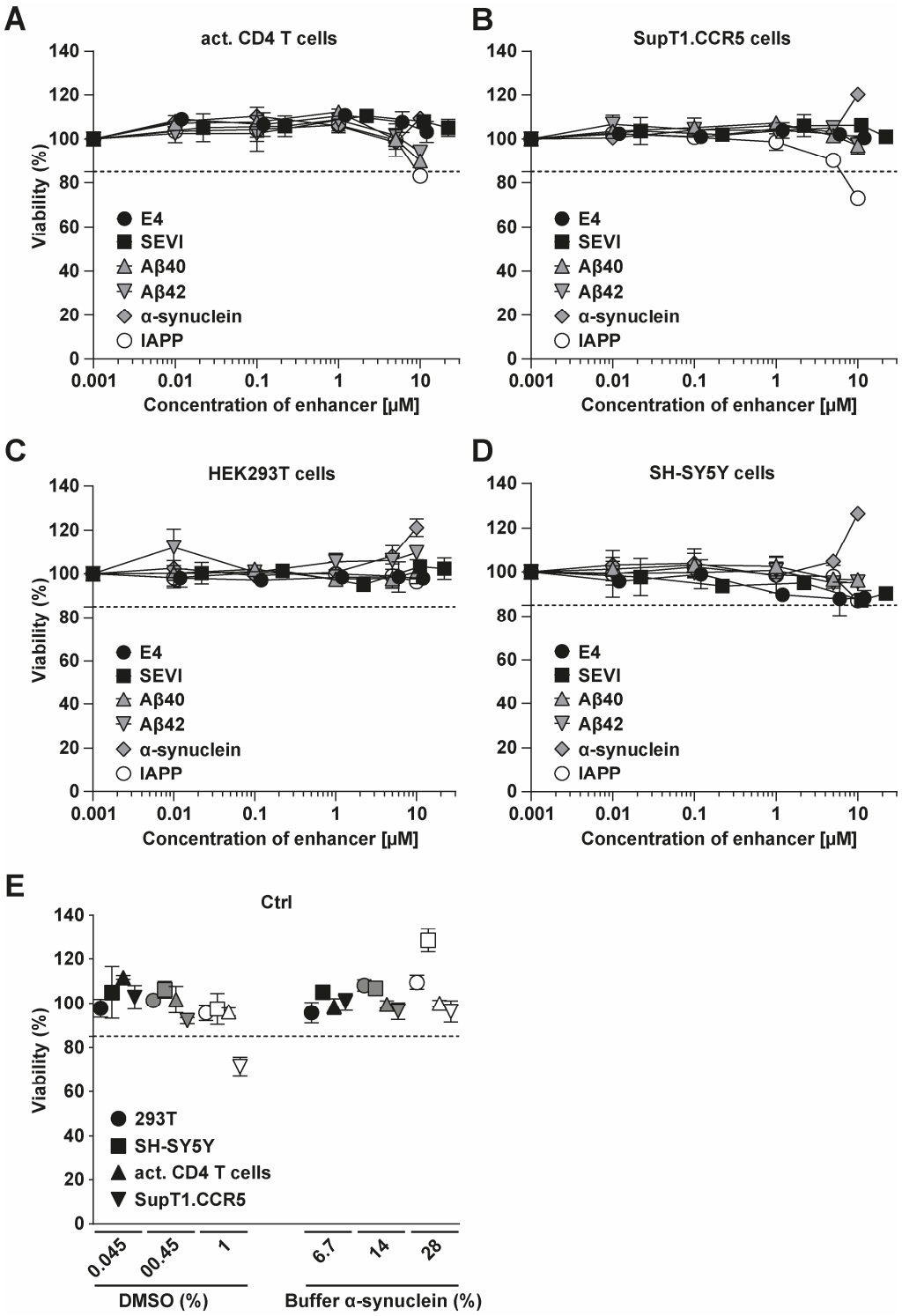

Figure S20: Amyloid enhancers used in infection experiments are not cytotoxic to cells types used in infection enhancement experiments. Primary activated CD4 T cells (three donor pool) (**A**), SupT1.CCR5 cells (**B**), HEK293T cells (**C**) or SH-SY5Y cells (**D**) were incubated with increasing concentrations of either HPV16 E4, SEVI, Aβ40, Aβ42, α-synuclein, or IAPP and incubated for 44 h (**A+B**) or 20 h (**C+D**). Solvent controls were used (**E**). Next, Resazurin (final concentration of 24 µg/ml) was added and incubated for 4 h in the dark in a cell culture incubator. Fluorescence (590 +/- 8 nm) was measured using the Clariostar plate reader. Background was subtracted and data were normalized for untreated cells, which were set to be 100% viable. Depicted are the arithmetic mean and standard deviation of three technical replicates. Supplementary figure for **Fig. 38-40**.

6 References

1. Deeks, S.G., et al., *HIV infection.* Nat Rev Dis Primers, 2015. **1**: p. 15035.
2. Peeters, M., M. Jung, and A. Ayouba, *The origin and molecular epidemiology of HIV.* Expert Rev Anti Infect Ther, 2013. **11**(9): p. 885-96.
3. Shaw, G.M. and E. Hunter, *HIV transmission.* Cold Spring Harb Perspect Med, 2012. **2**(11).
4. Joseph, S.B., et al., *Bottlenecks in HIV-1 transmission: insights from the study of founder viruses.* Nat Rev Microbiol, 2015. **13**(7): p. 414-25.
5. Parrish, N.F., et al., *Phenotypic properties of transmitted founder HIV-1.* Proc Natl Acad Sci U S A, 2013. **110**(17): p. 6626-33.
6. Xu, H., X. Wang, and R.S. Veazey, *Mucosal immunology of HIV infection.* Immunol Rev, 2013. **254**(1): p. 10-33.
7. Pandrea, I., et al., *Mucosal simian immunodeficiency virus transmission in African green monkeys: susceptibility to infection is proportional to target cell availability at mucosal sites.* J Virol, 2012. **86**(8): p. 4158-68.
8. Casartelli, N., *HIV-1 Cell-to-Cell Transmission and Antiviral Strategies: An Overview.* Curr Drug Targets, 2016. **17**(1): p. 65-75.
9. Lucas, S. and A.M. Nelson, *HIV and the spectrum of human disease.* J Pathol, 2015. **235**(2): p. 229-41.
10. Chang, C.C., et al., *HIV and co-infections.* Immunol Rev, 2013. **254**(1): p. 114-42.
11. Shepherd, B.L., et al., *HLA Correlates of Long-Term Survival in Vertically Infected HIV-1-Positive Adolescents in Harare, Zimbabwe.* AIDS Res Hum Retroviruses, 2015. **31**(5): p. 504-7.
12. *Human Immunodeficiency Virus (HIV).* Transfusion Medicine and Hemotherapy, 2016. **43**(3): p. 203-222.
13. Briggs, J.A. and H.G. Krausslich, *The molecular architecture of HIV.* J Mol Biol, 2011. **410**(4): p. 491-500.
14. Zhu, P., et al., *Distribution and three-dimensional structure of AIDS virus envelope spikes.* Nature, 2006. **441**(7095): p. 847-52.
15. Goodsell, D.S., *Illustrations of the HIV life cycle.* Curr Top Microbiol Immunol, 2015. **389**: p. 243-52.
16. Campbell, E.M. and T.J. Hope, *HIV-1 capsid: the multifaceted key player in HIV-1 infection.* Nat Rev Microbiol, 2015. **13**(8): p. 471-83.
17. Chen, L., O.T. Keppler, and C. Scholz, *Post-translational Modification-Based Regulation of HIV Replication.* Front Microbiol, 2018. **9**: p. 2131.
18. Sauter, D. and F. Kirchhoff, *HIV replication: a game of hide and sense.* Curr Opin HIV AIDS, 2016. **11**(2): p. 173-81.
19. Sheehy, A.M., et al., *Isolation of a human gene that inhibits HIV-1 infection and is suppressed by the viral Vif protein.* Nature, 2002. **418**(6898): p. 646-50.
20. Neil, S.J., T. Zang, and P.D. Bieniasz, *Tetherin inhibits retrovirus release and is antagonized by HIV-1 Vpu.* Nature, 2008. **451**(7177): p. 425-30.
21. Baldauf, H.M., et al., *SAMHD1 restricts HIV-1 infection in resting CD4(+) T cells.* Nat Med, 2012. **18**(11): p. 1682-7.
22. Baldauf, H.M., et al., *Vpx overcomes a SAMHD1-independent block to HIV reverse transcription that is specific to resting CD4 T cells.* Proc Natl Acad Sci U S A, 2017. **114**(10): p. 2729-2734.

23. Descours, B., et al., *SAMHD1 restricts HIV-1 reverse transcription in quiescent CD4(+) T-cells.* Retrovirology, 2012. **9**: p. 87.
24. Laguette, N., et al., *SAMHD1 is the dendritic- and myeloid-cell-specific HIV-1 restriction factor counteracted by Vpx.* Nature, 2011. **474**(7353): p. 654-7.
25. Rosa, A., et al., *HIV-1 Nef promotes infection by excluding SERINC5 from virion incorporation.* Nature, 2015. **526**(7572): p. 212-7.
26. Usami, Y., Y. Wu, and H.G. Gottlinger, *SERINC3 and SERINC5 restrict HIV-1 infectivity and are counteracted by Nef.* Nature, 2015. **526**(7572): p. 218-23.
27. Sood, C., et al., *SERINC5 protein inhibits HIV-1 fusion pore formation by promoting functional inactivation of envelope glycoproteins.* J Biol Chem, 2017. **292**(14): p. 6014-6026.
28. Kanters, S., et al., *Comparative efficacy and safety of first-line antiretroviral therapy for the treatment of HIV infection: a systematic review and network meta-analysis.* Lancet HIV, 2016. **3**(11): p. e510-e520.
29. Bavinton, B.R., et al., *Viral suppression and HIV transmission in serodiscordant male couples: an international, prospective, observational, cohort study.* Lancet HIV, 2018. **5**(8): p. e438-e447.
30. Chow, E.P.F., A.E. Grulich, and C.K. Fairley, *Epidemiology and prevention of sexually transmitted infections in men who have sex with men at risk of HIV.* Lancet HIV, 2019.
31. Rodger, A.J., et al., *Risk of HIV transmission through condomless sex in serodifferent gay couples with the HIV-positive partner taking suppressive antiretroviral therapy (PARTNER): final results of a multicentre, prospective, observational study.* Lancet, 2019.
32. Wilen, C.B., J.C. Tilton, and R.W. Doms, *HIV: cell binding and entry.* Cold Spring Harb Perspect Med, 2012. **2**(8).
33. Mortier, V., et al., *Frequency and predictors of HIV-1 co-receptor switch in treatment naive patients.* PLoS One, 2013. **8**(11): p. e80259.
34. Novembre, J., A.P. Galvani, and M. Slatkin, *The geographic spread of the CCR5 Delta32 HIV-resistance allele.* PLoS Biol, 2005. **3**(11): p. e339.
35. Merk, A. and S. Subramaniam, *HIV-1 envelope glycoprotein structure.* Curr Opin Struct Biol, 2013. **23**(2): p. 268-76.
36. Munro, J.B. and W. Mothes, *Structure and Dynamics of the Native HIV-1 Env Trimer.* J Virol, 2015. **89**(11): p. 5752-5.
37. Kim, J.H., J.L. Excler, and N.L. Michael, *Lessons from the RV144 Thai phase III HIV-1 vaccine trial and the search for correlates of protection.* Annu Rev Med, 2015. **66**: p. 423-37.
38. Rerks-Ngarm, S., et al., *Vaccination with ALVAC and AIDSVAX to prevent HIV-1 infection in Thailand.* N Engl J Med, 2009. **361**(23): p. 2209-20.
39. Karnasuta, C., et al., *Comparison of Antibody Responses Induced by RV144, VAX003, and VAX004 Vaccination Regimens.* AIDS Res Hum Retroviruses, 2017. **33**(5): p. 410-423.
40. de Souza, M.S., et al., *The Thai Phase III Trial (RV144) Vaccine Regimen Induces T Cell Responses That Preferentially Target Epitopes within the V2 Region of HIV-1 Envelope.* The Journal of Immunology, 2012. **188**(10): p. 5166.
41. Fouda, G.G., et al., *Systemic administration of an HIV-1 broadly neutralizing dimeric IgA yields mucosal secretory IgA and virus neutralization.* Mucosal Immunol, 2017. **10**(1): p. 228-237.
42. Barouch, D.H., et al., *Mosaic HIV-1 vaccines expand the breadth and depth of cellular immune responses in rhesus monkeys.* Nat Med, 2010. **16**(3): p. 319-23.

43. Barouch, D.H. and L.J. Picker, *Novel vaccine vectors for HIV-1.* Nat Rev Microbiol, 2014. **12**(11): p. 765-71.
44. Barouch, D.H., et al., *Evaluation of a mosaic HIV-1 vaccine in a multicentre, randomised, double-blind, placebo-controlled, phase 1/2a clinical trial (APPROACH) and in rhesus monkeys (NHP 13-19).* Lancet, 2018. **392**(10143): p. 232-243.
45. Burton, D.R. and J.R. Mascola, *Antibody responses to envelope glycoproteins in HIV-1 infection.* Nat Immunol, 2015. **16**(6): p. 571-6.
46. Malbec, M., et al., *Broadly neutralizing antibodies that inhibit HIV-1 cell to cell transmission.* J Exp Med, 2013. **210**(13): p. 2813-21.
47. Horwitz, J.A., et al., *HIV-1 suppression and durable control by combining single broadly neutralizing antibodies and antiretroviral drugs in humanized mice.* Proc Natl Acad Sci U S A, 2013. **110**(41): p. 16538-43.
48. Bradley, T., et al., *Structural Constraints of Vaccine-Induced Tier-2 Autologous HIV Neutralizing Antibodies Targeting the Receptor-Binding Site.* Cell Rep, 2016. **14**(1): p. 43-54.
49. Klein, F., et al., *HIV therapy by a combination of broadly neutralizing antibodies in humanized mice.* Nature, 2012. **492**(7427): p. 118-22.
50. Scheid, J.F., et al., *Broad diversity of neutralizing antibodies isolated from memory B cells in HIV-infected individuals.* Nature, 2009. **458**(7238): p. 636-40.
51. Mouquet, H., *Antibody B cell responses in HIV-1 infection.* Trends Immunol, 2014. **35**(11): p. 549-61.
52. Pancera, M., A. Changela, and P.D. Kwong, *How HIV-1 entry mechanism and broadly neutralizing antibodies guide structure-based vaccine design.* Curr Opin HIV AIDS, 2017. **12**(3): p. 229-240.
53. Scharf, L., et al., *Broadly Neutralizing Antibody 8ANC195 Recognizes Closed and Open States of HIV-1 Env.* Cell, 2015. **162**(6): p. 1379-90.
54. Doores, K.J., *The HIV glycan shield as a target for broadly neutralizing antibodies.* FEBS J, 2015. **282**(24): p. 4679-91.
55. Seaman, M.S., et al., *Tiered categorization of a diverse panel of HIV-1 Env pseudoviruses for assessment of neutralizing antibodies.* J Virol, 2010. **84**(3): p. 1439-52.
56. Reh, L., et al., *Capacity of Broadly Neutralizing Antibodies to Inhibit HIV-1 Cell-Cell Transmission Is Strain- and Epitope-Dependent.* PLoS Pathog, 2015. **11**(7): p. e1004966.
57. Gautam, R., et al., *A single injection of anti-HIV-1 antibodies protects against repeated SHIV challenges.* Nature, 2016. **533**(7601): p. 105-109.
58. Klein, F., et al., *Enhanced HIV-1 immunotherapy by commonly arising antibodies that target virus escape variants.* J Exp Med, 2014. **211**(12): p. 2361-72.
59. Halper-Stromberg, A., et al., *Broadly neutralizing antibodies and viral inducers decrease rebound from HIV-1 latent reservoirs in humanized mice.* Cell, 2014. **158**(5): p. 989-999.
60. Bournazos, S., et al., *Broadly neutralizing anti-HIV-1 antibodies require Fc effector functions for in vivo activity.* Cell, 2014. **158**(6): p. 1243-1253.
61. Kong, R., et al., *Improving neutralization potency and breadth by combining broadly reactive HIV-1 antibodies targeting major neutralization epitopes.* J Virol, 2015. **89**(5): p. 2659-71.
62. Ramirez Valdez, K.P., et al., *Complementary and synergistic activities of anti-V3, CD4bs and CD4i antibodies derived from a single individual can cover a wide range of HIV-1 strains.* Virology, 2015. **475**: p. 187-203.

63. Bar-On, Y., et al., *Safety and antiviral activity of combination HIV-1 broadly neutralizing antibodies in viremic individuals.* Nat Med, 2018. **24**(11): p. 1701-1707.
64. Caskey, M., et al., *Viraemia suppressed in HIV-1-infected humans by broadly neutralizing antibody 3BNC117.* Nature, 2015. **522**(7557): p. 487-91.
65. Scheid, J.F., et al., *HIV-1 antibody 3BNC117 suppresses viral rebound in humans during treatment interruption.* Nature, 2016. **535**(7613): p. 556-60.
66. Hard, T. and C. Lendel, *Inhibition of amyloid formation.* J Mol Biol, 2012. **421**(4-5): p. 441-65.
67. Lee, Y.H. and A. Ramamoorthy, *Semen-derived amyloidogenic peptides-Key players of HIV infection.* Protein Sci, 2018. **27**(7): p. 1151-1165.
68. Baxa, U., *Structural basis of infectious and non-infectious amyloids.* Curr Alzheimer Res, 2008. **5**(3): p. 308-18.
69. Hewetson, A., et al., *Functional Amyloids in Reproduction.* Biomolecules, 2017. **7**(3).
70. Chu, H., et al., *Human alpha-defensin 6 promotes mucosal innate immunity through self-assembled peptide nanonets.* Science, 2012. **337**(6093): p. 477-81.
71. Barnhart, M.M. and M.R. Chapman, *Curli biogenesis and function.* Annu Rev Microbiol, 2006. **60**: p. 131-47.
72. Bergman, P., et al., *Amyloid formation: functional friend or fearful foe?* J Intern Med, 2016. **280**(2): p. 139-52.
73. Sabatte, J., et al., *The role of semen in sexual transmission of HIV: beyond a carrier for virus particles.* Microbes Infect, 2011. **13**(12-13): p. 977-82.
74. Munch, J., et al., *Semen-derived amyloid fibrils drastically enhance HIV infection.* Cell, 2007. **131**(6): p. 1059-71.
75. Wojtowicz, W.M., et al., *Stimulation of enveloped virus infection by beta-amyloid fibrils.* J Biol Chem, 2002. **277**(38): p. 35019-24.
76. Roan, N.R., et al., *The cationic properties of SEVI underlie its ability to enhance human immunodeficiency virus infection.* J Virol, 2009. **83**(1): p. 73-80.
77. Brender, J.R., et al., *Helical conformation of the SEVI precursor peptide PAP248-286, a dramatic enhancer of HIV infectivity, promotes lipid aggregation and fusion.* Biophys J, 2009. **97**(9): p. 2474-83.
78. Munch, J., et al., *Effect of semen and seminal amyloid on vaginal transmission of simian immunodeficiency virus.* Retrovirology, 2013. **10**: p. 148.
79. Van Dis, E.S., et al., *No SEVI-mediated enhancement of rectal HIV-1 transmission of HIV-1 in two humanized mouse cohorts.* Virology, 2016. **488**: p. 88-95.
80. Roan, N.R., et al., *Peptides released by physiological cleavage of semen coagulum proteins form amyloids that enhance HIV infection.* Cell Host Microbe, 2011. **10**(6): p. 541-50.
81. Linke, R.P., et al., *Senile seminal vesicle amyloid is derived from semenogelin I.* J Lab Clin Med, 2005. **145**(4): p. 187-93.
82. Roan, N.R. and W.C. Greene, *A seminal finding for understanding HIV transmission.* Cell, 2007. **131**(6): p. 1044-6.
83. Roan, N.R., et al., *Liquefaction of semen generates and later degrades a conserved semenogelin peptide that enhances HIV infection.* J Virol, 2014. **88**(13): p. 7221-34.
84. Martellini, J.A., et al., *Cationic polypeptides contribute to the anti-HIV-1 activity of human seminal plasma.* FASEB J, 2009. **23**(10): p. 3609-18.

85. Roan, N.R., et al., *Interaction of fibronectin with semen amyloids synergistically enhances HIV infection.* J Infect Dis, 2014. **210**(7): p. 1062-6.
86. Tang, Q., N.R. Roan, and Y. Yamamura, *Seminal plasma and semen amyloids enhance cytomegalovirus infection in cell culture.* J Virol, 2013. **87**(23): p. 12583-91.
87. Torres, L., T. Ortiz, and Q. Tang, *Enhancement of herpes simplex virus (HSV) infection by seminal plasma and semen amyloids implicates a new target for the prevention of HSV infection.* Viruses, 2015. **7**(4): p. 2057-73.
88. Bart, S.M., et al., *Enhancement of Ebola virus infection by seminal amyloid fibrils.* Proc Natl Acad Sci U S A, 2018. **115**(28): p. 7410-7415.
89. Muller, J.A., et al., *Semen inhibits Zika virus infection of cells and tissues from the anogenital region.* Nat Commun, 2018. **9**(1): p. 2207.
90. Camus, C., et al., *Comparison of the effect of semen from HIV-infected and uninfected men on CD4+ T-cell infection.* AIDS, 2016. **30**(8): p. 1197-208.
91. Balandya, E., et al., *Semen protects CD4+ target cells from HIV infection but promotes the preferential transmission of R5 tropic HIV.* J Immunol, 2010. **185**(12): p. 7596-604.
92. Chen, J.C., et al., *Seminal plasma induces global transcriptomic changes associated with cell migration, proliferation and viability in endometrial epithelial cells and stromal fibroblasts.* Hum Reprod, 2014. **29**(6): p. 1255-70.
93. Doncel, G.F., S. Anderson, and I. Zalenskaya, *Role of semen in modulating the female genital tract microenvironment--implications for HIV transmission.* Am J Reprod Immunol, 2014. **71**(6): p. 564-74.
94. Ferreira, Z., et al., *Reproduction and immunity-driven natural selection in the human WFDC locus.* Mol Biol Evol, 2013. **30**(4): p. 938-50.
95. Hurle, B., et al., *Comparative sequence analyses reveal rapid and divergent evolutionary changes of the WFDC locus in the primate lineage.* Genome Res, 2007. **17**(3): p. 276-86.
96. Roan, N.R., et al., *Semen amyloids participate in spermatozoa selection and clearance.* Elife, 2017. **6**.
97. LoRicco, J.G., et al., *Gallic Acid Is an Antagonist of Semen Amyloid Fibrils That Enhance HIV-1 Infection.* J Biol Chem, 2016. **291**(27): p. 14045-55.
98. Roan, N.R., et al., *Aminoquinoline surfen inhibits the action of SEVI (semen-derived enhancer of viral infection).* J Biol Chem, 2010. **285**(3): p. 1861-9.
99. Sievers, S.A., et al., *Structure-based design of non-natural amino-acid inhibitors of amyloid fibril formation.* Nature, 2011. **475**(7354): p. 96-100.
100. Widera, M., et al., *The D-amino acid peptide D3 reduces amyloid fibril boosted HIV-1 infectivity.* AIDS Res Ther, 2014. **11**(1): p. 1.
101. de Villiers, E.M., et al., *Classification of papillomaviruses.* Virology, 2004. **324**(1): p. 17-27.
102. Bottalico, D., et al., *The oral cavity contains abundant known and novel human papillomaviruses from the Betapapillomavirus and Gammapapillomavirus genera.* J Infect Dis, 2011. **204**(5): p. 787-92.
103. Graham, S.V., *The human papillomavirus replication cycle, and its links to cancer progression: a comprehensive review.* Clin Sci (Lond), 2017. **131**(17): p. 2201-2221.
104. Buck, C.B., P.M. Day, and B.L. Trus, *The papillomavirus major capsid protein L1.* Virology, 2013. **445**(1-2): p. 169-74.
105. Wang, J.W. and R.B. Roden, *L2, the minor capsid protein of papillomavirus.* Virology, 2013. **445**(1-2): p. 175-86.

106. Smith, L. and M.P. Angarone, *Sexually Transmitted Infections.* Urol Clin North Am, 2015. **42**(4): p. 507-18.
107. zur Hausen, H., *Papillomaviruses in the causation of human cancers - a brief historical account.* Virology, 2009. **384**(2): p. 260-5.
108. Stanley, M., *Pathology and epidemiology of HPV infection in females.* Gynecol Oncol, 2010. **117**(2 Suppl): p. S5-10.
109. Martin, C.M. and J.J. O'Leary, *Histology of cervical intraepithelial neoplasia and the role of biomarkers.* Best Pract Res Clin Obstet Gynaecol, 2011. **25**(5): p. 605-15.
110. Venkatesan, N.N., H.S. Pine, and M.P. Underbrink, *Recurrent respiratory papillomatosis.* Otolaryngol Clin North Am, 2012. **45**(3): p. 671-94, viii-ix.
111. Andersen, A.S., et al., *The interplay between HPV and host immunity in head and neck squamous cell carcinoma.* Int J Cancer, 2014. **134**(12): p. 2755-63.
112. Schellenbacher, C., et al., *Efficacy of RG1-VLP vaccination against infections with genital and cutaneous human papillomaviruses.* J Invest Dermatol, 2013. **133**(12): p. 2706-2713.
113. Lee, S.J., et al., *Immunotherapy for human papillomavirus-associated disease and cervical cancer: review of clinical and translational research.* J Gynecol Oncol, 2016. **27**(5): p. e51.
114. Huber, B., et al., *Chimeric L2-Based Virus-Like Particle (VLP) Vaccines Targeting Cutaneous Human Papillomaviruses (HPV).* PLoS One, 2017. **12**(1): p. e0169533.
115. Doorbar, J., *Model systems of human papillomavirus-associated disease.* J Pathol, 2016. **238**(2): p. 166-79.
116. Doorbar, J., *Host control of human papillomavirus infection and disease.* Best Pract Res Clin Obstet Gynaecol, 2018. **47**: p. 27-41.
117. Moody, C., *Mechanisms by which HPV Induces a Replication Competent Environment in Differentiating Keratinocytes.* Viruses, 2017. **9**(9).
118. de Freitas, A.C., et al., *Human papillomavirus and lung cancinogenesis: an overview.* J Cancer Res Clin Oncol, 2016. **142**(12): p. 2415-2427.
119. Wang, C.J., J. Sparano, and J.M. Palefsky, *Human Immunodeficiency Virus/AIDS, Human Papillomavirus, and Anal Cancer.* Surg Oncol Clin N Am, 2017. **26**(1): p. 17-31.
120. Freeman, E.E., et al., *Herpes simplex virus 2 infection increases HIV acquisition in men and women: systematic review and meta-analysis of longitudinal studies.* AIDS, 2006. **20**(1): p. 73-83.
121. Chin-Hong, P.V., et al., *Anal human papillomavirus infection is associated with HIV acquisition in men who have sex with men.* AIDS, 2009. **23**(9): p. 1135-42.
122. Averbach, S.H., et al., *The association between cervical human papillomavirus infection and HIV acquisition among women in Zimbabwe.* AIDS, 2010. **24**(7): p. 1035-42.
123. Smith-McCune, K.K., et al., *Type-specific cervico-vaginal human papillomavirus infection increases risk of HIV acquisition independent of other sexually transmitted infections.* PLoS One, 2010. **5**(4): p. e10094.
124. Veldhuijzen, N.J., et al., *Factors affecting transmission of mucosal human papillomavirus.* Lancet Infect Dis, 2010. **10**(12): p. 862-74.
125. Houlihan, C.F., et al., *Human papillomavirus infection and increased risk of HIV acquisition. A systematic review and meta-analysis.* AIDS, 2012. **26**(17): p. 2211-22.

126. Rositch, A.F., et al., *Risk of HIV acquisition among circumcised and uncircumcised young men with penile human papillomavirus infection.* AIDS, 2014. **28**(5): p. 745-52.
127. Dreyer, G., *Clinical implications of the interaction between HPV and HIV infections.* Best Pract Res Clin Obstet Gynaecol, 2018. **47**: p. 95-106.
128. Camargo, M., et al., *Association of HIV status with infection by multiple HPV types.* Trop Med Int Health, 2018. **23**(11): p. 1259-1268.
129. Auvert, B., et al., *Association of oncogenic and nononcogenic human papillomavirus with HIV incidence.* J Acquir Immune Defic Syndr, 2010. **53**(1): p. 111-6.
130. Scott, M., M. Nakagawa, and A.B. Moscicki, *Cell-mediated immune response to human papillomavirus infection.* Clin Diagn Lab Immunol, 2001. **8**(2): p. 209-20.
131. Laurson, J., et al., *Epigenetic repression of E-cadherin by human papillomavirus 16 E7 protein.* Carcinogenesis, 2010. **31**(5): p. 918-26.
132. Doorbar, J., *The E4 protein; structure, function and patterns of expression.* Virology, 2013. **445**(1-2): p. 80-98.
133. McIntosh, P.B., et al., *Structural analysis reveals an amyloid form of the human papillomavirus type 16 E1--E4 protein and provides a molecular basis for its accumulation.* J Virol, 2008. **82**(16): p. 8196-203.
134. Ashmole, I., P.H. Gallimore, and S. Roberts, *Identification of conserved hydrophobic C-terminal residues of the human papillomavirus type 1 E1E4 protein necessary for E4 oligomerisation in vivo.* Virology, 1998. **240**(2): p. 221-31.
135. Doorbar, J., et al., *Specific interaction between HPV-16 E1-E4 and cytokeratins results in collapse of the epithelial cell intermediate filament network.* Nature, 1991. **352**(6338): p. 824-7.
136. Davy, C., et al., *A novel interaction between the human papillomavirus type 16 E2 and E1--E4 proteins leads to stabilization of E2.* Virology, 2009. **394**(2): p. 266-75.
137. Davy, C.E., et al., *Human papillomavirus type 16 E1 E4-induced G2 arrest is associated with cytoplasmic retention of active Cdk1/cyclin B1 complexes.* J Virol, 2005. **79**(7): p. 3998-4011.
138. Davy, C.E., et al., *Identification of a G(2) arrest domain in the E1 wedge E4 protein of human papillomavirus type 16.* J Virol, 2002. **76**(19): p. 9806-18.
139. Doorbar, J., et al., *The E1E4 protein of human papillomavirus type 16 associates with a putative RNA helicase through sequences in its C terminus.* J Virol, 2000. **74**(21): p. 10081-95.
140. Prescott, E.L., et al., *Human papillomavirus type 1 E1^E4 protein is a potent inhibitor of the serine-arginine (SR) protein kinase SRPK1 and inhibits phosphorylation of host SR proteins and of the viral transcription and replication regulator E2.* J Virol, 2014. **88**(21): p. 12599-611.
141. Khan, J., et al., *Role of calpain in the formation of human papillomavirus type 16 E1^E4 amyloid fibers and reorganization of the keratin network.* J Virol, 2011. **85**(19): p. 9984-97.
142. Murphy, M.P. and H. LeVine, 3rd, *Alzheimer's disease and the amyloid-beta peptide.* J Alzheimers Dis, 2010. **19**(1): p. 311-23.
143. Goedert, M., *NEURODEGENERATION. Alzheimer's and Parkinson's diseases: The prion concept in relation to assembled Abeta, tau, and alpha-synuclein.* Science, 2015. **349**(6248): p. 1255555.
144. Masters, C.L., et al., *Alzheimer's disease.* Nat Rev Dis Primers, 2015. **1**: p. 15056.

145. Atik, A., T. Stewart, and J. Zhang, *Alpha-Synuclein as a Biomarker for Parkinson's Disease.* Brain Pathol, 2016. **26**(3): p. 410-8.
146. Alam, U., et al., *General aspects of diabetes mellitus.* Handb Clin Neurol, 2014. **126**: p. 211-22.
147. Ninomiya, T., *Diabetes mellitus and dementia.* Curr Diab Rep, 2014. **14**(5): p. 487.
148. Akter, R., et al., *Islet Amyloid Polypeptide: Structure, Function, and Pathophysiology.* J Diabetes Res, 2016. **2016**: p. 2798269.
149. Westermark, P., A. Andersson, and G.T. Westermark, *Islet amyloid polypeptide, islet amyloid, and diabetes mellitus.* Physiol Rev, 2011. **91**(3): p. 795-826.
150. Ge, X., et al., *Islet Amyloid Polypeptide Promotes Amyloid-Beta Aggregation by Binding-Induced Helix-Unfolding of the Amyloidogenic Core.* ACS Chem Neurosci, 2018. **9**(5): p. 967-975.
151. Kollias, C.M., et al., *Animal models of herpes simplex virus immunity and pathogenesis.* J Neurovirol, 2015. **21**(1): p. 8-23.
152. Ghanem, A. and K.K. Conzelmann, *G gene-deficient single-round rabies viruses for neuronal circuit analysis.* Virus Res, 2016. **216**: p. 41-54.
153. Fooks, A.R., et al., *Rabies.* Nat Rev Dis Primers, 2017. **3**: p. 17091.
154. Rota, P.A., et al., *Measles.* Nat Rev Dis Primers, 2016. **2**: p. 16049.
155. Delpeut, S., et al., *Host factors and measles virus replication.* Curr Opin Virol, 2012. **2**(6): p. 773-83.
156. Kukhanova, M.K., A.N. Korovina, and S.N. Kochetkov, *Human herpes simplex virus: life cycle and development of inhibitors.* Biochemistry (Mosc), 2014. **79**(13): p. 1635-52.
157. Su, Y.H., et al., *Stability and circularization of herpes simplex virus type 1 genomes in quiescently infected PC12 cultures.* J Gen Virol, 2002. **83**(Pt 12): p. 2943-50.
158. Weller, S.K. and D.M. Coen, *Herpes simplex viruses: mechanisms of DNA replication.* Cold Spring Harb Perspect Biol, 2012. **4**(9): p. a013011.
159. Albertini, A.A., R.W. Ruigrok, and D. Blondel, *Rabies virus transcription and replication.* Adv Virus Res, 2011. **79**: p. 1-22.
160. Bhattacharjee, S. and P.K. Yadava, *Measles virus: Background and oncolytic virotherapy.* Biochem Biophys Rep, 2018. **13**: p. 58-62.
161. Goncalves, M.A. and A.A. de Vries, *Adenovirus: from foe to friend.* Rev Med Virol, 2006. **16**(3): p. 167-86.
162. Ison, M.G. and R.T. Hayden, *Adenovirus.* Microbiol Spectr, 2016. **4**(4).
163. Schrenzel, M., et al., *Characterization of a new species of adenovirus in falcons.* J Clin Microbiol, 2005. **43**(7): p. 3402-13.
164. Sanchala, D.S., L.K. Bhatt, and K.S. Prabhavalkar, *Oncolytic Herpes Simplex Viral Therapy: A Stride toward Selective Targeting of Cancer Cells.* Front Pharmacol, 2017. **8**: p. 270.
165. Watanabe, D. and F. Goshima, *Oncolytic Virotherapy by HSV.* Adv Exp Med Biol, 2018. **1045**: p. 63-84.
166. Russell, W.C., *Adenoviruses: update on structure and function.* J Gen Virol, 2009. **90**(Pt 1): p. 1-20.
167. Pizzato, M., et al., *A one-step SYBR Green I-based product-enhanced reverse transcriptase assay for the quantitation of retroviruses in cell culture supernatants.* J Virol Methods, 2009. **156**(1-2): p. 1-7.
168. Cavrois, M., C. De Noronha, and W.C. Greene, *A sensitive and specific enzyme-based assay detecting HIV-1 virion fusion in primary T lymphocytes.* Nat Biotechnol, 2002. **20**(11): p. 1151-4.

169. Muthumani, K., et al., *Vpr-GFP virion particle identifies HIV-infected targets and preserves HIV-1Vpr function in macrophages and T-cells.* DNA Cell Biol, 2000. **19**(3): p. 179-88.
170. Riss, T.L., et al., *Cell Viability Assays*, in *Assay Guidance Manual*, G.S. Sittampalam, et al., Editors. 2004: Bethesda (MD).
171. Qian, K., S.L. Morris-Natschke, and K.H. Lee, *HIV entry inhibitors and their potential in HIV therapy.* Med Res Rev, 2009. **29**(2): p. 369-93.
172. Coffin, J. and R. Swanstrom, *HIV pathogenesis: dynamics and genetics of viral populations and infected cells.* Cold Spring Harb Perspect Med, 2013. **3**(1): p. a012526.
173. Guo, J., et al., *Spinoculation triggers dynamic actin and cofilin activity that facilitates HIV-1 infection of transformed and resting CD4 T cells.* J Virol, 2011. **85**(19): p. 9824-33.
174. Ochsenbauer, C., et al., *Generation of transmitted/founder HIV-1 infectious molecular clones and characterization of their replication capacity in CD4 T lymphocytes and monocyte-derived macrophages.* J Virol, 2012. **86**(5): p. 2715-28.
175. Hemalatha, R., et al., *Evaluation of vaginal pH for detection of bacterial vaginosis.* Indian J Med Res, 2013. **138**(3): p. 354-9.
176. Zhou, J., et al., *The Semen pH Affects Sperm Motility and Capacitation.* PLoS One, 2015. **10**(7): p. e0132974.
177. Bitterman, W., et al., *Contact pH of rectal mucosa in humans and dogs.* Dis Colon Rectum, 1969. **12**(2): p. 96-8.
178. LeVine, H., 3rd, *Quantification of beta-sheet amyloid fibril structures with thioflavin T.* Methods Enzymol, 1999. **309**: p. 274-84.
179. Zirafi, O., et al., *Semen enhances HIV infectivity and impairs the antiviral efficacy of microbicides.* Sci Transl Med, 2014. **6**(262): p. 262ra157.
180. Herfs, M., et al., *Mucosal junctions: open doors to HPV and HIV infections?* Trends Microbiol, 2011. **19**(3): p. 114-20.
181. Lissouba, P., P. Van de Perre, and B. Auvert, *Association of genital human papillomavirus infection with HIV acquisition: a systematic review and meta-analysis.* Sex Transm Infect, 2013. **89**(5): p. 350-6.
182. van der Loeff, M.F., A.G. Nyitray, and A.R. Giuliano, *HPV vaccination to prevent HIV infection: time for randomized controlled trials.* Sex Transm Dis, 2011. **38**(7): p. 640-3.
183. Yolamanova, M., et al., *Peptide nanofibrils boost retroviral gene transfer and provide a rapid means for concentrating viruses.* Nat Nanotechnol, 2013. **8**(2): p. 130-6.
184. Scharf, L., et al., *Antibody 8ANC195 reveals a site of broad vulnerability on the HIV-1 envelope spike.* Cell Rep, 2014. **7**(3): p. 785-95.
185. Scutari, R., et al., *The Role of HIV Infection in Neurologic Injury.* Brain Sci, 2017. **7**(4).
186. Mzingwane, M.L. and C.T. Tiemessen, *Mechanisms of HIV persistence in HIV reservoirs.* Rev Med Virol, 2017. **27**(2).
187. Riva, N., et al., *Acute human herpes virus 7 (HHV-7) encephalitis in an immunocompetent adult patient: a case report and review of literature.* Infection, 2017. **45**(3): p. 385-388.
188. Gewurz, B.E., et al., *Human herpesvirus 6 encephalitis.* Curr Infect Dis Rep, 2008. **10**(4): p. 292-9.
189. Itzhaki, R.F., *Herpes simplex virus type 1 and Alzheimer's disease: possible mechanisms and signposts.* FASEB J, 2017. **31**(8): p. 3216-3226.

190. Bourgade, K., et al., *Anti-Viral Properties of Amyloid-beta Peptides.* J Alzheimers Dis, 2016. **54**(3): p. 859-878.
191. Nair, S., et al., *Enterovirus infection induces cytokine and chemokine expression in insulin-producing cells.* J Med Virol, 2010. **82**(11): p. 1950-7.
192. Ericsson, M. and O. Skog, *Presence of Human Herpesvirus 6B in the Pancreas of Subjects With and Without Type 1 Diabetes.* Pancreas, 2017. **46**(10): p. 1341-1346.
193. Kim, K.W., et al., *Higher abundance of enterovirus A species in the gut of children with islet autoimmunity.* Sci Rep, 2019. **9**(1): p. 1749.
194. Krogvold, L., et al., *Detection of a low-grade enteroviral infection in the islets of langerhans of living patients newly diagnosed with type 1 diabetes.* Diabetes, 2015. **64**(5): p. 1682-7.
195. Riedner, G., et al., *Baseline survey of sexually transmitted infections in a cohort of female bar workers in Mbeya Region, Tanzania.* Sex Transm Infect, 2003. **79**(5): p. 382-7.